EXTREME MEDICINE

SCIENTIFIC AND PRACTICAL REVIEWED JOURNAL OF FMBA OF RUSSIA

Indexed in Scopus in 2022

Indexed in RSCI. IF 2018: 0,570

Listed in HAC 31.01.2020 (№ 1292)

Open access to archive

МЕДИЦИНА ЭКСТРЕМАЛЬНЫХ СИТУАЦИЙ

НАУЧНО-ПРАКТИЧЕСКИЙ РЕЦЕНЗИРУЕМЫЙ ЖУРНАЛ ФМБА РОССИИ

Contents
Содержание

NEUTRALIZING ANTIBODY CREATION TECHNOLOGIES: CASE OF SARS-COV-2

Baklaushev VP[1,2,3] ✉, Samoilova EM[1,2], Kuznetsova SM[1], Ermolaeva EV[2], Yusubalieva GM[1,2], Kalsin VA[1,2], Lipatova AV[2], Troitsky AV[1]

[1] Federal Scientific and Clinical Center of Specialized Types of Medical Care and Medical Technologies, Federal Medical Biological Agency of Russia, Moscow, Russia

[2] Engelhardt Institute of Molecular Biology, Russian Academy of Sciences, Moscow, Russia

[3] Research Institute of Pulmonology, Federal Medical Biological Agency of Russia, Moscow, Russia

Monoclonal antibodies (mAbs) are the most promising and most intensively replenished type of bioactive pharmaceuticals. Currently, there are over 100 different mAbs approved by the FDA and other regulating agencies for treatment of oncological, infectious, systemic, autoimmune and other diseases. Design of antibodies neutralizing pathogens of socially significant infections, such as HIV, hepatitis viruses, SARS-CoV-2, is a separate direction. The SARS-CoV-2 pandemic has shown how urgent it is to have a technological platform enabling production of fully human antibodies. The development of recombinant DNA technology and antibody phage display enabled compilation of libraries of antigen-binding fragments and screening with target antigens. This review discusses the advantages and disadvantages of phage display, including use of single-domain antibody technology based on the heavy chain variable domain. We describe the state-of-the-art (and practical results of its application) technology enabling production of human antibodies by sorting and sequencing the genome of individual memory B cells, using monoclonal virus-neutralizing antibodies against SARS-CoV-2 as an example. The prospects of further development of the recombinant human antibody production technology are discussed; in particular, we consider creation of sequences of variable fragments of antibodies with the help of artificial intelligence.

✉ **Correspondence should be addressed:** Vladimir P. Baklaushev
Orexovyj bul'var, 28, g. Moscow, 115682, Russia; baklaushev.vp@fnkc-fmba.ru

ТЕХНОЛОГИИ СОЗДАНИЯ ВИРУСНЕЙТРАЛИЗУЮЩИХ АНТИТЕЛ ЧЕЛОВЕКА НА ПРИМЕРЕ SARS-COV-2

В. П. Баклаушев[1,2,3] ✉, Е. М. Самойлова[1,2], С. М. Кузнецова[1], Е. В. Ермолаева[2], Г. М. Юсубалиева[1,2], В. А. Кальсин[1,2], А. В. Липатова[2], А. В. Троицкий[1]

[1] Федеральный научно-клинический центр специализированных видов медицинской помощи и медицинских технологий Федерального медико-биологического агентства, Москва, Россия

[2] Институт молекулярной биологии имени В. А. Энгельгардта Российской академии наук, Москва, Россия

[3] Научно-исследовательский институт пульмонологии Федерального медико-биологического агентства, Москва, Россия

Моноклональные антитела (мАт) — самый перспективный и наиболее интенсивно пополняемый вид биоактивных фармпрепаратов. В настоящее время более 100 различных мАт одобрены FDA и другими регуляторами для терапии онкологических, инфекционных, системных, аутоиммунных и других заболеваний. Отдельным современным направлением является получение вируснейтрализующих антител к возбудителям социально значимых инфекций, таких как ВИЧ, вирусы гепатита, SARS-CoV-2. Пандемия новой коронавирусной инфекции показала, насколько актуально может быть наличие технологической платформы по производству полностью гуманизированных антител человека. Развитие технологии рекомбинантных ДНК и разработка фагового дисплея антител позволили создавать библиотеки антигенсвязывающих фрагментов и проводить скрининг с целевыми антигенами. В обзоре обсуждаются достоинства и недостатки фагового дисплея, в том числе с применением технологии однодоменных антител на основе вариабельного домена тяжелой цепи. Представлены описание и практические результаты наиболее современной технологии получения антител человека путем сортировки и секвенирования генома отдельных В-клеток памяти на примере получения моноклональных вируснейтрализующих антител против SARS-CoV-2. Описаны перспективы дальнейшего развития технологии получения рекомбинантных антител человека, в частности — создание последовательностей вариабельных фрагментов антител с помощью искусственного интеллекта.

✉ **Для корреспонденции:** Владимир Павлович Баклаушев
Ореховый бульвар, д. 28, г. Москва, 115682, Россия; baklaushev.vp@fnkc-fmba.ru

Since Köhler and Milstein developed the technology of production of monoclonal antibodies (hybridoma technology) in 1975 [1], hundreds of diagnostic and therapeutic antibodies have been designed, tested, registered, applied and discontinued [2]. This technology enabled production of Muromonab-CD3, the first registered therapeutic antibody produced in mice [3]. Advancements of the recombinant DNA technology allowed humanization of mouse immunoglobulins, partial or complete, which was the next step in the development of the therapeutic (monoclonal) antibodies production technology [4]. Approximately simultaneously with the first human trials of mouse monoclonal antibodies the phage display technique was developed, first for peptides [5], then for antibodies [6]. Arguably, this technique became the most powerful tool enabling creation and "improvement of monoclonal antibodies; gradually, it replaced the hybridoma technology [2, 7]. Development of single cell sequencing yielded an alternative to phage display, a technique that allowed producing human monoclonal antibodies by cloning variable antibody fragments from a specific clone of plasma cells [8].

One of the most promising directions of medical application of human monoclonal antibodies is production of neutralizing antibodies (NAbs) and their use in prevention and treatment of socially significant infectious diseases. The COVID-19

pandemic made development of the SARS-CoV-2 neutralizing antibodies a particularly urgent task [9]. Over 20 NAbs have been designed, clinically tested and registered with the FDA and other regulating agencies since the beginning of the pandemic. Emergence of the new variants of SARS-CoV-2 rendered most NAbs ineffective, but a number of them have demonstrated a broad neutralizing activity against the most common subvariants of Omicron [8, 11]. Despite a significant decrease in the proportion of severe COVID-19 cases, NAbs still remain the most effective agents of etiotropic therapy, which is especially relevant for patients with oncological and hematological diseases and other primary and secondary immunodeficiencies [12].

The purpose of this review is to describe the current state of production of recombinant human antibodies using the example of neutralizing antibodies designed against SARS-CoV-2.

Antibody phage display

The antibody phage display method was developed independently by several groups of researchers, the first of which was the group of McCafferty from the University of Cambridge [6]. The method implies compilation of a phage library containing all possible variants of immunoglobulin variable regions. For this purpose, the antigen-binding antibody sequences are cloned into the pIII surface protein sequence of filamentous bacteriophages M13, fd or f1, which produces a number of unique clones, each of which presents a variable fragment of a certain specificity on its surface. The next step is to screen and select phages by this or that useful property, e.g., by the binding affinity to an antigen immobilized on the solid phase, followed by cloning of the selected sequences into vectors for antibody expression [6]. A phage library can be compiled from variable regions of immunoglobulin sequence of an immunized animal or human, but it can also be a random set of synthetic peptides [13].

Compared to other technologies, such as ribosome display [14], yeast display [15] or mammalian cell display [16], phage display libraries can have the variety of unique clones greater than 1011, with all of them stored for considerable periods in a state ready for screening with any antigen panel [7]. The variable fragments of antibodies in phage libraries can be antigen-binding Fab-fragments [17] or single-domain scFv-fragments (single chain fragment variable) [18, 19]. ScFv are monovalent fragments of antibodies with molecular weight of 25–27 kDa, consisting of the variable domains of heavy (VH) and light (VL) immunoglobulin chains connected by a peptide linker [20]. Fab are relatively large fragments of immunoglobulins that consist of V_H, V_L, C_L, and C_H1 domains. Compared to Fab, scFv offers a higher level of expression in phages, which is an advantage somewhat offset by the risk of loss of affinity upon conversion to Fab or full-length IgG [7]. There are variants of antibody phage libraries, those which include single-domain antibodies (human V_H, camelid VHH, and shark V_{NAR}, respectively); they are covered in a separate section below.

The antibody phage display enabled production of NAbs acting against HIV [21], anthrax toxin [22], tick-borne encephalitis [23], and, of course, SARS-CoV-2 [24]. The latter study demonstrated that phage display can produce high-affinity NAbs against the SARS-CoV-2 S protein with ID_{50} < 2 ng/mL from a semi-synthetic library of variable fragments of naive antibodies. Thus, compilation of an accurate CDR library of naïve B cells is the key factor ensuring stable pairing of V_H and V_L domains and, as a result, production of high-affinity neutralizing antibodies [24]. At the same time, it should be noted that far from all attempts at this task are successful, and the vast majority of highly active NAbs are obtained from samples of hyperimmune convalescents [8].

A noteworthy shortcoming of the canonical oligomeric antibody phage display technique is the fact that the resulting antibodies, as a rule, mismatch the natural repertoire, since they are generated from random pairs of VH and VL. One of the possible solutions to the VH/VL domain pairing problem involves use of phage libraries of the camelid family single-domain antibodies, the so-called nanobodies [25, 26].

Single-domain antibodies as a developmental platform for immunity preparations produced using the phage display technology

Single-domain antibodies, or nanobodies, are recombinant variable domains of VHH heavy chains derived from non-canonical immunoglobulins, with the Fab fragment consisting only of a shortened heavy chain, without a light chain. Normally, such antibodies are present in cartilaginous fish and the Camelidae in addition to the "classical" immunoglobulins G, which are comprised of two heavy and two light chains [25]. The key advantage of nanobodies is that the VHH domain, represented by a single polypeptide sequence, can be easily cloned in prokaryotic or yeast expression systems. The size of a nanobody is 12–15 kDa; they are highly soluble and capable of refolding after denaturing purification [25]. The increased solubility of VHH is the results of peculiarities of their amino acid composition. Compared to conventional antibodies, which have the V_H and V_L domains pairing interface dressed with hydrophobic amino acid residues, VHH have the hydrophobic amino acids in homologous regions replaced by more hydrophilic ones, which increases solubility of the recombinant products by reducing aggregation capacity [27].

With their small size and single-domain nature, nanobodies can penetrate structures inaccessible to full-length antibodies, and bind epitopes that are sterically shielded for conventional antibodies [25, 28–30]. Another reason behind the single-domain antibodies' capacity to penetrate steric shielding is the CDR3 loop in the VHH domain: it is longer than that of conventional antibodies, which allows single-domain antibodies to bind antigens located, for example, in the catalytic clefts of enzymes or in three-dimensional congruent regions of the ligand-receptor interaction [7]. With SARS-CoV-2 in particular, greater mobility allows single-domain antibodies to recognize the RBD of the S protein in its "down" conformation and disrupt the transition to the "up" conformation, rendering the protein nonfunctional [31] (see below).

The affinity of single domain antibodies is similar to that of conventional heavy and light chain antibodies, but nanobodies, unlike classical antibodies, are highly stable over a wide range of ionic strengths, pH values and temperatures [32]. The production of nanobodies in bacteria is cheaper than production of classical antibodies. The level of homology of framework regions of single-domain camelid VHH and human IgG3 subclass VH domains is high, which means the former can be easily humanized and retain their functional properties in the process [25]. All of the above translates into the prerequisites justifying research and practical application of recombinant single-domain antibodies both for diagnostic and therapeutic purposes [33, 34].

Bi- and trispecific/valence nanobodies

Small size of single-domain antibodies awards them rapid kinetics in the systemic circulation; they are eliminated

through the kidneys within a few hours. On the one hand, this is an advantage usable, for example, in development of radioisotope diagnostic tools [26]. On the other hand, it limits the use of nanobodies as preventive and therapeutic agents and necessitates additional efforts aimed at increasing their half-life in the bloodstream. The solution to the problem of rapid elimination of nanobodies from the body is their oligomerization and/or creation of bi- and trispecific antibodies. Heterodimerized and bi- and trivalent nanobodies have significantly longer pharmacokinetic persistence. An example thereof is the ALX-0061 heterodimeric bispecific nanobody produced by Ablynx; it consists of a high affinity VHH domain binding the IL6 receptor with an affinity coefficient of 0.19 pM and a VHH domain specific to serum albumin. The latter brings the half-life of the heterodimeric complex up to 6.6 days, with the molecular weight of the former of 26 kDa [35] and this is clearly not the ultimate limit. This high an affinity of the ALX-0061 nanobody is the result of "affinity maturation", also enabled by phage display; the technology increased the affinity 200-fold compared to the initial VHH domain [35]. Another example of a therapeutic antibody produced through heterooligomerization of nanobodies is Ozoralizumab, a humanized bispecific trivalent antibody including two TNFα-binding VHH domains and one serum albumin-binding VHH domain [36]. Supplementing the bi- and trivalent antibodies with VHH domain that binds serum albumin can be considered one of the standard approaches to augmentation of half-life of recombinant nanobodies [37].

Oligomerization of VHH domains to create bi- and trivalent antibodies not only increases the half-life of these antibodies but also enhances their functionality by building up the avidity of such antibodies [38]. Another way to boost half-life and functionality of nanobodies is through creation of fusion proteins with the Fc fragment of human immunoglobulins. A nanobody modified with an Fc fragment has a significantly longer half-life in the bloodstream; the fusion also promotes activation of the Fc-mediated effector functions (antibody-dependent cell-mediated cytotoxicity, complement-dependent cytotoxicity, etc.) [39, 40].

Virus neutralizing nanobodies

In the pre-pandemic era, different groups of researchers designed nanobodies neutralizing the respiratory syncytial virus [41], MERS-CoV [42], pandemic variants of the influenza (H1N1 [43], H5N1 [44]), as well as multidomain broad-spectrum influenza neutralizing nanobodies that bind hemagglutinin [45]. When the SARS-CoV-2 pandemic began, this technological knowledge enabled development of neutralizing nanobodies acting against the new pathogen. For example, yeast display technology [46] allowed producing synthetic neutralizing mNb6-tri nanobodies targeting the SARS-CoV-2 S-protein. These nanobodies were shown to bind with the S trimer in the "down" conformation, stabilize it in this inactive form and thus make interaction with the ACE2 impossible [31]. Genetic engineering optimization gave trivalent mNb6-tri antibodies femtomolar affinity and picomolar concentration for complete SARS-CoV-2 virus neutralization. These antibodies retain their properties having undergone lyophilization, heating, aerosolization, and thus can be used in inhalations for the purpose of virus neutralization in the bronchoalveolar tree [31].

A panel of RBD-specific nanobodies was obtained from a library of VHH phage displays created from B-cells of a Bactrian camel immunized with recombinant RBD [47]. Three clones, P2C5, P5F8, and P2G1, were selected with *in vitro* virus neutralization test as completely suppressing the cytopathic effect of SARS-CoV-2 at concentrations of 12–48 nM. Seeking to further improve antivirus properties of the antibodies, a group of researchers produced homodimeric and heterodimeric forms of nanobody clones that had 100-fold (minimum, some were more potent) higher virus neutralizing potency compared to monomers [47].

The new variants of SARS-CoV-2 that are better at avoiding virus-neutralizing antibodies add urgency to the task of creation of broadly neutralizing antibodies that bind all possible SARS-CoV-2 variants. At least one option thereof has been produced with the help of the single-domain antibody technology. A group of researchers immunized a llama alternately with the S protein of SARS-CoV-1 and MERS-CoV, then derived a phage library of antibody variable domains and screened it against the S protein of SARS-CoV-2, among other things. They found the VHH72 nanobody, which boasts high cross-neutralizing activity against SARS-CoV-1 and SARS-CoV-2. The researchers have created a bivalent antibody based on VHH72 as a fusion protein with the Fc fragment of human Ig, and shown its promise as a possible base for a broadly neutralizing antiviral drug [48]. Phage display and VHH have enabled design of other virus-neutralizing nanobodies that inactivate SARS-CoV-2 [49].

Thus, using the single-domain antibody technology, a number of promising homo- and heterodimeric NAbs were produced, all of them showing promise as base for an etiotropic drug for treatment and prevention of COVID-19.

Production of recombinant human antibodies from individual B cells

From the historical and methodological points of view, the approach to production of human monoclonal antibodies most advanced currently is direct isolation of specific B cells followed by sequencing of the genomes of individual cells and identification of variable fragments of MAbs produced by them [50]. There are three variations of this approach, each with its own methodology of the first stage (identification and cultivation of the antigen-specific clone of B cells). For example, the hybridoma technology allows producing hybridomas of target B cells with myeloma cells and carrying out selection on the HAT medium, and then collect hybridomas with the desired specificity (1); or, isolate, culture and collect memory B cells (2); or, directly isolate memory B cells with a target BCR interacting with a fluorescently or magnetically labeled antigen, and then analyze the repertoire of specific B cell clones using the single-cell sequence technology (3). The latter option is the most advanced one; it allows producing panels of specific NAbs in a relatively short time [8]. Antigen-specific memory B cells can be obtained from the plasma of hyperimmune patients or from transgenic mice carrying human immunoglobulin loci and producing fully human antibodies in response to immunization with the target antigen [51]. There is a number of technological solutions that improve performance of screening of individual antibody-producing cells, like microfluidic sorting of B-cells with assessment of BCR specificity, followed by bar-coding of VH and VL pairs and high-throughput sequencing [52].

The advantage of the new technology is that its result does not depend on the diversity of the library of variable domains, but, at the same time, it is always a variant of the natural repertoire of antibodies, which means an acceptable safety profile and a significantly lower probability of non-specific (off-target) interactions with its own antigenic determinants [50]. Along with single-cell NGS sequencing, high-performance technological solutions enable simultaneous analysis of hundreds of different clones of memory B-cells secreting

antibodies of a given specificity and subsequent selection by various useful properties (affinity, avidity, overlapping antigenic epitopes, etc.) [8, 52].

The approach implying production of NAbs from individual clones of B cells the with the help of the single cell sequence technique has proven to be highly efficient in creation of broadly neutralizing antibodies that block the CD4 binding site in the V1/V2 and V3 regions of gp120, as well as HIV gp41 [53, 54]. In addition, this technology is behind design of MAbs against cytomegalovirus [55], S-antigen of hepatitis B virus (HBsAg) [56] and a large number of NAbs against the SARS-CoV-2 S protein [57–60].

Some of the first neutralizing antibodies REGN10933 (casirivimab) and REGN10897 (imdevimab) were obtained by applying the single B cell assay technology to the material collected from immunized humanized mice and convalescents after COVID-19 [58]. NGS sequencing and 3D mapping of antigenic epitopes (done with hydrogen-deuterium exchange mass spectrometry) enabled analysis of a panel of more than 200 virus-neutralizing antibodies, which ultimately yielded four antibodies characterized by non-overlapping epitopes. Used in a cocktail, the pairs of these antibodies effectively neutralized all SARS-CoV-2 variants known at that time.

A similar study aimed at creation of a panel of SARS-CoV-2 virus-neutralizing antibodies was conducted in 2021 [8]. As a result of NGS sequencing of clones of B cells from patients that had severe COVID-19, 18 high-affinity antibodies to RBD with KD in the range of 0.47–13.3 nM and virus-neutralizing capacity were produced; four of them have shown 100% virus neutralization at concentrations below 16 ng/ml [8]. The next step was to do a competitive analysis of interaction of the obtained antibodies with a panel of commercially available neutralizing antibodies with a known 3D structure of the antigenic epitope. COVA2-15 [59] and COV2-2504 [60] can be named here in addition to the already mentioned REGN10933 (casirivimab) and REGN10897 (imdevimab) [58]. The results of the competitive analysis and a series of SARS-CoV-2 RBD (with known point mutations) viral neutralization experiments allowed an accurate identification of antigenic epitopes of the obtained ultra-neutralizing antibodies. By combining antibodies complementing each other NAb cocktails that effectively neutralize all studied variants of SARS-CoV-2 were mixed. This experience shows that a comprehensive panel of broadly neutralizing antibodies from individual memory B cells that covers all possible antigenic epitopes and avoids point mutations allows compilation of effective virus-neutralizing cocktails against any new variant of SARS-CoV-2. If necessary, the panel of broadly neutralizing antibodies can be supplemented with targeted mutagenesis of antigen-binding sites.

There was developed a number of microfluidic platforms that significantly increase cloning throughput and single antibody expression. One of them is the 10x Genomics platform: drops containing one antibody-producing cell each, as well as a lysis buffer with microbeads coated with bar-coded primers, are generated in a microfluidic device to encode cDNA of specific native pairs of VH and VL domains [61].

A recent advancement is LIBRA-seq (linking B cell receptor to fntigen specificity through sequencing) a technology enabling high-throughput BCR screening by binding B lymphocytes to antigens barcoded using oligonucleotides, followed by NGS sequencing [62]. Using this technology, several thousand B cells from HIV-infected patients were screened for antigenic specificity, which yielded confirmation of the predicted specificity for antibodies to HIV, influenza and SARS-CoV-2, including known and unknown NAbs.

The MAbs produced using the single B cell technology can be genetically modified in the same way as antibodies obtained by phage display. For example, it is possible to modify the Fc fragment to increase the circulation of antibodies in the bloodstream. Among the most advanced modified antibodies to SARS-CoV-2 is sotrovimab, also known as VIR-7831 and GSK4182136, designed by Vir Biotechnology and GlaxoSmithKline, approved by the FDA in 2021. The Fc fragment of sotrovimab includes amino acid substitutions M428L and N434S (LS modification), which prolongs its half-life [63]. Another example is AZD7442, a cocktail of tixagevimab (AZD8895) and Cilgavimab (AZD1061) [64] compiled by AstraZeneca. Both NAbs, combined, have engineered Fc domains including L234F/L235/P331S substitutions (TM modification), resulting in little or no binding to various FcγRs or C1q complement protein, and insignificant to non-existent manifestations of the effector function *in vitro* [64].

Prospects of artificial intelligence (AI) in further development of the human antibody design technologies

Today, there is an already established candidate for the role of a fundamentally new human antibody modeling technology: AI-enabled in silico antibody structure prediction [65]. The AlphaFold2 neural network launched in 2021 can predict spatial structure of proteins from their primary sequence with accuracy at the atomic level [66]. AlphaFold2 is the first successful application of machine learning to the task of modeling tertiary structure of a protein. AlphaFold2 relies on the so-called multiple sequence alignment (MSA), analyzing information about the pairing of amino acid residues and structural templates for the primary sequence [67].

The AbAdapt service was developed specifically to predict the 3D structure of antibodies and antigenic epitopes; it combines structural modeling of antibodies and antigens with modeling of their interaction. By default, AbAdapt takes primary sequences as input and uses the Repertoire Builder [68], a high performance antibody structure modeling service. In 2022, AlphaFold and AbAdapt were merged to build the AbAdapt-AF system [69], which more accurately predicts the structure of paratopes and antigenic epitopes specific to antibodies. The authors used the service to analyze the virus-neutralizing antibody to RBD domain of SARS-CoV-2 and showed that their system is best in modeling the antigen-antibody interaction. The recently built Ablooper [70] and DeepAb [71] specialized neural networks have proven to have a better throughput than the Rosetta Antibody Benchmark and AlphaFold2 networks.

In August 2022, there was launched the NanoNet neural network, which is optimized to predict the 3D structure of VHH [72]. Its architecture includes a high-precision neural network (CNN) and two additional neural networks (ResNet). The first, ResNet, analyzes scaffolds and hypervariable CDR cycles, while the second perceives interactions between amino acid residues. Comparison of NanoNet and AlphaFold2 in terms of prediction of 3D structure of the known 16 VHHs deposited in the PDB in 2021, which means they were not part of the dataset AlphaFold2 was trained on, revealed that NanoNet offered better accuracy on the atomic level. Thus, NanoNet is a very promising new tool for modeling the structure of VHH; it is used, inter alia, to optimize the predictions of structure of CDR3 loops that neutralize VHH acting against SARS-CoV-2 [73].

It can be concluded that today, it is already theoretically possible to create high-affinity variable domains of antibodies *in silico*, i.e., without actual use of B cells and immunization. There is no doubt that in the future, selection of a high affinity

sequence for specific antigenic epitopes with the help of machine learning will be a routine method of production of human antibodies.

CONCLUSION

Currently, the monoclonal human neutralizing antibody production technologies rely on phage display and derivation of antibodies from individual B cells. Each technology has its own advantages and limitations. Phage display allows rapid screening of phage libraries with antigen-binding site sequences, such a screening done against novel antigens. The

VHH single-domain antibody technology allows creating bi- and trispecific antibodies, optimization of the affinity and capacity to neutralize new variants of SARS-CoV-2. The technology for obtaining antibodies from individual B cells, enhanced by high-throughput screening based on microfluidics and NGS sequencing, enables compilation of panels of virus-neutralizing antibodies that can be combined to cover any SARS-CoV-2 RBD modification. Future advancements of the monoclonal antibody production technology involve neural networks and machine learning that are used to predict the primary structure of variable domains of antibodies based on the tertiary structure of the target antigen.

References

1. Köhler G, Milstein C. Continuous cultures of fused cells secreting antibody of predefined specificity. Nature. 1975; 256 (5517): 495–7.
2. Frenzel A, Kügler J, Helmsing S, Meier D, Schirrmann T, Hust M, et al. Designing human antibodies by phage display. Transfus Med Hemother. 2017; 44 (5): 312–8.
3. Emmons C, Hunsicker LG. Muromonab-CD3 (Orthoclone OKT3): the first monoclonal antibody approved for therapeutic use. Iowa Med. 1987; 77 (2): 78–82.
4. Presta LG. Engineering of therapeutic antibodies to minimize immunogenicity and optimize function. Adv Drug Deliv Rev. 2006; 58: 640–56.
5. Smith GP. Filamentous fusion phage: novel expression vectors that display cloned antigens on the virion surface. Science. 1985; 228: 1315–7.
6. McCafferty J, Griffiths AD, Winter G, Chiswell DJ. Phage antibodies: filamentous phage displaying antibody variable domains. Nature. 1990; 348 (6301): 552–4.
7. Ledsgaard L, Ljungars A, Rimbault C, Sørensen CV, Tulika T, Wade J, et al. Advances in antibody phage display technology. Drug Discov. Today. 2022; 27 (8): 2151–69.
8. Gorchakov AA, Kulemzin SV, Guselnikov SV, Baranov KO, Belovezhets TN, Mechetina LV, et al. Isolation of a panel of ultra-potent human antibodies neutralizing SARS-CoV-2 and viral variants of concern. Cell Discov. 2021; 7 (1): 96.
9. Baklaushev VP, Kulemzin SV, Gorchakov AA, Lesnyak VN, Yusubalieva GM, Sotnikova AG. COVID-19. Aetiology, pathogenesis, diagnosis and treatment. Journal of Clinical Practice. 2020; 11 (1): 7–20.
10. Coronavirus disease (COVID-19) pandemic. World Health Organization. 2021. Available from: https://www.who.int/emergencies/diseases/novel-coronavirus-2019.
11. Baklaushev VP, Yusubalieva GM, Bychinin MV, Yusubalieva SM, Kalsin VA, Troickij AV. Racional'naya strategiya podderzhaniya protivovirusnogo immuniteta k novym variantam SARS-CoV-2. Klinicheskaya praktika. 2022; 13 (3): 43–55. Russian.
12. Synowiec A, Szczepański A, Barreto-Duran E, Lie LK, Pyrc K. Severe acute respiratory syndrome coronavirus 2 (SARS-CoV-2): a systemic infection. Clin Microbiol Rev. 2021; 34: e00133–20.
13. Hoogenboom HR. Overview of antibody phage-display technology and its applications. Methods Mol Biol. 2002; 178: 1–37.
14. Hanes J, Plückthun A. In vitro selection and evolution of functional proteins by using ribosome display. Proc Natl Acad Sci U S A. 1997; 94 (10): 4937–42.
15. Boder ET, Wittrup KD. Yeast surface display for screening combinatorial polypeptide libraries. Nat Biotechnol. 1997; 15 (6): 553–7.
16. Beerli RR, Bauer M, Buser RB, Gwerder M, Muntwiler S, Maurer P, et al. Isolation of human monoclonal antibodies by mammalian cell display. Proc Natl Acad Sci U S A. 2008; 105 (38): 14336–41.
17. Hoet RM, Cohen EH, Kent RB, Rookey K, Schoonbroodt S, Hogan S, et al. Generation of high-affinity human antibodies by combining donor-derived and synthetic complementarity-determining-region diversity. Nat Biotechnol. 2005; 23: 344–8.
18. Vaughan TJ, Williams AJ, Pritchard K, Osbourn JK, Pope AR, Earnshaw JC, et al. Human antibodies with sub-nanomolar affinities isolated from a large non-immunized phage display library. Nat Biotechnol. 1996; 14: 309–14.
19. Chan CE, Chan AH, Lim AP, Hanson BJ. Comparison of the efficiency of antibody selection from semi-synthetic scFv and non-immune Fab phage display libraries against protein targets for rapid development of diagnostic immunoassays. J Immunol Methods. 201; 373 (1–2): 79–88.
20. Li K, Zettlitz KA, Lipianskaya J, Zhou Y, Marks JD, Mallick P, et al. A fully human scFv phage display library for rapid antibody fragment reformatting. Protein Eng Des Sel. 2015; 28 (10): 307–16.
21. Burton DR, Pyati J, Koduri R, Sharp SJ, Thornton GB, Parren PW, et al. Efficient neutralization of primary isolates of HIV-1 by a recombinant human monoclonal antibody. Science. 1994; 266 (5187): 1024–7.
22. Maynard JA, Maassen CB, Leppla SH, Brasky K, Patterson JL, Iverson BL, et al. Protection against anthrax toxin by recombinant antibody fragments correlates with antigen affinity. Nat Biotechnol. 2002; 20 (6): 597–601.
23. Matveev AL, Kozlova IV, Stronin OV, Khlusevich YA, Doroshchenko EK, Baykov IK, et al. Post-exposure administration of chimeric antibody protects mice against European, Siberian, and Far-Eastern subtypes of tick-borne encephalitis virus. PLoS One. 2019; 14 (4): e0215075.
24. Ferrara F, Erasmus MF, D'Angelo S, Leal-Lopes C, Teixeira AA, Choudhary A, et al. A pandemic-enabled comparison of discovery platforms demonstrates a naïve antibody library can match the best immune-sourced antibodies. Nat Commun. 2022; 13 (1): 462.
25. Tillib SV. Perspektivy ispol'zovaniya odnodomennyx antitel v biomedicine. Molekulyarnaya biologiya. 2020; 54 (3): 362–73.
26. Iezzi ME, Policastro L, Werbajh S, Podhajcer O, Canziani GA. Single-domain antibodies and the promise of modular targeting in cancer imaging and treatment. Front Immunol. 2018; 9: 273.
27. Vincke C, Loris R, Saerens D, Martinez-Rodriguez S, Muyldermans S, Conrath K. General strategy to humanize a camelid single-domain antibody and identification of a universal humanized nanobody scaffold. J Biol Chem. 2009; 284 (5): 3273–84.
28. De Genst E, Silence K, Decanniere K, Conrath K, Loris R, Kinne J, et al. Molecular basis for the preferential cleft recognition by dromedary heavy-chain antibodies. Proc Natl Acad Sci U S A. 2006; 103 (12): 4586–91.
29. Muyldermans S. Applications of nanobodies. Annu Rev Anim Biosci. 2021; 9: 401–21.
30. Zavrtanik U, Lukan J, Loris R, Lah J, Hadži S. Structural basis of epitope recognition by heavy-chain camelid antibodies. J Mol Biol. 2018; 430 (21): 4369–86.
31. Schoof M, Faust B, Saunders RA, Sangwan S, Rezelj V, Hoppe N, et al. An ultrapotent synthetic nanobody neutralizes SARS-CoV-2 by stabilizing inactive Spike. Science. 2020; 370 (6523): 1473–9.
32. Van der Linden RH, Frenken LG, de Geus B, Harmsen MM, Ruuls RC, Stok W, et al. Comparison of physical chemical properties of llama VHH antibody fragments and mouse monoclonal antibodies. Biochim Biophys Acta. 1999; 1431 (1): 37–46.

33. Jovčevska I, Muyldermans S. The therapeutic potential of nanobodies. BioDrugs. 2020; 34 (1): 11–26.

34. Muyldermans S. Nanobodies: natural single-domain antibodies. Annu Rev Biochem. 2013; 82: 775–97.

35. Van Roy M, Ververken C, Beirnaert E, Hoefman S, Kolkman J, Vierboom M, et al. The preclinical pharmacology of the high affinity anti-IL-6R Nanobody® ALX-0061 supports its clinical development in rheumatoid arthritis. Arthritis Res Ther. 2015; 17 (1): 135.

36. Ishiwatari-Ogata C, Kyuuma M, Ogata H, Yamakawa M, Iwata K, Ochi M, et al. Ozoralizumab, a humanized anti-TNFα NANOBODY® Compound, exhibits efficacy not only at the onset of arthritis in a human TNF transgenic mouse but also during secondary failure of administration of an anti-TNFα IgG. Front Immunol. 2022; 13: 853008.

37. Van Faassen H, Ryan S, Henry KA, Raphael S, Yang Q, Rossotti MA, et al. Serum albumin-binding VH Hs with variable pH sensitivities enable tailored half-life extension of biologics. FASEB J. 2020; 34 (6): 8155–71.

38. Saerens D, Ghassabeh GH, Muyldermans S. Single-domain antibodies as building blocks for novel therapeutics. Curr Opin Pharmacol. 2008; 8 (5): 600–8.

39. Godakova SA, Noskov AN, Vinogradova ID, Ugriumova GA, Solovyev AI, Esmagambetov IB, et al. Camelid VHHs fused to human Fc fragments provide long term protection against botulinum neurotoxin A in mice. Toxins (Basel). 2019; 11 (8): 464.

40. Günaydın G, Yu S, Gräslund T, Hammarström L, Marcotte H. Fusion of the mouse IgG1 Fc domain to the VHH fragment (ARP1) enhances protection in a mouse model of rotavirus. Sci Rep. 2016; 6: 30171.

41. Detalle L, Stohr T, Palomo C, Piedra PA, Gilbert BE, Mas V, et al. Generation and characterization of ALX-0171, a potent novel therapeutic nanobody for the treatment of respiratory syncytial virus infection. antimicrob agents chemother. 2015; 60 (1): 6–13.

42. Stalin Raj V, Okba NMA, Gutierrez-Alvarez J, Drabek D, van Dieren B, Widagdo W, et al. Chimeric camel/human heavy-chain antibodies protect against MERS-CoV infection. Sci Adv. 2018; 4 (8): eaas9667.

43. Hufton SE, Risley P, Ball CR, Major D, Engelhardt OG, Poole S. The breadth of cross sub-type neutralisation activity of a single domain antibody to influenza hemagglutinin can be increased by antibody valency. PLoS One. 2014; 9 (8): e103294.

44. Ibañez LI, De Filette M, Hultberg A, Verrips T, Temperton N, Weiss RA, et al. Nanobodies with in vitro neutralizing activity protect mice against H5N1 influenza virus infection. J Infect Dis. 2011; 203 (8): 1063–72.

45. Laursen NS, Friesen RHE, Zhu X, Jongeneelen M, Blokland S, Vermond J, et al. Universal protection against influenza infection by a multidomain antibody to influenza hemagglutinin. Science. 2018; 362 (6414): 598–602

46. McMahon C, Baier AS, Pascolutti R, Wegrecki M, Zheng S, Ong JX, et al. Yeast surface display platform for rapid discovery of conformationally selective nanobodies. Nat Struct Mol Biol. 2018; 25 (3): 289–96.

47. Favorskaya IA, Shcheblyakov DV, Esmagambetov IB, Dolzhikova IV, Alekseeva IA, Korobkova AI, et al. Single-Domain Antibodies Efficiently Neutralize SARS-CoV-2 Variants of Concern. Front Immunol. 2022; 13: 822159.

48. Wrapp D, De Vlieger D, Corbett KS, Torres GM, Wang N, Van Breedam W, et al. Structural basis for potent neutralization of betacoronaviruses by single-domain camelid antibodies. Cell. 2020; 181 (5): 1004–15.e15.

49. Chen F, Liu Z, Jiang F. Prospects of Neutralizing Nanobodies Against SARS-CoV-2. Front Immunol. 2021; 12: 690742.

50. Pedrioli, A, Oxenius, A. Single B cell technologies for monoclonal antibody discovery. Trends Immunol. 2021; 42: 1143–58.

51. Lee EC, Liang Q, Ali H, Bayliss L, Beasley A, Bloomfield-Gerdes T, et al. Complete humanization of the mouse immunoglobulin loci enables efficient therapeutic antibody discovery. Nat Biotechnol. 2014; 32 (4): 356–63.

52. Gérard A, Woolfe A, Mottet G, Reichen M, Castrillon C, Menrath V, et al. High-throughput single-cell activity-based screening

53. and sequencing of antibodies using droplet microfluidics. Nat Biotechnol. 2020; 38 (6): 715–21.

53. Scheid JF, Mouquet H, Feldhahn N, Seaman MS, Velinzon K, Pietzsch J, et al. Broad diversity of neutralizing antibodies isolated from memory B cells in HIV-infected individuals. Nature. 2009; 458 (7238): 636–40.

54. McCoy LE, Burton DR. Identification and specificity of broadly neutralizing antibodies against HIV. Immunol Rev. 2017; 275 (1): 11–20.

55. Macagno A, Bernasconi NL, Vanzetta F, Dander E, Sarasini A, Revello MG, et al. Isolation of human monoclonal antibodies that potently neutralize human cytomegalovirus infection by targeting different epitopes on the gH/gL/UL128-131A complex. J Virol. 2010; 84 (2): 1005–13.

56. Wang Q, Michailidis E, Yu Y, Wang Z, Hurley AM, Oren DA, et al. A combination of human broadly neutralizing antibodies against hepatitis B virus HBsAg with distinct epitopes suppresses escape mutations. Cell Host Microbe. 2020; 28 (2): 335–49.e6.

57. Hartley GE, Edwards ESJ, Aui PM, Varese N, Stojanovic S, McMahon J, et al. Rapid generation of durable B cell memory to SARS-CoV-2 spike and nucleocapsid proteins in COVID-19 and convalescence. Sci Immunol. 2020; 5 (54): eabf8891.

58. Hansen J, Baum A, Pascal KE, Russo V, Giordano S, Wloga E, et al. Studies in humanized mice and convalescent humans yield a SARS-CoV-2 antibody cocktail. Science. 2020; 369 (6506): 1010–4.

59. Brouwer PJM, Caniels TG, van der Straten K, Snitselaar JL, Aldon Y, Bangaru S, et al. Potent neutralizing antibodies from COVID-19 patients define multiple targets of vulnerability. Science. 2020; 369 (6504): 643–50.

60. Zost SJ, Gilchuk P, Case JB, Binshtein E, Chen RE, Nkolola JP, et al. Potently neutralizing and protective human antibodies against SARS-CoV-2. Nature. 2020; 584 (7821): 443–9.

61. Tanno H, McDaniel JR, Stevens CA, Voss WN, Li J, Durrett R, et al. A facile technology for the high-throughput sequencing of the paired VH:VL and TCRβ:TCRα repertoires. Sci Adv. 2020; 6 (17): eaay9093.

62. Setliff I, Shiakolas AR, Pilewski KA, Murji AA, Mapengo RE, Janowska K, et al. High-throughput mapping of B cell receptor sequences to antigen specificity. Cell. 2019; 179 (7): 1636–46.e15.

63. Gupta A, Gonzalez-Rojas Y, Juarez E, Crespo Casal M, Moya J, Falci DR, et al. Early treatment for covid-19 with SARS-CoV-2 neutralizing antibody sotrovimab. N Engl J Med. 2021; 385 (21): 1941–50.

64. Loo YM, McTamney PM, Arends RH, Abram ME, Aksyuk AA, Diallo S, et al. The SARS-CoV-2 monoclonal antibody combination, AZD7442, is protective in nonhuman primates and has an extended half-life in humans. Sci Transl Med. 2022; 14 (635): eabl8124.

65. Vishwakarma P, Vattekatte AM, Shinada N, Diharce J, Martins C, Cadet F, et al. VHH structural modelling approaches: a critical review. Int J Mol Sci. 2022; 23 (7): 3721.

66. Senior AW, Evans R, Jumper J, Kirkpatrick J, Sifre L, Green T, et al. Improved protein structure prediction using potentials from deep learning. Nature. 2020; 577: 706–10.

67. Jumper J, Evans R, Pritzel A, Green T, Figurnov M, Ronneberger O, et al. Highly accurate protein structure prediction with AlphaFold. Nature. 2021; 596 (7873): 583–9.

68. Schritt D, Li S, Rozewicki J, Katoh K, Yamashita K, Volkmuth W, et al. Repertoire Builder: high-throughput structural modeling of B and T cell receptors. Mol Sys. Des Eng. 2019; 4: 761–8.

69. Xu Z, Davila A, Wilamowski J, Teraguchi S, Standley DM. Improved antibody-specific epitope prediction using AlphaFold and AbAdapt. Chembiochem. 2022; 23 (18): e202200303.

70. Abanades B, Georges G, Bujotzek A, Deane CM. ABlooper: fast accurate antibody CDR loop structure prediction with accuracy estimation. Bioinformatics. 2022; 38 (7): 1877–80. DOI: 10.1093/bioinformatics/btac016.

71. Ruffolo JA, Sulam J, Gray JJ. Antibody structure prediction using interpretable deep learning. Patterns (NY). 2021; 3 (2): 100406. DOI: 10.1016/j.patter.2021.100406. PMID: 35199061; PMCID: PMC8848015.

72. Cohen T, Halfon M, Schneidman-Duhovny D. NanoNet: Rapid and

accurate end-to-end nanobody modeling by deep learning. Front Immunol. 2022; 13: 958584. DOI: 10.3389/fimmu.2022.958584.

73. Sun D, Sang Z, Kim YJ, Xiang Y, Cohen T, Belford AK, et al. Potent

neutralizing nanobodies resist convergent circulating variants of SARS-CoV-2 by targeting diverse and conserved epitopes. Nat Commun. 2021; 12: 4676.

Литература

1. Köhler G, Milstein C. Continuous cultures of fused cells secreting antibody of predefined specificity. Nature. 1975; 256 (5517): 495–7.

2. Frenzel A, Kügler J, Helmsing S, Meier D, Schirrmann T, Hust M, et al. Designing human antibodies by phage display. Transfus Med Hemother. 2017; 44 (5): 312–8.

3. Emmons C, Hunsicker LG. Muromonab-CD3 (Orthoclone OKT3): the first monoclonal antibody approved for therapeutic use. Iowa Med. 1987; 77 (2): 78–82.

4. Presta LG. Engineering of therapeutic antibodies to minimize immunogenicity and optimize function. Adv Drug Deliv Rev. 2006; 58: 640–56.

5. Smith GP. Filamentous fusion phage: novel expression vectors that display cloned antigens on the virion surface. Science. 1985; 228: 1315–7.

6. McCafferty J, Griffiths AD, Winter G, Chiswell DJ. Phage antibodies: filamentous phage displaying antibody variable domains. Nature. 1990; 348 (6301): 552–4.

7. Ledsgaard L, Ljungars A, Rimbault C, Sørensen CV, Tulika T, Wade J, et al. Advances in antibody phage display technology. Drug Discov. Today. 2022; 27 (8): 2151–69.

8. Gorchakov AA, Kulemzin SV, Guselnikov SV, Baranov KO, Belovezhets TN, Mechetina LV, et al. Isolation of a panel of ultra-potent human antibodies neutralizing SARS-CoV-2 and viral variants of concern. Cell Discov. 2021; 7 (1): 96.

9. Baklaushev VP, Kulemzin SV, Gorchakov AA, Lesnyak VN, Yusubalieva GM, Sotnikova AG. COVID-19. Aetiology, pathogenesis, diagnosis and treatment. Journal of Clinical Practice. 2020; 11 (1): 7–20.

10. Coronavirus disease (COVID-19) pandemic. World Health Organization. 2021. Available from: https://www.who.int/emergencies/diseases/novel-coronavirus-2019.

11. Баклаушев В. П., Юсубалиева Г. М., Бычинин М. В., Юсубалиева С. М., Кальсин В. А., Троицкий А. В. Рациональная стратегия поддержания противовирусного иммунитета к новым вариантам SARS-CoV-2. Клиническая практика. 2022; 13 (3): 43–55.

12. Synowiec A, Szczepański A, Barreto-Duran E, Lie LK, Pyrc K. Severe acute respiratory syndrome coronavirus 2 (SARS-CoV-2): a systemic infection. Clin Microbiol Rev. 2021; 34: e00133–20.

13. Hoogenboom HR. Overview of antibody phage-display technology and its applications. Methods Mol Biol. 2002; 178: 1–37.

14. Hanes J, Plückthun A. In vitro selection and evolution of functional proteins by using ribosome display. Proc Natl Acad Sci U S A. 1997; 94 (10): 4937–42.

15. Boder ET, Wittrup KD. Yeast surface display for screening combinatorial polypeptide libraries. Nat Biotechnol. 1997; 15 (6): 553–7.

16. Beerli RR, Bauer M, Buser RB, Gwerder M, Muntwiler S, Maurer P, et al. Isolation of human monoclonal antibodies by mammalian cell display. Proc Natl Acad Sci U S A. 2008; 105 (38): 14336–41.

17. Hoet RM, Cohen EH, Kent RB, Rookey K, Schoonbroodt S, Hogan S, et al. Generation of high-affinity human antibodies by combining donor-derived and synthetic complementarity-determining-region diversity. Nat Biotechnol. 2005; 23: 344–8.

18. Vaughan TJ, Williams AJ, Pritchard K, Osbourn JK, Pope AR, Earnshaw JC, et al. Human antibodies with sub-nanomolar affinities isolated from a large non-immunized phage display library. Nat Biotechnol. 1996; 14: 309–14.

19. Chan CE, Chan AH, Lim AP, Hanson BJ. Comparison of the efficiency of antibody selection from semi-synthetic scFv and non-immune Fab phage display libraries against protein targets for rapid development of diagnostic immunoassays. J Immunol Methods. 201; 373 (1–2): 79–88.

20. Li K, Zettlitz KA, Lipianskaya J, Zhou Y, Marks JD, Mallick P, et al. A fully human scFv phage display library for rapid antibody

fragment reformatting. Protein Eng Des Sel. 2015; 28 (10): 307–16.

21. Burton DR, Pyati J, Koduri R, Sharp SJ, Thornton GB, Parren PW, et al. Efficient neutralization of primary isolates of HIV-1 by a recombinant human monoclonal antibody. Science. 1994; 266 (5187): 1024–7.

22. Maynard JA, Maassen CB, Leppla SH, Brasky K, Patterson JL, Iverson BL, et al. Protection against anthrax toxin by recombinant antibody fragments correlates with antigen affinity. Nat Biotechnol. 2002; 20 (6): 597–601.

23. Matveev AL, Kozlova IV, Stronin OV, Khlusevich YA, Doroshchenko EK, Baykov IK, et al. Post-exposure administration of chimeric antibody protects mice against European, Siberian, and Far-Eastern subtypes of tick-borne encephalitis virus. PLoS One. 2019; 14 (4): e0215075.

24. Ferrara F, Erasmus MF, D'Angelo S, Leal-Lopes C, Teixeira AA, Choudhary A, et al. A pandemic-enabled comparison of discovery platforms demonstrates a naïve antibody library can match the best immune-sourced antibodies. Nat Commun. 2022; 13 (1): 462.

25. Тиллиб С. В. Перспективы использования однодоменных антител в биомедицине. Молекулярная биология. 2020; 54 (3): 362–73.

26. Iezzi ME, Policastro L, Werbajh S, Podhajcer O, Canziani GA. Single-domain antibodies and the promise of modular targeting in cancer imaging and treatment. Front Immunol. 2018; 9: 273.

27. Vincke C, Loris R, Saerens D, Martinez-Rodriguez S, Muyldermans S, Conrath K. General strategy to humanize a camelid single-domain antibody and identification of a universal humanized nanobody scaffold. J Biol Chem. 2009; 284 (5): 3273–84.

28. De Genst E, Silence K, Decanniere K, Conrath K, Loris R, Kinne J, et al. Molecular basis for the preferential cleft recognition by dromedary heavy-chain antibodies. Proc Natl Acad Sci U S A. 2006; 103 (12): 4586–91.

29. Muyldermans S. Applications of nanobodies. Annu Rev Anim Biosci. 2021; 9: 401–21.

30. Zavrtanik U, Lukan J, Loris R, Lah J, Hadži S. Structural basis of epitope recognition by heavy-chain camelid antibodies. J Mol Biol. 2018; 430 (21): 4369–86.

31. Schoof M, Faust B, Saunders RA, Sangwan S, Rezelj V, Hoppe N, et al. An ultrapotent synthetic nanobody neutralizes SARS-CoV-2 by stabilizing inactive Spike. Science. 2020; 370 (6523): 1473–9.

32. Van der Linden RH, Frenken LG, de Geus B, Harmsen MM, Ruuls RC, Stok W, et al. Comparison of physical chemical properties of llama VHH antibody fragments and mouse monoclonal antibodies. Biochim Biophys Acta. 1999; 1431 (1): 37–46.

33. Jovčevska I, Muyldermans S. The therapeutic potential of nanobodies. BioDrugs. 2020; 34 (1): 11–26.

34. Muyldermans S. Nanobodies: natural single-domain antibodies. Annu Rev Biochem. 2013; 82: 775–97.

35. Van Roy M, Ververken C, Beirnaert E, Hoefman S, Kolkman J, Vierboom M, et al. The preclinical pharmacology of the high affinity anti-IL-6R Nanobody® ALX-0061 supports its clinical development in rheumatoid arthritis. Arthritis Res Ther. 2015; 17 (1): 135.

36. Ishiwatari-Ogata C, Kyuuma M, Ogata H, Yamakawa M, Iwata K, Ochi M, et al. Ozoralizumab, a humanized anti-TNFα NANOBODY® Compound, exhibits efficacy not only at the onset of arthritis in a human TNF transgenic mouse but also during secondary failure of administration of an anti-TNFα IgG. Front Immunol. 2022; 13: 853008.

37. Van Faassen H, Ryan S, Henry KA, Raphael S, Yang Q, Rossotti MA, et al. Serum albumin-binding VHHs with variable pH sensitivities enable tailored half-life extension of biologics. FASEB J. 2020; 34 (6): 8155–71.

38. Saerens D, Ghassabeh GH, Muyldermans S. Single-domain

antibodies as building blocks for novel therapeutics. Curr Opin Pharmacol. 2008; 8 (5): 600–8.

39. Godakova SA, Noskov AN, Vinogradova ID, Ugriumova GA, Solovyev AI, Esmagambetov IB, et al. Camelid VHHs fused to human Fc fragments provide long term protection against botulinum neurotoxin A in mice. Toxins (Basel). 2019; 11 (8): 464.

40. Günaydın G, Yu S, Gräslund T, Hammarström L, Marcotte H. Fusion of the mouse IgG1 Fc domain to the VHH fragment (ARP1) enhances protection in a mouse model of rotavirus. Sci Rep. 2016; 6: 30171.

41. Detalle L, Stohr T, Palomo C, Piedra PA, Gilbert BE, Mas V, et al. Generation and characterization of ALX-0171, a potent novel therapeutic nanobody for the treatment of respiratory syncytial virus infection. antimicrob agents chemother. 2015; 60 (1): 6–13.

42. Stalin Raj V, Okba NMA, Gutierrez-Alvarez J, Drabek D, van Dieren B, Widagdo W, et al. Chimeric camel/human heavy-chain antibodies protect against MERS-CoV infection. Sci Adv. 2018; 4 (8): eaas9667.

43. Hufton SE, Risley P, Ball CR, Major D, Engelhardt OG, Poole S. The breadth of cross sub-type neutralisation activity of a single domain antibody to influenza hemagglutinin can be increased by antibody valency. PLoS One. 2014; 9 (8): e103294.

44. Ibañez LI, De Filette M, Hultberg A, Verrips T, Temperton N, Weiss RA, et al. Nanobodies with in vitro neutralizing activity protect mice against H5N1 influenza virus infection. J Infect Dis. 2011; 203 (8): 1063–72.

45. Laursen NS, Friesen RHE, Zhu X, Jongeneelen M, Blokland S, Vermond J, et al. Universal protection against influenza infection by a multidomain antibody to influenza hemagglutinin. Science. 2018; 362 (6414): 598–602.

46. McMahon C, Baier AS, Pascolutti R, Wegrecki M, Zheng S, Ong JX, et al. Yeast surface display platform for rapid discovery of conformationally selective nanobodies. Nat Struct Mol Biol. 2018; 25 (3): 289–96.

47. Favorskaya IA, Shcheblyakov DV, Esmagambetov IB, Dolzhikova IV, Alekseeva IA, Korobkova AI, et al. Single-Domain Antibodies Efficiently Neutralize SARS-CoV-2 Variants of Concern. Front Immunol. 2022; 13: 822159.

48. Wrapp D, De Vlieger D, Corbett KS, Torres GM, Wang N, Van Breedam W, et al. Structural basis for potent neutralization of betacoronaviruses by single-domain camelid antibodies. Cell. 2020; 181 (5): 1004–15.e15.

49. Chen F, Liu Z, Jiang F. Prospects of Neutralizing Nanobodies Against SARS-CoV-2. Front Immunol. 2021; 12: 690742.

50. Pedrioli, A, Oxenius, A. Single B cell technologies for monoclonal antibody discovery. Trends Immunol. 2021; 42: 1143–58.

51. Lee EC, Liang Q, Ali H, Bayliss L, Beasley A, Bloomfield-Gerdes T, et al. Complete humanization of the mouse immunoglobulin loci enables efficient therapeutic antibody discovery. Nat Biotechnol. 2014; 32 (4): 356–63.

52. Gérard A, Woolfe A, Mottet G, Reichen M, Castrillon C, Menrath V, et al. High-throughput single-cell activity-based screening and sequencing of antibodies using droplet microfluidics. Nat Biotechnol. 2020; 38 (6): 715–21.

53. Scheid JF, Mouquet H, Feldhahn N, Seaman MS, Velinzon K, Pietzsch J, et al. Broad diversity of neutralizing antibodies isolated from memory B cells in HIV-infected individuals. Nature. 2009; 458 (7238): 636–40.

54. McCoy LE, Burton DR. Identification and specificity of broadly neutralizing antibodies against HIV. Immunol Rev. 2017; 275 (1): 11–20.

55. Macagno A, Bernasconi NL, Vanzetta F, Dander E, Sarasini A, Revello MG, et al. Isolation of human monoclonal antibodies that potently neutralize human cytomegalovirus infection by targeting different epitopes on the gH/gL/UL128-131A complex. J Virol.

2010; 84 (2): 1005–13.

56. Wang Q, Michailidis E, Yu Y, Wang Z, Hurley AM, Oren DA, et al. A combination of human broadly neutralizing antibodies against hepatitis B virus HBsAg with distinct epitopes suppresses escape mutations. Cell Host Microbe. 2020; 28 (2): 335–49.e6.

57. Hartley GE, Edwards ESJ, Aui PM, Varese N, Stojanovic S, McMahon J, et al. Rapid generation of durable B cell memory to SARS-CoV-2 spike and nucleocapsid proteins in COVID-19 and convalescence. Sci Immunol. 2020; 5 (54): eabf8891.

58. Hansen J, Baum A, Pascal KE, Russo V, Giordano S, Wloga E, et al. Studies in humanized mice and convalescent humans yield a SARS-CoV-2 antibody cocktail. Science. 2020; 369 (6506): 1010–4.

59. Brouwer PJM, Caniels TG, van der Straten K, Snitselaar JL, Aldon Y, Bangaru S, et al. Potent neutralizing antibodies from COVID-19 patients define multiple targets of vulnerability. Science. 2020; 369 (6504): 643–50.

60. Zost SJ, Gilchuk P, Case JB, Binshtein E, Chen RE, Nkolola JP, et al. Potently neutralizing and protective human antibodies against SARS-CoV-2. Nature. 2020; 584 (7821): 443–9.

61. Tanno H, McDaniel JR, Stevens CA, Voss WN, Li J, Durrett R, et al. A facile technology for the high-throughput sequencing of the paired VH:VL and TCRβ:TCRα repertoires. Sci Adv. 2020; 6 (17): eaay9093.

62. Setliff I, Shiakolas AR, Pilewski KA, Murji AA, Mapengo RE, Janowska K, et al. High-throughput mapping of B cell receptor sequences to antigen specificity. Cell. 2019; 179 (7): 1636–46.e15.

63. Gupta A, Gonzalez-Rojas Y, Juarez E, Crespo Casal M, Moya J, Falci DR, et al. Early treatment for covid-19 with SARS-CoV-2 neutralizing antibody sotrovimab. N Engl J Med. 2021; 385 (21): 1941–50.

64. Loo YM, McTamney PM, Arends RH, Abram ME, Aksyuk AA, Diallo S, et al. The SARS-CoV-2 monoclonal antibody combination, AZD7442, is protective in nonhuman primates and has an extended half-life in humans. Sci Transl Med. 2022; 14 (635): eabl8124.

65. Vishwakarma P, Vattekatte AM, Shinada N, Diharce J, Martins C, Cadet F, et al. VHH structural modelling approaches: a critical review. Int J Mol Sci. 2022; 23 (7): 3721.

66. Senior AW, Evans R, Jumper J, Kirkpatrick J, Sifre L, Green T, et al. Improved protein structure prediction using potentials from deep learning. Nature. 2020; 577: 706–10.

67. Jumper J, Evans R, Pritzel A, Green T, Figurnov M, Ronneberger O, et al. Highly accurate protein structure prediction with AlphaFold. Nature. 2021; 596 (7873): 583–9.

68. Schritt D, Li S, Rozewicki J, Katoh K, Yamashita K, Volkmuth W, et al. Repertoire Builder: high-throughput structural modeling of B and T cell receptors. Mol Sys. Des Eng. 2019; 4: 761–8.

69. Xu Z, Davila A, Wilamowski J, Teraguchi S, Standley DM. Improved antibody-specific epitope prediction using AlphaFold and AbAdapt. Chembiochem. 2022; 23 (18): e202200303.

70. Abanades B, Georges G, Bujotzek A, Deane CM. ABlooper: fast accurate antibody CDR loop structure prediction with accuracy estimation. Bioinformatics. 2022; 38 (7): 1877–80. DOI: 10.1093/bioinformatics/btac016.

71. Ruffolo JA, Sulam J, Gray JJ. Antibody structure prediction using interpretable deep learning. Patterns (NY). 2021; 3 (2): 100406. DOI: 10.1016/j.patter.2021.100406. PMID: 35199061; PMCID: PMC8848015.

72. Cohen T, Halfon M, Schneidman-Duhovny D. NanoNet: Rapid and accurate end-to-end nanobody modeling by deep learning. Front Immunol. 2022; 13: 958584. DOI: 10.3389/fimmu.2022.958584.

73. Sun D, Sang Z, Kim YJ, Xiang Y, Cohen T, Belford AK, et al. Potent neutralizing nanobodies resist convergent circulating variants of SARS-CoV-2 by targeting diverse and conserved epitopes. Nat Commun. 2021; 12: 4676.

IMMUNOCHROMATOGRAPHY-BASED PORTABLE EQUIPMENT FOR INDICATION OF PATHOGENIC MICROORGANISMS AND TOXINS

Yarkov SP ✉, Shilenko IV, Tretyakov SI, Ishkov YN, Styazhkin KK

Federal State Unitary Enterprise "State Scientific Research Institute of Biological Engineering" FMBA of Russia (FSUE "SSRIBE"), Moscow, Russia

This review looks at analytical capabilities and composition of portable equipment based on lateral flow immunoassay for rapid indication of human pathogenic bacteria, viruses and toxins which was developed by the State Research Institute of Biological Instrumentation under the auspices of the Federal Medical and Biological Agency of Russia. The review presents technical characteristics and composition of portable test kits UIHE-1 designed for taking monoanalytical and multi-analytical lateral flow immunoassay on pathogenic microorganisms and toxins in washes from environmental objects surfaces and in culture media; it also describes kits EkB and EkB-01 for analysis of biological aerosol samplers contents. Information is given on the analytical properties of luminescence lateral flow immunoassay kit ULI-1, an on the experimental prototype of fluorimeter-reflectometer "Zondazh". The technical characteristics of indication kits were compared with those of foreign origin, areas for improvement of portable equipment based on lateral flow immunoassay were indicated.

Author contribution: Yarkov SP — idea, development planning, analysis of findings, participation in tests, manuscript preparation; Shilenko IV — creation of multi-analysis lateral flow immunoassays, implementation of tests of EkB sets, analysis of obtained results; Tretyakov SI — creation of lateral flow immunoassays, models and kits, tests, analysis of research results; Ishkov YN — study management, manuscript editing; Stiazhkin KK — management, manuscript editing.

✉ **Correspondence should be addressed:** Sergei P. Yarkov
Volokolamskoye, 75, str. 1, 125424, Moscow, Russia; diasol@dol.ru

ТЕХНИЧЕСКИЕ СРЕДСТВА НА ОСНОВЕ ИММУНОХРОМАТОГРАФИИ ДЛЯ ИНДИКАЦИИ ПАТОГЕННЫХ МИКРООРГАНИЗМОВ И ТОКСИНОВ

С. П. Ярков ✉, И. В. Шиленко, С. И. Третьяков, Ю. Н. Ишков, К. К. Стяжкин

Государственный научно-исследовательский институт биологического приборостроения Федерального медико-биологического агентства, Москва, Россия

В обзоре рассмотрены аналитические возможности и состав технических средств на основе иммунохроматографии для экспрессной индикации патогенных для человека бактерий, вирусов и токсинов, разработанных в Государственном научно-исследовательском институте биологического приборостроения ФМБА России. Рассмотрены технические характеристики и состав серийных укладок УИХЭ-1, предназначенных для осуществления моноаналитного и мультианалитного иммунохроматографического анализа патогенных микроорганизмов и токсинов в смывах с поверхностей объектов окружающей среды, в культуральных средах, комплектов ЭкБ и ЭкБ-01 для анализа содержимого пробоотборников биологического аэрозоля. Приведены сведения об аналитических свойствах укладки для люминесцентного иммунохроматографического анализа УЛИ-1, экспериментальном образце флуориметра-рефлектометра «Зондаж». Проведено сравнение технических характеристик индикационных укладок и комплектов с зарубежными аналогами, указаны направления совершенствования технических средств на основе иммунохроматографии.

Вклад авторов: С. П. Ярков — идея, планирование опытно-конструкторских работ, анализ результатов, участие в испытаниях, подготовка рукописи; И. В. Шиленко — создание мультианалитных иммунохроматографических тестов, осуществление испытаний комплектов ЭкБ, анализ полученных результатов; С. И. Третьяков — создание иммунохроматографических тестов, макетов и укладок, проведение испытаний, анализ результатов исследований; Ю. Н. Ишков — руководство исследованием, редактирование рукописи; К. К. Стяжкин — руководство, редактирование рукописи.

✉ **Для корреспонденции:** Сергей Петрович Ярков
Волоколамское шоссе, д. 75, корпус 1, 125424, г. Москва, Россия; diasol@dol.ru

Immunochemical analysis in which liquid immunochromatography processes are based on specific (immune) interactions between an analyte and specific receptor molecules deposited on a porous thin membrane is called lateral flow immunoassay, or LFIA. The history of the method began in the 1980s with the development of urine chorionic gonadotropin test strips, which allowed the detection of pregnancy outside the laboratory (1). A schematic of a test strip for the sandwich version of the LFIA is shown in Fig. 1.

Typically, an lateral flow immunoassay uses a multi-membrane composite consisting of several membranes of different chemical structure and porosity, fixed to a substrate that provides structural rigidity and housed in a polymeric frame.

The principle of the sandwich version of LFIA has been described many times in the literature [2–4]. A liquid sample, potentially containing analyte antigens, is placed on a substrate for the sample to be applied. Capillary forces move the liquid through the multi-membrane composite. First the colloidal gold nanoparticles (CGN) conjugate with specific antibodies is solubilized. The CGN conjugate is cherry colored and its movement along the membrane can be observed visually. When a detectable antigen is present in the sample, an antigenic immune complex is formed, which starts to move along the analytical membrane with an excess of conjugate with the flow of liquid. The immune complex is then immobilized on the analytical membrane by specific antibodies in the

analytical region (AR), forming a 'sandwich', while unbound conjugate antibodies are immobilized by antibodies located in the control region (CR) of the test strip resulting in two colored lines. In the absence of antigen in the sample, no antigenic immune complex is formed, so a single visible line is formed by the binding of the conjugate antibody and the CR antibody (antispecific to the conjugate antibody) only in the CR.

Depending on the task at hand, additional reagents can be added to the test strip and some membranes can be added, combined or eliminated. However, the general design and principle of analytical interactions during the movement of reagents along the membranes is retained. Simplification of the assay with respect to the Enzime Linked Immunosorbent Assay (ELISA) can be achieved by avoiding additional treatments, washes, signal-enhancing incubations, and visual assessment of the results. Typical LFIA times are 10–25 min, sensitivity for bacterial suspensions is 10^5–10^6 CFU/ml, for viral suspensions 10^4–10^6 PFU/ml; for protein toxins, sensitivity ranges from 1–100 ng/ml, depending on toxin type. Since immunochemical interactions at the membrane are in non-equilibrium mode, LFIA is considered to be inferior to ELISA in sensitivity. At the same time, there are techniques and methods to increase the sensitivity of LFIA to protein antigens to 0.1 ng/ml and to 103 cells/ml, but this requires either additional reagents or instrumental registration and significantly increases assay time.

The focus on the LFIA method has emerged against a backdrop of external global events affecting the interests of the world's major economic powers and global public health. Four waves of interest in LFIA methods can be distinguished, related to the mass use of human pathogenic bacteria, toxins and the emergence of new viral infectious diseases.

1. For the US Army's Operation Desert Storm in January-February 1991 immunofiltration personalized anthrax detection devices were created that were included in military equipment. In the event of use of anthrax spores by the Iraqi army, rapid detection was expected to reduce personnel casualties.

2. Acts of individual bioterrorism, such as mailing envelopes to US government agencies containing anthrax spores in August-October 2001. Several firms in the US have produced LFIA sandwich test strips to detect anthrax spores and other dangerous pathogens (plague, tularemia, brucellosis).

3. The US Iraq War 2003-2011. There has been an expansion in the nomenclature of tests for the detection of pathogens in environmental media.

4. COVID-19 pandemic from late 2020 — up to the present. Rapid LFIA tests have become available to detect the nucleocapsid antigen of SARS-CoV-2 coronavirus and antibodies to it in exposed individuals in nasopharyngeal wipes and serum. Production of immunochromatographic test strips has reached hundreds of millions worldwide.

Biosecurity is extremely important in modern society. Information on the presence of pathogens and toxins in environmental media should preferably be obtained immediately and directly at the sampling site. In addition to the biological threats posed by individual bioterrorism, there are concerns about the presence of biological laboratories working with highly dangerous pathogens, funded by unfriendly states, in CIS countries. The activities of these biolaboratories are not transparent and are not monitored by the local administration.

The application of LFIA in sanitation and hygiene is driven not only by biosafety issues, but also by the need for rapid information on commodities of mass consumption, e.g. the quality of agricultural raw materials entering the plant and finished food products destined for the retail chain [5]. The last decade has seen an increase in the development of modifications to the LFIA that allow for highly sensitive analysis while retaining the key strengths of speed of execution, ease of implementation and interpretation of results [6–8].

The above makes the development and serial production of domestic technical means of rapid indication of pathogenic microorganisms and toxins, suitable both for medical needs and for the control of environmental objects urgent.

Federal State Unitary Enterprise "State Scientific Research Institute of Biological Engineering" FMBA of Russia (FSUE "SSRIBE") is the only agency in the country which is actively involved in development and massive production of portable equipment for indicating pathogens in environmental objects, based on LFIA principle.

This overview is to present the characteristics of domestic LFIA-based means for indication of pathogenic microorganisms and toxins in environmental objects (wipes from surfaces, liquids, contents of biological aerosol samplers) developed by FSUE "SSRIBE" and to compare with similar items of foreign origin.

A kit of lateral flow immunoassay indicator elements UIHE-1

The UIHE-1 kit was developed for the detection of plague, anthrax, tularemia, glanders and botulinum toxin type A in wipes from environmental objects. The kit consists of lateral flow immunoassay indicator elements and surface sampling equipment, brushes, assay buffer container, sterile swab and assay chart, all stowed in a water and dust-proof polymer case. The kit has enough consumables for 10 tests to be carried out for five different types of pathogens. A refill set is available to quickly replace expended indicator elements and assay buffer and other disposable accessories. In the regulatory documents of FMBA of Russia the kit is recommended for use in the practical work of the centers of hygiene and sanitation acting under the auspices of FMBA of Russia. The main technical characteristics of the kit are given in Table 1.
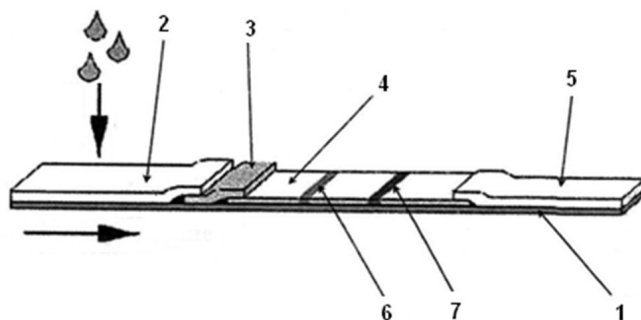
Fig. 1. Schematics of the test strip for the LFIA. 1 — rigid plastic substrate; 2 — substrate for sample application; 3 — conjugate substrate with dried conjugate of colloidal gold nanoparticles (CGN) with specific antibodies; 4 — analytical membrane with applied lines of antibody solutions; 6 — analytical zone; 7 — control zone; 5 — adsorbent substrate. The vertical arrow indicates the application of the liquid sample on the substrate, the horizontal arrow indicates the direction of flow of the test sample

Table 1. Comparative characteristics of domestic and foreign technical tools for the indication of pathogens in environmental media based on lateral flow immunoassays

Features	Domestic kits and sets — EkB, EkB-01 (376.00.00.000;)	UIHE-1 304.00.00.000	UIHE-1 304.00.00.000-01	MID	Pro Strips™	RAID	NIDS	Toxin Screen	IMASS	RAMP**	BADD	KBTB
1	2	3	4	5	6	7	8	9	10	11	12	13
Manufacturer	Federal State Unitary Enterprise "SRIBE", Russia	Federal State Unitary Enterprise "SRIBE", Russia	Federal State Unitary Enterprise "SRIBE", Russia	Federal State Unitary Enterprise "SRIBE", Russia	ADVNT Biotech-nologies, USA	Alexeter Tech-nologies, USA	ANP Tech-nologies, USA	Gen Prime, USA	BBI Detection, U.K.	Responce Biome-dical Corp., Canada	Osborne Scientific, USA	CEA, France
Number of pathogens detected	17	5	10	5	6	3, 5, 2008	3, 5	3	9	5	3	6
Name of pathogens, infectious agents and toxins detected by the technical detection aid	Anthrax, plague, brucellosis, tularemia, glanders/melioidosis, botulinum toxins types A and B, ricin, SEB***, cholera exotoxin, Ebola virus, orthopoxvirus, Lassa virus/Machupo virus, virus and rickettsial growth medium based on chicken embryo	Depending on configuration: Anthrax, plague, brucellosis, tularemia, glanders/ melioidosis, legionellosis, salmonellosis, Bernet's rickettsia, orthopoxviruses, botulinum toxins types A and B, ricin, SEB, cholera exotoxin	Anthrax, plague, brucellosis, tularemia, glanders/ melioidosis, botulinum toxins types A and B, ricin, SEB, cholera exotoxin	MID bacteria: anthrax, plague, brucellosis, tularemia, glanders/ meliodosis. MID toxins: botulinum toxins type A and B, ricin, SEB, cholera exotoxin	Anthrax, plague, botulinum toxins types A and B, ricin, SEB	Depending on configuration: anthrax, plague, brucellosis, tularemia, botulinum toxins, ricin, SEB, smallpox virus	Depending on configuration: anthrax, plague, brucellosis, tularemia, toxins ricin, SEB, cholera exo-toxin, smallpox virus	Botulinum toxins, ricin, SEB	Anthrax, plague, brucellosis, tularemia, glanders/ mel-iodosis, botulinum toxin, ricin, SEB	Anthrax, plague, botulinum toxins, ricin, smallpox virus	Anthrax, plague, botulinum toxins, ricin	Anthrax, plague, tularemia, botulinum toxins, ricin, SEB
Sensitivity threshold: spore forms of bacteria, m.c./ml; vegetative forms of bacteria, m.c./ml; Viruses, PFU/mL; Bacterial and plant toxins, ng/ml	1×10^6 / 1×10^6 / $(1...100) \times 10^5$ / 30–250	1×10^6 / 1×10^6 / 1×10 PFU/mL / 50–1000	1×10^6 / 1×10^6 / Not detectable / 20–500	1×10^6 / 1×10^6 / Not detectable / 20–500	$1,5 \times 10^4$ – $8,3 \times 10^4$ / 1×10^6 / Not detectable 10–500	1×10^6 / $3,6 \times 10^4$ – $1,6 \times 10^6$ / $1,6 \times 10^6$ / 6–30	no data / no data / no data / no data	Not detectable / Not detectable / Not detectable 400	5×10^6–5×10^7 / 1×10^6 – / 1×10^3 Not detectable 10–20	$1,5 \times 10^4$ / no data / 3,8 ng/mL 19–38	1×10^6 / 1×10^5 / Not detectable 10–500	no data / no data / Not detectable / no data
Operating time, min	25	25–30	25–30	25–30	15	15	no data	15	no data	15	15–25	15
Number of samples to be analysed	50/5	10	4	1	1	1	10	3	10	5	5	5
Availability of sampling equipment	Sampling equipment is available											
Availability of sample preparation tools for assay	yes	yes	yes	no	yes	yes	no	yes	no	yes	yes	yes
Operating temperature range, °C	+10...+ 40	+10....+ 35	+10....+ 35		from 4	no data	no data	+20...+ 42	no data	no data	from 4	no data
Shelf life, years	2	2	2	2	2	2	2	1	no data	no data	2	2
Weight, kg	30 /0,405	5,5	2	0,03	no data	no data	4,54	no data	no data	9,08	no data	no data
Dimensions, mm	994 × 600 × 445 / 200 × 128 × 90	490 × 390 × 190	235 × 195 × 108	140 × 140 × 20	no data	no data	no data	no data	no data	no data	no data	no data
Method of recording the results of the analysis	Visual/ Instrumental (mains or internal battery supply)	Visual	Visual	Visual			Instrumental. Battery powered	Visual. Instrumental	Visual	Instrumental. Battery and mains powered	Visual	Visual. Instrumental
Mono/multi-analytical tests	Multi	Mono	Multi	Multi	Multi	Multi	Multi	Multi	Multi	Mono	Mono	Mono

Note: * — the decimal numbers of the design documentation are indicated; ** — lateral flow immunoassays use a fluorescent tag; *** — SEB — Staphylococcal enterotoxin type B; The table contains manufacturers' information on indication equipment such as portable kits and sets to counteract the bioterrorist threat. The list of individual lateral flow immunoassays produced in Russia and abroad for medical purposes for the diagnosis of particularly dangerous and dangerous infectious diseases is more extensive.

Table 2. Comparative characteristics of UIHE-1 kit and other methods of rapid pathogen indication [9]

Concentration mln cl./ml	PCR time (2,0 h)	IHR time (3,5 h)	ELISA time (2,0 h)	UIHE-1 time (15–20 min)
Y. pestis 0,1	+	+	+	+
Y. pestis 0,01	+	–	–	+/–
B. anthracis 1,0	+	+	+	+
B. anthracis 0,1	+	+/–	+	+/–
B. anthracis 0,01	+	–	–	–
Fr. tularensis 0,1	+	+	+	+
Fr. tularensis 0,01	+	–	–	+/–

Note: PCR — polymerase chain reaction; IHR — indirect haemoagglutination reaction; ELISA — enzyme linked immunosorbent assay.

The characteristics of lateral flow immunoassay indicator elements of the kit in terms of sensitivity and speed, in comparison with other lateral flow immunoassay express methods of pathogen indication are given in Table 2. The data were obtained in the course of exercises on detection of microbial cells of vaccine strains of anthrax, plague and tularemia pathogens [9].

As can be seen from comparative tests, the LFIA method and the UIHE-1 lateral flow immunoassay indicator elements have sensitivity comparable to indirect haemagglutination reaction (IHR) and ELISA, and outperform them in terms of speed. The range of lateral flow immunoassay indicator elements that can be optionally supplied with the kit has now been extended to 15 items [10, 11]. As a further effort, a version of UIHE-1 kit was created which is complete with multi-analyte lateral flow immunoassay indicator devices (MID) designed for the detection of bacteria and toxins [12]. The test strips in the MID are arranged in separable polymeric rims of 5 pieces each, whereby the selected liquid sample has to be introduced into the sample application hole and distributed evenly over all test strips. The top cover of the polymeric MID rim has rectangular slots for visual recording of assay results and appropriate labeling. The use of the MID has made the kit more compact and increased the nomenclature of bacteria (five names) and toxins (five names) detected in a single assay cycle. The causative agents of glanders and melioidosis have no species distinction in LFIA, due to the close antigenic structure of the Burkholderia genus. Both versions of UIHE-1 kit have high resistance to mechanical and climatic factors and are used in mobile biolaboratories. The plastic kit cases are resistant to disinfectants. The small dimensions and weights of 5.5 kg and 2.0 kg make them also suitable for use as a portable specific indication.

Express Kit-Bio

The Express Kit Bio (EkB) is designed for:
– sampling and preparing samples of the contents of biological aerosol samplers, culture media after the biological enrichment stage, wipes from environmental objects;
– detection of viruses (orthopoxviruses, Lassa and Machupo haemorrhagic fevers, Dengue fever, West Nile fever, virus accumulation medium and rickettsia (antigens of growing chicken embryos), vegetative and spore forms of bacteria (plague pathogens, glanders and melioidosis, brucellosis, anthrax spores, tularemia), bacterial and plant toxins (botulinum toxin type A (BTA), botulinum toxin type B (BTB), staphylococcal enterotoxin type B (SEB), cholera exotoxin, ricin;
– recording the results of the LFIA and transmitting the results to authorities.

The kit is designed for sampling, preparation and carrying out assays of 50 samples and is operated between +10 °C and +40°C [13]. It consists of a kit of accessories for the preparation of selected samples for carrying out assays, which includes a device for elution of the sample from solid sorbent media of aerosol samplers; a set of multi-analyte lateral flow immunoassays (MLFIA). The indication capability of the kit is provided by three types of MLFIA: Bacterial MLFIA, Virus and Accumulation Medium MLFIA and Toxin MLFIA (Fig. 2).

The detection and indication of glanders and melioidosis pathogens is indistinguishable from the bacterial species.
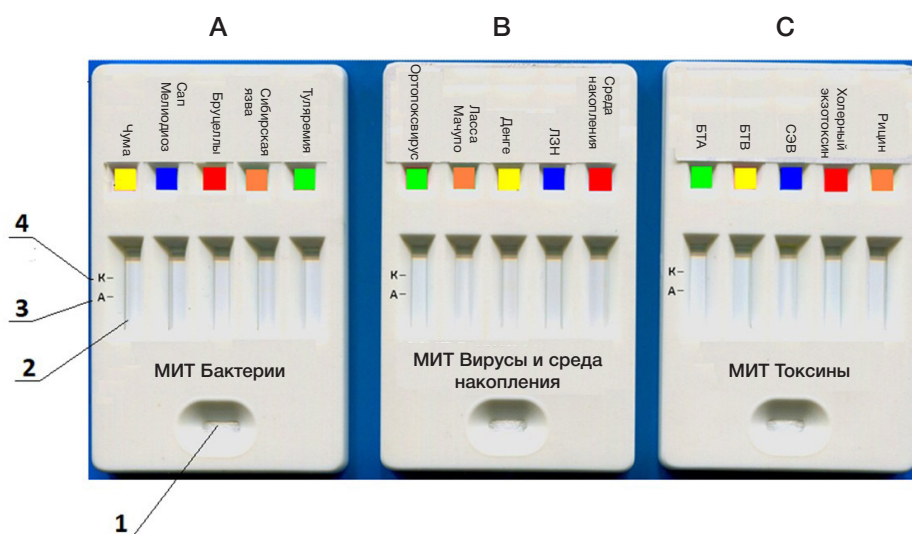
Fig. 2. Appearance of the multi-analyte lateral flow immunoassays included in the EkB and EkB-01 kits. **A**. Bacteria for multi-analyte lateral flow immunoassays. **B**. Viruses and accumulation media for multi-analyte lateral flow immunoassays. **C**. Toxins for multi-analyte lateral flow immunoassays 1 — sample put-in opening; 2 — opening for recording the test finding; 3 — analytical area; 4 — control area

In the case of orthopoxviruses, Lassa fever and Machupo fever viruses, detection and indication by LFIA is also without species distinction. This is due to a lack of antibodies capable of differentiating the antigens of these pathogens at the species level. The kit is equipped with a reflectometric device (Fig. 3) whose software allows automatic recognition of positive analysis results, setting of intensity thresholds for coloring MLFIA zones, archiving of assay data and transmission by email to higher authorities for decision-making.

The computer used in the reflectometer device is highly resistant to mechanical stress and moisture. The EkB kit is fully autonomous, has its own power supply for the reflectometer and can be deployed both in the laboratory and in the field. The kit is housed in four impact-resistant, waterproof polymer cases and contains all the necessary accessories for carrying out an assay of the contents of the aerosol sampler when sampling into liquids, filters or dense sorbent media. The kit is also equipped with a transport container, allowing it to be transported by all means of air and ground transport.

Portable version of the kit "Express-kit-Bio"

A portable version of the "Express-Kit-Bio " (EkB-01), (Fig. 4) allows it to be used as a means of individual control of the biological situation. The EkB-01 kit is designed to analyze five samples for 17 types of pathogens. The device is designed for LFIA of prepared samples of the contents of aerosol samplers, immunochemical verification of microbial colonies after sample enrichment on culture media, making wipes from the surfaces of environmental objects and their analysis.

The portable version of the kit uses the same MLFIA as for the EkB, the kit casing is dustproof, made of carbon composite material, the total weight of the kit is 0.405 kg.

Development of indication tools based on luminescent tags in lateral flow immunoassay

Luminescent tag molecules have also been successfully used in LFIA, along with NCG. For example, Response

Fig. 3. Exterior view of the reflectometer device of EkB kit

Biomedical Corp. (Canada) created the RAMP analyzer for lateral flow immunoassay detection of pathogenic bacteria, orthopoxviruses, and toxins. Technical specifications are presented in Table 1.

The Federal State Unitary Enterprise "SSRIBE" under FMBA of Russia developed and tested a prototype of luminescent lateral flow immunoassay kit ULI-1 containing luminescent lateral flow immunoassay indicator elements based on latex sub-micron particles functionalized with carboxyl groups. Obtaining conjugates of antibodies with latex particles was performed by covalent binding. The ULI-1 kit also contains a battery-operated LED visualizing device that allows the operator to observe the luminescence of the analytical and test zones of the lateral flow immunoassay indicator element and perform visual registration of the assay results [14]. There is an advantage in terms of detection sensitivity when using

Fig. 4. Exterior view of the EkB-01 kit. **A**. Kit with open cover. **B**. Attachment of the kit to the operator's uniform

fluorescent tags, compared with NCG -based lateral flow immunoassays, and namely: for the spore form of the anthrax pathogen it is twice as much, for the vegetative forms of the plague pathogen it is twice as much, for the F1 antigen of the plague microbe it is five times higher, and for various types of botulinum toxin it is two to four times higher.

For the purpose of recording LFIA results, an experimental prototype reflectometer-fluorometer "Zondazh" was also developed to record the intensity of light reflection from an analytical or control zone of an lateral flow immunoassay in four spectral ranges of visible light: white (400–800 nm), red (650 nm), green (525 nm) and blue (470 nm). The spectral range of the instrument makes it possible to record reflectograms not only of CGN conjugates but also of colored latex particles of different colors, often used as a dispersed phase in the LFIA. In the luminescence intensity measurement mode the "Zondazh" instrument allows the recording of luminescent immunochromatograms. It provides a luminescence excitation wavelength of 380 nm and emission wavelength of 490 nm. The device operates based on the reflectometry of digital images of immunochromatograms, or the recording of luminescence intensity in the case of luminescence tests. Emitting LEDs are used as light sources. A solid-state video camera serves as an image receptor. The device is electrically powered (220V/50Hz) and weighs 1.30 kg. The software allows not only setting of recording parameters but also integral peak intensities of immunochromatograms and quantitative comparison of different samples. The LFIA logs are stored in memory and can be transmitted by email.

Directions for improving LFIA for pathogen indication

Ways to improve LFIA are to increase sensitivity, specificity and speed of the method. A review of the literature suggests that a pre-analytical sample concentration procedure, the selection of high affinity receptor molecules, the use of colloidal tags with a low detection threshold, instrumentation and methods for recording these tags are promising for this purpose. The use of magnetosorbents to concentrate bacteria and viruses is effective in the pre-analytical phase [15, 16]. In order to select the most efficient receptor molecules, it should be taken into account that immune reactions in LFIA are carried out in a kinetic mode. Therefore, it does not matter whether the detected complexes dissociate within hours or days. Their number is determined primarily by the kinetic association constants, which are similar in magnitude and vary within a limited range for receptors and antigens with the same structure. Additionally, the affinity can be increased by genetic modification (targeted design) of the antibody active centre. The use of these methods is still very limited, despite the confirmation of their efficacy [17].

With the development of molecular biology techniques, the production of modified traditional receptors (antibodies) and new receptors — aptamers [18–20], single domain antibodies [21] are becoming available. Targeted immobilization of antibodies on the dispersed phase via receptor staphylococcal protein A and streptococcal protein G, avidin-biotin interactions [22–25], occurs without loss of antibody affinity, as often occurs with physical adsorption on the dispersed phase, indicating the utility of this approach.

In the search for optimal markers, attention should be paid to the use of new optical markers based on highly branched colloidal gold [26, 27], colloidal carbon [28–30], graphene oxide and carboxylated graphene oxide [31]. The limitation to the registration of only surface label molecules existing in LFIA is of no relevance to analytical methods in which label registration is based on other physical principles. A temperature contrast amplifier reader has been developed for the registration of gold nanoparticles on immunochromatographic membranes [32]. This reader reduces the detection limit by a factor of eight for influenza virus LFIA, also for malaria, Clostridium difficile LFIA, compared to an optical reader.

The magnetic properties of the nanodispersed tag are also used to record the LFIA signal [33–35]. In recent studies, a commercially available glucometer with electrochemical detection has been proposed as a recorder of LFIA results [36].

Future test systems should be expected to be integrated with recording systems (reflectometers, fluorometers) as well as tools for collecting, storing and processing information to record and record results. The literature summarizes trends in the transformation of LFIA from a visual to an instrumental method [37] and presents the current state of the art in mobile/ smartphone based analytical technologies [38, 39].

CONCLUSION

Data from the literature and the authors' own studies show that LFIA is widely used for the identification of human pathogenic bacteria, viruses and toxins.

A comparison of the technical characteristics of the developed sets and kits for pathogen indication with similar foreign samples (Table 1) showed that our work followed the global trend of the method development: from the creation of mono-type individual lateral flow immunoassays to multiplex analysis, the search for the most sensitive methods of registration, and the expansion of the range of pathogens detected [40]. Kits EkB and EkB-01 are better than foreign analogues as they have a wider range of detected pathogens, automation of registration of results of the analysis (EkB) at comparable, or better threshold of sensitivity. The indicated means of pathogen indication are in demand in practice of centers of hygiene and epidemiology, specialized laboratories of other departments, providing biological safety.

The ways of improvement discussed in this review suggest that immunochromatographic analytical systems will be able to detect pathogens of bacterial, viral- rickettsial and toxin nature more effectively. At the same time, the specificity of the analysis will increase to the strain level, in the case of bacterial pathogens, making it possible to carry out a process of specific indication of pathogens and toxins on a new technological basis.

References

1. Leavitt SA. A Thin Blue Line: The History of the Pregnancy Test Kits. 2003 (cited 2022, Nov. 14); Available from: https:// www. history.nih.gov/exhibits /thinblueline/ introduction.html.
2. de Puig H, Bosch I, Gehrke L, Hamad-Schifferli K. Challenges of the nano-bio interface in lateral flow and dipstick immunoassays. Trends in Biotechnology. 2017; 35 (12):1169–80.
3. Li J, Macdonald J. Multiplexed lateral flow biosensors: Technological advances for radically improving point-of-care diagnoses. Biosensors and Bioelectronics. 2016; 83: 177–92.
4. Posthuma-Trumpie GA, Korf J, van Amerongen A. Lateral flow

(immuno) assay: Its strengths, weaknesses, opportunities and threats. A literature survey. Analytical and Bioanalytical Chemistry. 2009; 393 (2): 569–82.

5. Dzantiev BB, Byzova NA, Urusov AE, Zherdev AV. Immunochromatographic methods in food analysis. TrAC Trends in Analytical Chemistry. 2014; 55: 81–93.

6. Bahadır EB, Sezgintürk MK. Lateral flow assays: Principles, designs and labels. TrAC Trends in Analytical Chemistry. 2016; 82: 286–306.

7. Quesada-González D, Merkoçi A. Nanoparticle-based lateral flow biosensors. Biosensors and Bioelectronics. 2015; 73: 47–63.

8. Zherdev AV, Dzantiev BB. Ways to Reach Lower Detection Limits of Lateral Flow Immunoassays. Rapid Test - Advances in Design, Format and Diagnostic Applications, 2018. DOI: 10.5772/intechopen.76926.

9. Karimova TV, Pryadkina EN, Yakunina OYu, Ivanova LK, Duben LG, Kuzubov VI, i dr. Ispol'zovanie immunoxromatograficheskogo analiza dlya indikacii patogennyx biologicheskix agentov. V sbornike: Materialy IX Mezhgosudarstvennoj nauchno-prakticheskoj konferencii «Sovremennye texnologii v realizacii global'noj strategii bor'by s infekcionnymi boleznyami na territorii gosudarstv-uchastnikov Sodruzhestva Nezavisimyx Gosudarstv»; 2 oktyabrya 2008 g. Rossijskaya Federaciya, g. Volgograd. 87–88. Russian.

10. Yarkov SP, Basharova LA, Tret'yakov SI, Zlobin VN. Sozdanie indikatornyx immunoxromatograficheskix ehlementov dlya vyyavleniya rikketsij Berneta. Problemy osobo opasnyx infekcij. 2013; 4: 79–81. Russian.

11. Shilenko IV, Yarkov SP, Artemov AV, Smirnov AM, Kononenko AB. Otechestvennyj immunoxromatograficheskij test dlya vyyavleniya sal'monell razlichnyx serogrupp. Veterinariya i kormlenie. 2011; 4: 12–13. Russian.

12. Yarkov SP, Shilenko IV, Titov AA, Brovkina AN, Tret'yakov SI, Xramov EN. Razrabotka mul'tianalitnogo immunoxromatograficheskogo testa dlya indikacii toksinov. Problemy osobo opasnyx infekcij. 2015; 4: 103–08. Russian.

13. Yarkov SP, Shilenko IV, Tretyakov SI, Naumov PV. Nosimyj komplekt biologicheskogo kontrolya dlya specificheskoj indikacii biologicheskix porazhayushhix agentov v ob"ektax okruzhayushhej sredy EhkB-01. V cbornike: II Vserossijskaya nauchno-prakticheskaya konferenciya «Issledovanie voprosov radiacionnoj, ximicheskoj i biologicheskoj zashhity v mirnoe i voennoe vremya». 14–15 sentyabrya 2021 g. Kostroma; s. 301–306. Russian.

14. Shilenko IV, Yarkov SP, Zlobin VN. Nosimyj komplekt dlya vyyavleniya vozbuditelej osobo opasnyx infekcij na principe lyuminescentnoj immunoxromatografii. Zhurnal infekcionnoj patologii. 2009; 16 (3): 222–23. Russian.

15. Li Q, Zhang S, Cai Y, Yang Y, Hu F, Liu X, et al. Rapid detection of Listeria monocytogenes using fluorescence immunochromatographic assay combined with immunomagnetic separation technique. International Journal of Food Science & Technology. 2017; 52 (7): 1559–66.

16. Razo SC, Panferov VG, Safenkova IV, Varitsev YA, Zherdev AV, Dzantiev BB. Double enhanced lateral flow immunoassay for potato virus X based on a combination of magnetic and gold nanoparticles. Analytica Chimica Acta. 2018; 1007: 50–60.

17. Kim H-Y, Stojadinovic A, Izadjoo MJ. Affinity maturation of monoclonal antibodies by multi-site-directed mutagenesis. In: Monoclonal Antibodies. Totowa, NJ, USA: Springer, Humana Press, 2014; p. 407–20. Available from: https://link.springer.com/book/10.1007%2F978-1-62703-992-5#about.

18. Dias AM, Roque AC. The future of protein scaffolds as affinity reagents for purification. Biotechnology and Bioengineering. 2017; 114 (3): 481–91.

19. Jauset-Rubio M, El-Shahawi MS, Bashammakh AS, Alyoubi AO. Advances in aptamers-based lateral flow assays. TrAC Trends in Analytical Chemistry. 2017; 97: 385–98.

20. Chen A, Yang S. Replacing antibodies with aptamers in lateral flow immunoassay. Biosensors and Bioelectronics. 2015; 71: 230–42.

21. Leow CH, Fischer K, Leow CY, Cheng Q, Chuah C, McCarthy J. Sigle domain antibodies as new biomarker detectors. Diagnostics. 2017; 7 (4): 52.

22. Welch NG, Scoble JA, Muir BW, Pigram PJ. Orientation and characterization of immobilized antibodies for improved immunoassays. Biointerphases. 2017; 12 (2): 02D301.

23. Shen M, Rusling JF, Dixit CK. Site-selective orientated immobilization of antibodies and conjugates for immunodiagnostics development. Methods. 2017; 116: 95–111.

24. Iijima M, Si K. Scaffolds for oriented and close-packed immobilization of immunoglobulins. Biosensors and Bioelectronics. 2017; 89: 810–21.

25. Kruljec N, Bratkovič T. Alternative affinity ligands for immunoglobulins. Bioconjugate Chemistry. 2017; 28 (8): 2009–30.

26. Serebrennikova KV, Samsonova JV, Osipov AP, Senapati D, Kuznetsov DV. Gold nanoflowers and gold nanospheres as labels in lateral flow immunoassay of procalcitonin. Nano Hybrids and Composites. 2017; 13: 47–53.

27. Xu P, Li J, Huang X, Duan H, Ji Y, Xiong Y. Effect of the tip length of multi-branched AuNFs on the detection performance of immunochromatographic assays. Analytical Methods. 2016; 8 (16): 3316–24.

28. van Amerongen A, Besselink G, Blazkova M, Posthuma-Trumpie GA, Koets M, Beelen- Thomissen M. Chapter 19: Carbon nanoparticles as detection label for diagnostic antibody microarrays. In: Abuelzein E, Editor. Trends in Immunolabelled and Related Techniques. Rijeka, Croatia: InTech, 2012; p. 311–330.

29. Suárez-Pantaleón C, Wichers J, Abad-Somovilla A, van Amerongen A, Abad-Fuentes A. Development of an immunochromatographic assay based on carbon nanoparticles for the determination of the phytoregulator forchlorfenuron. Biosensors and Bioelectronics. 2013; 42: 170–6.

30. Liu B, Wang L, Tong B, Zhang Y, Sheng W, Pan M, et al. Development and comparison of immunochromatographic strips with three nanomaterial labels: Colloidal gold, nanogold-polyaniline-nanogold microspheres (GPGs) and colloidal carbon for visual detection of salbutamol. Biosensors and Bioelectronics. 2016; 85: 337–42.

31. Yu L, Li P, Ding X, Zhang Q. Graphene oxide and carboxylated graphene oxide: Viable two-dimensional nanolabels for lateral flow immunoassays. Talanta. 2017; 165: 167–75.

32. Wang Y, Qin Z, Boulware DR, Pritt BS, Sloan LM, González IJ, et al. Thermal contrast amplification reader yielding 8-fold analytical improvement for disease detection with lateral flow assays. Analytical Chemistry. 2016; 88 (23): 11774–82.

33. Barnett JM, Wraith P, Kiely J, Persad R, Hurley K, Hawkins P, et al. An inexpensive, fast and sensitive quantitative lateral flow magneto-immunoassay for total prostate specific antigen. Biosensors. 2014; 4 (3): 204–20.

34. Chen Y, Wang K, Liu Z, Sun R, Cui D, He J. Rapid detection and quantification of tumor marker carbohydrate antigen 72–4 (CA72–4) using a superparamagnetic immunochromatographic strip. Analytical and Bioanalytical Chemistry. 2016; 408 (9): 2319–27.

35. Lago-Cachón D, Oliveira-Rodríguez M, Rivas M, Blanco-López MC, Martínez-García JC, Moyano A, et al. Scanning magneto-inductive sensor for quantitative assay of prostate- specific antigen. IEEE Magnetics Letters. 2017; 8: 1–5.

36. Zhao Y, Chen X, Lin S, Du D, Lin Y. Integrated immunochromatographic strip with glucometer readout for rapid quantification of phosphorylated proteins. Analytica Chimica Acta. 2017; 964: 1–6.

37. Mak WC, Beni V, Turner AP. Lateral-flow technology: From visual to instrumental. TrAC Trends in Analytical Chemistry. 2016; 79: 297–305.

38. Quesada-González D, Merkoçi A. Mobile phone-based biosensing: An emerging "diagnostic and communication" technology. Biosensors and Bioelectronics. 2017; 92: 549–62.

39. Zarei M. Portable biosensing devices for point-of-care diagnostics: Recent developments and applications. TrAC Trends in Analytical Chemistry. 2017; 91: 26–41.

40. Yarkov SP, Tretyakov SI, Shilenko IV, Titov AA, Basharova LA, Khramov EN. Experience of pathogens identification tools development in the environment using immunochromatography. The 13th CBRNe Protection Symposium. Science for Safety&Security. September 24th–26th Malmö, Sweden, 2019; p. 118.

Литература

1. Leavitt SA. A Thin Blue Line: The History of the Pregnancy Test Kits. 2003 (cited 2022, Nov. 14); Available from: https:// www. history.nih.gov/exhibits /thinblueline/ introduction.html.

2. de Puig H, Bosch I, Gehrke L, Hamad-Schifferli K. Challenges of the nano-bio interface in lateral flow and dipstick immunoassays. Trends in Biotechnology. 2017; 35 (12):1169–80.

3. Li J, Macdonald J. Multiplexed lateral flow biosensors: Technological advances for radically improving point-of-care diagnoses. Biosensors and Bioelectronics. 2016; 83: 177–92.

4. Posthuma-Trumpie GA, Korf J, van Amerongen A. Lateral flow (immuno) assay: Its strengths, weaknesses, opportunities and threats. A literature survey. Analytical and Bioanalytical Chemistry. 2009; 393 (2): 569–82.

5. Dzantiev BB, Byzova NA, Urusov AE, Zherdev AV. Immunochromatographic methods in food analysis. TrAC Trends in Analytical Chemistry. 2014; 55: 81–93.

6. Bahadır EB, Sezgintürk MK. Lateral flow assays: Principles, designs and labels. TrAC Trends in Analytical Chemistry. 2016; 82: 286–306.

7. Quesada-González D, Merkoçi A. Nanoparticle-based lateral flow biosensors. Biosensors and Bioelectronics. 2015; 73: 47–63.

8. Zherdev AV, Dzantiev BB. Ways to Reach Lower Detection Limits of Lateral Flow Immunoassays. Rapid Test - Advances in Design, Format and Diagnostic Applications, 2018. DOI: 10.5772/ intechopen.76926.

9. Каримова Т. В., Прядкина Е. Н., Якунина О. Ю., Иванова Л. К., Дубень Л. Г., Кузубов В. И., и др. Использование иммунохроматографического анализа для индикации патогенных биологических агентов. В сборнике: Материалы IX Межгосударственной научно-практической конференции «Современные технологии в реализации глобальной стратегии борьбы с инфекционными болезнями на территории государств-участников Содружества Независимых Государств»; 2 октября 2008 г. Российская Федерация, г. Волгоград. 87–88.

10. Ярков С. П., Башарова Л. А., Третьяков С. И., Злобин В. Н. Создание индикаторных иммунохроматографических элементов для выявления риккетсий Бернета. Проблемы особо опасных инфекций. 2013; 4: 79–81.

11. Шиленко И. В., Ярков С. П., Артемов А. В., Смирнов А. М., Кононенко А. Б. Отечественный иммунохроматографический тест для выявления сальмонелл различных серогрупп. Ветеринария и кормление. 2011; 4: 12–13.

12. Ярков С. П., Шиленко И. В., Титов А. А., Бровкина А. Н., Третьяков С. И., Храмов Е. Н. Разработка мультианалитного иммунохроматографического теста для индикации токсинов. Проблемы особо опасных инфекций. 2015; 4: 103–08.

13. Ярков С. П., Шиленко И. В., Третьяков С. И., Наумов П. В. Носимый комплект биологического контроля для специфической индикации биологических поражающих агентов в объектах окружающей среды ЭкБ-01. В сборнике: II Всероссийская научно-практическая конференция «Исследование вопросов радиационной, химической и биологической защиты в мирное и военное время». 14–15 сентября 2021 г. Кострома; с. 301–306.

14. Шиленко И. В., Ярков С. П., Злобин В. Н. Носимый комплект для выявления возбудителей особо опасных инфекций на принципе люминесцентной иммунохроматографии. Журнал инфекционной патологии. 2009; 16 (3): 222–23.

15. Li Q, Zhang S, Cai Y, Yang Y, Hu F, Liu X, et al. Rapid detection of Listeria monocytogenes using fluorescence immunochromatographic assay combined with immunomagnetic separation technique. International Journal of Food Science & Technology. 2017; 52 (7): 1559–66.

16. Razo SC, Panferov VG, Safenkova IV, Varitsev YA, Zherdev AV, Dzantiev BB. Double enhanced lateral flow immunoassay for potato virus X based on a combination of magnetic and gold nanoparticles. Analytica Chimica Acta. 2018; 1007: 50–60.

17. Kim H-Y, Stojadinovic A, Izadjoo MJ. Affinity maturation of monoclonal antibodies by multi-site-directed mutagenesis. In: Monoclonal Antibodies. Totowa, NJ, USA: Springer, Humana Press, 2014; p. 407–20. Available from: https://link.springer.com/ book/10.1007%2F978-1-62703-992-5#about.

18. Dias AM, Roque AC. The future of protein scaffolds as affinity reagents for purification. Biotechnology and Bioengineering. 2017; 114 (3): 481–91.

19. Jauset-Rubio M, El-Shahawi MS, Bashammakh AS, Alyoubi AO. Advances in aptamersbased lateral flow assays. TrAC Trends in Analytical Chemistry. 2017; 97: 385–98.

20. Chen A, Yang S. Replacing antibodies with aptamers in lateral flow immunoassay. Biosensors and Bioelectronics. 2015; 71: 230–42.

21. Leow CH, Fischer K, Leow CY, Cheng Q, Chuah C, McCarthy J. Sigle domain antibodies as new biomarker detectors. Diagnostics. 2017; 7 (4): 52.

22. Welch NG, Scoble JA, Muir BW, Pigram PJ. Orientation and characterization of immobilized antibodies for improved immunoassays. Biointerphases. 2017; 12 (2): 02D301.

23. Shen M, Rusling JF, Dixit CK. Site-selective orientated immobilization of antibodies and conjugates for immunodiagnostics development. Methods. 2017; 116: 95–111.

24. Iijima M, Si K. Scaffolds for oriented and close-packed immobilization of immunoglobulins. Biosensors and Bioelectronics. 2017; 89: 810–21.

25. Kruljec N, Bratkovič T. Alternative affinity ligands for immunoglobulins. Bioconjugate Chemistry. 2017; 28 (8): 2009–30.

26. Serebrennikova KV, Samsonova JV, Osipov AP, Senapati D, Kuznetsov DV. Gold nanoflowers and gold nanospheres as labels in lateral flow immunoassay of procalcitonin. Nano Hybrids and Composites. 2017; 13: 47–53.

27. Xu P, Li J, Huang X, Duan H, Ji Y, Xiong Y. Effect of the tip length of multi-branched AuNFs on the detection performance of immunochromatographic assays. Analytical Methods. 2016; 8 (16): 3316–24.

28. van Amerongen A, Besselink G, Blazkova M, Posthuma-Trumpie GA, Koets M, Beelen- Thomissen M. Chapter 19: Carbon nanoparticles as detection label for diagnostic antibody microarrays. In: Abuelzein E, Editor. Trends in Immunolabelled and Related Techniques. Rijeka, Croatia: InTech, 2012; p. 311–330.

29. Suárez-Pantaleón C, Wichers J, Abad-Somovilla A, van Amerongen A, Abad-Fuentes A. Development of an immunochromatographic assay based on carbon nanoparticles for the determination of the phytoregulator forchlorfenuron. Biosensors and Bioelectronics. 2013; 42: 170–6.

30. Liu B, Wang L, Tong B, Zhang Y, Sheng W, Pan M, et al. Development and comparison of immunochromatographic strips with three nanomaterial labels: Colloidal gold, nanogold-polyaniline-nanogold microspheres (GPGs) and colloidal carbon for visual detection of salbutamol. Biosensors and Bioelectronics. 2016; 85: 337–42.

31. Yu L, Li P, Ding X, Zhang Q. Graphene oxide and carboxylated graphene oxide: Viable two-dimensional nanolabels for lateral flow immunoassays. Talanta. 2017; 165: 167–75.

32. Wang Y, Qin Z, Boulware DR, Pritt BS, Sloan LM, González IJ, et al. Thermal contrast amplification reader yielding 8-fold analytical improvement for disease detection with lateral flow assays. Analytical Chemistry. 2016; 88 (23): 11774–82.

33. Barnett JM, Wraith P, Kiely J, Persad R, Hurley K, Hawkins P, et al. An inexpensive, fast and sensitive quantitative lateral flow magneto-immunoassay for total prostate specific antigen. Biosensors. 2014; 4 (3): 204–20.

34. Chen Y, Wang K, Liu Z, Sun R, Cui D, He J. Rapid detection and quantification of tumor marker carbohydrate antigen 72–4 (CA72–4) using a superparamagnetic immunochromatographic strip. Analytical and Bioanalytical Chemistry. 2016; 408 (9): 2319–27.

35. Lago-Cachón D, Oliveira-Rodríguez M, Rivas M, Blanco-López MC, Martínez-García JC, Moyano A, et al. Scanning magneto-inductive sensor for quantitative assay of prostate- specific antigen. IEEE Magnetics Letters. 2017; 8: 1–5.

36. Zhao Y, Chen X, Lin S, Du D, Lin Y. Integrated immunochromatographic strip with glucometer readout for rapid quantification of phosphorylated proteins. Analytica Chimica Acta. 2017; 964: 1–6.

37. Mak WC, Beni V, Turner AP. Lateral-flow technology: From visual to instrumental. TrAC Trends in Analytical Chemistry. 2016; 79: 297–305.

38. Quesada-González D, Merkoçi A. Mobile phone-based biosensing: An emerging "diagnostic and communication" technology. Biosensors and Bioelectronics. 2017; 92: 549–62.

39. Zarei M. Portable biosensing devices for point-of-care diagnostics: Recent developments and applications. TrAC Trends in Analytical Chemistry. 2017; 91: 26–41.

40. Yarkov SP, Tretyakov SI, Shilenko IV, Titov AA, Basharova LA, Khramov EN. Experience of pathogens identification tools development in the environment using immunochromatography. The 13th CBRNe Protection Symposium. Science for Safety&Security. September 24th–26th Malmö, Sweden, 2019; p. 118.

REGULATORY T CELLS AND T HELPER 17 CELLS EXPRESSING CD39 AND CD73 ECTONUCLEOTIDASE IN CHILDREN WITH SEVERE INJURY

Zakirov RSh[1,2] ✉, Kuptsova DG[1], Freidlin EV[1], Semikina EL[1], Petrichuk SV[1], Karaseva OV[1,2]

[1] National Medical Research Center for Children's Health, Moscow, Russia

[2] Institute of Urgent Children Surgery and Traumatology, Moscow, Russia

Frequent resulting disability and case mortality support the urgency of investigation of the immune response mechanisms triggered by severe injury (SI) in children. This study aimed to determine the informative immunological criteria of traumatic injury severity and prognosis in children ($n = 43$) based on the assessment of expression of CD39 and CD73 ectonucleotidase in populations of regulatory T cells (Treg, CD4+CD127^{low}CD25^{high}) and T-helper 17 cells (Th17, CD4+CD161+CD3±) in SI cases grouped by the outcome (favorable (SIfav, $n = 24$), unfavorable (Slunfav, $n = 17$) and lethal ($n = 2$)). With the help of flow cytometry, we identified a pronounced decrease in the absolute number of T_{reg} and Th17, as well as T_{reg} and Th17 expressing CD39 and CD73, in the early post-traumatic period. In the SIfav and Slunfav groups the relative number of T_{reg} and Th17 cells expressing CD39 differed significantly ($p <0.05$); it was substantially higher form the first to the third day post injury in the Slunfav group. The level of Treg CD39 (44.4%) is a premise for an unfavorable outcome in children surviving an SI. In fatality cases, we registered extremely low ectonucleotidase expression rates: CD39+T_{reg} — 9.52% (9.52–13.75) and CD39+Th17 — 0.92% (0.74–1.1). In the Slunfav group, the intensity of fluorescence (FL) of CD39 on T_{reg} cells in the early post-traumatic period was higher than seen in the SIfav group. The threshold value for the average fluorescence intensity (FL) of CD39 on T_{reg} was 8.25 c.u. In fatality cases, the T_{reg} CD39 FL values were extremely low: 3.95 c.u. (3.7–4.67). The results of the study indicate that in children, the expression of CD39 and CD73 in T_{reg} and Th17 populations is significantly associated with the severity of injury and outcome of the traumatic disease.

Keywords: children, severe injury, T_{reg}, Th17, CD39, CD73, immune suppression

✉ Correspondence should be addressed: Rustam Shakirovich Zakirov
Lomonosovsky prospect, 2/1, Moscow, 119296, Russia; zakirov.rsh@nczd.ru

РЕГУЛЯТОРНЫЕ Т-КЛЕТКИ И Т-ХЕЛПЕРЫ 17-ГО ТИПА С ЭКСПРЕССИЕЙ ЭКТОНУКЛЕОТИДАЗ CD39 И CD73 ПРИ ТЯЖЕЛОЙ МЕХАНИЧЕСКОЙ ТРАВМЕ У ДЕТЕЙ

Р. Ш. Закиров[1,2] ✉, Д. Г. Купцова[1], Е. В. Фрейдлин[1], Е. Л. Семикина[1], С. В. Петричук[1], О. В. Карасева[1,2]

[1] Национальный медицинский исследовательский центр здоровья детей Минздрава России, Москва, Россия

[2] Научно-исследовательский институт неотложной детской хирургии и травматологии Департамента здравоохранения г. Москвы, Москва, Россия

Исследование механизмов развития иммунного ответа при тяжелой механической травме (ТМТ) у детей — актуальная и социально значимая задача по причине высокой инвалидизации и летальности. Целью работы было определение информативных иммунологических критериев тяжести и прогноза исхода травматической болезни у детей ($n = 43$) на основе оценки экспрессии эктонуклеотидаз CD39 и CD73 в популяциях регуляторных Т-клеток (T_{reg}, CD4+CD127^{low}CD25^{high}) и Т-хелперов 17-го типа (Th17, CD4+CD161+CD3+) при ТМТ в группах с благоприятным (ТМТбл, $n = 24$), неблагоприятным (ТМТнебл, $n = 17$) и летальным исходом ($n = 2$). С помощью метода проточной цитофлуориметрии было выявлено выраженное снижение абсолютного количества T_{reg} и Th17, а также T_{reg} и Th17, экспрессирующих CD39 и CD73, в раннем посттравматическом периоде ТМТ. В группах ТМТбл и ТМТнебл относительное число T_{reg} и Th17, экспрессирующих CD39, значимо различалось ($p <0,05$) и было существенно повышено с первых по третьи сутки после травмы для ТМТнебл. Уровень T_{reg} CD39 (44,4 %) является предпосылкой неблагоприятного исхода у выживших детей при ТМТ. Для больных с летальным исходом были получены крайне низкие показатели экпрессии эктонуклеотидаз: CD39+T_{reg} — 9,52% (9,52–13,75) и CD39+Th17 — 0,92% (0,74–1,1). Для ТМТнебл интенсивность флюоресценции (FL) CD39 на T_{reg} в раннем посттравматическом периоде была повышена в сравнении с ТМТбл. Для средней интенсивности флуоресценции (FL) CD39 на T_{reg} пороговое значение составило 8,25 у.е. Для пациентов с летальным исходом значения FL CD39 на T_{reg} выявлены крайне низкие: 3,95 у.е. (3,7–4,67). Полученные результаты показывают, что экспрессия CD39 и CD73 в популяциях T_{reg} и Th17 в значительной степени связана с тяжестью и исходом травматической болезни у детей.

Ключевые слова: дети, тяжелая травма, регуляторные Т-лимфоциты, Т-хелперы 17-го типа, CD39, CD73, иммуносупрессия

✉ Для корреспонденции: Рустам Шакирович Закиров
Ломоносовский проспект, д. 2/1, г. Москва, 119296, Россия; zakirov.rsh@nczd.ru

Severe mechanical injury (SI) is one of the main reasons behind children's disability and mortality [1, 2]. SI triggers decompensation of the body's life support systems as a result of combined effect of such damage factors as traumatic mechanical damage, blood loss and hypoxia. Mechanical damage is the initiating factor: it triggers the release of damage-associated molecular patterns (DAMPs), which, in turn, can disrupt the cellular immune response to exogenous antigens and pathogen-associated molecular patterns (PAMPs), thus promoting dysfunction of the immune system. Extracellular ATP (eATP) is one of the endogenous tissue DAMPs that trigger and regulate the immune response to damage [3]. In trauma cases, the level of eATP grows persistently in the injury [4, 5]. This compound is one of the main components of the purinergic system; being a strong pro-inflammatory signal, eATP plays an important part in the T cell functioning regulation. As a powerful damage-associated molecular pattern, eATP basically initiates inflammatory response through purinergic P2R receptors. At the same time, the end product of eATP degradation, extracellular adenosine, being an immunosuppressor, plays an important part in limiting that response. Extracellular adenosine functions through the A2A adenosine receptors, blocks the T cell receptor (TCR) signal by inhibiting phosphorylation of the zeta-associated protein 70 (ZAP-70) and activates the activating protein 1 (AP-1), thus decreasing the production of IL2, expression of CD25 and inhibiting the T cell proliferation. The levels of eATP and extracellular adenosine, as well as their biological effects, are strictly regulated by the catalytic effects of CD39 (E-NTPDasa1) and CD73 (Ecto5'NTasa), ectoenzymes expressed on the plasma membrane of immune cells. CD39 metabolizes ATP to ADP, pyrophosphate and AMP. CD73 ectonucleotidase degrades AMP into adenosine and phosphate. Thus, CD39 and CD73 exonucleotidase secure a balance between pro-inflammatory action of ATP and anti-inflammatory action of adenosine in the focus of inflammation [6–9]. In case of a severe trauma, there is usually a period of prominent immunosuppression the pathogenesis of which is largely shaped by the decreasing level of T-lymphocytes. Absolute and relative number of T helper subpopulations is a significant marker in determining the severity of the pathological process and predicting its outcome [10–13]. Establishing the levels of expression of CD39 and CD73 exonucleotidase on various populations of circulating lymphocytes is of great clinical importance in the context of diagnosing and predicting the outcome of a wide range of diseases [14]. Therefore, the purpose of this study was to identify informative immunological criteria for the traumatic disease severity and outcome prognosis as applicable to children. The identification relies on the assessment of absolute and relative number of T lymphocyte subpopulations and the level of expression of CD39 and CD73 ectonucleotidase in T_{reg} and Th17 populations in severe mechanical trauma cases.

METHODS

The study involved 43 patients (28 boys (65.1%), 15 girls (34.9%); 116 observation sessions) with SI, treated at the Department of Anesthesiology and Resuscitation of the Research Institute of Emergency Pediatric Surgery and Traumatology, Moscow, in 2020–2021. We used the laboratory of the National Medical Research Center for Children's Health for laboratory studies, which were prescribed 1 to 5 times, depending on the length of stay of a given child at the Department of Anesthesiology and Resuscitation (DAR). The mean age of the children was 13.0 (6.0–15.0) years (Me (Q_{25}–Q_{75})). The time options for laboratory studies were the first, third, fifth, seventh and 14th days from the day of injury.

The control group was comprised of 41 apparently healthy children; all of them underwent medical examination at the National Medical Research Center for Children's Health. The children were comparable in age and sex: age — 12.41 (7.4–16.2) years; 26 boys (63.4%), 15 girls (36.6%).

Assessing the injury, we relied on the Injury Severity Score (ISS), the Glasgow Coma Scale (GCS) and its modification for patients under 2 years old, the pediatric GCS (pGCS) [15].

The outcome of an SI was assessed with the help of the Glasgow Outcome Scale (GOS) and the Severe Injury Outcomes Scale (OISS) [16], which suggest the following categories: category 1 — full recovery (the patient can live and be as active as before the injury); category 2 — good recovery (there are consequences that do not limit the level of social adaptation, but the patient cannot return to the pre-injury level of functional activity and needs further treatment or rehabilitation); category 3 — moderate disability (there are consequences that disallow return to the pre-injury functional level, but the patient retains independent living skills); category 4 — severe disability (the patient needs assistance of others and cannot live independently); category 5 — death. These scales were applied to assess the condition of the patient at discharge from the hospital.

The patients were included in the study if they had an SI (ISS ≥ 16) and were treated in the ICU. Concomitant acute inflammatory and chronic diseases were a reason for exclusion.

At the first stage, we analyzed the results from the control group and the SI group. At the second stage, we analyzed the two groups formed with the help of GOS and OISS, the favorable outcome group (SIfav, $n = 24$) and the unfavorable outcome group (Slunfav, $n = 17$) (Table 1). The distribution into these groups was based on the scores: patients were allocated to the SIfav group if they scored 4–5 points on the GOS scale and 1–2 points on the OISS scale, and to the Slunfav group if they scored 2–3 points on the GOS scale and 3-4 points on the OISS scale. A group of fatal cases (SIdeath, $n = 2$) was described separately (Table 1).

We assessed the quantity of Th17 lymphocytes (Th17 — CD3+CD4+CD161+), regulatory T lymphocytes (T_{reg} — CD4+CD127lowCD25high) in the patients and established the level of expression of purinergic signaling receptors on T_{reg} (CD39+T_{reg} — CD4+CD127lowCD25highCD39+ and CD73+T_{reg} — CD4+CD127lowCD25highCD73+) and Th17 lymphocytes (CD39+Th17 — CD3+CD4+CD161+CD39+ and CD39+Th17 — CD3+CD4+CD161+CD73+). Two-platform technology enabled assessment of the quantitative indicators of the subpopulation composition of peripheral blood T lymphocytes. The absolute number of lymphocytes was calculated with the help of a Sysmex XT-2000i hematology analyzer (Sysmex Corporation; Japan). The preparation of samples for cytofluorimetric analysis included incubation of 100 µl of whole blood with 10 µl of monoclonal antibodies tagged with fluorochromes for 20 min in a dark place. The erythrocytes were lysed with BD FACS™ Lysing Solution (BD Biosciences; USA); the duration of incubation therewith in the dark at room temperature did not exceed 10–12 minutes. The resulting samples were analyzed in a Novocyte flow cytometer (ACEA Biosciences; USA). The surface markers used to determine lymphocyte subpopulations were as follows: CD45, IgG1, IgG2a, CD3, CD4, CD25, CD127, CD161, CD39, CD73 (Beckman Coulter, USA; BD Biosciences, USA; SONY corp., Japan).

We used MS Excel 2016 (Microsoft corp.; USA), Statistica 10 (StatSoft, Inc.; USA), and IBM SPSS Statistics 25 (IBM corp.; USA)

Table 1. Clinical characteristics of patients

Factor		SI outcome		
		SIfav	SIunfav	SIdeath
n		24	17	2
Sex, %	girls	9 (37.5)	6 (35.3)	–
	boys	15 (62.5)	11 (64.7)	2 (100.0)
Age (Me [IQR]), years		12.5 [6.0–15.0]	13.0 [8.0–14.0]	7.5 [4.7–10.2]
Days in DAR (Me [IQR])		9.00 [7.00–13.25]	16.00 [10.00–25.00]	6.00 [6.00–6.00]
Total days in hospital (Me [IQR])		23.00 [16.00–29.25]	53.00 [23.00–58.00]	6.00 [6.00–6.00]
ISS (Me [IQR])		26 (19–29)	27 (26–34)	25 и 35
TBI, %		21 (87.5)	16 (94.1)	100
GCS (Me [IQR]), points		12 (8–12)	7 (4–13)	7 и 3
Coma, %		5 (20.8)	8 (47.0)	2 (100)
Concomitant injury, %		21 (87.5)	16 (94.1)	2 (100)
Multiple trauma, %		11 (45.8)	7 (41.1)	1 (50)
Blood loss, %		16 (66.6)	13 (76.4)	1 (50)
Unstable hemodynamics, %		8 (33.3)	12 (70.5)	2 (100)
Respiratory support (ALV), %		16 (66.6)	16 (94.1)	2 (100)
Multiple organ failure, %		1 (4.1)	2 (11.7)	2 (100)

to process the data obtained. The results are presented as a median (Me) and quartiles (Q_{25}–Q_{75}). Mann–Whitney *U*-test with Bonferroni correction enabled comparison of differences in the attributes. Spearman's rank correlation coefficient (R) was used to assess relations between the attributes. The significance of quantitative indicators was assessed and threshold values (cut-off points) chosen with the help of the receiver operating characteristic curve (ROC curve). The threshold values were determined factoring in the maximum sensitivity and specificity requirements. The conclusions were considered significant at $p < 0.05$ (*).

RESULTS

The analysis of data from the control and SI groups revealed a pronounced decline in the absolute number of T_{reg} and Th17 in the early post-traumatic period. The values of these indicators in SI patients were significantly different from the respective values registered in the control group (Table 2, 3). Third to fifth day post injury, the T_{reg}/Th17 ratio was decreased in the SI group compared to the control group, which is the result of gradual growth of the level of Th17 from the third day on (Tables 2, 3).

Table 2. Subpopulations of CD4+-lymphocytes, T_{reg} and Th17 expressing CD39 and CD73, and ectonucleotidase fluorescence intensity on T_{reg} and Th17 in SI and control groups, regardless of the traumatic disease outcome

Indicators	Control group	SI (days elapsed since injury)				
		1st day	3rd day	5th day	7th day	14th day
	n = 41	*n* = 18	*n* = 33	*n* = 16	*n* = 21	*n* = 24
T_{reg}, abs	72.2 [57.3–86.2]	34.9 [22–48]*	38.3 [24.2–54.4]*	36.5 [24–67.2] *	36.5 [24–67.2]*	61 [49.1–78.9]
Th17, abs	144.6 [97.7–150.6]	78.1 [54.7–97.2]*	87.2 [64.4–136.3]*	93.2 [75.3–145.9]	93.2 [75.3–145.9]	163.3 [118.4–232.9]
T_{reg}/Th17	0.6 [0.5–0.8]	0.4 [0.3–0.7]	0.4 [0.3–0.5]*	0.4 [0.3–0.5]*	0.4 [0.3–0.5]	0.4 [0.3–0.5]*
CD39+, % T_{reg}	35.2 [29.1–39.4]	27.6 [17.3–43.1]	33.3 [15.4–53.2]*	36.4 [15.8–49.6]	36.4 [15.8–49.6]	43.4 [28–52]
CD39+, abs T_{regs}	27 [18.3–31.7]	9.3 [5.9–13.1*	10 [7–14.2]*	12.4 [6.7–18.8]*	12.4 [6.7–18.8] *	23.2 [10.9–38.7]
CD39+, % Th17	9.6 [8.6–12.1]	9.8 [6.5–12.4]	7.7 [3.4–10.6]*	6.8 [5.3–10.7]*	6.8 [5.3–10.7]	7.3 [4–8.9] *
CD39+, abs Th17	12.5 [10.9–14.7]	7.9 [3.5–9.2]*	6.0 [2.2–9.6]*	7.1 [4–10.5]*	7.1 [4–10.5]	11.3 [4.3–18.5]
CD73+, % T_{reg}	8.9 [7.3–11.1]	6.5 [4.1–13.1]	6.9 [4.9–11.8]	11.2 [5.1–22.3]	11.2 [5.1–22.3]	6.7 [4.6–16.9]
CD73+, abs T_{regs}	8 [3–10]	2.7 [1.3–3.3]*	2.2 [1.6–4.7]*	5.2 [2.7–6.5]	5.2 [2.7–6.5]	4.3 [2.5–8]
CD73+, % Th17	10.2 [7.3–14.4]	8.1 [6.1–13.7]	10.8 [7.4–19]	13.8 [10.6–16.5]	13.8 [10.6–16.5]	15* [9.2–19.8]
CD73+, abs Th17	13.6 [8.4–17]	6.5 [3.3–9.2]*	10.3 [4.3–22.4]	14.7 [11.9–28.2]	14.7 [11.9–28.2]	26.7 [12.3–34.9]*
CD39/CD73 T_{reg}	3.4 [2.6–5.1]	3.9 [1.9–6.9]	4.5 [1.9–7.8]	2.8 [1.6–5.4]	2.8 [1.6–5.4]	4.6 [2.5–9.1]
CD39/CD73 Th17	1.1 [0.7–1.7]	1.4 [0.5–2.2]	0.7 [0.2–1.3]	0.5 [0.2–1.3]	0.5 [0.2–1.3]	0.5 [0.1–0.7]*
FL CD39 T_{reg}	7.9 [7–9.2]	8 [6.7–13]	8.4 [6.2–11.3]	8.1 [5.6–10]	8.1 [5.6–10]	9.4 [7.1–12]
FL CD39 Th17	7.2 [5.8–8.9]	6.6 [5.4–7.7]	7.8 [6.2–9.3]	7.2 [6.6–9.1]	7.2 [6.6–9.1]	7.8 [6.8–8.8]
FL CD73 T_{reg}	3.3 [2.7–3.7]	3.2 [2.7–4.1]	4.2 [3.2–6.2]*	3.3 [2.8–4.7]	3.3 [2.8–4.7]	4.4 [3.6–5.7]*
FL CD73 Th17	3.6 [3.3–4.7]	4 [3.2–6.1]	4.6 [3.2–5.7]	4.1 [3.9–6.8]	4.1 [3.9–6.8]	4 [3.3–6.4]

Note: Me [Q_{25}–Q_{75}%]; * — $p < 0.05$, Mann–Whitney *U*-test with Bonferroni correction, compared groups (healthy children, SI).

Table 3. Adjusted level of reliability of the analyzed parameters (with Bonferroni correction), control and SI groups, regardless of the traumatic disease outcome

Parameter	Mann–Whitney U-test (control group/SI)				
Days since injury	1	3	5	7	14
# of observation sessions	18	33	16	21	24
T_{reg}, abs	0.0000*	0.0000*	0.006*	0.03 *	0.605
Th17, abs	0.0000*	0.003*	0.215	1.407	0.232
T_{reg}/Th17	0.1035	0.005*	0.015*	0.3665	0.011*
CD39+, % T_{reg}	0.509	4.1445	3.206	4.2395	0.3365
CD39+, abs T_{reg}	0.0000*	0.0000*	0.002*	0.017*	1.9045
CD39+, % Th17	4.13	0.0335*	0.0125*	1.9935	0.0015*
CD39+, abs Th17	0.0005*	0.0000*	0.0165*	0.2125	1.091
CD73+, % T_{reg}	2.2375	1.0035	2.6035	1.836	3.6035
CD73+, abs T_{reg}	0.0015*	0.0000*	0.206	0.98	0.926
CD73+, % Th17	1.6255	1.418	0.758	2.152	0.063
CD73+, abs Th17	0.006*	2.032	1.1885	4.7335	0.0065*
CD39/CD73 T_{reg}	4.3845	4.1865	1.2375	1.4005	1.9915
CD39/CD73 Th17	4.462	0.1255	0.0885	1.2715	0.007*
FL CD39 T_{reg}	4.8375	4.8275	3.333	3.079	1.4725
FL CD39 Th17	1.936	1.105	2.7475	2.547	2.438
FL CD73 T_{reg}	2.5445	0.0245 *	3.462	0.1695	0.0005*
FL CD73 Th17	1.584	0.5755	0.223	2.6665	0.993

Note: Me [Q_{25}–Q_{75}%]; * — $p < 0{,}05$, Mann–Whitney U-test, compared groups (control group, SI).

The dynamics of the absolute number of Treg and Th17 cells expressing CD39 and CD79 was similar to the dynamics of small subpopulations of CD4+ lymphocytes during the acute post-traumatic period, but the changes were more pronounced in case of T_{reg} cells (Tables 2, 3). The relative amount of CD39+T_{reg} in children with SI varied from 6.3 to 76.6% and significantly exceeded the value of CD39+Th17 (range of variability: 0.3–24.1%) (Table 2). As for CD73, the relative number of this marker was significantly higher on Th17 (range of variability: 2.6–99.9%) than on T_{reg} (range of variability: 0.5–55.2%). We uncovered no significant differences with the control group.

However, at some observation sessions the registered values significantly exceeded the maximum levels seen in the control group (Table 2).

The analysis of ectonucleotidase mean fluorescence intensity (FL) on T_{reg} and Th17 revealed differences for CD73 on T_{reg}. Compared to the control group, the FL values for CD73 three days after the injury were increased (Tables 2, 3).

Correlation analysis revealed a relationship between the percentage of T_{reg} and Th17 expressing CD39 and CD73 and the intensity of marker fluorescence. In case of Th17, the percentage of enzyme-expressing cells increases slightly

A
CD39+, % Th17: FL CD39 Th17: $r = 0{,}2701$; $p = 0{,}0019$

B
CD39+, % T_{regs}: FL CD39 T_{reg}: $r = 0{,}7121$; $p = 0{,}0000$

C
CD39+, % Th17: FL CD39 Th17: $r = 0{,}2041$; $p = 0{,}0189$

D
CD39+, % T_{regs}: FL CD39 T_{reg}: $r = 0{,}1857$; $p = 0{,}0259$
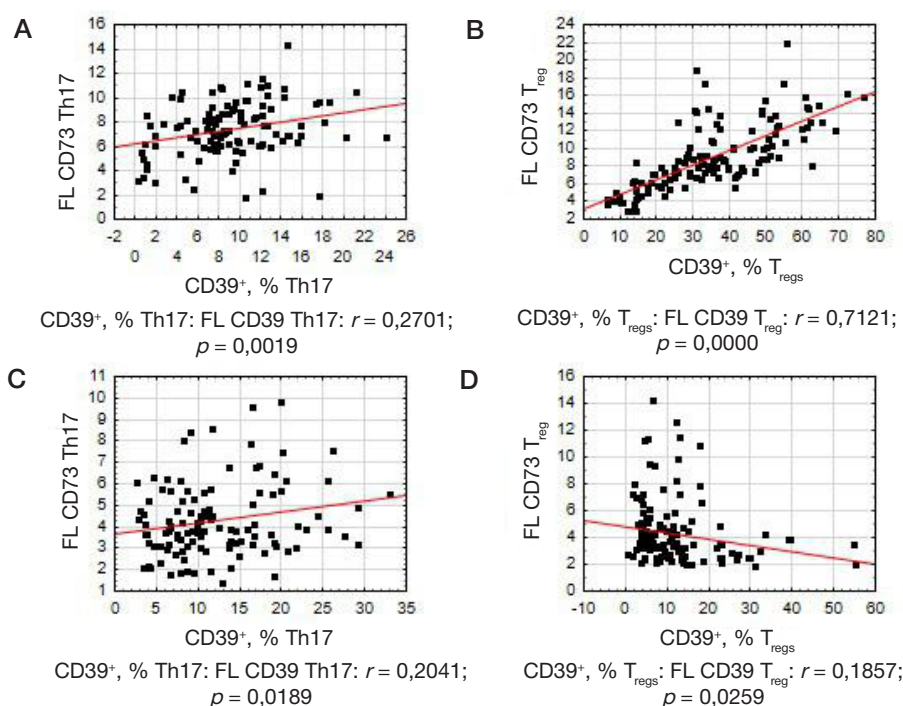
Fig. 1. Dependence of the percentage of T_{reg} and Th17 cells expressing CD39 and CD73 enzymes on the intensity of fluorescence (FL) of CD39 and CD73. **A**. FL CD39 Th17: CD39+, Th17%. **B**. FL CD39 T_{reg}: CD39+, T_{reg}%. **C**. FL CD73 Th17: CD73+, Th17%. **D**. FL CD73 T_{reg}: CD73+, %T_{reg}

Table 4. Relative amount of T_{reg} and Th17 cells expressing CD39 and CD73 enzymes, first through third days, children with SI

Indicator	Slunfav	Slfav	SIdeath	Statistical significance level *p*, Slunfav and Slfav
# of observation sessions	19	28	3	
T_{reg}, % CD4	9.24 [8.12–10.84]	8.9 [8.48–11.4]	9.9 [8.84–10.5]	0.968
CD39, % T_{reg}	52.33 [43.7–62.2]*	21.7 [14.9–25.2]	9.52 [9.52–13.75]	0.000026
CD73, % T_{reg}	6.24 [3.2–8.8]	6.54 [4.0–9.2]	4.9 [3.53–7.2]	0.84
Th17, % CD4	30.76 [25.2–35.2]*	15.5 [12.2–17.8]	19.5 [17.91–28.5]	0.0008
CD39, % Th17	14.55 [8.9–19.1]*	6.72 [3.14–9.0]	0.92 [0.74–1.1]	0.012
CD73, % Th17	12.38 [7.7–19.21]	10.38 [4.15–15.77]	5.7 [4.7–6.7]	0.599

Note: Me [Q_{25}–Q_{75}%]; Mann–Whitney *U*-test, compared groups: Slunfav, Slfav.

as the intensity of fluorescence of CD39 ($r = 0.27$; $p = 0.002$) and CD73 ($r = 0.20$; $p = 0.018$) grows (Fig. 1A, B). In case of Treg, as the fluorescence intensity grows, the share of enzyme-expressing cells increases for CD39 ($r = 0.71$; $p < 0.001$) and decreases slightly for CD73 ($r = -0.18$; $p < 0.05$; Fig. 1). The strongest direct dependence was found for CD39$^+$$T_{reg}$ (Fig. 1B).

A comparative analysis of the post-traumatic period data from Slfav and Slunfav groups has shown a significant increase in the relative amount of Th17 that occurred first through third days in the Slunfav group. At the same time, there were no differences between groups in terms of the number of T_{reg} cells (Table 4). The levels of expression of CD39 on T_{reg} and Th17 lymphocytes differed significantly in the Slfav and Slunfav groups: patients from the latter group had it considerably higher (Table 4, Fig. 2). We did not do the comparative analysis for the STMdeath group ($n = 2$) because of the small number of observation sessions (three), but it can be noted that in case of such patients, with the relative amounts of T_{reg} and Th17 being comparable, the registered expression of ectonucleotidase on T_{reg} and Th17 was extremely low (Table 4).

The following clinical cases show the dynamics of CD39 expression on T_{reg} and Th17 in patients with unfavorable (Case #1, Fig. 3) and favorable (Case #2, Fig. 3) injury outcome.

The analysis of fluorescence of ectonucleotidase on T_{reg} and Th17 in children from the Slfav and Slunfav groups revealed that the respective parameter differed significantly between the groups in case of CD39 on T_{reg}. In the Slunfav group we registered a slight increase in the fluorescence of CD39 on T_{reg} days 1 through 7 post-injury (Table 5). As for the SIdeath group, the fluorescence values there were as follows: FL CD39 T_{reg} — 3.95 (3.7–4.67), FL CD73 T_{reg} — 4 (2.55–4.55), FL CD39 Th17 — 6 .77 (5–8.55), FL CD73 Th17 3.52 (3.1–3.95). Compared to Slfav and Slunfav, the FL CD39 T_{reg} values there were extremely low (Table 5).

We built a ROC curve (both Slfav and Slunfav groups) for the indicators that proved to be of high prognostic significance in traumatic disease cases in children. A good quality division model was generated for CD39$^+$ T_{reg} % (AUC = 0.741) and FL CD39 T_{reg} (AUC = 0.721). The resulting cut-off for CD39$^+$$T_{reg}$ was 44.4% (sensitivity — 66.6, specificity — 84.7) and FL CD39 Treg — 8.25 c.u. (sensitivity — 87.5, specificity — 62.5).

DISCUSSION

This study shows that a severe mechanical trauma in children unbalances the T_{reg}/Th17 ratio in the early post-injury period, the imbalance translating into a slight shift towards Th17 while the absolute number of T_{reg} and Th17 cells decreases noticeably. These findings are consistent with the data published by other researchers [11–13, 17]. Among Treg and Th17, the
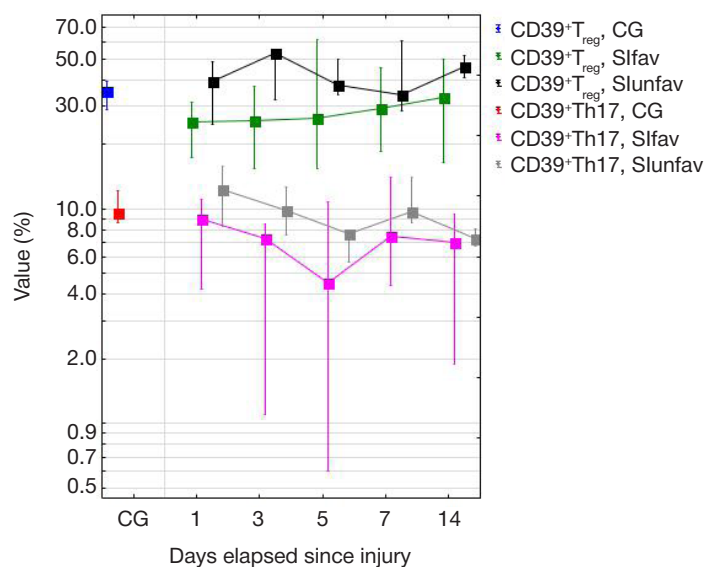
Fig. 2. Relative amount of Th17 and T_{reg} cells expressing CD39, Slfav and Slunfav and control groups. Me [Q_{25}–Q_{75}%]; compared groups: Slunfav, Slfav, control group (CG)
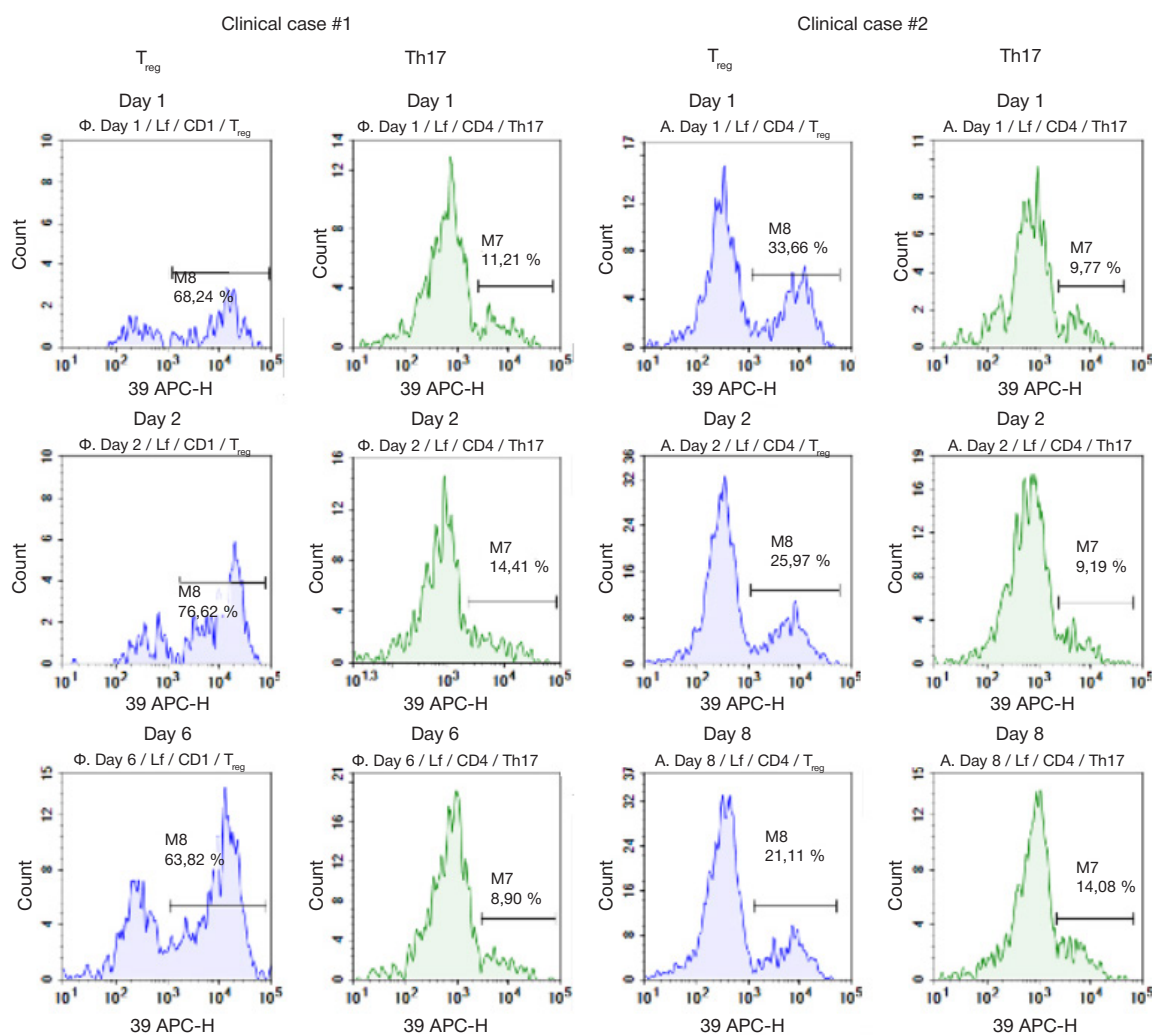
Fig. 3. Dynamics of the relative amount of Th17 and T_{reg} expressing CD39, critical period, severe injury, children with unfavorable (Case #1) and favorable (Case #2) outcome

absolute number of cells expressing CD39 and CD73 also proportionally decreases in the critical period of traumatic disease.

The analysis of cells expressing CD39 and CD73 ectonucleotidase in CD4+-lymphocyte populations in children with SI revealed that the highest expression of CD39 in the Treg population is up to 76.6%, that of CD73 in Th17 — up to 99.9%. In apparently healthy children, by contrast, the CD39 expression in the Treg population ranged from 19 to 49%, and that of CD73 by Th17 — from 7 to 35% [18].

We have established that depending on the traumatic disease outcome, the expression of ectonucleotidase in children going through the early post-injury period may be different. Compared to the patients for whom the outcome was favorable, children from the Slunfav group had the percentage of CD39 on T_{reg} and Th17 increasing and the intensity of CD39 fluorescence on T_{reg} growing on days first through seventh post-injury. A possible reason therefor is the role played by ectonucleotidases, especially CD39, in enhancing the hydrolysis of eATP and accumulation of extracellular adenosine

Table 5. Fluorescence parameters (FL) of CD39 and CD73 purinergic signaling on T_{reg} and Th17, critical period, SI, children

Indicators	SIfav, days since injury					Slunfav, days since injury				
	1	3	5	7	14	1	3	5	7	14
	$n = 10$	$n = 18$	$n = 6$	$n = 14$	$n = 12$	$n = 6$	$n = 13$	$n = 8$	$n = 7$	$n = 12$
FL CD39 T_{reg}	7.7 [5.1–9.3]*	7.3 [6.2–9] *	9.7 [5.6–14.8]	7.7 [5.6–9.9] *	7.5 [6.3–11.8]	10.7 [8.5–14]	10.8 [8.8–12.4]	8.5 [7.9–8.8]	12.9 [9.4–14.1]	10.3 [8.3–12]
FL CD39 Th17	6.5 [5.4–7]	7.3 [5.7–8.4]	9.9 [6.1–10.6]	7.9 [6.4–8.2]	7.3 [6.1–8.8]	7.3 [6–8.7]	8.7 [7.1–9.8]	7 [6.8–7.9]	9.3 [5.3–10.3]	8.2 [7.1–9]
FL CD73 T_{reg}	3.2 [2.7–5.9]	3.8 [3–4.8]	3.2 [3.1–4.9]	3.9 [2.4–4.8]	4.6 [2.8–6]	3.2 [2.6–3.7]	5.1 [3.7–8.7]	3.4 [2.8–5.5]	4.7 [4.3–7.1]	4.4 [3.8–5.6]
FL CD73 Th17	3.7 [3.1–6.1]	4.2 [3.7–4.8]	4.1 [3.9–5.1]	3.9 [3.1–5.7]	4.3 [3.3–7.4]	4.3 [4–6.9]	5.1 [3.3–8.4]	4.5 [3.9–7.9]	4.7 [3.3–5.9]	3.9 [3.2–5.3]

Note: Me [Q_{25}–Q_{75}%]; p is the adjusted significance level (Bonferroni correction applied); * — $p < 0.05$ significance level, Mann–Whitney U-test, compared groups (SIfav and Slunfav on the first, third, fifth, seventh, and 14th days post injury).

in the injury locus, which triggers a cascade of reactions through the A2R system of adenosine receptors, this cascade ultimately leading to suppression of the immune response to prevent massive tissue damage [14]. The direct correlation between the level of CD39 fluorescence and the percentage of $CD39^+T_{reg}$ that we discovered indicates that the proportion of Treg abundantly expressing CD39 ectonucleotidase increases in response to injury. Previous studies that involved healthy adult donors have shown that cells with a large amount of CD39 on T_{reg} hydrolyze ATP more efficiently [8]. As for the CD73 ectonucleotidase, we established no correlation between its percentage and fluorescence intensity, probably due to the fact that CD73 is found both on the cell membrane and in soluble form [19]. In the deceased patients, the identified values of ectonucleotidase expression were extremely low, which may

signal of development of decompensation of the immune system functions when the injuries are extremely severe.

CONCLUSIONS

The results of the study indicate that in children, the expression of CD39 and CD73 in T_{reg} and Th17 populations is significantly associated with the severity of injury and may be used to predict outcome of the traumatic disease. A deeper understanding of the role of purinergic signaling in the pathogenesis of traumatic disease suggests therapeutic potential of biopreparations based on the soluble forms of ectonucleotidase that may be designed to manipulate the immune system in such critical conditions as severe traumatic injury [20].

References

1. Timofeev VV, Bondarenko AV. Epidemiological aspects of polytrauma in children in major city. Polytrauma. 2012; (4): 5–8. Russian.
2. Bondarenko AV The organization of specialized care for polytrauma in a large city. N.N. Priorov Journal of Traumatology and Orthopedics. 2005; (4): 81–84. Russian.
3. Cauwels A, Rogge E, Vandendriessche B, Shiva S, Brouckaert P. Extracellular ATP drives systemic inflammation, tissue damage and mortality. Cell Death Dis. 2014; 5 (3): e1102.
4. Moro N, Ghavim SS, Sutton RL. Massive efflux of adenosine triphosphate into the extracellular space immediately after experimental traumatic brain injury. Exp Ther Med. 2021; 21 (6): 575.
5. Faroqi AH, Lim MJ, Kee EC, Lee JH, Burgess JD, Chen R, Di Virgilio F, Delenclos M, McLean PJ. In Vivo Detection of Extracellular Adenosine Triphosphate in a Mouse Model of Traumatic Brain Injury. J Neurotrauma. 2021; 38 (5): 655–64.
6. Golovkin AS, Serebryakova MK, Zhiduleva EV, Murtazalieva PM, Titov VA, Irtuga OB, Moiseeva OM, Krobinec II, Kudryavtsev IV. Purinergic signaling receptors expression on peripheral T-lymphocites of healthy donors. Translational Medicine. 2017; 4 (5): 46–60. Russian.
7. Takenaka MC, Robson S, Quintana FJ. Regulation of the T Cell Response by CD39. Trends Immunol. 2016; 37 (7): 427–39.
8. Timperi E, Barnaba V. CD39 Regulation and Functions in T Cells. Int J Mol Sci. 2021; 22 (15): 8068.
9. Borsellino G, Kleinewietfeld M, Di Mitri D, et al. Expression of ectonucleotidase CD39 by Foxp3+Treg cells: Hydrolysis of extracellular ATP and immune suppression. Blood. 2007; 110 (4): 1225–32.
10. Zhang C, Li L, Feng K, Fan D, Xue W, Lu J: 'Repair' Treg Cells in Tissue Injury. Cell Physiol Biochem. 2017; 43: 2155–69.
11. Sturm R, Xanthopoulos L, Heftrig D, Oppermann E, Vrdoljak T, Dunay IR, et al. Regulatory T Cells Modulate CD4 Proliferation after Severe Trauma via IL10. J Clin Med. 2020; 9 (4): 1052.

12. Zhang Y, Li XF, Wu W, Chen Y. Dynamic changes of circulating T-helper cell subsets following severe thoracic trauma. Int J Clin Exp Med. 2015; 8 (11): 21106–13.
13. Hein F, Massin F, Cravoisy-Popovic A, Barraud D, Levy B, Bollaert PE, et al. The relationship between CD4+CD25+CD127-regulatory T cells and inflammatory response and outcome during shock states. Crit Care. 2010; 14 (1): R19.
14. Han L, Sugiyama H, Zhang Q, Yan K, Fang X, McCormick TS, et al. Phenotypical analysis of ectoenzymes CD39/CD73 and adenosine receptor 2A in CD4+ CD25high Foxp3+ regulatory T-cells in psoriasis. Australas J Dermatol. 2018; 59 (1): e31–e38.
15. Holmes JF, Palchak MJ, MacFarlane T, Kuppermann N. Performance of the pediatric Glasgow coma scale in children with blunt head trauma. Acad Emerg Med. 2005; 12: 814.
16. Karaseva O, Roshal L. Pediatric Trauma in Earthquakes: General Principles of Care in Pediatric Trauma During Earthquakes. In: Wolfson N, Lerner A, Roshal L, eds. Orthopedics in Disasters: Orthopedic Injuries in Natural Disasters and Mass Casualty Events. Berlin Heidelberg: Springer, 2016.
17. Zhou X, Yao J, Lin J, Liu J, Dong L, Duan M. Th17/Regulatory T-Cell Imbalance and Acute Kidney Injury in Patients with Sepsis. J Clin Med. 2022; 11 (14): 4027.
18. Radygina TV, Kuptsova DG, Petrichuk SV, et al. Expression of CD39 and CD73 ectonucleotidases in CD4+ lymphocyte populations in healthy children. Russian Journal of Immunology. 2022; 25 (3): 283–290. Russian.
19. Vaara ST, Hollmén M, Korhonen AM, Maksimow M, Ala-Kokko T, Salmi M, et al. FINNAKI Study Group. Soluble CD73 in Critically Ill Septic Patients — Data from the Prospective FINNAKI Study. PLoS One. 2016; 11 (10): e0164420.
20. Zhai X, Chen K, Yang H, Li B, Zhou T, Wang H, et al. Extracellular vesicles derived from CD73 modified human umbilical cord mesenchymal stem cells ameliorate inflammation after spinal cord injury. J Nanobiotechnology. 2021; 19 (1): 274.

Литература

1. Тимофеев В. В., Бондаренко А. В. Эпидемиологические аспекты политравмы у детей в крупном городе. Политравма. 2012; (4): 5–8.
2. Бондаренко А. В. Организация специализированной помощи при политравме в крупном городе. Вестник травматологии и ортопедии им. Н. Н. Приорова. 2005; (4): 81–84.
3. Cauwels A, Rogge E, Vandendriessche B, Shiva S, Brouckaert P. Extracellular ATP drives systemic inflammation, tissue damage and mortality. Cell Death Dis. 2014; 5 (3): e1102.
4. Moro N, Ghavim SS, Sutton RL. Massive efflux of adenosine triphosphate into the extracellular space immediately after experimental traumatic brain injury. Exp Ther Med. 2021; 21 (6): 575.

5. Faroqi AH, Lim MJ, Kee EC, Lee JH, Burgess JD, Chen R, Di Virgilio F, Delenclos M, McLean PJ. In Vivo Detection of Extracellular Adenosine Triphosphate in a Mouse Model of Traumatic Brain Injury. J Neurotrauma. 2021; 38 (5): 655–64.
6. Головкин А. С., Серебрякова М. К., Жидулева Е. В., Муртазалиева П. М., Титов В. А. Экспрессия рецепторов пуринергического сигналинга на Т-лимфоцитах периферической крови здоровых доноров. Трансляционная медицина. 2017; 4 (5): 46–60.
7. Takenaka MC, Robson S, Quintana FJ. Regulation of the T Cell Response by CD39. Trends Immunol. 2016; 37 (7): 427–39.
8. Timperi E, Barnaba V. CD39 Regulation and Functions in T Cells.

Int J Mol Sci. 2021; 22 (15): 8068.

9. Borsellino G, Kleinewietfeld M, Di Mitri D, et al. Expression of ectonucleotidase CD39 by Foxp3+Treg cells: Hydrolysis of extracellular ATP and immune suppression. Blood. 2007; 110 (4): 1225–32.

10. Zhang C, Li L, Feng K, Fan D, Xue W, Lu J: 'Repair' Treg Cells in Tissue Injury. Cell Physiol Biochem. 2017; 43: 2155–69.

11. Sturm R, Xanthopoulos L, Heftrig D, Oppermann E, Vrdoljak T, Dunay IR, et al. Regulatory T Cells Modulate CD4 Proliferation after Severe Trauma via IL10. J Clin Med. 2020; 9 (4): 1052.

12. Zhang Y, Li XF, Wu W, Chen Y. Dynamic changes of circulating T-helper cell subsets following severe thoracic trauma. Int J Clin Exp Med. 2015; 8 (11): 21106–13.

13. Hein F, Massin F, Cravoisy-Popovic A, Barraud D, Levy B, Bollaert PE, et al. The relationship between CD4+CD25+CD127- regulatory T cells and inflammatory response and outcome during shock states. Crit Care. 2010; 14 (1): R19.

14. Han L, Sugiyama H, Zhang Q, Yan K, Fang X, McCormick TS, et al. Phenotypical analysis of ectoenzymes CD39/CD73 and adenosine receptor 2A in CD4+ CD25high Foxp3+ regulatory T-cells in psoriasis. Australas J Dermatol. 2018; 59 (1): e31–e38.

15. Holmes JF, Palchak MJ, MacFarlane T, Kuppermann N. Performance of the pediatric Glasgow coma scale in children with blunt head trauma. Acad Emerg Med. 2005; 12: 814.

16. Karaseva O, Roshal L. Pediatric Trauma in Earthquakes: General Principles of Care in Pediatric Trauma During Earthquakes. In: Wolfson N, Lerner A, Roshal L, eds. Orthopedics in Disasters: Orthopedic Injuries in Natural Disasters and Mass Casualty Events. Berlin Heidelberg: Springer, 2016.

17. Zhou X, Yao J, Lin J, Liu J, Dong L, Duan M. Th17/Regulatory T-Cell Imbalance and Acute Kidney Injury in Patients with Sepsis. J Clin Med. 2022; 11 (14): 4027.

18. Радыгина Т. В., Купцова Д. Г., Петричук С. В., Семикина Е. Л., Фисенко А. П. Экспрессия эктонуклеотидаз CD39 и CD73 в популяциях CD4+ лимфоцитов у условно здоровых детей. Российский иммунологический журнал. 2022; 25 (3): 283–90.

19. Vaara ST, Hollmén M, Korhonen AM, Maksimow M, Ala-Kokko T, Salmi M, et al. FINNAKI Study Group. Soluble CD73 in Critically Ill Septic Patients — Data from the Prospective FINNAKI Study. PLoS One. 2016; 11 (10): e0164420.

20. Zhai X, Chen K, Yang H, Li B, Zhou T, Wang H, et al. Extracellular vesicles derived from CD73 modified human umbilical cord mesenchymal stem cells ameliorate inflammation after spinal cord injury. J Nanobiotechnology. 2021; 19 (1): 274.

FABRICATION OF CARTILAGE TISSUE SUBSTITUTES FROM CELLS WITH INDUCED PLURIPOTENCY

Eremeev AV[1,3] ✉, Pikina AS[1,2], Ruchko ES[1], Sidorov VS[1], Ragozin AO[1]

[1] Federal State Budgetary Institution Federal Research and Clinical Center of Physical-Chemical Medicine of the Federal Medical Biological Agency, Moscow, Russia

[2] Lomonosov Moscow State University, Moscow, Russia

[3] Koltzov Institute of Developmental Biology, Moscow, Russia

One of the approaches to cartilage tissue restoration problem relies on cellular technologies that use iPSCs, induced pluripotency stem cells that are an unlimited source of cellular material for tissue engineering with significant differentiation potential. However, there are no standardized protocols for chondrogenic differentiation of iPSCs. This study aimed to make cartilage tissue samples using 3D spheroid cultures and following four chondrogenic differentiation protocols, then compare characteristics of the cartilage samples made under different protocols and isolate the most effective way of differentiation. The iPSCs were differentiated chondrogenically, the four protocols were "long", "short", "combined" and with conditioned medium from a primary culture of autologous chondrocytes; the combinations of TGFβ1, BMP2, Chir 99021, and PK factors varied. Microwell plates were used to make spheroids. Immunocytochemical staining, real-time PCR and histological staining enabled assessment of the synthesis and expression profiles. High rates of synthesis and expression of chondrogenic markers Sox9, aggrecan, type II collagen were observed in spheroids experimented with under the "long", "combined" protocols and the conditioned medium protocol. The "combined" differentiation protocol made chondrogenesis most effective, and conditioned medium was highly efficient in inducing and supporting chondrogenic differentiation.

Keywords: tissue engineering, articular cartilage, induced pluripotency stem cells (iPSCs), spheroids, chondrogenesis

✉ Correspondence should be addressed: Artem V. Eremeev
Malaya Pirogovskaya, 1a, 119435, Moscow, Russia; art-eremeev@yandex.ru

ПОЛУЧЕНИЕ ХРЯЩЕПОДОБНЫХ СТРУКТУР ИЗ СТВОЛОВЫХ КЛЕТОК С ИНДУЦИРОВАННОЙ ПЛЮРИПОТЕНТНОСТЬЮ

А. В. Еремеев[1,3] ✉, А. С. Пикина[1,2], Е. С. Ручко[1,3], В. С. Сидоров[1], А. О. Рагозин[1]

[1] Федеральный научно-клинический центр физико-химической медицины Федерального медико-биологического агентства, Москва, Россия

[2] Московский государственный университет имени М. В. Ломоносова, Москва, Россия

[3] Институт биологии развития имени Н. К. Кольцова, Москва, Россия

Одним из подходов для решения проблемы восстановления хрящевой ткани является использование клеточных технологий с применением ИПСК, обладающих большим потенциалом к дифференцировке и являющихся неограниченным источником клеточного материала для тканевой инженерии. Однако стандартизированных протоколов хондрогенной дифференцировки ИПСК нет. Целью работы было получить хрящеподобные образцы ткани с помощью метода 3D-культивирования сфероидов с использованием четырех протоколов хондрогенной дифференцировки, сравнить характеристики хрящеподобных образцов, полученных с помощью разных протоколов, и определить наиболее эффективный способ дифференцировки. ИПСК дифференцировали по хондрогенному пути с помощью четырех протоколов («долгий», «короткий», «комбинированный», с кондиционированной средой от первичной культуры аутологичных хондроцитов) при различном сочетании факторов TGFβ1, BMP2, Chir 99021 и PK. Для получения сфероидов использовали планшеты с микролунками. Профили синтеза и экспрессии оценивали с помощью методов иммуноцитохимического окрашивания, ПЦР в реальном времени, а также гистологического окрашивания. Высокие показатели синтеза и экспрессии хондрогенных маркеров Sox9, аггрекана, коллагена II типа наблюдали в сфероидах «долгого», «комбинированного» протоколов и протокола с кондиционированной средой. Хондрогенез наиболее эффективно проходит при использовании «комбинированного» протокола дифференцировки. Высокую эффективность показало также использование кондиционированной среды для индукции и поддержания хондрогенной дифференцировки.

Ключевые слова: тканевая инженерия, суставной хрящ, индуцированные плюрипотентные стволовые клетки (ИПСК), сфероиды, хондрогенез

✉ Для корреспонденции: Артём Валерьевич Еремеев
ул. Малая Пироговская, д. 1а, 119435, г. Москва, Россия; art-eremeev@yandex.ru

Peculiarities of morphology of the hyaline cartilage tissue make its ability to heal rather low. Without proper therapy, most defects of the cartilage caused by trauma, focal lesions or degeneration processes progress, for example, into arthrosis, which negatively affects the quality of life. Cellular technologies that can cover losses of functionally active cells in the damaged tissue area and trigger effective healing offer a promising approach to this problem.

CO.DON, a German company, has been using such cellular technologies in the clinic for over 10 years: the respective protocols of treatment of the damaged articular cartilage rely on autologous chondrocytes, which ensure development of a phenotypically stable cartilage during healing [1–3]. However, transplantation of autologous chondrocytes, although a proven successful approach to the damaged hyaline cartilage restoration, is quite invasive: collection of the donor material requires a biopsy [4, 5]. In addition, the amount of cellular material collected is quite small, which necessitates long-term cultivation that puts the cells at risk of losing chondrogenic qualities and differentiating into fibroblasts, which can lead to fibrosis after transplantation [4, 5]. In connection with these shortcomings, it is especially important to have a selection of alternative cellular resources.

Induced pluripotent stem cells (iPSCs) are one of the promising sources of cellular material. Their properties, such as pluripotency, a wide potential for differentiation into all types of somatic cells, including chondrocytes, as well as the unlimited self-renewal ability, make iPSCs an equivalent of embryonic stem cells (ESCs) that lacks the ethical problems associated with derivation of the latter [4, 6, 7]. Any type of somatic cells of the body can be used to make iPSCs [5, 8].

Chondrocytes differentiated from iPSCs have a juvenile phenotype, which translates into a high proliferation rate and increased production of extracellular matrix (ECM). This quality makes healing of articular defects more effective [4, 5]. Thus, iPSCs are a promising source of cells that can yield a large amount of biomaterial for cellular technologies. However, despite a large number of studies investigating the subject, there is still no standardized protocol that ensures quality chondrogenic differentiation [9]. An actively used method is that of directed differentiation, which roughly reproduces the process of chondrogenesis [10]. The common choice in this context are recombinant proteins that are similar to the main chondroinducers in the developmental processes, as well as various combinations thereof (Fig. 1).

Proteins of the transforming growth factor — (TGFβ) superfamily, such as TGFβ proper and those of the bone morphogenetic protein family (BMP2), are widely used for in vitro chondrogenic differentiation. One study [11] had TGFβ3 as the only differentiation factor, and the resulting chondrogenesis in iPSC cultures was registered as incomplete. Another group of researchers relied on a combination of TGFβ1 and BMP2 [12], and the results they achieved were of better quality. The effectiveness of *in vitro* chondrogenesis may also be increased through differentiation into an MSC-like cell population as a preparative step; this approach was used in the "classic" protocol [3], which implies preliminary induction of mesenchymal precursors with Wnt3a and Activin A. The next step was to induce chondrogenesis using TGFβ1 and BMP2, thus creating cartilage structures with a high expression of chondrogenic markers and a low level of hypertrophy. A similar protocol that differed in longer cultivation time has also yielded effective chondrogenesis; the
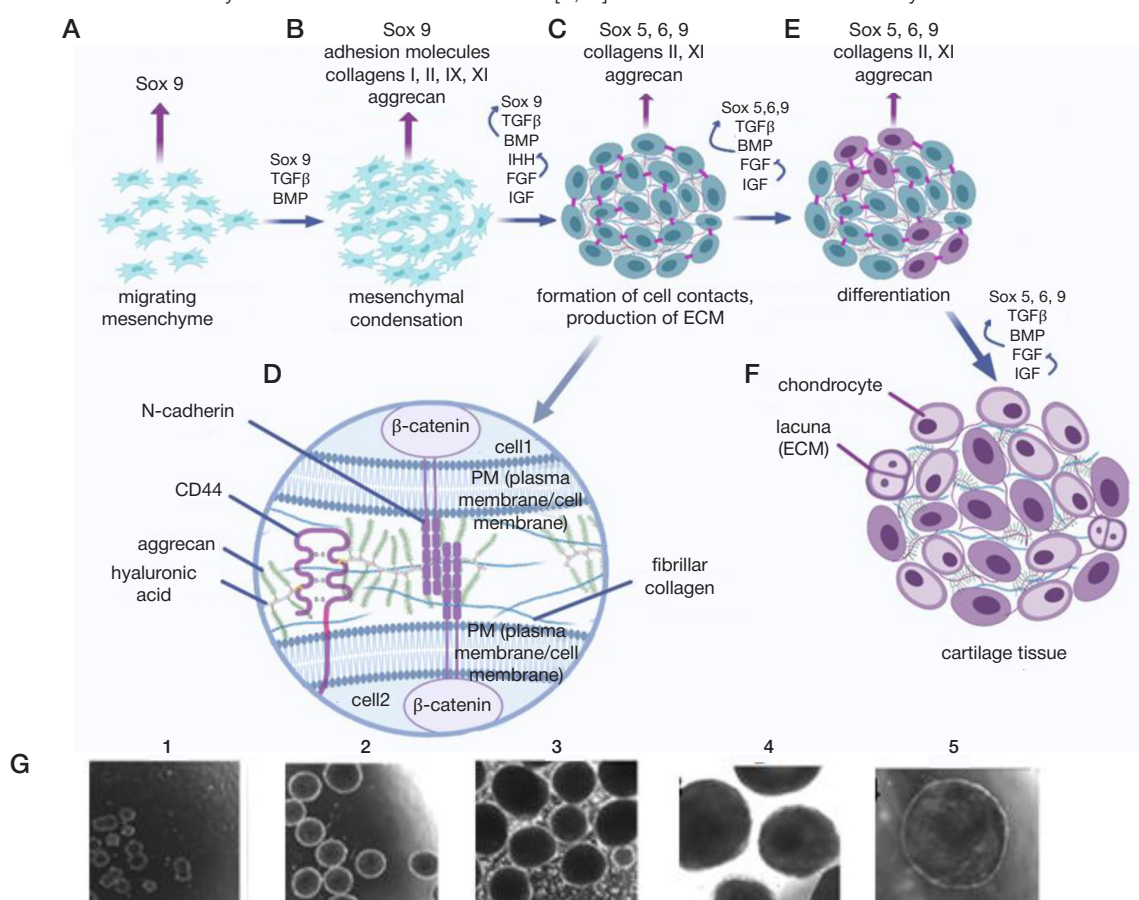
Fig. 1. General sequence of chondrogenesis processes. **A**. Migration of the mesenchyme. **B**. Prechondrogenic mesenchymal condensation. **C**. Formation of cell contacts, synthesis of ECM. **D**. Intercellular space and microenvironment of differentiating cells. **E**. Beginning of chondrogenic differentiation. **F**. Cartilage formation **G**. Phase contrast microscopy pictures, magnification x10: 1–5 — spheroids after 1, 2, 3, 4 and 5 weeks of cultivation, 3D cultivation condition

Table 1. Chondrogenic differentiation protocols

Protocol name	Differentiation (35 days)	
	In monolayer culture (7 days)	In 3D culture (28 days)
"Long"	TGFβ₁, BMP2, FBS 10%	
"Short"	Chir 99021, RA — 2 days RA — 5 days	Base medium with additives
"Combined"		TGFβ1, BMP2, FBS 10%
with conditioned medium		Conditioned medium from chondrocytes, GlutaMAX
Control groups		
Positive control	Base medium with additives, FBS 15%	Base medium with additives, FBS 10%
Negative control	TeSR1, Essential8 (1 : 3)	Base medium without additives

resulting structure was transplanted subcutaneously to a mouse with subsequent formation of a cartilage of a juvenile phenotype with a high content of proteoglycans [4]. Retinoic acid (RA) and retinoids are necessary for the development of limbs, since they trigger activation of Hox genes involved in determining the area of bud formation [13]. *In vitro*, a combination of Chir 99021 (6-[[2-[[4-(2,4-dichlorophenyl)-5-(5-methyl-1H-imidazol-2-yl)-2-pyrimidinyl]amino]ethyl]amino]-3-pyridinecarbonitrile, an inhibitor of glycogen synthase kinase 3 (GSK-3)) and RA promoted directed differentiation into chondrocytes within a short period of time [14]. In addition, low molecular weight compounds are quite simple to use, non-immunogenic and can be efficiently delivered to cells [15].

The standard 2D culture approach does not match the natural environment of the cells and limits differentiation significantly [16]. Both in vivo and *in vitro*, cells need a 3D environment.

One of the common methods of 3D cell cultivation and differentiation is the production of spheroids [17, 18]. Spheroid cultures were shown to significantly improve cell proliferation while maintaining the phenotype and key signals [16, 19]. Moreover, this 3D culturing technique mimics the process of mesenchymal condensation at the early stage of cartilage development [20]. There are various methods yielding spheroids, including the hanging drop method [21, 22], centrifugation of a suspension of cells of certain density [23–25], self-aggregation into spheroids in suspension cultures [2], formation in U-shaped microwell plates [26–28], as well as methods involving biomaterials [29, 30]. The finished constructs can be effectively cultured under dynamic conditions, for example, in a 3D orbital shaker [8].

In this work, we followed four protocols of the 3D spheroid culturing method to form cartilage tissue. Two of the four protocols were developed by our laboratory. The main purpose of this study was to identify and compare the features of the resulting structures and single out the most effective way of differentiation.

METHODS

iPSC cultures

We used the FD4S iPSC line derived from human skin fibroblasts by the method described in [41], using a non-integrating Sendai viral vector carrying the genes of transcription factors OCT3/4, SOX2, KLF4, and C-MYC. The cells were cryopreserved at –80 °C.

Cultivation was conducted at 37 °C with CO_2 at 5%, in a mixture of growth media without a mTeSR1 feeder (STEMCELL Technologies; Canada) and Essential 8 (Thermo Fisher Scientific; USA), at a 1 : 3 ratio, with 40 µg/ml of gentamicin (PanEco; Russia). The medium was changed once a day. Upon appearance of a monolayer, we subcultured the culture at 1 : 3 ratio; to improve cell viability after this procedure, we used 10 µM of the Y27632 Rock kinase inhibitor (StemMACS, Miltenyi Biotec; Germany).

Differentiation protocols

Chondrogenic differentiation of iPSCs was conducted following the four tested protocols (Table 1):
- "long" [3];
- "short" [14];
- "combined";
- with conditioned medium.

Cultures of human chondrocytes and fragments of human articular cartilage were used as a positive control. Cultures of iPSCs and 3D structures from them served as negative control.

Monolayer cultures

Monolayer iPSC cultures were differentiated for 7 days in Advanced DMEM base medium (Gibco, Thermo Fisher Scientific; USA) supplemented with 10 ng/ml of bFGF (STEMCELL Technologies; Canada), 100× GlutaMAX (Gibco, Thermo Fisher Scientific; USA), 50x B27 (Gibco, Thermo Fisher Scientific; USA), 1% insulin transferrin selenite (ITS) (PanEco; Russia), 50 µg/ml ascorbic acid (Sigma Aldrich; USA), 50 µM β-mercaptoethanol, 5 µg/ml plasmacin, gentamicin (PanEco; Russia) and 40 µg/ml gentamicin solution (PanEco; Russia).

For the "long" protocol we also added 10 ng/ml of TGFβ1 (Miltenyi Biotec; Germany), 10 ng/ml of BMP2 and 10% FBS to the base medium. For the "short", "combined" and conditioned medium protocols the supplements were 10 µM of Chir 99021 (Miltenyi Biotec; Germany) and 10 nM of RA (Sigma Aldrich; USA) introduced together for two days, and after that — only 10 nM of RA.

The medium was changed once a day. On the third or fourth day we subcultured the cultures at the ratio of 1:3 with a 0.25% trypsin solution.

The previously obtained culture of human chondrocytes was thawed from the cryobank of the Federal Research And Clinical Center of Physical-Chemical Medicine. The process implied heating the cryovial in a water bath until the ice completely disappeared and then washing the DMSO cryoprotector off the cells in 10 ml of pure Advanced DMEM medium preheated to +37 °C, the washing done by centrifuging in a 15 ml test tube (Servicebio; China) at 1000 RPM for 5 min. The precipitate with chondrocytes was diluted for subsequent cultivation in Advanced DMEM supplemented with 15% FBS or 10% human serum. The medium was changed every 4 days; the conditioned medium was taken out and filtered twice through syringe filters (0.45 µm pore and 0.22 µm pore, respectively).

3D cultures

The spheroids were formed in AggreWell 800 microwell plates (STEMCELL Technologies; Canada) with Anti-Adherence Rinsing Solution (STEMCELL Technologies; Canada); we followed the protocol provided by the manufacturer [31].

Factoring in the number of cells, we added 1 or 2 ml of medium with 10 μM Y27632, as per the protocol of chondrogenic differentiation in 3D cultures, seeking to reach the concentration of $1–1.5 \times 10^6$ cells/ml. Each well of a plate contained 1 ml of this suspension. The plates with cells evenly distributed in microwells were incubated at 37°C with CO_2 at 5% for 24 h.

To prepare Petri dishes for cultivation of spheroids we applied chloroform-plastic glue strictly to the center of 60 mm Ultra Low Attachment Petri dishes (Corning Inc.; USA). The applied chloroform-plastic glue had the shape of a drop with the diameter of about 1 cm. Then, the cups without lids were placed under ultraviolet light for 6 hours. Before use, we rinsed the surface several times with Versene solution [32].

After 24 h of incubation in microwell plates, we carefully collected spherical cell aggregates using pipettes with tips cut off (to avoid damage to the spheroids) and then transferred them to prepared Petri dishes, the medium therein as per the differentiation protocol. Dishes with spheroids were subjected to dynamic processing in a 3D orbital shaker at 37°C and with CO_2 at 5%.

For the differentiation of 3D cultures under the "long", "short" and "combined" protocols, as well as to cultivate the positive control spheroids, we used the Advanced DMEM base medium supplemented with 10 ng/ml of bFGF (STEMCELL Technologies; Canada), 100× GlutaMAX (Gibco , Thermo Fisher Scientific; USA), 50× B27 (Gibco, Thermo Fisher Scientific; USA), 1% insulin-transferrin selenite (ITS) (PanEco; Russia), 50 μg/ml of ascorbic acid (Sigma Aldrich; USA), 50 μM of β-mercaptoethanol, 5 μg/ml of plasmacin, gentamicin (PanEco; Russia) and 10 ml/L 100x penicillin/streptomycin solution (PanEco; Russia). For the "long" and "combined" protocols we also added 10 ng/ml of TGFβ1 (Miltenyi Biotec; Germany), 10 ng/ml of BMP2, 10% FBS to the medium. For the conditioned medium protocol we used the conditioned medium from a culture of human articular chondrocytes supplemented with 200x GlutaMAX. For cultivation of the positive control spheroids the medium was supplemented with 10% FBS. Negative control spheroids were cultured in Advanced DMEM supplemented with antibiotics and 200x GlutaMAX.

The period of differentiation of spheroids was 28 days. The medium was changed every 4 days. We evaluated morphology of the spheroids every 7 days using an Olympus IX53F phase contrast microscope (Olympus; Japan) and CellSens Standart morphometry software.

Immunofluorescence analysis

For the purposes of immunocytochemical staining of 3D cultures, every 7 days of cultivation we transferred the spheroids into 48-well plates that had bottoms of wells preliminarily covered with a 0.1% gelatin solution. Within 1 to 2 days, the spheroids attached and spread over the surface.

Monolayer cultures fixed with 4% paraformaldehyde (PFA) and attached organelles were treated with 0.1% Triton as follows: for 20 minutes in order to stain for the nuclear marker; for 10 minutes — to stain for the surface and cytoplasmic markers. After permeabilization, the cultures were treated (for 30 minutes) with a 0.01 M PBS blocking solution containing 3% goat serum and 0.1% Tween.

Monolayer cultures, as well as spheroids at all stages of differentiation, were stained with primary antibodies to the nuclear marker of chondrogenesis Sox 9 (Rabbit, 1 : 400, Invitrogen; Thermo Fisher Scientific, USA), to the proteoglycan cartilage ECM marker agrecan (Mouse, 1 : 500, Invitrogen; Thermo Fisher Scientific, USA), fibrillar ECM hyaline cartilage marker type II collagen (Rabbit, 1 : 200; Abcam, UK) and fibrocartilage marker type I collagen (Rabbit, 1 : 800, Invitrogen; Thermo Fisher Scientific, USA), as well as the surface marker of CD105 prechondrogenic mesenchyme (Human, 1 : 500; Sony, Japan). At room temperature, the staining with primary antibody solutions based on blocking solution lasted for 1.5 hours, while at 4 °C the duration thereof was 12 hours.

Alexa Fluor 488 (Goat, Anti-Mouse, 1 : 500), Alexa Fluor 555 (Goat, Anti-Rabbit, 1 : 500), and Alexa Fluor 546 (Goat, Anti-Human, 1 : 500) were used for staining with secondary antibodies (Invitrogen; Thermo Fisher Scientific, USA). The process lasted 1 hour and was conducted in the dark. Nuclei were stained with 100 ng/ml DAPI (Sigma Aldrich; USA).

Stained preparations were examined using an Olympus IX53F fluorescence microscope with four fluorescence filters (Olympus; Japan) and CellSens Standard morphometry software.

Real-time polymerase chain reaction (PCR)

To initiate cell lysis in monolayer cultures and spheroids we used RLT buffer (QIAGEN; Germany) supplemented with 10 μl/ml of β-mercaptoethanol. Spheroids, in batches of 3 to 5 pieces, depending on their size, and monolayer cultures were pipetted into 600 μl of RLT for lysing.

To isolate the total RNA, we used RNeasy Plus Mini Kit (QIAGEN; Germany) following the instructions supplied therewith [33]. Total RNA was purified from genomic DNA with the help of DNase solution (SibEnzyme; Russia)

MMLV RT kit (Evrogen; Russia) was used, as described in the manual [34], to synthesize the first cDNA strand from the RNA template.

For real-time PCR, we added 5 μl of 5× qPCRmix-HS SYBR (Evrogen; Russia), 0.8 μl of 10 μM primer, 18.2 μl of water and 1 μl of cDNA matrix (Table 2) to each well of a 96-well plate (SSIbio, Scientific Specialties; USA), . The reaction was enabled by a C10000 Touch version of 1000 CFX Manager nucleic acid amplification thermal cycler (Bio-Rad; USA) and CFX Manager software. The number of cycles was 39. SYBR (Evrogen; Russia) was used as the probe. To increase specificity of the reaction we used a "hot start" polymerase, HS Taq DNA polymerase (Evrogen; Russia), and selected the optimal primer annealing temperature (60 °C). cDNA

Table 2. Primers used in the work

Gene name	Sequence 5'→3'	Product length, b.p.
SOX9	F: GAAGTCGGTGAAGAACGGGC R: CACGTCGCGGAAGTCGATAG	283
ACAN	F: AGGAGTCCCTGACCTGGTTT R: CCTGACAGATCTGCCTCTCC	167
COL1A2	F: AGGGTGAGACAGGCGAACA R: CCGTTGAGTCCATCTTTGC	184
COL2A1	F: TGGACGCCATGAAGGTTTTCT R: CCATTGATGGTTTCTCCAAACC	142
YWHAZ	F: ACTTTTGGTACATTGTGGCTTCAA R: CCGCCAGGACAAACCAGTAT	94
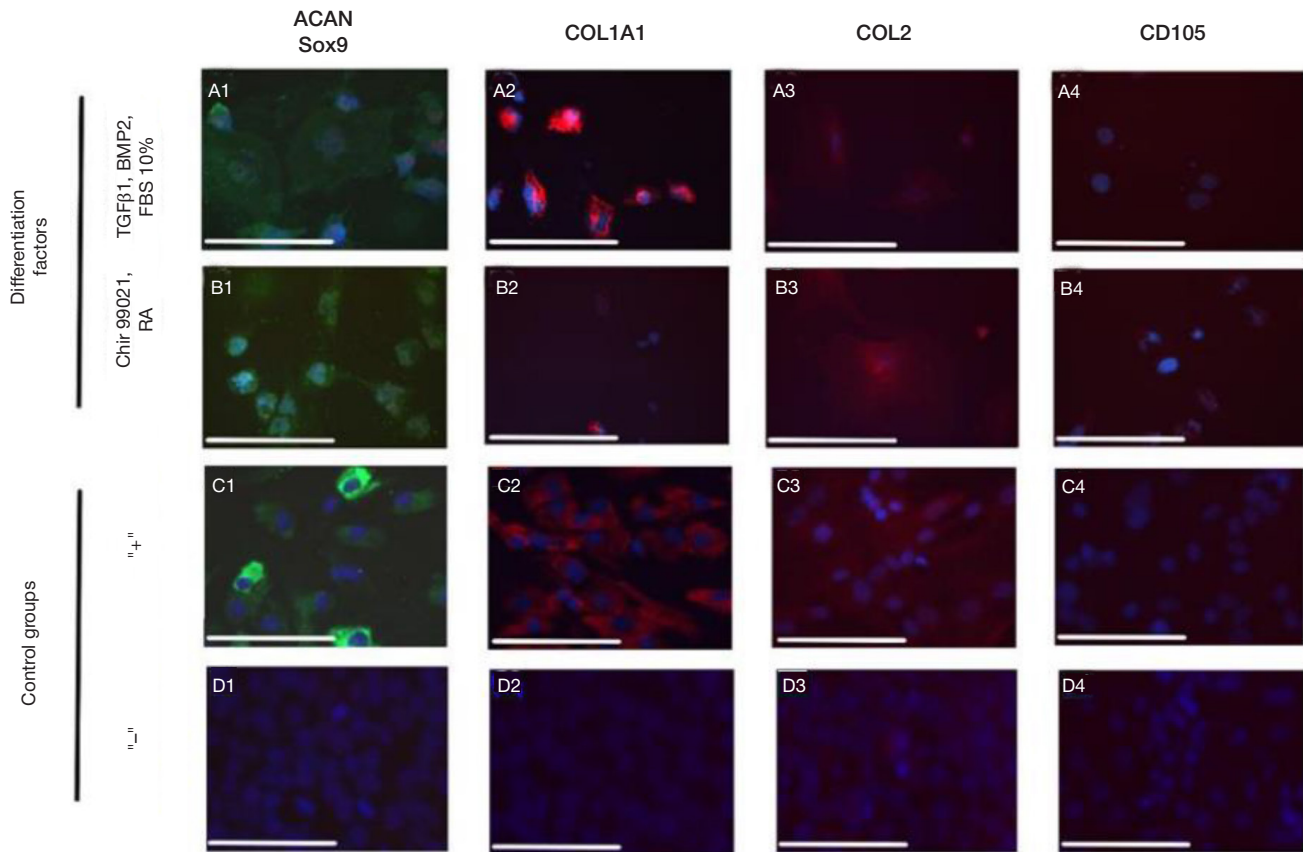
Fig. 2. Immunocytochemical analysis of monolayer cultures. **A**. Use of TGFβ1, BMP2 and 10% FBS. **B**. Using Chir99021 and RA. **C**. Articular chondrocyte culture, positive control. **E**. FD4S iPSC culture, negative control. 1 — aggrecan (*green*) and Sox9 (*red*), 2 — type I collagen (red), 3 — type II collagen (*red*), 4 — CD105 (*red*). Scale bar — 200 microns

isolated from iPSCs was used as a negative control in assessment of specificity of the reaction once the results were available.

Microsoft Excel enabled analysis of the results (ΔΔCt method). Mean values and confidence intervals are shown. For statistical analysis, we used the Welch's t-test that accounts for the possible differences in standard deviations of means of two groups of independent samples.

Histological analysis

To make paraffin sections, we sequentially fixed spheroids and fragments of cartilage, treated them with xylene and ethanol (concentrations of 70, 80, 96, and 100%) to dehydrate and degrease, and poured liquid paraffin. Then we cut series of paraffin sections 4 µm thick. Cryosections of spheroids (7 µm thick) were prepared according to the protocol described earlier [35]. For that purpose, we used the Shandon Cryotome FSE resin (Thermo Fisher Scientific; USA) to form a histological block. The sections were stained with hematoxylin-eosin, picrosirius red, and safranin O. After staining they were dehydrated and embedded in polystyrene.

The photographed of the sections were taken with a DM4000 B LED microscope (Leica; Germany).

RESULTS

Differentiation in monolayer cultures

Undifferentiated iPSC cultures were dense colonies of small cells with a high nuclear-cytoplasmic ratio; the morphology of such colonies was described earlier [36]. On the second day of differentiation by exposure to Chir 99021 and RA

or recombinant factors TGFβ1, BMP2, and 10% FBS, the cells assumed a rounded shape. Following the Chir 99021 differentiation protocols, we registered growth in cell mortality, which was assessed by staining with a trypan blue solution (the volume of dead cells that included the dye reached 30–35% of the population). On the 4th day of differentiation the cells assumed a polygonal and elongated shape. On the 7th day we noticed individual populations of chondrocyte-like cells that had a rounded shape and a large nucleus. Also, on the second and third day of differentiation we observed budding cell clusters in the experimental group cultures, the effect especially pronounced in cultures differentiated according to the Chir 99021 protocol.

Analyzing the results of immunocytochemistry we discovered a significant fluorescence on the part of aggrecan and type I and II collagens in monolayer cultures obtained following protocols implying the use of both recombinant factors TGFβ1 and BMP2 and Chir 99021 and RA (Fig. 2). However, the Sox9 synthesis was most effective in cultures differentiated with the help of TGFβ1 and BMP2 (Fig. 2A1). As for the CD105 mesodermal marker, it synthesis was low in experimental and control groups (Fig. 2A4–E4), although a small signal was observed in cultures differentiated with Chir 99021 (Fig. 2B4).

The analysis of results of real-time PCR revealed that the indicators of expression of chondrogenic markers in the samples were comparable to those registered in the positive control group. The use of protein factors TGFβ1 and BMP2 made the expression of SOX9 higher than application of Chir 99021 and RA (Fig. 3).

Differentiation in spheroid cultures

Immediately after the formed cell aggregates were put in 3D cultivation conditions they acquired an irregular shape and their
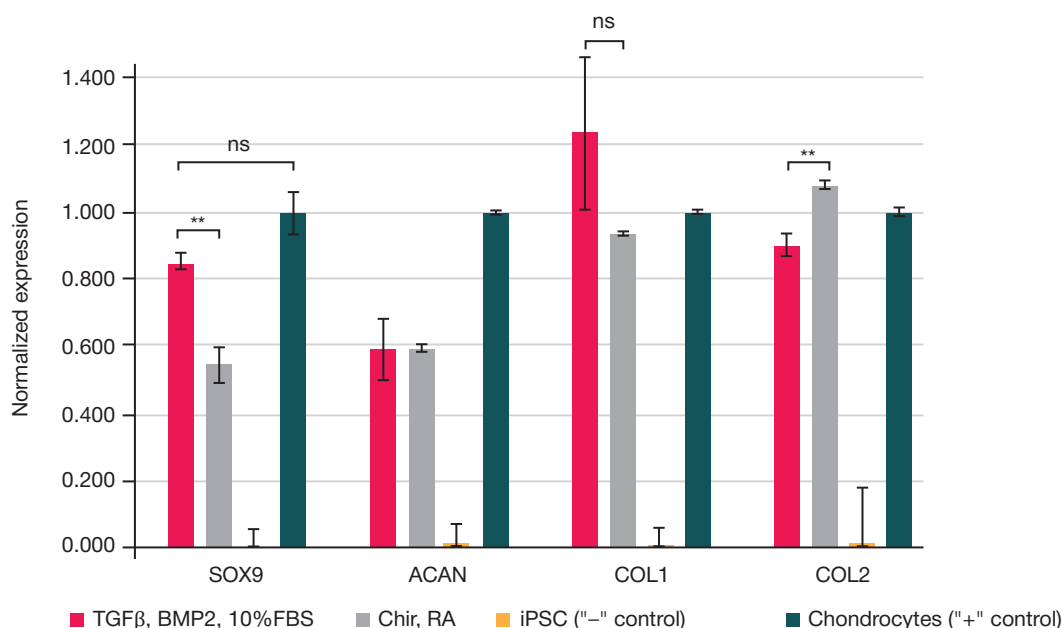
Fig. 3. Indicators of gene expression of chondrogenic markers in monolayer cultures. Error bar is the standard deviation. Significance of differences between groups: ns, $p > 0.05$; * — $p < 0.05$; ** — $p < 0.01$; *** — $p < 0.001$

ACAN, SOX9
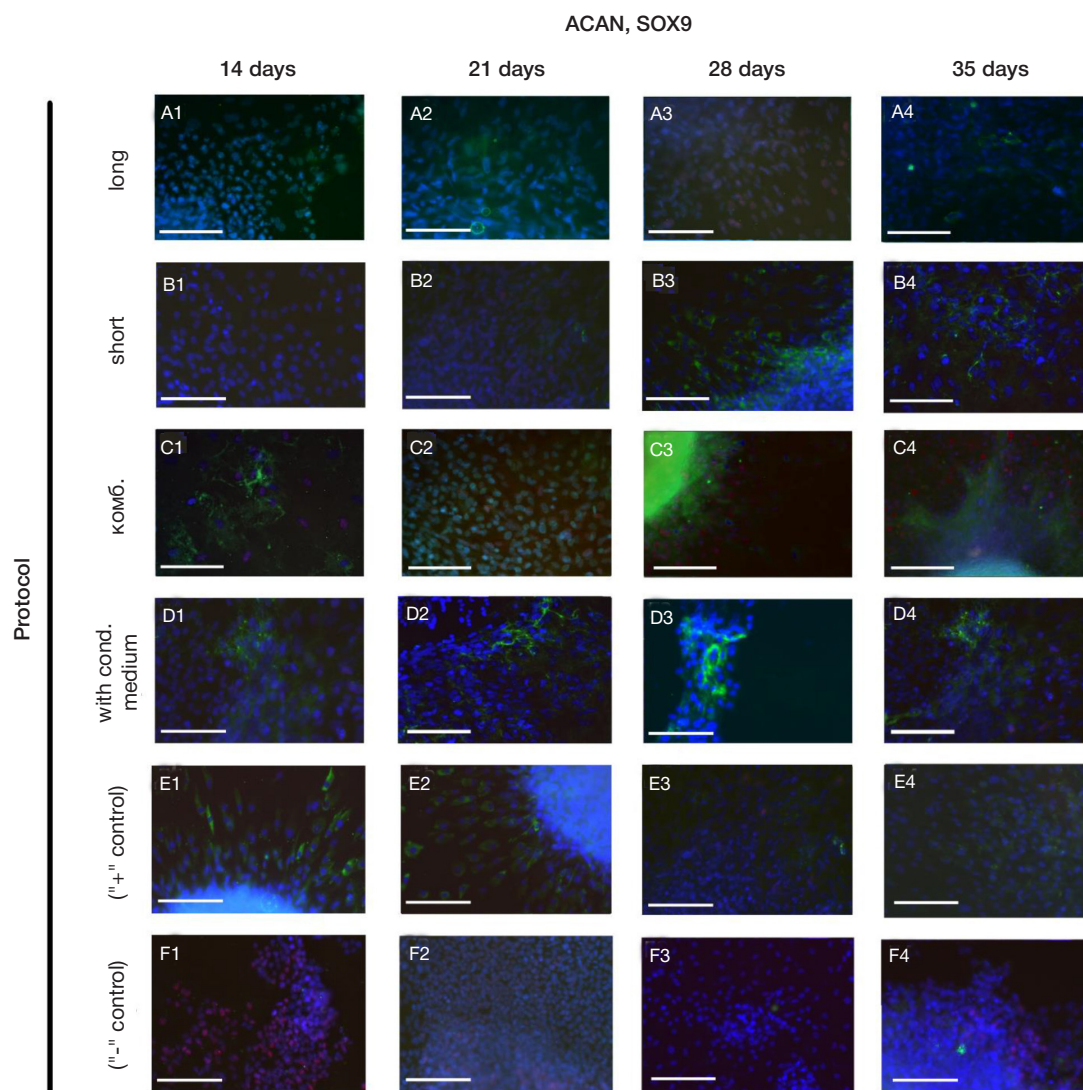
Fig. 4. Immunocytochemical analysis of aggrecan (*green*) and Sox9 (*red*) synthesis in 3D spheroid cultures of different protocols. **A–D**. Differentiation protocols: "long" (**A**), "short" (**B**), "combined" (**C**), with conditioned medium (**D**). **E**. Spheroids of the positive control group. **F**. Spheroids of the negative control group. Duration of differentiation: 1 — 14 days, 2 — 21 days, 3 — 28 days, 4 — 35 days. Scale bar — 200 microns
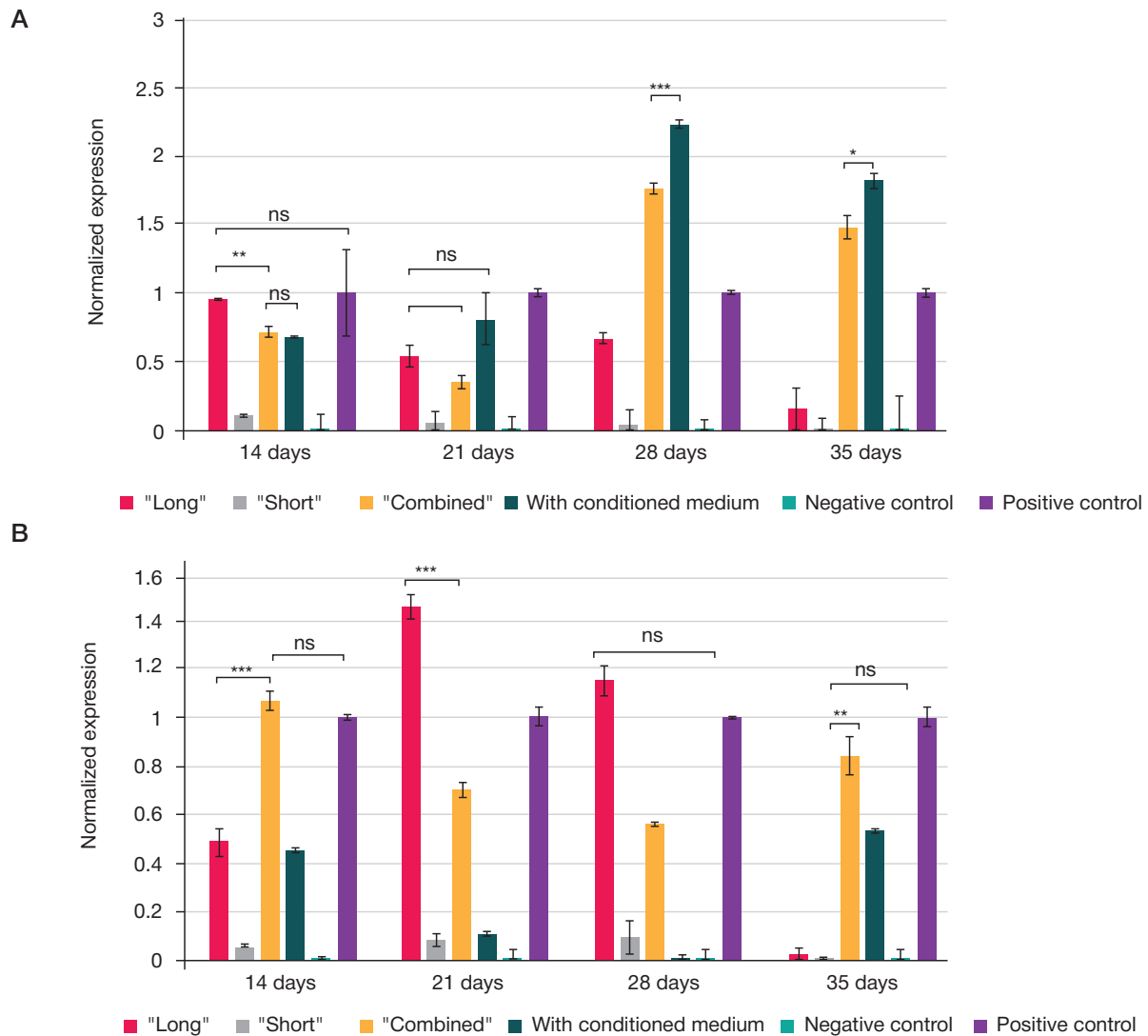
Fig. 5. A. ACAN expression indicators in 3D spheroid cultures of various protocols. **B**. SOX9 expression indicators. Abscissa, duration of differentiation; ordinate, value of normalized expression. Error bar is the standard deviation. Significance of differences between groups: ns, $p > 0.05$; * — $p < 0.05$; ** — $p < 0.01$; *** — $p < 0.001$

surface became uneven, but on the 35th day of differentiation all spheroids (all protocol groups and control groups) became whitish translucent structures with a smooth shiny surface (Fig. 1G). The only exception were the cultures developing in 3D cultivation conditions following the conditioned medium protocol.

On the 14th and 21st day of differentiation we observed nonintense fluorescence of aggrecan in the constructs of cultures of spheroids cultivated in 3D conditions, all protocols (Fig. 4). The highest fluorescence intensity of this marker was recorded on days 28 and 35 in spheroids of the "combined" protocol (Fig. 4B3, 4). On the 21st and 28th days we also registered a high level of synthesis of aggrecan in spheroids obtained following the conditioned medium protocol (Fig. 4D1–3). In the "long", "combined" and conditioned medium protocols the level of ACAN expression was comparable to that in the spheroids of the positive control group. At the same time, on the 28th and 35th days of differentiation, ACAN expression significantly increased in the spheroids of "combined" and conditioned medium protocols (Fig. 5A).

The synthesis of Sox9 was observed in rspheroids formed following the "combined" protocol at each step, and the intensity of fluorescence of this marker was increasing as differentiation progressed (Fig. 4B1–4). As for other protocols, we registered intense Sox9 fluorescence signals on the 28th day in the "long"

protocol spheroids and on the 35th day in the conditioned medium protocol spheroids (Fig. 4A3, D4). The fluorescence associated with this marker was also seen in spheroids of the negative control group (Fig. 4E1–4). The results of PCR analysis of SOX9 expression show its comparability with the indicators peculiar to the positive control group in samples of the "long" and "combined" protocol groups (Fig. 5B).

The intensity of fluorescence of type I collagen was recorded as high in all experimental groups, but the highest values were registered in the "long" and "combined" protocol groups. The expression of COL1A2 increased with the progress of differentiation in spheroids of all protocol groups (Fig. 6A). The highest rates were observed in the "long" and "combined" protocol group samples.

In the spheroids formed following "long", "combined" and conditioned medium protocols the observed intensity of fluorescence of type II collagen was high, and it can be said that it increased with time. The expression of COL2A1 was pronounced in spheroids of all differentiation protocol groups (Fig. 6B). The maximum values were registered in the samples of "long" and "combined" protocol groups: they were several times greater than expression seen in the positive control group.

The synthesis of CD105 was detected at the beginning of cultivation under 3D conditions. The fluorescence of this marker was well expressed in the "long" and "combined"

A

"Long"   "Short"   "Combined"   With conditioned medium   Negative control   Positive control

B

"Long"   "Short"   "Combined"   With conditioned medium   Negative control   Positive control
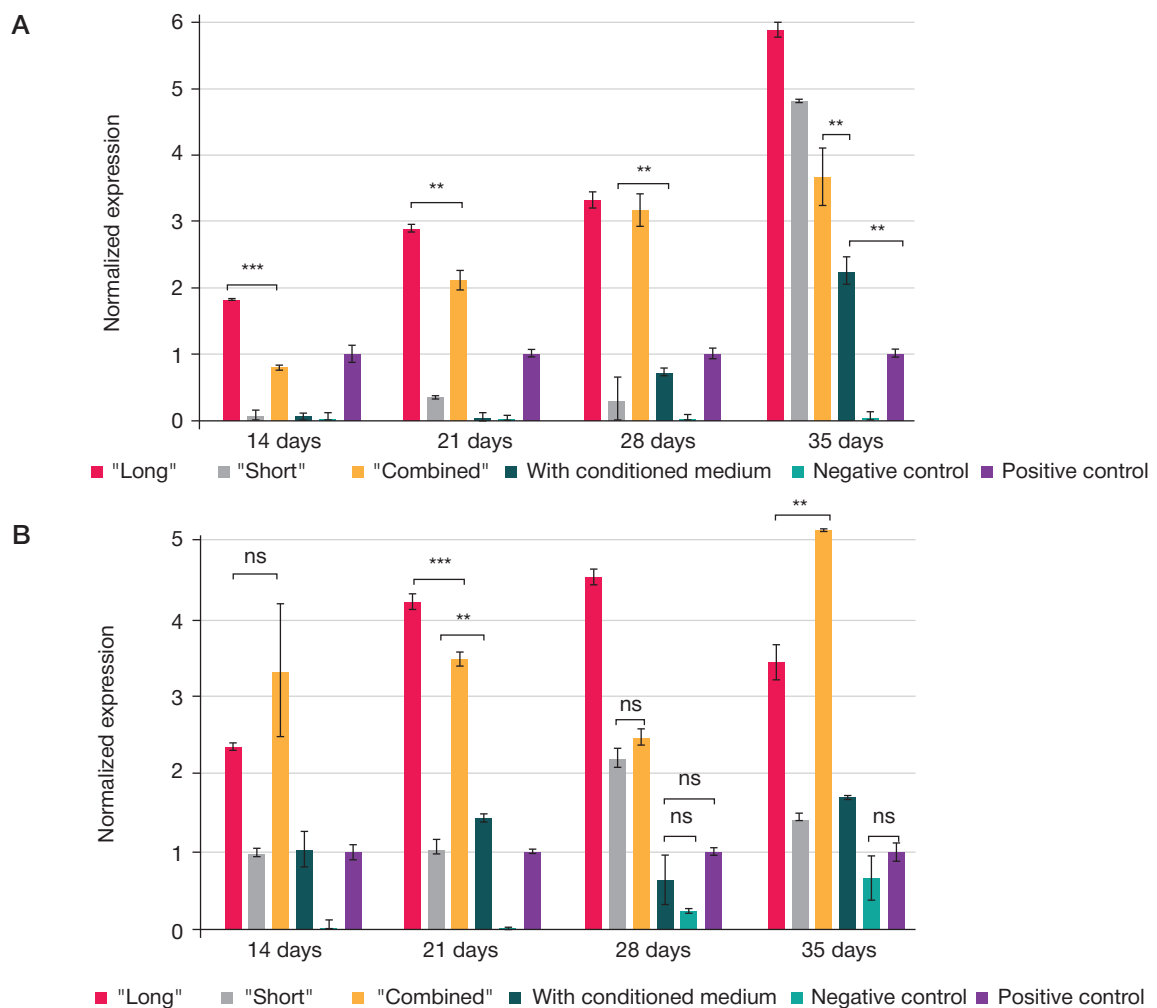
Fig. 6. A. COL1A2 expression indicators in 3D spheroid cultures of various protocols. **B**. COL2A1 expression indicators. Abscissa, duration of differentiation; ordinate, value of normalized expression. Error bar is the standard deviation. Significance of differences between groups: ns, $p > 0.05$; * — $p < 0.05$; ** — $p < 0.01$; *** — $p < 0.001$

protocol spheroids, but it significantly decreased by the end of differentiation.

Examining the sections of "long" and "combined" protocol spheroids stained with picrosirius red we saw bright pink collagen fibers covering the entire area of said sections (Fig. 7). However, staining of spheroids of all protocol groups with safranin O was not intense (Fig. 7).

DISCUSSION

Comparing the morphological characteristics of monolayer cultures, we noted that iPSC differentiation can be induced with both Chir 99021 and RA and TGFβ, BMP2, and 10% FBS. The elongated polygonal shape the cells assume on the 4th day may indicate that their morphology becomes MSC-like
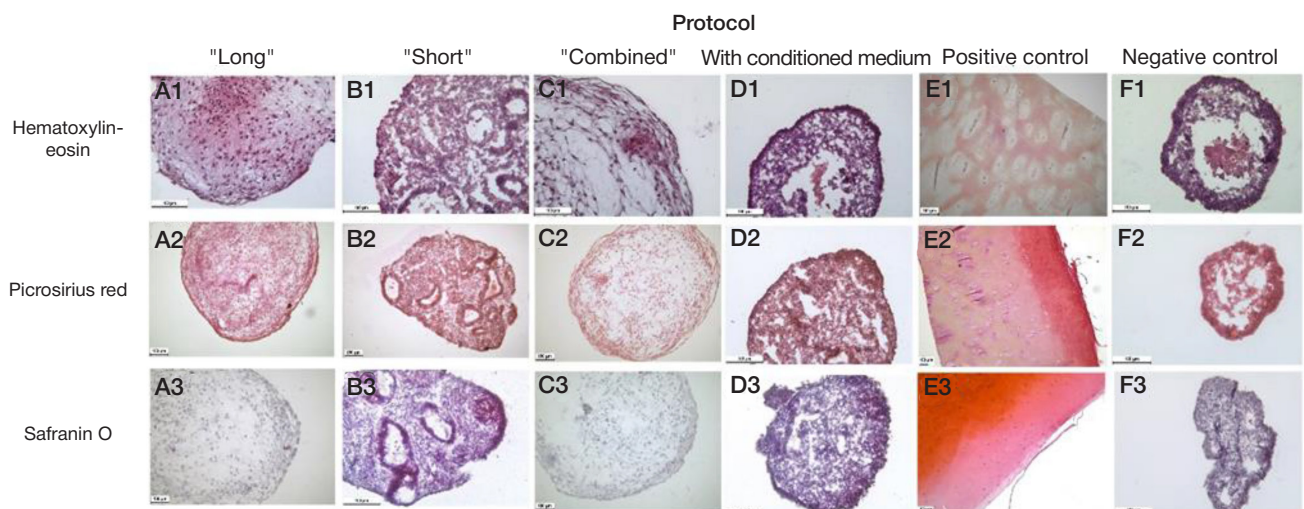
Protocol

Fig. 7. Histological analysis of 3D spheroid cultures of different differentiation protocols. Differentiation protocols: "long" (**A**), "short" (**B**), "combined" (**C**), with conditioned medium (**D**). Control groups: positive control (fragments of articular cartilage) (**E**), negative control (**F**). Type of histological staining: 1 — hematoxylin-eosin, 2 — picrosirius red, 3 — safranin O

during chondrogenic induction. The increased cell death that we observed in cultures differentiated with Chir 99021 and RA is most likely associated with the action of Chir 99021, since, as shown in the past experiments, this molecule enhances apoptotic activity [14]. Self-aggregation of cells with the formation of hyaline-like structures peculiar to the early stages of chondrogenic differentiation, when adhesion molecules actively form and accumulate (10).

The positive effect exogenous presence of TGFβ1 and BMP2 has on the synthesis and expression of Sox9 in monolayer cultures is most likely the result of participation of these molecules in stimulation and stabilization of production of this transcription factor [37]. Since Chir 99021 mimics mesoderm-inducing signals, the presence of CD105 can be explained by similarity of the culture, at that stage of differentiation, to the early prechondrogenic mesenchyme [1, 14]. It can be concluded that use of both TGFβ1, BMP2, and 10% FBS and Chir 99021 and RA triggers fairly efficient differentiation in monolayer cultures.

Microwell plates were used to make spheroids. In such plates, cell aggregation is gravity-driven, which may lead to formation of cell conglomerates of irregular shapes [27]. Cartilage structures that were obtained by other researchers from spheroid cultures were ultimately translucent and whitish, with a smooth surface [3]. At the final stages of cultivation, the spheroids of all protocol groups except for the conditioned medium group has similar characteristics. The exception may be the result of a slower compaction rate, which disallows the outer layer cells to generate a sufficient number of intercellular contact molecules.

In our study, the expression of chondrogenic markers in groups using TGFβ1 and BMP2 were fairly high. In addition, we saw spontaneous differentiation of iPSCs in negative control spheroids, which coincided with registration of fluorescent signals of Sox9 and type II collagen, as well as expression of COL2A1. The production of cartilage ECM is largely a mechanodependent process, therefore, we could observe the synthesis of type II collagen in response to the presence of cells in dynamic conditions [38, 39].

The synthesis of CD105 in spheroid cultures on the 14th and 21st days can be explained by the transition from MSC-like to chondrocyte phenotype, which was happening as cells in spheroids were differentiating. *in vivo*, CD105, along with other surface markers such as CD34, CD44, and CD45, is one of the markers characteristic of prechondrogenic mesenchymal cells [1, 40].

The increased synthesis and expression of type I collagen in spheroids of all protocol groups indicate that the resulting cartilage structures have a mixed phenotype, combining hyaline and fibrous tissues. The strongest expression of COL1A2 was observed in spheroids formed following the protocols that used 10% FBS. Some studies mention the fibrotic effect of serum associated with the increased synthesis of type I collagen, so it is likely that the high levels of this collagen may be conditioned by its presence in the differentiation medium [41, 42].

Histological analysis revealed no significant presence of the proteoglycan matrix in preparations stained with safranin O. In this connection, it can be assumed that the resulting structures are similar to cartilage at an early stage of chondrogenesis. Probably, generation of a greater amount of proteoglycan matrix that would be detectable with the help of safranin O requires longer culturing. Previous research has shown that on the 28th day of cultivation spheroids could be stained with safranin O marginally, while on the 42th day such staining was intense [3].

CONCLUSIONS

Our study yielded samples of cartilage tissue formed following four protocols. A comparative analysis of these protocols has shown that chondrogenesis is most effective in cultures of 3D spheroids differentiated under a "combined" protocol, which, as we suggest, relies on Chir 99021 and RA for differentiation of monolayer cultures and TGFβ1, BMP2 and 10% FBS for differentiation of spheroid cultures. High rates of synthesis and expression of chondrogenic markers were also registered in constructs obtained following the "long" and conditioned medium protocols. The use of conditioned medium, obtained from the primary culture of chondrocytes from donor tissue and exposed to Chir 99021 and RA, increases the efficacy of differentiation. In our opinion, use of a conditioned medium reduces the cost of the technology, but complicates its standardization the because of the variability of different cultures of chondrocytes obtained from different donors. This problem can be solved by using cultures of chondrocytes derived iPSCs. This protocol needs further optimization, as it enables formation of cartilage samples with a mixed phenotype that combine characteristics of both hyaline and fibrous cartilage, as is the case with immature tissue in the early stages of chondrogenesis. Nevertheless, samples of cartilage tissue obtained using the studied protocols can be effectively used to model the processes of chondrogenesis in basic research. After optimization of the differentiation protocols, it is possible to use the resulting cartilage structures to make prototype cell products for preclinical and, possibly, subsequent clinical testing.

References

1. Diederichs S, Gabler J, Autenrieth J. Differential regulation of SOX9 protein during chondrogenesis of induced pluripotent stem cells versus mesenchymal stromal cells: a shortcoming for cartilage formation. Stem Cells and Development. 2016; (April): 1–34.
2. Tsumaki N, Okada M, Yamashita A. iPS cell technologies and cartilage regeneration. Bone. 2015; 70: 48–54. Available from: http://dx.doi.org/10.1016/j.bone.2014.07.011.
3. Yamashita A, Morioka M, Yahara Y, Okada M, Kobayashi T, Kuriyama S, et al. Generation of scaffoldless hyaline cartilaginous tissue from human iPSCs. Stem Cell Reports. 2015; 4 (3): 404–18.
4. Kimura T, Yamashita A, Ozono K, Tsumaki N. Limited Immunogenicity of Human Induced Pluripotent Stem Cell-Derived Cartilages. Tissue Engineering — Part A. 2016; 22 (23–24): 1367–75.
5. Lietman SA. Induced pluripotent stem cells in cartilage repair.

World Journal of Orthopedics. 2016; 7 (3): 149–55.
6. Narsinh KH, Plews J, Wu JC. Comparison of human induced pluripotent and embryonic stem cells: Fraternal or identical twins? Molecular Therapy. 2011; 19 (4): 635–8. Available from: http://dx.doi.org/10.1038/mt.2011.41/nature06264.
7. Cheng B, Tu T, Shi X, Liu Y, Zhao Y, Zhao Y, et al. A novel construct with biomechanical flexibility for articular cartilage regeneration. Stem Cell Research and Therapy. 2019; 10 (1): 1–16.
8. Limraksasin P, Kosaka Y, Zhang M, Horie N, Kondo T, Okawa H, et al. Shaking culture enhances chondrogenic differentiation of mouse induced pluripotent stem cell constructs. Scientific Reports. 2020; 10 (1): 1–15. Available from: https://doi.org/10.1038/s41598-020-72038-y.
9. Suchorska WM, Augustyniak E, Richter M, Trzeciak T. Comparison

of Four Protocols to Generate Chondrocyte-Like Cells from Human Induced Pluripotent Stem Cells (hiPSCs). Stem Cell Reviews and Reports. 2017; 13 (2): 299–308.

10. Castro-Viñuelas R, Sanjurjo-Rodríguez C, Piñeiro-Ramil M, Hermida-Gómez T, Fuentes-Boquete IM, de Toro-Santos FJ, et al. Induced pluripotent stem cells for cartilage repair: Current status and future perspectives. European Cells and Materials. 2018; 36 (2006): 96–109.

11. Qu C, Puttonen KA, Lindeberg H, Ruponen M, Hovatta O, Koistinaho J, et al. Chondrogenic differentiation of human pluripotent stem cells in chondrocyte co-culture. International Journal of Biochemistry and Cell Biology. 2013; 45 (8): 1802–12.

12. Chijimatsu R, Ikeya M, Yasui Y, Ikeda Y, Ebina K, Moriguchi Y, et al. Characterization of Mesenchymal Stem Cell-Like Cells Derived from Human iPSCs via Neural Crest Development and Their Application for Osteochondral Repair. Stem Cells International. 2017: 1–18.

13. Karen Niederreither JV, Vermot J, Schuhbaur B, Chambon P, Dollé P. Embryonic retinoic acid synthesis is required for forelimb growth andanteroposterior patterning in the mouse. Development. 2002: 129 (15): 3563–74.

14. Kawata M, Mori D, Kanke K, Hojo H, Ohba S, Chung U il, et al. Simple and Robust Differentiation of Human Pluripotent Stem Cells toward Chondrocytes by Two Small-Molecule Compounds. Stem Cell Reports. 2019; 13 (3): 530–44.

15. Kreuser U, Buchert J, Haase A, Richter W, Diederichs S. Initial WNT/β-Catenin Activation Enhanced Mesoderm Commitment, Extracellular Matrix Expression, Cell Aggregation and Cartilage Tissue Yield From Induced Pluripotent Stem Cells. Frontiers in Cell and Developmental Biology. 2020; 8: 581331. DOI: 10.3389/fcell.2020.581331.

16. Lee NH, Bayaraa O, Zechu Z, Kim HS. Biomaterials-assisted spheroid engineering for regenerative therapy. BMB Reports. 2021; 54 (7): 356–67.

17. Martin I, Suetterlin R, Baschong W, Heberer M, Vunjak-Novakovic G, Freed LE. Enhanced cartilage tissue engineering by sequential exposure of chondrocytes to FGF-2 during 2D expansion and BMP-2 during 3D cultivation. J Cell Biochem. 2001; 83 (1): 121–8. DOI: 10.1002/jcb.1203.

18. Kim J, Tomida K, Matsumoto T, Adachi T. Spheroid culture for chondrocytes triggers the initial stage of endochondral ossification. Biotechnol Bioeng. 2022; 119 (11): 3311–8. DOI: 10.1002/bit.28203.

19. Sulaiman S, Chowdhury SR, Fauzi MB, Rani RA, Mohamadyahaya NH, Tabata Y, et al. 3d culture of MSCS on a gelatin microsphere in a dynamic culture system enhances chondrogenesis. International Journal of Molecular Sciences. 2020; 21 (8): 1–17.

20. Gionet-Gonzales MA, Leach JK. Engineering principles for guiding spheroid function in the regeneration of bone, cartilage, and skin. Biomedical Materials (Bristol). 2018; 13 (3): 034109. DOI: 10.1088/1748-605X/aab0b3.

21. Sridharan BP, Laflin AD, Detamore MS. Generating Chondromimetic Mesenchymal Stem Cell Spheroids by Regulating Media Composition and Surface Coating. Cellular and Molecular Bioengineering. 2018; 11 (2): 99–115.

22. Wang G, An Y, Zhang X, Ding P, Bi H, Zhao Z. Chondrocyte Spheroids Laden in GelMA/HAMA Hybrid Hydrogel for Tissue-Engineered Cartilage with Enhanced Proliferation, Better Phenotype Maintenance, and Natural Morphological Structure. Gels. 2021; 7 (4): 247. Available from: https://www.mdpi.com/2310-2861/7/4/247.

23. Jang Y, Jung H, Ju JH. Chondrogenic differentiation induction of adipose-derived stem cells by centrifugal gravity. Journal of Visualized Experiments. 2017; 2017 (120). DOI: 10.3791/54934.

24. Jang J, Lee J, Lee E, Lee EA, Son Y. Disc-type hyaline cartilage reconstruction using 3D-cell sheet culture of human bone marrow stromal cells and human costal chondrocytes and maintenance of its shape and phenotype after transplantation. Tissue Engineering

25. Salonius E, Kontturi L, Laitinen A, Haaparanta AM, Korhonen M, Nystedt J, et al. Chondrogenic differentiation of human bone marrow-derived mesenchymal stromal cells in a three-dimensional environment. Journal of Cellular Physiology. 2020; 235 (4): 3497–507.

26. Markway BD, Tan GK, Brooke G, Hudson JE, Cooper-White JJ, Doran MR. Enhanced chondrogenic differentiation of human bone marrow-derived mesenchymal stem cells in low oxygen environment micropellet cultures. Cell Transplantation. 2010; 19 (1): 29–42.

27. Rogan H, Ilagan F, Yang F. Comparing Single Cell Versus Pellet Encapsulation of Mesenchymal Stem Cells in Three-Dimensional Hydrogels for Cartilage Regeneration. Tissue Engineering — Part A. 2019; 25 (19–20): 1404–12.

28. Zhang M, Shi J, Xie M, Wen J, Niibe K, Zhang X, et al. Recapitulation of cartilage/bone formation using iPSCs via biomimetic 3D rotary culture approach for developmental engineering. Biomaterials. 2020; 260. DOI: 10.1016/j.biomaterials.

29. Zhang K, Yan S, Li G, Cui L, Yin J. In-situ birth of MSCs multicellular spheroids in poly(L-glutamic acid)/chitosan scaffold for hyaline-like cartilage regeneration. Biomaterials. 2015; 71: 24–34.

30. Stuart MP, Matsui RAM, Santos MFS, Côrtes I, Azevedo MS, Silva KR, et al. Successful low-cost scaffold-free cartilage tissue engineering using human cartilage progenitor cell spheroids formed by micromolded nonadhesive hydrogel. Stem Cells International. 2017; 2017. DOI: 10.1155/2017/7053465. Epub 2017 Dec 20.

31. STEMCELL Technologies. Reproducible and Uniform Embryoid Bodies Using AggreWellTM Plates. 2011. Available from: https://www.stemcell.com/media/files/brochure/BR29150-AggreWell_Reproducible_Uniform_Embryoid_Bodies.pdf.

32. Eremeev AV, Volovikov EA, Shuvalova LD, Davi denko AV, Khomyakova EA, Bogomiakova ME, Lebedeva OS, Zubkova OA, Lagarkova MA. "Necessity is the Mother of Invention" or Inexpensive, Reliable, and Reproducible Protocol for Generating Organoids. Biochemistry (Moscow). 2019; 84 (3): 321–28. DOI: 10.1134/S0006297919030143.

33. QIAGEN. RNeasy ® Plus Mini Handbook. 2020, 47 p. https://www.qiagen.com/us/resources/resourcedetail?id=16b8f578-d192-4613-ae32-8e02e0b0fa77&lang=en

34. Evrogen. MMLV RT kit. 2021. Available from: www.evrogen.ru. Russian.

35. Molecular Cellular and Developmental Biology. Cryostat Procedure. 2012; 5 p. Available from: https://labs.mcdb.ucsb.edu/fisher/steven/Website/protocols/Cryosectioning.pdf.

36. Shuvalova LD, Eremeev AV, Bogomazova EV, Novosadova EV, Zerkalenkova EA, Olshanskaya YV, et al. Generation of induced pluripotent stem cell line RCPCMi004-A derived from patient with Parkinson's disease with deletion of the exon 2 in PARK2 gene. Stem Cell Res. 2020; 44: 101733. DOI: 10.1016/j.scr.2020.101733.

37. Goldring MB, Tsuchimochi K, Ijiri K. The control of chondrogenesis. Journal of Cellular Biochemistry. 2006; 97: 33–44.

38. Rutgers M, Saris DB, Vonk LA, van Rijen MH, Akrum V, Langeveld D, et al. Effect of collagen type I or type II on chondrogenesis by cultured human articular chondrocytes. Tissue Engineering — Part A. 2013; 19 (1–2): 59–65.

39. Theodoropoulos JS, DeCroos AJN, Petrera M, Park S, Kandel RA. Mechanical stimulation enhances integration in an in vitro model of cartilage repair. Knee Surgery, Sports Traumatology, Arthroscopy. 2016; 24 (6): 2055–64.

40. Endo K, Fujita N, Nakagawa T, Nishimura R. Effect of Fibroblast Growth Factor-2 and Serum on Canine Mesenchymal Stem Cell Chondrogenesis. Tissue Engineering — Part A. 2019; 25 (11–12): 901–10.

41. Wu CL, Dicks A, Steward N, Tang R, Katz DB, Choi YR, et al. Single cell transcriptomic analysis of human pluripotent stem cell chondrogenesis. Nature Communications. 2021; 12 (1): 1–18.

and Regenerative Medicine. 2016; 13 (4): 352–63.

Литература

1. Diederichs S, Gabler J, Autenrieth J. Differential regulation of SOX9 protein during chondrogenesis of induced pluripotent stem cells versus mesenchymal stromal cells: a shortcoming for cartilage formation. Stem Cells and Development. 2016; (April): 1–34.

2. Tsumaki N, Okada M, Yamashita A. iPS cell technologies and cartilage regeneration. Bone. 2015; 70: 48–54. Available from: http://dx.doi.org/10.1016/j.bone.2014.07.011.

3. Yamashita A, Morioka M, Yahara Y, Okada M, Kobayashi T, Kuriyama S, et al. Generation of scaffoldless hyaline cartilaginous tissue from human iPSCs. Stem Cell Reports. 2015; 4 (3): 404–18.

4. Kimura T, Yamashita A, Ozono K, Tsumaki N. Limited Immunogenicity of Human Induced Pluripotent Stem Cell-Derived Cartilages. Tissue Engineering — Part A. 2016; 22 (23–24): 1367–75.

5. Lietman SA. Induced pluripotent stem cells in cartilage repair. World Journal of Orthopedics. 2016; 7 (3): 149–55.

6. Narsinh KH, Plews J, Wu JC. Comparison of human induced pluripotent and embryonic stem cells: Fraternal or identical twins? Molecular Therapy. 2011; 19 (4): 635–8. Available from: http://dx.doi.org/10.1038/mt.2011.41/nature06264.

7. Cheng B, Tu T, Shi X, Liu Y, Zhao Y, Zhao Y, et al. A novel construct with biomechanical flexibility for articular cartilage regeneration. Stem Cell Research and Therapy. 2019; 10 (1): 1–16.

8. Limraksasin P, Kosaka Y, Zhang M, Horie N, Kondo T, Okawa H, et al. Shaking culture enhances chondrogenic differentiation of mouse induced pluripotent stem cell constructs. Scientific Reports. 2020; 10 (1): 1–15. Available from: https://doi.org/10.1038/s41598-020-72038-y.

9. Suchorska WM, Augustyniak E, Richter M, Trzeciak T. Comparison of Four Protocols to Generate Chondrocyte-Like Cells from Human Induced Pluripotent Stem Cells (hiPSCs). Stem Cell Reviews and Reports. 2017; 13 (2): 299–308.

10. Castro-Viñuelas R, Sanjurjo-Rodríguez C, Piñeiro-Ramil M, Hermida-Gómez T, Fuentes-Boquete IM, de Toro-Santos FJ, et al. Induced pluripotent stem cells for cartilage repair: Current status and future perspectives. European Cells and Materials. 2018; 36 (2006): 96–109.

11. Qu C, Puttonen KA, Lindeberg H, Ruponen M, Hovatta O, Koistinaho J, et al. Chondrogenic differentiation of human pluripotent stem cells in chondrocyte co-culture. International Journal of Biochemistry and Cell Biology. 2013; 45 (8): 1802–12.

12. Chijimatsu R, Ikeya M, Yasui Y, Ikeda Y, Ebina K, Moriguchi Y, et al. Characterization of Mesenchymal Stem Cell-Like Cells Derived from Human iPSCs via Neural Crest Development and Their Application for Osteochondral Repair. Stem Cells International. 2017: 1–18.

13. Karen Niederreither JV, Vermot J, Schuhbaur B, Chambon P, Dollé P. Embryonic retinoic acid synthesis is required for forelimb growth andanteroposterior patterning in the mouse. Development. 2002: 129 (15): 3563–74.

14. Kawata M, Mori D, Kanke K, Hojo H, Ohba S, Chung U il, et al. Simple and Robust Differentiation of Human Pluripotent Stem Cells toward Chondrocytes by Two Small-Molecule Compounds. Stem Cell Reports. 2019; 13 (3): 530–44.

15. Kreuser U, Buchert J, Haase A, Richter W, Diederichs S. Initial WNT/β-Catenin Activation Enhanced Mesoderm Commitment, Extracellular Matrix Expression, Cell Aggregation and Cartilage Tissue Yield From Induced Pluripotent Stem Cells. Frontiers in Cell and Developmental Biology. 2020; 8: 581331. DOI: 10.3389/fcell.2020.581331.

16. Lee NH, Bayaraa O, Zechu Z, Kim HS. Biomaterials-assisted spheroid engineering for regenerative therapy. BMB Reports. 2021; 54 (7): 356–67.

17. Martin I, Suetterlin R, Baschong W, Heberer M, Vunjak-Novakovic G, Freed LE. Enhanced cartilage tissue engineering by sequential exposure of chondrocytes to FGF-2 during 2D expansion and BMP-2 during 3D cultivation. J Cell Biochem. 2001; 83 (1): 121–8. DOI: 10.1002/jcb.1203.

18. Kim J, Tomida K, Matsumoto T, Adachi T. Spheroid culture for chondrocytes triggers the initial stage of endochondral ossification. Biotechnol Bioeng. 2022; 119 (11): 3311–8. DOI: 10.1002/bit.28203.

19. Sulaiman S, Chowdhury SR, Fauzi MB, Rani RA, Mohamadyahaya NH, Tabata Y, et al. 3d culture of MSCS on a gelatin microsphere in a dynamic culture system enhances chondrogenesis. International Journal of Molecular Sciences. 2020; 21 (8): 1–17.

20. Gionet-Gonzales MA, Leach JK. Engineering principles for guiding spheroid function in the regeneration of bone, cartilage, and skin. Biomedical Materials (Bristol). 2018; 13 (3): 034109. DOI: 10.1088/1748-605X/aab0b3.

21. Sridharan BP, Laflin AD, Detamore MS. Generating Chondromimetic Mesenchymal Stem Cell Spheroids by Regulating Media Composition and Surface Coating. Cellular and Molecular Bioengineering. 2018; 11 (2): 99–115.

22. Wang G, An Y, Zhang X, Ding P, Bi H, Zhao Z. Chondrocyte Spheroids Laden in GelMA/HAMA Hybrid Hydrogel for Tissue-Engineered Cartilage with Enhanced Proliferation, Better Phenotype Maintenance, and Natural Morphological Structure. Gels. 2021; 7 (4): 247. Available from: https://www.mdpi.com/2310-2861/7/4/247.

23. Jang Y, Jung H, Ju JH. Chondrogenic differentiation induction of adipose-derived stem cells by centrifugal gravity. Journal of Visualized Experiments. 2017; 2017 (120). DOI: 10.3791/54934.

24. Jang J, Lee J, Lee E, Lee EA, Son Y. Disc-type hyaline cartilage reconstruction using 3D-cell sheet culture of human bone marrow stromal cells and human costal chondrocytes and maintenance of its shape and phenotype after transplantation. Tissue Engineering and Regenerative Medicine. 2016; 13 (4): 352–63.

25. Salonius E, Kontturi L, Laitinen A, Haaparanta AM, Korhonen M, Nystedt J, et al. Chondrogenic differentiation of human bone marrow-derived mesenchymal stromal cells in a three-dimensional environment. Journal of Cellular Physiology. 2020; 235 (4): 3497–507.

26. Markway BD, Tan GK, Brooke G, Hudson JE, Cooper-White JJ, Doran MR. Enhanced chondrogenic differentiation of human bone marrow-derived mesenchymal stem cells in low oxygen environment micropellet cultures. Cell Transplantation. 2010; 19 (1): 29–42.

27. Rogan H, Ilagan F, Yang F. Comparing Single Cell Versus Pellet Encapsulation of Mesenchymal Stem Cells in Three-Dimensional Hydrogels for Cartilage Regeneration. Tissue Engineering — Part A. 2019; 25 (19–20): 1404–12.

28. Zhang M, Shi J, Xie M, Wen J, Niibe K, Zhang X, et al. Recapitulation of cartilage/bone formation using iPSCs via biomimetic 3D rotary culture approach for developmental engineering. Biomaterials. 2020; 260. DOI: 10.1016/j.biomaterials.

29. Zhang K, Yan S, Li G, Cui L, Yin J. In-situ birth of MSCs multicellular spheroids in poly(L-glutamic acid)/chitosan scaffold for hyaline-like cartilage regeneration. Biomaterials. 2015; 71: 24–34.

30. Stuart MP, Matsui RAM, Santos MFS, Côrtes I, Azevedo MS, Silva KR, et al. Successful low-cost scaffold-free cartilage tissue engineering using human cartilage progenitor cell spheroids formed by micromolded nonadhesive hydrogel. Stem Cells International. 2017. 2017; DOI: 10.1155/2017/7053465. Epub 2017 Dec 20.

31. STEMCELL Technologies. Reproducible and Uniform Embryoid Bodies Using AggreWellTM Plates. 2011. Available from: https://www.stemcell.com/media/files/brochure/BR29150-AggreWell_Reproducible_Uniform_Embryoid_Bodies.pdf.

32. Eremeev AV, Volovikov EA, Shuvalova LD, Davi denko AV, Khomyakova EA, Bogomiakova ME, Lebedeva OS, Zubkova OA, Lagarkova MA. "Necessity is the Mother of Invention" or Inexpensive, Reliable, and Reproducible Protocol for Generating Organoids. Biochemistry (Moscow). 2019; 84 (3): 321–28. DOI: 10.1134/S0006297919030143.

33. QIAGEN. RNeasy ® Plus Mini Handbook. 2020, 47 p. https://www.qiagen.com/us/resources/resourcedetail?id=16b8f578-d192-4613-ae32-8e02e0b0fa77&lang=en

34. Евроген. MMLV RT kit. 2021. Available from: www.evrogen.ru.

35. Molecular Cellular and Developmental Biology. Cryostat Procedure. 2012; 5 p. Available from: https://labs.mcdb.ucsb.edu/fisher/steven/Website/protocols/Cryosectioning.pdf.

36. Shuvalova LD, Eremeev AV, Bogomazova AN, Novosadova EV, Zerkalenkova EA, Olshanskaya YV, et al. Generation of induced pluripotent stem cell line RCPCMi004-A derived from patient

with Parkinson's disease with deletion of the exon 2 in PARK2 gene. Stem Cell Res. 2020; 44: 101733. DOI: 10.1016/j.scr.2020.101733.

37. Goldring MB, Tsuchimochi K, Ijiri K. The control of chondrogenesis. Journal of Cellular Biochemistry. 2006; 97: 33–44.

38. Rutgers M, Saris DB, Vonk LA, van Rijen MH, Akrum V, Langeveld D, et al. Effect of collagen type I or type II on chondrogenesis by cultured human articular chondrocytes. Tissue Engineering — Part A. 2013; 19 (1–2): 59–65.

39. Theodoropoulos JS, DeCroos AJN, Petrera M, Park S, Kandel RA.

Mechanical stimulation enhances integration in an in vitro model of cartilage repair. Knee Surgery, Sports Traumatology, Arthroscopy. 2016; 24 (6): 2055–64.

40. Endo K, Fujita N, Nakagawa T, Nishimura R. Effect of Fibroblast Growth Factor-2 and Serum on Canine Mesenchymal Stem Cell Chondrogenesis. Tissue Engineering — Part A. 2019; 25 (11–12): 901–10.

41. Wu CL, Dicks A, Steward N, Tang R, Katz DB, Choi YR, et al. Single cell transcriptomic analysis of human pluripotent stem cell chondrogenesis. Nature Communications. 2021; 12 (1): 1–18.

ASSESSMENT OF CYTOTOXICITY AND ANTIVIRAL ACTIVITY AGAINST SARS-COV-2 OF THE MIXTURE OF LACTOFERRIN, ARTEMISININ, AND AZITHROMYCIN *IN VITRO*

Ryabchenkova AA[1]✉, Kopat VV[1], Chirak ER[1], Chirak EL[1], Leneva IA[2], Glubokova EA[2], Kartashova NP[2], Kolmakov NN[3], Dukhovlinov IV[1]

[1] ATG Service Gen LLC, St. Petersburg, Russia

[2] Mechnikov Research Institute of Vaccines and Sera, Moscow, Russia

[3] Institute of Experimental Medicine, St. Petersburg, Russia

Lactoferrin, artemisinin, and azithromycin exhibit a broad spectrum of antiviral, immunomodulatory, and anti-inflammatory effects. The experiments show that these drugs partially inhibit the infection caused by SARS-CoV-2 *in vitro*. This allows us to conclude that the effects on the entry of virions into cells mediated by each of these substances taken separately are insufficient for complete inhibition of the SARS-CoV-2 infection. The study was aimed to perform *in vitro* assessment of cytotoxicity and antiviral activity against the laboratory SARS-CoV-2 strain of the mixture of active ingredients: lactoferrin, artemisinin, and azithromycin. We used the Vero CCL81 (ATCC) cell line and the Dubrovka laboratory strain of SARS-CoV-2 (GenBank ID: MW161041.1), isolated in the Vero CCL81 cell culture from the nasopharyngeal swab of patient with COVID-19. Cytotoxic effects and antiviral activity against SARS-CoV-2 of the drug mixture were assessed based on the cytopathic effects using the MTT (methylthiazolyldiphenyl-tetrazolium bromide) assay. Hydroxychloroquine was used as a reference drug. It has been shown that at high (MOI 100) and low (MOI 20) multiplicity of infection used in the Vero CCL 81 cell culture, the mixture of artemisinin, lactoferrin and azithromycin has a significant effect on the SARS-CoV-2 reproduction, and IC50 (half maximal inhibitory concentration) is estimated as the 1 : 2 dilution in both cases. The findings make it possible to conclude that the studied mixture is low toxic and shows significant antiviral effects *in vitro*.

Keywords: artemisinin, azithromycin, lactoferrin, cytotoxicity, antiviral activity, SARS-CoV-2, COVID-19, drug repurposing

✉ **Correspondence should be addressed:** Anastasia A. Ryabchenkova
Prospect Maly V.O., 57, k. 4, litera Zh, k. 5-H, St. Petersburg, 199178, Russia; riabchenkova@service-gene.ru

ОЦЕНКА ЦИТОТОКСИЧНОСТИ И ПРОТИВОВИРУСНОЙ АКТИВНОСТИ СМЕСИ ЛАКТОФЕРРИНА, АРТЕМИЗИНИНА И АЗИТРОМИЦИНА В ОТНОШЕНИИ SARS-COV-2 *IN VITRO*

А. А. Рябченкова[1]✉, В. В. Копать[1], Е. Р. Чирак[1], Е. Л. Чирак[1], И. А. Ленева[2], Е. А. Глубокова[2], Н. П. Карташова[2], Н. Н. Колмаков[3], И. В. Духовлинов[1]

[1] Общество с ограниченной ответственностью «АТГ Сервис Ген», Санкт-Петербург, Россия

[2] Научно-исследовательский институт вакцин и сывороток имени И. И. Мечникова Минобрнауки России, Москва, Россия

[3] Институт экспериментальной медицины Минобрнауки России, Санкт-Петербург, Россия

Лактоферрин, артемизинин и азитромицин обладают широким спектром противовирусного, иммуномодулирующего и противовоспалительного действия. Экспериментально показанное частичное ингибирование ими инфекции, вызванной SARS-CoV-2 *in vitro*, позволяет заключить, что влияния на проникновение вирионов в клетки, опосредованное каждым из этих веществ в отдельности, недостаточно для полного ингибирования инфекции SARS-CoV-2. Целью работы было оценить *in vitro* цитотоксичность и противовирусную активность смеси активных действующих веществ лактоферрина, артемизинина и азитромицина в отношении лабораторного штамма SARS-CoV-2. Использовали перевиваемую культуру клеток Vero CCL81 (ATCC) и лабораторный штамм коронавируса SARS-CoV-2 «Дубровка» (идентификационный № GenBank: MW161041.1), выделенный на культуре клеток Vero CCL81 из назофарингеального мазка больного COVID-19. Определение цитотоксического действия смеси препаратов и изучение противовирусной активности в отношении вируса SARS-CoV-2 оценивали по эффекту цитопатического действия с использованием MTT (метилтиазолилдифенил-тетразолия бромид). В качестве препарата сравнения использовали гидроксихлорохин. Показано, что при высокой множественности заражения (100 MOI) и низкой (20 MOI) в культуре клеток Vero CCL81 смеси артемизинина, лактоферрина и азитромицина оказывает значимый эффект на вирусную репродукцию SARS-CoV-2, ИК50 (полумаксимальная ингибирующая концентрация) оценивается в обоих случаях как разведение 1 : 2. Полученные результаты позволяют сделать вывод о низкой цитотоксичности изучаемой смеси и о наличии значимого противовирусного действия *in vitro*.

Ключевые слова: артемизинин, азитромицин, лактоферрин, цитотоксичность, противовирусная активность, SARS-CoV-2, COVID-19, перепрофилирование препарата

✉ **Для корреспонденции:** Анастасия Андреевна Рябченкова
пр-кт Малый В. О., д. 57, к. 4, литера Ж, помещение 5-Н, г. Санкт-Петербург, 199178, Россия; riabchenkova@service-gene.ru

Currently, the issue of the spread of COVID-19 coronavirus infection caused by SARS-CoV-2 is still relevant. Despite the fact that timely vaccination can decrease the risk of severe infection, the development of additional safeguard that can either alleviate severe course or prevent COVID-19 infection is still a priority, especially because antibodies against vaccine antigens may not recognize new variants of the virus.

To date, COVID-19 prevention and treatment consist primarily of the use and development of vaccines for the formation of neutralizing antibodies binding spike protein, immune sera and monoclonal antibodies, antiviral drugs [1], and drugs directed against hyperactivation of the immune response [2] along with the symptomatic supportive treatment and respiratory support of the infected individuals. During the fight against the COVID-19 pandemic, special attention was paid to drug repurposing, since the known safety and pharmacokinetic profiles allowed for timely introduction of the drugs, in contrast to the new medications that required full scale testing and registration. Currently, the most recent (16th) update of the Temporary Guidelines on the "Prevention, Diagnosis, and Treatment of Novel Coronavirus Infection (COVID-19)" includes favipiravir, molnupiravir, nirmatrelvir + ritonavir, remdesivir, and umifenovir as the direct-acting antiviral agents. Biotechnology medications are also recommended: interferon alpha, synthetic small interfering ribonucleic acid (double-stranded) [3]. However, the clinical trials of these drugs used for treatment of COVID-19 are limited and often controversial, there is no indisputable evidence and experience of using the drugs. The presence of multiple mutations in the S protein suggests its capability of acquiring new ligand specificity properties [4].

The mechanism underlying the SARS-CoV-2 cell entry, that is associated with the angiotensin converting enzyme 2 (ACE2), is a complex multifactorial process that involves many accessory molecules: proteinases, co-receptors and activators of their expression. Availability of co-receptors allows SARS-CoV-2 to infect cells with low ACE2 expression on the membranes.

Thus, as a glycoprotein, S protein can interact with receptors not only via its protein component, but also by binding to the lectin receptors via its carbohydrate component (N-glycans of S1 subunit containing oligomannose and complex carbohydrates that protect the virus against antibodies) [5, 6]. Binding of the lectin-like S1 sites to the target cell glycocalyx via O-acetylated sialic acids [7] and heparan sulfate [8] may facilitate cell infection. It has been shown that heparan sulfate promotes cell entry in viruses of many types [9], including SARS-CoV-2 [10]. The majority of polysaccharide chains found in the heparan sulfate proteoglycans are strongly negatively charged. This makes it possible to recruit SARS-CoV-2 viral particles on the cell surface due to interaction with S protein, thereby increasing its local concentration for further binding to ACE2. There are reasons to believe that the positively charged binding groove located in the S protein RBD domain might be the putative binding site for negatively charged polysaccharide chains of the heparan sulfate proteoglycans [8, 11], and the binding specificity depends largely on the complementary spatial arrangement of the main protein groups and of sulfate and carboxyl groups on the polysaccharide [12–14].

As for strong inhibitors of the SARS-CoV-2 cell entry, the drug repurposing screening has made it possible to identify a number of compounds targeting the heparan sulfate proteoglycans and dependent on them endocytosis pathways. One such compound is lactoferrin (LF), the naturally occurring non-toxic glycoprotein that is available as dietary supplement [15].

Assessment of the LF antiviral activity in the model of the human colon adenocarcinoma cell line Caco-2 and monkey kidney epithelial cell line Vero 6 infected with coronavirus has shown that LF partially inhibits infection and SARS-CoV-2 replication [16]. A number of studies focused on assessing the effects of LF binding with to the receptor show that binding affects various signaling systems and pathways, including NF-κB and various interferon regulatory factors. This results in modulation of antiviral immune response [17]. The effects of LF on regulation of TLR, especially TLR3 and TLR7, involved in recognition of RNA viruses [18, 19] and inhibition of cathepsin L [20] have been also shown. These result in blocking the SARS-CoV-2 entry into the human embryonic kidney 293/hACE2 cells [21]. The experimental study [16] shows that LF can inhibit the TGFB1 immunosuppressive cytokine expression, suppress the expression of thymic stromal lymphopoietin, high levels of which have been found on the bronchial mucosa of patients with asthma and chronic obstructive pulmonary disease, and reduce the expression of pro-inflammatory cytokines IL1B and IL6. These immunomodulatory effects of LF may counteract the cytokine storm activation.

Azithromycin that affects a variety of processes is one more promising repurposed drug. First of all, azithromycin affecting the decline in the expression of matrix metalloproteinases related to CD147 attracted attention of the researchers, who hypothesised that azithromycin was capable of inhibiting CD147 and eventually blocking viral entry into host cells [22]. It has been shown that CD147 induces the PI3K/AKT signaling pathway activation, thus promoting NF-κB induction and production of pro-inflammatory cytokines [23, 24]. The PI3K/AKT signaling pathway increases the TMPRSS2 serine protease expression, thus enchancing viral entry.

Immunomodulatory properties of azithromycin [25] may play a vital part in treatment of hyperinflammation caused by cytokine storm associated with COVID-19. *In vitro* studies of azithromycin have shown the decreased secretion of pro-inflammatory cytokines and chemokines [26, 27]. Furthermore, azithromycin reduces accumulation of inflammatory cell infiltrates in the bronchoalveolar lavage fluid [28]. In fibroblasts, azithromycin inhibits proliferation and collagen production by reducing the concentration of transforming growth factor (TGFβ) and demonstration of pulmonary antifibrotic activity [29, 30]. Azithromycin exhibits mucoregulatory effects: it reduces mucus hypersecretion and improves mucociliary clearance [31].

Research has shown that azithromycin can modify ACE2 glycosylation, thus preventing SARS-CoV-2 entry into cells. Molecular mimicry of azithromycin and cellular GM1 ganglioside (ganglioside-lipid that acts as a cofactor of the respiratory virus attachment to host cells) is the other proposed mechanism underlying antiviral effects. Azithromycin can bind the ganglioside-binding domain of S protein, thus blocking the S protein-GM1 interaction on the host cell plasma membrane [32].

Indirect blocking of furin system promoting viral entry after the S1-ACE2 binding is one more mechanism underlying the effects of azithromycin. The furin system is activated in the acidic conditions of the trans-Golgi network. In the active form furin cleavages S1 subunit from spike protein. It is assumed that azithromycin reduces furin activity by increasing the organellar pH [33]. Furthermore, azithromycin can alkalinize vesicles containing SARS-CoV-2 virions, thus preventing the pH-dependent membrane fusion.

Artemisinin, the anti-malarial drug that exhibits immunomodulatory properties is the third candidate remedy against SARS-CoV-2. Artemisinin, together with chloroquine and quinine, has a long history of clinical use, it shows a broad-

spectrum antiviral potential. It has been shown that chloroquine, the anti-malarial drug possessing immunomodulatory activity, that is well-known for decades, and hydroxychloroquine, the chloroquine derivative, can effectively inhibit SARS-CoV-2 in vitro [34, 35].

In addition to its role in treatment of malaria, artemisinin was studied for its potential effects on the immune responses under physiological and pathological conditions [36–38]. Many bacteria and viruses, including SARS-CoV-2, activate the NF-κB signaling pathway in human cells. Activation of the NF-κB signal transduction results in subsequent activation of the p50/p65 transcription factors. Artemisinin and artesunate can act as the NF-κB signaling pathway inhibitors by blocking the function of p50/p65. Research shows that artemisinin can interact with the cell surface via inhibition of the SARS-CoV-2 S protein binding to the cell surface receptors. This potentially prevents both endocytic entry of the virus and activation of the NF-κB signal transduction. Thus, artemisinin can prevent cytokine storm by inhibiting the IκB kinase [39–41]. However, the molecular docking studies show that artemisinins can also bind to coronavirus proteins, such as E protein, helicase protein, N protein, protein 3CL PRO, S protein, non-structural protein 3 (nsp3), nsp10, nsp14, nsp15, cathepsin L, and GRP78 [42, 43]. Therefore, biological activities of artemisinin may be partially based on inhibition of functions of these viral proteins.

Partial inhibition of the SARS-CoV-2 infection by lactoferrin, artemisinin, and azithromycin in vitro suggests that potential blocking of the entry of virions into cells mediated by each of these substances is insufficient for complete inhibition of the SARS-CoV-2 infection. However, the combination use of these drugs may be more promising in terms of clinical use. That is why the search and development of new drugs effective against novel coronavirus infection are going on, and the relevance of such studies is beyond doubt. The cell culture study of the drug antiviral activity is the first step of the search.

The study was aimed to assess cytotoxicity and antiviral activity of the mixture of active ingredients, lactoferrin, artemisinin, and azithromycin, against SARS-CoV-2 and to compare the mixture with hydroxychloroquine, since many in vitro studies that involved assessment of antiviral activity were limited by non-utilization of reference drugs.

METHODS

Viruses and cells

The experiments involved the Vero CCL81 (ATCC) kidney epithelial cells from the African green monkey that were obtained from the collection of the Mechnikov Research Institute of Vaccines and Sera and the Dubrovka laboratory strain of SARS-CoV-2 (GenBank ID: MW161041.1), isolated in the Vero CCL81 cell culture from the nasopharyngeal swab of patient with COVID-19. The virus was cultivated at 37 °C in the DMEM growth medium containing glutamine and glucose (4.5 g/L), 5% fetal bovine serum (FBS), L-glutamine (300 μg/mL), gentamicin (40 μg/mL) in the 5% CO_2 atmosphere conditions (growth medium, GM). The strain derived after 20 serial passages, it caused strong cytopathic effects (CPE) of the virus. The samples of viral material were stored at a temperature of °80 °C as aliquots. Aliquots of one stock were used in all the experiments.

Preparing the drug mixture

Ten milliliters of DMSO were added to 45 mg of azithromycin to obtain the solution with a concentration of 6 μmol/mL. Then

0.5 mL of phosphate buffer were added to 10 mg of lactoferrin to obtain the solution with a concentration of 20 mg/mL. Five milliliters of DMSO were added to 21 mg of artemisinin to obtain the solution with a concentration of 15 μmol/mL. To prepare the working solution, we mixed 5 μL of azithromycin solution, 125 μL of lactoferrin solution, and 50 μL of artemisinin solution, the growth medium was used to adjust the volume to 5 mL.

The concentrated solution of the reference drug (hydroxychloroquine) was prepared using the dosage form (the pill) that was diluted in the sterile distilled water individually for each experiment on the very day of use in equimolar amounts corresponding to the amount of pure substance in the drug. All the compounds, including hydroxychloroquine, were weighted to 0.1 mg using the analytical balance.

Cell culture assay for assessment of drug cytotoxicity

The cells were seeded in the 96-well Corning plates with the average seeding density of 20,000 cells per well and grown in the DMEM growth medium containing glutamine and glucose (4.5 g/L), 5% fetal bovine serum (FBS), L-glutamine (300 μg/mL), gentamicin (40 μg/mL) in the 5% CO_2 atmosphere conditions (GM) for three days until a monolayer was completely formed. Then the medium was removed, and 100 μL of the specified test drug concentrations (eight concentrations of each drug) in appropriate medium with no serum (working medium, WM) were added to the plate. Then 100 μL of WM were added to each well of the plate. Four iterations of each experimental step were performed ($n = 4$). Cells containing 200 μL of WM were used as negative controls. To define the thresholds of cytotoxicity concentration (TCD_{50}), the plates were incubated for 72 hrs at 37 °C in the 5% CO_2 atmosphere. When assessing antiviral activity, cells were incubated with drugs for five days, that is why the same incubation time (five days) was used for cytotoxicity assessment in the other series of experiments in order to rule out the toxic effects of the tested samples. Cytotoxic effects of the drugs were visually estimated based on the condition of cellular monolayer and quantified using the MTT assay. For that 160 μL of DMEM growth medium containing no phenol red and 40 μL of the 5 mg/mL methylthiazolyldiphenyl-tetrazolium bromide dye (MTT) solution were added to each well and incubated for 2 hrs at 37 °C in the 5% CO_2 atmosphere. The culture broth was removed, and 100 μL of DMSO were added to the wells, then the plates were incubated for 20 min at room temperature with continuous shaking. The optical density (OD) was measured at 530 nm taking into account the background values obtained at 620 nm using a spectrophotometer for plate reading. The maximum drug concentration that did not change the OD by more than 10–15% compared to control cells was considered as maximum tolerable concentration (MTC). The substance concentration that reduced OD by 50% compared to control cells was considered as TCD_{50}.

Assessment of drug antiviral activity against SARS-CoV-2 based on the cytopathic effect (CPE) using MTT assay

To assess antiviral activity of the samples, the Vero CCL81 cell culture was plated in the 96-well flat bottom cell culture plates (20,000 cells/well) and grown in aprropriate GM. On day three, after the monolayer was completely formed, the WM was removed from the plate wells. Then 100 μL of the tested drugs, undiluted or diluted with the WM to the specified concentrations (seven concentrations), were added to the wells. Some wells were used as virus control or cell control. Four iterations of each experimental step were performed ($n = 4$). In parallel, to rule out
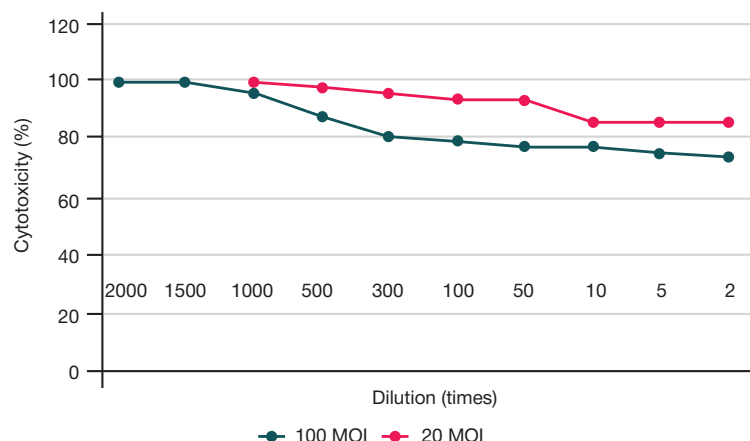
Fig. 1. Cytotoxicity of various dilutions of the mixture of active ingredients in the Vero CCL81 cell culture during the 3- and 5-day incubation

the cytotoxic effects of the drugs in the experiments focused on assessing antiviral activity, the same drug concentrations in the same conditions were added to the non-infected wells. After the 2-hrs incubation, the virus at a dose of infection (MOI) of 20 or 100 (per 100 μL) was added to all the wells, except for the cell control wells. Then the cells were incubated for five days at 37 °C in the 5% CO_2 atmosphere until the CPE was clearly visible in the virus control cells. The CPEs observed in the cells were quantified using the MTT assay as previously described. IC_{50} was calculated using the Excel application in accordance with the following formula:

$$\text{Inhibition} = \frac{100 - (OD_{\text{cell control}} - OD_{\text{experiment}})}{(OD_{\text{cell control}} - OD_{\text{virus control}})} \times 100 \ (\%)$$

Inhibition of viral reproduction of 30% or more was considered significant for exhibiting antiviral activity. The drug concentration that reduced OD by 50% was considered as IC_{50}.

The dosage form of hydroxychloroquine was used as a reference drug. Hydroxychloroquine concentration of 10 μg/mL that corresponded to IC_{50} was selected for the study [34, 44].

RESULTS

Assessing cytotoxic effects of the samples in the Vero CCL81 cell culture

In the first series of experiments we studied cytotoxicity of various dilutions of the tested drugs. We used the Vero CCL81 cell line that was later used to define antiviral activity. Visual assessment performed using the inverted microscope after the 72-hrs incubation showed that there were no cytotoxic/ morphological changes or cell monolayer breakdown. After adding some concentrations of substances, partial breakdown of monolayer was observed in experimental wells, the cells had a more rounded shape, and cell morphology was different from that of cell control. Complete breakdown of cell monolayer was observed in some wells. The research conducted by the more precise quantitative method involving MTT staining confirmed the data obtained by visual assessment of the cell condition. Based on the cell culture assessment of cytotoxic effects exhibited by the mixture with the use of the MTT assay, the dose–response curves were plotted (Fig. 1) that were used to define the MTC and TCD_{50} values: 1 : 500 and less than 1 : 2 for three-day incubation, 1 : 50 and less than 1 : 2 for five-day incubation, respectively. The method involving the use of MTT is also used to define antiviral activity, that is why the same dilutions of samples, with the same volume and time

of incubation as in the method of assessing antiviral activity involving no cell infection, were added to the cells for control to rule out the cytotoxic effects of the mixture during the five-day incubation.

Antiviral activity of the mixture of active ingredients against SARS-CoV-2 in the Vero CCL81 cell culture

Antiviral activity against SARS-CoV-2 was assessed in the Vero CCL81 by the method of viral CPE inhibition revealed using the MTT staining. Two multiplicity of infection values, MOI 100 and MOI 20, were used to infect the cells. Inhibition was observed at no more than 15-times dilution for both variants of infection. The data obtained are provided in Fig. 2. Adding mixture to the cells significantly suppressed (viral reproduction inhibition exceeded 30%) replication of the SARS-CoV-2 coronavirus. At the same time, hydroxychloroquine with a concentration of 10 μg/mL that was used as a reference drug showed SARS-CoV-2 reproduction inhibition of 65% (data not shown).

DISCUSSION

Several studies have shown that other co-receptors and cellular molecules in addition to ACE2 are required for SARS-CoV-2 infection [45]. Currently, the complete list of them is unknown to date. Initial step of viral entry is often triggered by the low-affinity binding to the attachment sites that promotes accumulation of virions on the cell surface. The subsequent binding to the high-affinity receptor triggers the viral entry [46, 47]. The study of molecular mechanisms underlying the SARS-CoV-2 cell infection has revealed a number of drugs that make it possible to inhibit infection.

The tested mixture of artemisinin, azithromycin, and lactoferrin is low toxic, it significantly inhibits the infection and SARS-CoV-2 replication *in vitro*. It is assumed that its mechanisms of action are mediated by active ingredients. Binding to the SARS-CoV-2 entry receptors and inhibition of viral protein functions may underlie prevention of cell infection with SARS-CoV-2, since these affect the related signaling systems and pathways, including NF-κB, PI3K/AKT, various interferon regulatory factors, and pro-inflammatory cytokine production [23, 24]. Furthermore, the decrease in furin activity provided by azithromycin significantly reduces cell infection. Moreover, azithromycin can alkalinize vesicles containing SARS-CoV-2 virions and prevent the pH-dependent membrane fusion.

CONCLUSIONS

The findings show that the mixture of active ingredients containing azithromycin, lactoferrin, and artemisinin shows low
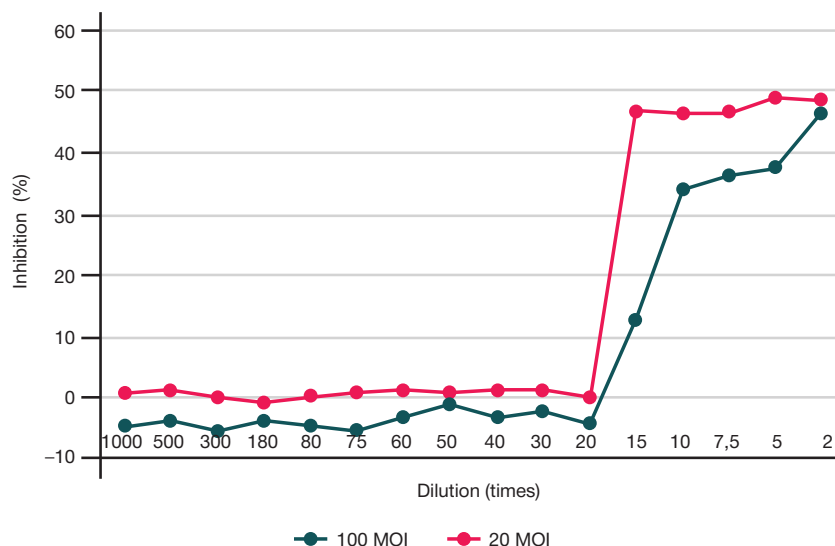
Fig. 2. Antiviral activity of the mixture of active ingredients in the culture of Vero CCL81 cells infected with MOI 20 and MOI 100 of the SARS-CoV-2 coronavirus

toxicity during the three-day and five-day incubation in the Vero CCL 81 cell culture. All the dilutions reduce cell viability by no more than 10–30%, the estimated TCD50 values are lower than the lowest dilution that is available for assessment (1 : 2). At high (MOI 100) and low (MOI 20) multiplicity of infection used in the Vero CCL 81 cell culture, the mixture has a significant effect on the SARS-CoV-2 reproduction, and IC50 is estimated as the 1 : 2 dilution in both cases. Thus, IC50 of the mixture is achieved by using the following concentrations of active ingredients: 3 μmol/L of azithromycin, 5 mg/L of lactoferrin, and 7.5 μmol/L of artemisinin.

Such molecular mechanisms underlying cell infection with the SARS-CoV-2 virions are still poorly understood, however, the combination mixtures have some benefits due to synergistic effects of the ingredients. The results obtained for the mixture of artemisinin, azithromycin, and lactoferrin *in vitro* show that the mixture can be used as a potential effective and useful adjuvant therapeutic supplement for treatment and prevention of COVID-19. Theoretical background and antiviral activity shown by the mixture of artemisinin, azithromycin, and lactoferrin during the study encourage us to plan further preclinical and clinical studies focused on assessing its safety and antiviral activity against SARS-CoV-2 *in vivo*, as well as on studying the dosage regimens of the drug and its combinations with other antivirals.

References

1. Martinez MA. Compounds with Therapeutic Potential against Novel Respiratory 2019 Coronavirus. Antimicrob Agents Chemother. 2020; 64 (5): e00399-20. https://doi.org/10.1128/AAC.00399-20.
2. Convertino I, Tuccori M, Ferraro S, Valdiserra G, Cappello E, Focosi D, et al. Exploring pharmacological approaches for managing cytokine storm associated with pneumonia and acute respiratory distress syndrome in COVID-19 patients. Crit Care. 2020; 24 (1): 331. https://doi.org/10.1186/s13054-020-03020-3.
3. Временные методические рекомендации «Профилактика, диагностика и лечение новой коронавирусной инфекции (COVID-19)» версия 16 от 18.08.2022. 2022; 249 с.
4. Weisblum Y, Schmidt F, Zhang F, DaSilva J, Poston D, Lorenzi JC, et al. Escape from neutralizing antibodies by SARS-CoV-2 spike protein variants. Elife. 2020; 9: e61312. Available from: https://doi.org/10.7554/eLife.61312.
5. Zhang Q, Xiang R, Huo S, Zhou Y, Jiang S, Wang Q, et al. Molecular mechanism of interaction between SARS-CoV-2 and host cells and interventional therapy. Signal Transduct Target Ther. 2021; 6 (1): 233. Available from: https://doi.org/10.1038/s41392-021-00653-w.
6. Lokhande KB, Apte GR, Shrivastava A, Singh A, Pal JK, K Venkateswara Swamy, et al. Sensing the interactions between carbohydrate-binding agents and N-linked glycans of SARS-CoV-2 spike glycoprotein using molecular docking and simulation studies. J Biomol Struct Dyn. 2022; 40 (9): 3880–98. Available from: https://doi.org/10.1080/07391102.2020.1851303.
7. Kim CH. SARS-CoV-2 Evolutionary Adaptation toward Host Entry and Recognition of Receptor O-Acetyl Sialylation in Virus-Host Interaction. Int J Mol Sci. 2020; 21 (12): 4549. Available from: https://doi.org/10.3390/ijms21124549.
8. Clausen TM, Sandoval DR, Spliid CB, Pihl J, Perrett HR, Painter CD, et al. SARS-CoV-2 Infection Depends on Cellular Heparan Sulfate and ACE2. Cell. 2020; 183 (4): 1043–57. Available from: https://doi.org/10.1016/j.cell.2020.09.033.
9. Cagno V, Tseligka ED, Jones ST, Tapparel C. Heparan Sulfate Proteoglycans and Viral Attachment: True Receptors or Adaptation Bias? Viruses. 2019; 11 (7): 596. Available from: https://doi.org/10.3390/v11070596.
10. Tree JA, Turnbull JE, Buttigieg KR, Elmore MJ, Coombes N, Hogwood J, et al. Unfractionated heparin inhibits live wild type SARS-CoV-2 cell infectivity at therapeutically relevant concentrations. Br J Pharmacol. 2021; 178 (3): 626–35. https://doi.org/10.1111/bph.15304.
11. Kim SY, Jin W, Sood A, Montgomery DW, Grant OC, Fuster MM, et al. Characterization of heparin and severe acute respiratory syndrome-related coronavirus 2 (SARS-CoV-2) spike glycoprotein binding interactions. Antiviral Res. 2020; 181: 104873. Available from: https://doi.org/10.1016/j.antiviral.2020.104873.
12. Ori A, Wilkinson MC, Fernig DG. The heparanome and regulation of cell function: structures, functions and challenges. Front Biosci. 2008; 13: 4309–38. Available from: https://doi.org/10.2741/3007.
13. Rudd TR, Preston MD, Yates EA. The nature of the conserved basic amino acid sequences found among 437 heparin binding proteins determined by network analysis. Mol Biosyst. 2017; 13 (5): 852–65. Available from: https://doi.org/10.1039/c6mb00857g.
14. Meneghetti MC, Hughes AJ, Rudd TR, Nader HB, Powell AK, Yates EA, et al. Heparan sulfate and heparin interactions with

proteins. J R Soc Interface. 2015; 12 (110): 0589. Available from: https://doi.org/10.1098/rsif.2015.0589.

15. Zhang Q, Chen CZ, Swaroop M, Xu M, Wang L, Lee J, et al. Heparan sulfate assists SARS-CoV-2 in cell entry and can be targeted by approved drugs in vitro. Cell Discov. 2020; 6 (1): 80. Available from: https://doi.org/10.1038/s41421-020-00222-5.

16. Salaris C, Scarpa M, Elli M, Bertolini A, Guglielmetti S, Pregliasco F, et al. Protective Effects of Lactoferrin against SARS-CoV-2 Infection In Vitro. Nutrients. 2021; 13 (2): 328. Available from: https://doi.org/10.3390/nu13020328.

17. Kell DB, Heyden EL, Pretorius E. The Biology of Lactoferrin, an Iron-Binding Protein That Can Help Defend Against Viruses and Bacteria. Front Immunol. 2020; 11: 1221. Available from: https://doi.org/10.3389/fimmu.2020.01221.

18. Kawasaki T, Kawai T. Toll-like receptor signaling pathways. Front Immunol. 2014; 5: 461. Available from: https://doi.org/10.3389/fimmu.2014.00461.

19. Channappanavar R, Fehr AR, Zheng J, Wohlford-Lenane C, Abrahante JE, Mack M, et al. IFN-I response timing relative to virus replication determines MERS coronavirus infection outcomes. J Clin Invest. 2019; 129 (9): 3625–39. Available from: https://doi.org/10.1172/JCI126363.

20. Sano E, Miyauchi R, Takakura N, Yamauchi K, Murata E, Trang Le Q, et al. Cysteine protease inhibitors in various milk preparations and its importance as a food, Food Research International, 2005: 38 (4): 427–33, https://doi.org/10.1016/j.foodres.2004.10.011.

21. Ou X, Liu Y, Lei X, Li P, Mi D, Ren L, et al. Characterization of spike glycoprotein of SARS-CoV-2 on virus entry and its immune cross-reactivity with SARS-CoV. Nat Commun. 2020; 11 (1): 1620. Available from: https://doi.org/10.1038/s41467-020-15562-9.

22. Ulrich H, Pillat MM. CD147 as a Target for COVID-19 Treatment: Suggested Effects of Azithromycin and Stem Cell Engagement. Stem Cell Rev Rep. 2020; 16 (3): 434–40. Available from: https://doi.org/10.1007/s12015-020-09976-7.

23. Chen Y, Zhang H, Gou X, Horikawa Y, Xing J, Chen Z. Upregulation of HAb18G/CD147 in activated human umbilical vein endothelial cells enhances the angiogenesis. Cancer Lett. 2009; 278 (1): 113–21. Available from: https://doi.org/10.1016/j.canlet.2009.01.004.

24. Fang F, Wang L, Zhang S, Fang Q, Hao F, Sun Y. CD147 modulates autophagy through the PI3K/Akt/mTOR pathway in human prostate cancer PC-3 cells. Oncol Lett. 2015; 9 (3): 1439–43. Available from: https://doi.org/10.3892/ol.2015.2849

25. Wilms EB, Touw DJ, Heijerman HG. Pharmacokinetics of azithromycin in plasma, blood, polymorphonuclear neutrophils and sputum during long-term therapy in patients with cystic fibrosis. Ther Drug Monit. 2006; 28 (2): 219–25. Available from: https://doi.org/10.1097/01.ftd.0000195617.69721.a5.

26. Tsai WC, Rodriguez ML, Young KS. Azithromycin blocks neutrophil recruitment in Pseudomonas endobronchial infection. Am J Respir Crit Care Med. 2004; 170 (12): 1331–9. Available from: https://doi.org/10.1164/rccm.200402-200OC

27. Culic O, Erakovic V, Cepelak I. Azithromycin modulates neutrophil function and circulating inflammatory mediators in healthy human subjects. Eur J Pharmacol. 2002; 450 (3): 277–89. Available from: https://doi.org/10.1016/S0014-2999(02)02042-3.

28. Tsai WC, Standiford TJ. Immunomodulatory effects of macrolides in the lung: lessons from in-vitro and in-vivo models. Curr Pharm des. 2004; 10 (25): 3081–93. Available from: https://doi.org/10.2174/1381612043383430.

29. Stamatiou R, Paraskeva E, Boukas K, Gourgoulianis KI, Molyvdas PA, Hatziefthimiou AA. Azithromycin has an antiproliferative and autophagic effect on airway smooth muscle cells. Eur Respir J. 2009; 34 (3): 721–30. Available from: https://doi.org/10.1183/09031936.00089407.

30. Cigana C, Assael BM, Melotti P. Azithromycin selectively reduces tumor necrosis factor alpha levels in cystic fibrosis airway epithelial cells. Antimicrob Agents Chemother. 2007; 51 (3): 975–81. Available from: https://doi.org/10.1128/AAC.01142-06.

31. Halldorsson S, Gudjonsson T, Gottfredsson M, Singh PK, Gudmundsson GH, Baldursson O. Azithromycin maintains airway epithelial integrity during Pseudomonas aeruginosa infection. Am J Respir Cell Mol Biol. 2010; 42 (1): 62–8. Available from: https://doi.org/10.1165/rcmb.2008-0357OC

32. Pani A, Lauriola M, Romandini A, Scaglione F. Macrolides and viral infections: focus on azithromycin in COVID-19 pathology. Int J Antimicrob Agents. 2020; 56 (2): 106053. Available from: https://doi.org/10.1016/j.ijantimicag.2020.106053

33. Khoshnood S, Shirani M, Dalir A, Moradi M, Haddadi M, Sadeghifard N, et al. Antiviral effects of azithromycin: A narrative review, Biomedicine & Pharmacotherapy. 2022; 147: 112682, Available from: https://doi.org/10.1016/j.biopha.2022.112682.

34. Wang M, Cao R, Zhang L, Yang X, Liu J, Xu M, et al. Remdesivir and chloroquine effectively inhibit the recently emerged novel coronavirus (2019-nCoV) in vitro. Cell Res. 2020; 30 (3): 269–71. Available from: https://doi.org/10.1038/s41422-020-0282-0.

35. Hedya SA, Safar MM, Bahgat AK. Hydroxychloroquine antiparkinsonian potential: Nurr1 modulation versus autophagy inhibition. Behav Brain Res. 2019; 365: 82–88. Available from: https://doi.org/10.1016/j.bbr.2019.02.033.

36. Efferth T, Marschall M, Wang X, Huong SM, Hauber I, Olbrich A, et al. Antiviral activity of artesunate towards wild-type, recombinant, and ganciclovir-resistant human cytomegaloviruses. J Mol Med (Berl). 2002; 80 (4): 233–42. Available from: https://doi.org/10.1007/s00109-001-0300-8.

37. Aldieri E, Atragene D, Bergandi L, Riganti C, Costamagna C, Bosia A, et al. Artemisinin inhibits inducible nitric oxide synthase and nuclear factor NF-kB activation. FEBS Lett. 2003; 552: 141–4. Available from: https://doi.org/10.1016/S0014-5793(03)00905-0

38. Nunes JJ, Pandey SK, Yadav A, Goel S, Ateeq B. Targeting NF-kappa B Signaling by Artesunate Restores Sensitivity of Castrate-Resistant Prostate Cancer Cells to Antiandrogens. Neoplasia. 2017; 19 (4): 333–45. Available from: https://doi.org/10.1016/j.neo.2017.02.002.

39. Gendrot M, Duflot I, Boxberger M, Delandre O, Jardot P, Le Bideau M, et al. Antimalarial artemisinin-based combination therapies (ACT) and COVID-19 in Africa: In vitro inhibition of SARS-CoV-2 replication by mefloquine-artesunate. Int J Infect Dis. 2020; 99: 437–40. Available from: https://doi.org/10.1016/j.ijid.2020.08.032.

40. Rolta R, Salaria D, Sharma P, Sharma B, Kumar V, Rathi B, et al. Phytocompounds of Rheum emodi, Thymus serpyllum, and Artemisia annua Inhibit Spike Protein of SARS-CoV-2 Binding to ACE2 Receptor: In Silico Approach. Curr Pharmacol Rep. 2021; 7 (4): 135–49. Available from: https://doi.org/10.1007/s40495-021-00259-4.

41. Uckun FM, Saund S, Windlass H, Trieu V. Repurposing Anti-Malaria Phytomedicine Artemisinin as a COVID-19 Drug. Front Pharmacol. 2021; 12: 649532. Available from: https://doi.org/10.3389/fphar.2021.649532.

42. Fuzimoto AD. An overview of the anti-SARS-CoV-2 properties of Artemisia annua, its antiviral action, protein-associated mechanisms, and repurposing for COVID-19 treatment. J Integr Med. 2021; 19 (5): 375–88. Available from: https://doi.org/10.1016/j.joim.2021.07.003.

43. Ribaudo G, Coghi P, Yang LJ, Ng JPL, Mastinu A, Memo M, et al. Computational and experimental insights on the interaction of artemisinin, dihydroartemisinin and chloroquine with SARS-CoV-2 spike protein receptor-binding domain (RBD). Nat Prod Res. 2021; 12: 1–6. Available from: https://doi.org/10.1080/14786419.2021.1925894.

44. Gendrot M, Andreani J, Boxberger M, Jardot P, Fonta I, Le Bideau M, et al. Antimalarial drugs inhibit the replication of SARS-CoV-2: An in vitro evaluation. Trav Med Infect Dis. 2020; 37: 101873. Available from: https://doi.org/10.1016/j.tmaid.2020.101873.

45. Chen J, Subbarao K. The Immunobiology of SARS*. Annu Rev Immunol. 2007; 25: 443–72. Available from: https://doi.org/10.1146/annurev.immunol.25.022106.141706.

46. Sapp M, Bienkowska-Haba M. Viral entry mechanisms: human papillomavirus and a long journey from extracellular matrix to the nucleus. FEBS J. 2009; 276 (24): 7206–16. Available from: https://doi.org/10.1111/j.1742-4658.2009.07400.x.

47. Leistner CM, Gruen-Bernhard S, Glebe D. Role of glycosaminoglycans for binding and infection of hepatitis B virus. Cell Microbiol. 2008; 10 (1): 122–33. Available from: https://doi.org/10.1111/j.1462-5822.2007.01023.x.

Литература

1. Martinez MA. Compounds with Therapeutic Potential against Novel Respiratory 2019 Coronavirus. Antimicrob Agents Chemother. 2020; 64 (5): e00399-20. https://doi.org/10.1128/AAC.00399-20.

2. Convertino I, Tuccori M, Ferraro S, Valdiserra G, Cappello E, Focosi D, et al. Exploring pharmacological approaches for managing cytokine storm associated with pneumonia and acute respiratory distress syndrome in COVID-19 patients. Crit Care. 2020; 24 (1): 331. https://doi.org/10.1186/s13054-020-03020-3.

3. Временные методические рекомендации «Профилактика, диагностика и лечение новой коронавирусной инфекции (COVID-19)» версия 16 от 18.08.2022. 2022; 249 с.

4. Weisblum Y, Schmidt F, Zhang F, DaSilva J, Poston D, Lorenzi JC, et al. Escape from neutralizing antibodies by SARS-CoV-2 spike protein variants. Elife. 2020; 9: e61312. Available from: https://doi.org/10.7554/eLife.61312.

5. Zhang Q, Xiang R, Huo S, Zhou Y, Jiang S, Wang Q, et al. Molecular mechanism of interaction between SARS-CoV-2 and host cells and interventional therapy. Signal Transduct Target Ther. 2021; 6 (1): 233. Available from: https://doi.org/10.1038/s41392-021-00653-w.

6. Lokhande KB, Apte GR, Shrivastava A, Singh A, Pal JK, K Venkateswara Swamy, et al. Sensing the interactions between carbohydrate-binding agents and N-linked glycans of SARS-CoV-2 spike glycoprotein using molecular docking and simulation studies. J Biomol Struct Dyn. 2022; 40 (9): 3880–98. Available from: https://doi.org/10.1080/07391102.2020.1851303.

7. Kim CH. SARS-CoV-2 Evolutionary Adaptation toward Host Entry and Recognition of Receptor O-Acetyl Sialylation in Virus-Host Interaction. Int J Mol Sci. 2020; 21 (12): 4549. Available from: https://doi.org/10.3390/ijms21124549.

8. Clausen TM, Sandoval DR, Spliid CB, Pihl J, Perrett HR, Painter CD, et al. SARS-CoV-2 Infection Depends on Cellular Heparan Sulfate and ACE2. Cell. 2020; 183 (4): 1043–57. Available from: https://doi.org/10.1016/j.cell.2020.09.033.

9. Cagno V, Tseligka ED, Jones ST, Tapparel C. Heparan Sulfate Proteoglycans and Viral Attachment: True Receptors or Adaptation Bias? Viruses. 2019; 11 (7): 596. Available from: https://doi.org/10.3390/v11070596.

10. Tree JA, Turnbull JE, Buttigieg KR, Elmore MJ, Coombes N, Hogwood J, et al. Unfractionated heparin inhibits live wild type SARS-CoV-2 cell infectivity at therapeutically relevant concentrations. Br J Pharmacol. 2021; 178 (3): 626–35. https://doi.org/10.1111/bph.15304.

11. Kim SY, Jin W, Sood A, Montgomery DW, Grant OC, Fuster MM, et al. Characterization of heparin and severe acute respiratory syndrome-related coronavirus 2 (SARS-CoV-2) spike glycoprotein binding interactions. Antiviral Res. 2020; 181: 104873. Available from: https://doi.org/10.1016/j.antiviral.2020.104873.

12. Ori A, Wilkinson MC, Fernig DG. The heparanome and regulation of cell function: structures, functions and challenges. Front Biosci. 2008; 13: 4309–38. Available from: https://doi.org/10.2741/3007.

13. Rudd TR, Preston MD, Yates EA. The nature of the conserved basic amino acid sequences found among 437 heparin binding proteins determined by network analysis. Mol Biosyst. 2017; 13 (5): 852–65. Available from: https://doi.org/10.1039/c6mb00857g.

14. Meneghetti MC, Hughes AJ, Rudd TR, Nader HB, Powell AK, Yates EA, et al. Heparan sulfate and heparin interactions with proteins. J R Soc Interface. 2015; 12 (110): 0589. Available from: https://doi.org/10.1098/rsif.2015.0589.

15. Zhang Q, Chen CZ, Swaroop M, Xu M, Wang L, Lee J, et al. Heparan sulfate assists SARS-CoV-2 in cell entry and can be targeted by approved drugs in vitro. Cell Discov. 2020; 6 (1): 80. Available from: https://doi.org/10.1038/s41421-020-00222-5.

16. Salaris C, Scarpa M, Elli M, Bertolini A, Guglielmetti S, Pregliasco F, et al. Protective Effects of Lactoferrin against SARS-CoV-2 Infection In Vitro. Nutrients. 2021; 13 (2): 328. Available from: https://doi.org/10.3390/nu13020328.

17. Kell DB, Heyden EL, Pretorius E. The Biology of Lactoferrin, an Iron-Binding Protein That Can Help Defend Against Viruses and Bacteria. Front Immunol. 2020; 11: 1221. Available from: https://doi.org/10.3389/fimmu.2020.01221.

18. Kawasaki T, Kawai T. Toll-like receptor signaling pathways. Front Immunol. 2014; 5: 461. Available from: https://doi.org/10.3389/fimmu.2014.00461.

19. Channappanavar R, Fehr AR, Zheng J, Wohlford-Lenane C, Abrahante JE, Mack M, et al. IFN-I response timing relative to virus replication determines MERS coronavirus infection outcomes. J Clin Invest. 2019; 129 (9): 3625–39. Available from: https://doi.org/10.1172/JCI126363.

20. Sano E, Miyauchi R, Takakura N, Yamauchi K, Murata E, Trang Le Q, et al. Cysteine protease inhibitors in various milk preparations and its importance as a food, Food Research International, 2005: 38 (4): 427–33, https://doi.org/10.1016/j.foodres.2004.10.011.

21. Ou X, Liu Y, Lei X, Li P, Mi D, Ren L, et al. Characterization of spike glycoprotein of SARS-CoV-2 on virus entry and its immune cross-reactivity with SARS-CoV. Nat Commun. 2020; 11 (1): 1620. Available from: https://doi.org/10.1038/s41467-020-15562-9.

22. Ulrich H, Pillat MM. CD147 as a Target for COVID-19 Treatment: Suggested Effects of Azithromycin and Stem Cell Engagement. Stem Cell Rev Rep. 2020; 16 (3): 434–40. Available from: https://doi.org/10.1007/s12015-020-09976-7.

23. Chen Y, Zhang H, Gou X, Horikawa Y, Xing J, Chen Z. Upregulation of HAb18G/CD147 in activated human umbilical vein endothelial cells enhances the angiogenesis. Cancer Lett. 2009; 278 (1): 113–21. Available from: https://doi.org/10.1016/j.canlet.2009.01.004.

24. Fang F, Wang L, Zhang S, Fang Q, Hao F, Sun Y. CD147 modulates autophagy through the PI3K/Akt/mTOR pathway in human prostate cancer PC-3 cells. Oncol Lett. 2015; 9 (3): 1439–43. Available from: https://doi.org/10.3892/ol.2015.2849

25. Wilms EB, Touw DJ, Heijerman HG. Pharmacokinetics of azithromycin in plasma, blood, polymorphonuclear neutrophils and sputum during long-term therapy in patients with cystic fibrosis. Ther Drug Monit. 2006; 28 (2): 219–25. Available from: https://doi.org/10.1097/01.ftd.0000195617.69721.a5.

26. Tsai WC, Rodriguez ML, Young KS. Azithromycin blocks neutrophil recruitment in Pseudomonas endobronchial infection. Am J Respir Crit Care Med. 2004; 170 (12): 1331–9. Available from: https://doi.org/10.1164/rccm.200402-200OC

27. Culic O, Erakovic V, Cepelak I. Azithromycin modulates neutrophil function and circulating inflammatory mediators in healthy human subjects. Eur J Pharmacol. 2002; 450 (3): 277–89. Available from: https://doi.org/10.1016/S0014-2999(02)02042-3.

28. Tsai WC, Standiford TJ. Immunomodulatory effects of macrolides in the lung: lessons from in-vitro and in-vivo models. Curr Pharm des. 2004; 10 (25): 3081–93. Available from: https://doi.org/10.2174/1381612043383430.

29. Stamatiou R, Paraskeva E, Boukas K, Gourgoulianis KI, Molyvdas PA, Hatziefthimiou AA. Azithromycin has an antiproliferative and autophagic effect on airway smooth muscle cells. Eur Respir J. 2009; 34 (3): 721–30. Available from: https://doi.org/10.1183/09031936.00089407.

30. Cigana C, Assael BM, Melotti P. Azithromycin selectively reduces tumor necrosis factor alpha levels in cystic fibrosis airway epithelial cells. Antimicrob Agents Chemother. 2007; 51 (3): 975–81. Available from: https://doi.org/10.1128/AAC.01142-06.

31. Halldorsson S, Gudjonsson T, Gottfredsson M, Singh PK, Gudmundsson GH, Baldursson O. Azithromycin maintains airway epithelial integrity during Pseudomonas aeruginosa infection. Am J Respir Cell Mol Biol. 2010; 42 (1): 62–8. Available from: https://doi.org/10.1165/rcmb.2008-0357OC

32. Pani A, Lauriola M, Romandini A, Scaglione F. Macrolides and viral infections: focus on azithromycin in COVID-19 pathology. Int J Antimicrob Agents. 2020; 56 (2): 106053. Available from: https://doi.org/10.1016/j.ijantimicag.2020.106053

33. Khoshnood S, Shirani M, Dalir A, Moradi M, Haddadi M, Sadeghifard N, et al. Antiviral effects of azithromycin: A narrative review, Biomedicine & Pharmacotherapy. 2022; 147: 112682, Available from: https://doi.org/10.1016/j.biopha.2022.112682.

34. Wang M, Cao R, Zhang L, Yang X, Liu J, Xu M, et al. Remdesivir and chloroquine effectively inhibit the recently emerged novel coronavirus (2019-nCoV) in vitro. Cell Res. 2020; 30 (3): 269–71.

Available from: https://doi.org/10.1038/s41422-020-0282-0.

35. Hedya SA, Safar MM, Bahgat AK. Hydroxychloroquine antiparkinsonian potential: Nurr1 modulation versus autophagy inhibition. Behav Brain Res. 2019; 365: 82–88. Available from: https://doi.org/10.1016/j.bbr.2019.02.033.

36. Efferth T, Marschall M, Wang X, Huong SM, Hauber I, Olbrich A, et al. Antiviral activity of artesunate towards wild-type, recombinant, and ganciclovir-resistant human cytomegaloviruses. J Mol Med (Berl). 2002; 80 (4): 233–42. Available from: https://doi.org/10.1007/s00109-001-0300-8.

37. Aldieri E, Atragene D, Bergandi L, Riganti C, Costamagna C, Bosia, A, et al. Artemisinin inhibits inducible nitric oxide synthase and nuclear factor NF-kB activation. FEBS Lett. 2003; 552: 141–4. Available from: https://doi.org/10.1016/S0014-5793(03)00905-0

38. Nunes JJ, Pandey SK, Yadav A, Goel S, Ateeq B. Targeting NF-kappa B Signaling by Artesunate Restores Sensitivity of Castrate-Resistant Prostate Cancer Cells to Antiandrogens. Neoplasia. 2017; 19 (4): 333–45. Available from: https://doi.org/10.1016/j.neo.2017.02.002.

39. Gendrot M, Duflot I, Boxberger M, Delandre O, Jardot P, Le Bideau M, et al. Antimalarial artemisinin-based combination therapies (ACT) and COVID-19 in Africa: In vitro inhibition of SARS-CoV-2 replication by mefloquine-artesunate. Int J Infect Dis. 2020; 99: 437–40. Available from: https://doi.org/10.1016/j.ijid.2020.08.032.

40. Rolta R, Salaria D, Sharma P, Sharma B, Kumar V, Rathi B, et al. Phytocompounds of Rheum emodi, Thymus serpyllum, and Artemisia annua Inhibit Spike Protein of SARS-CoV-2 Binding to ACE2 Receptor: In Silico Approach. Curr Pharmacol Rep. 2021; 7 (4): 135–49. Available from: https://doi.org/10.1007/s40495-021-00259-4.

41. Uckun FM, Saund S, Windlass H, Trieu V. Repurposing Anti-Malaria Phytomedicine Artemisinin as a COVID-19 Drug. Front Pharmacol. 2021; 12: 649532. Available from: https://doi.org/10.3389/fphar.2021.649532.

42. Fuzimoto AD. An overview of the anti-SARS-CoV-2 properties of Artemisia annua, its antiviral action, protein-associated mechanisms, and repurposing for COVID-19 treatment. J Integr Med. 2021; 19 (5): 375–88. Available from: https://doi.org/10.1016/j.joim.2021.07.003.

43. Ribaudo G, Coghi P, Yang LJ, Ng JPL, Mastinu A, Memo M, et al. Computational and experimental insights on the interaction of artemisinin, dihydroartemisinin and chloroquine with SARS-CoV-2 spike protein receptor-binding domain (RBD). Nat Prod Res. 2021; 12: 1–6. Available from: https://doi.org/10.1080/14786419.2021.1925894.

44. Gendrot M, Andreani J, Boxberger M, Jardot P, Fonta I, Le Bideau M, et al. Antimalarial drugs inhibit the replication of SARS-CoV-2: An in vitro evaluation. Trav Med Infect Dis. 2020; 37: 101873. Available from: https://doi.org/10.1016/j.tmaid.2020.101873.

45. Chen J, Subbarao K. The Immunobiology of SARS*. Annu Rev Immunol. 2007; 25: 443–72. Available from: https://doi.org/10.1146/annurev.immunol.25.022106.141706.

46. Sapp M, Bienkowska-Haba M. Viral entry mechanisms: human papillomavirus and a long journey from extracellular matrix to the nucleus. FEBS J. 2009; 276 (24): 7206–16. Available from: https://doi.org/10.1111/j.1742-4658.2009.07400.x.

47. Leistner CM, Gruen-Bernhard S, Glebe D. Role of glycosaminoglycans for binding and infection of hepatitis B virus. Cell Microbiol. 2008; 10 (1): 122–33. Available from: https://doi.org/10.1111/j.1462-5822.2007.01023.x.

ISOLATION AND CHARACTERIZATION OF *KLEBSIELLA PNEUMONIAE* BACTERIOPHAGES ENCODING POLYSACCHARIDE DEPOLYMERASES WITH RARE CAPSULE SPECIFICITY

Gorodnichev RB[1]✉, Kornienko MA[1], Bespiatykh DA[1], Malakhova MV[1], Veselovsky VA[1], Goloshchapov OV[2], Chukhlovin AB[2,3], Bespyatykh JA[1], Shitikov EA[1]

[1] Federal Research and Clinical Center of Physical-Chemical Medicine of the Federal Medical Biological Agency, Moscow, Russia
[2] Pavlov First Saint Petersburg State Medical University, Saint Petersburg, Russia
[3] Pediatric Research and Clinical Center of Infectious Diseases of the Federal Medical Biological Agency, Saint Petersburg, Russia

Bacterial infections caused by antibiotic resistant strains of *Klebsiella pneumoniae* are among the most dangerous threats for the world's public healthcare. Treatment with bacteriophages and/or their derivatives could become one of the alternative methods for therapy of infections caused by *K. pneumoniae*. The study was aimed to isolate from the environment and characterize the capsule-specific *K. pneumoniae* bacteriophages that are useful for therapy and possess the polysaccharide depolymerase genes. Bacteriophages were isolated from the river water samples by enrichment method. The host range of bacteriophages were assessed using the collection of 180 *K. pneumoniae* clinical strains. Bacteriophage whole genome sequencing was performed on the MiSeq platform (Illumina). Four new bacteriophages from different taxonomic groups were isolated and characterized during the study: vB_KpnM_NDO71 (*Vequintavirinae* family), vB_KpnS_MAG26fr (*Casjensviridae* family), vB_KpnS_MDA2066 (*Ackermannviridae* family), and vB_KpnS_PMM-G3 (*Drexlerviridae* family). Bacteriophages vB_KpnM_NDO71, vB_KpnS_MAG26fr, and vB_KpnS_PMM-G3 had a narrow lytic spectrum and lysed all strains with the capsular type of the host: KL45, KL19 or KL28, respectively. Bacteriophage vB_KpnS_MDA2066 showed lytic activity against strains with two different capsular types: KL19 and KL107. Bacteriophages were strictly virulent and contained no integrase genes, potentially dangerous toxin genes or antibiotic resistance determinants. This allows them to be used in therapeutic practice. Receptor-binding proteins represented by polysaccharide depolymerases were predicted for each bacteriophage.

Keywords: virulent bacteriophages, *Klebsiella pneumoniae*, antibiotic resistance, bacteriophage therapy, polysaccharide depolymerases

ВЫДЕЛЕНИЕ И ХАРАКТЕРИСТИКА БАКТЕРИОФАГОВ *KLEBSIELLA PNEUMONIAE*, КОДИРУЮЩИХ ПОЛИСАХАРИД-ДЕПОЛИМЕРАЗЫ С УНИКАЛЬНОЙ КАПСУЛЬНОЙ СПЕЦИФИЧНОСТЬЮ

Р. Б. Городничев[1]✉, М. А. Корниенко[1], Д. А. Беспятых[1], М. В. Малахова[1], В. А. Веселовский[1], О. В. Голощапов[2], А. Б. Чухловин[2,3], Ю. А. Беспятых[1], Е. А. Шитиков[1]

[1] Федеральный научно-клинический центр физико-химической медицины Федерального медико-биологического агентства, Москва, Россия
[2] Первый Санкт-Петербургский государственный медицинский университет им. акад. И. П. Павлова, Санкт-Петербург, Россия
[3] Детский научно-клинический центр инфекционных болезней Федерального медико-биологического агентства, Санкт-Петербург, Россия

Бактериальные инфекции, вызываемые устойчивыми к антибиотикам штаммами *Klebsiella pneumoniae*, входят в список самых опасных угроз для мирового общественного здравоохранения. Одним из альтернативных способов терапии инфекций, вызванных *K. pneumoniae*, может стать терапия бактериофагами и/или их производными. Целью работы было выделить из внешней среды и охарактеризовать капсуло-специфичные бактериофаги *K. pneumoniae*, пригодные для терапевтического применения и несущие гены полисахарид-деполимераз. Бактериофаги выделяли из проб речной воды методом накопительных культур. Спектр хозяев бактериофагов оценивали на коллекции из 180 клинических штаммов *K. pneumoniae*. Полногеномное секвенирование бактериофагов выполняли на платформе MiSeq (Illumina). В рамках исследования выделено и охарактеризовано четыре новых бактериофага, принадлежащих к различным таксономическим группам: vB_KpnM_NDO71 (подсемейство *Vequintavirinae*), vB_KpnS_MAG26fr (семейство *Casjensviridae*), vB_KpnS_MDA2066 (семейство *Ackermannviridae*) и vB_KpnS_PMM-G3 (семейство *Drexlerviridae*). Бактериофаги vB_KpnM_NDO71, vB_KpnS_MAG26fr и vB_KpnS_PMM-G3 обладали узким спектром литической активности и лизировали все штаммы с капсульным типом штамма хозяина: KL45, KL19 или KL28 соответственно. Бактериофаг vB_KpnS_MDA2066 проявлял литическую активность в отношении штаммов двух различных капсульных типов: KL19 и KL107. Бактериофаги обладали строго вирулентной природой и не несли в своем составе генов интеграз, а также потенциально опасных генов токсинов и детерминант устойчивости к антибиотикам, что позволяет применять их в терапевтической практике. Для каждого бактериофага предсказаны рецептор-связывающие белки, представленные полисахарид-деполимеразами.

Ключевые слова: вирулентные бактериофаги, *Klebsiella pneumoniae*, антибиотикорезистентность, фаготерапия, полисахарид-деполимеразы

Klebsiella pneumoniae is a Gram-negative non-motile facultative anaerobic bacterium that occurs everywhere in nature and can constitute a part of normal flora in humans and other animals [1, 2]. At the same time, *K. pneumoniae* is the second most common nosocomial pathogen in the world capable of causing numerous infections, such as abscesses, purulent wounds, pneumonia, urinary tract and gastrointestinal tract infections [3]. The Russian study "Marathon 2015–2016" has shown that *K. pneumoniae* strains prevail (47.2%) among all nosocomial strains of Enterobacterales [4]. According to the same study and the map of antibiotic resistance in Russia [5], the share of carbapenem-resistant isolates is 6.9–41.6%, 80.1–90.2% are resistant to III-IV generation cephalosporins, and 6.11% are resistant to colistin. The *K. pneumoniae* strains associated with antibiotic resistance rank third in terms of mortality rate among antibiotic-resistant bacteria [6].

Treatment with bacteriophages and/or their derivatives could become one of the alternative methods for therapy of infections caused by *K. pneumoniae* [7]. Bacteriophages are the most widely spread and abundant group of viruses that are described as natural parasites of bacteria in natural populations [8]. Bacteriophages have been used as antimicrobial agents since early XX century due to their ability to infect and lyse bacterial cells [9]. Phage therapy has a number of advantages, such as the ability to lyse bacteria regardless of their antibiotic resistance, and no side effects to patients, which make it possible to use bacteriophage even for therapy of children and immunocompromised patients [10]. Today, the therapeutic use of bacteriophages is undergoing a rebirth, and the reports of successful treatment cases are more and more often found in the literature [11–13].

Along with the use of bacteriophages, close attention is currently paid to certain phage proteins showing activity against the bacterial surface structures. One such example are polysaccharide depolymerases [14]. These proteins can destroy bacterial capsular polysaccharides, thus providing sensitization of bacteria to antimicrobial drugs and the immune system [15]. Depolymerases usually show narrow specificity limited to certain type of the bacterial capsular polysaccharide [14]. In this regard, the search and description of bacteriophages encoding depolymerases that show activity against a broad range of capsular types of the clinically significant bacteria is an urgent task of the innovative approaches to therapy of infections caused by multidrug-resistant bacteria.

The study was aimed to isolate from the environment and characterize the capsule-specific *K. pneumoniae* bacteriophages that are useful for therapy and contain genes encoding polysaccharide depolymerases.

METHODS

Bacterial strains and their characteristics

The study involved a total of 180 K. pneumoniae clinical isolates collected in 2019–2022 in the Gorbacheva Research Institute of Pediatric Oncology, Hematology and Transplantation (Saint Petersburg, Russia) and the Clinical Hospital № 123 (Odintsovo, Russia), including 12 strains obtained from the State Collection of Pathogenic Microorganisms and Cell Cultures (Obolensk, Russia). Bacterial strains were grown in the lysogeny broth (LB) (Himedia; India) at 37 °C. Species identification was performed by the direct bacterial lysate mass spectrometry profiling in accordance with the previously reported method [16]. Mass spectra were acquired using the Microflex time-of-flight mass spectrometer (Bruker Daltonics; Germany). The

flexControl 3.0 and flexAnalysis 3.0 software packages (Bruker Daltonics; Germany) were used for recording, processing and analysis of mass spectra. Species identification was performed in the MALDI Biotyper 3.0 software package (Bruker Daltonics; Germany). The *K. pneumoniae* capsular type was defined by the wzi gene sequencing [17].

Bacteriophage isolation and purification

The river water sample was used as a source of phages. The sample was centrifuged (4000 g, 10 min), and supernatant was filtered through the 0.22 μm filters (Merk Millipore; USA) to remove the bacterial fraction. Equal aliquots (15 mL each) of filtered water and double concentration LB broth were mixed and inoculated with 20 μm of the potential host strain overnight culture. The mixture was incubated overnight at 37 °C on the rocking shaker. The resulting suspension was sterilized by filtration through the 0.22 μm filter, and the filtrate was tested for the presence of bacteriophages by the spot test assay [18]. Phage isolates were purified by triple passage through a single plaque.

Host range determination

The phage host range were defined by the spot test assay [18]. For that 100 μm of the culture of each strain being through the logarithmic phase of growth were added to 5 mL of the unset semi-solid LB agar (0.7% agar) and poured onto Petri dishes containing a thin layer of LB agar (1.5% agar). Testing was performed by applying 5 μL of the bacteriophage serial dilutions onto the fresh lawns of the strains. The Petri dishes were incubated overnight at 37 °C. The bacteriophage lytic activity was defined by the presence of the zones of solid bacterial cell lysis matching the drops by shape. The presence of translucent halo surrounding the lysis zone or a single phage plaque was interpreted as bacteriophage polysaccharide depolymerase activity.

DNA sequencing and analysis

Genomic DNA of the phage was extracted using the standard phenol–chloroform extraction protocol [19]. Sequencing was performed with the MiSeq tool (Illumina; USA) using the MiSeq Reagent Nano Kit v2 (500cycle) (Illumina; USA) in accordance with the manufacturer's recommendations. Genomes were assembled with the SPAdes tool (v.3.14.0). The GeneMarkS online service (ver. 4.32) was used for identification of open reading frames (ORFs) in the genome. The search for tRNA genes was performed with the ARAGORN tool.

The predicted genes were annotated manually using BLASTp, HHPred and InterPro. The absence of genes encoding toxins and antibiotic resistance determinants was confirmed by matching against the databases of the pathogenic bacteria virulence factors [20] and antibiotic resistance genes [21]. The annotated genome sequences of bacteriophages vB_KpnM_NDO71, vB_KpnS_MAG26fr, vB_KpnS_MDA2066, and vB_KpnS_PMM-G3 were deposited in the GenBank database with the numbers OP558001, OP558002, OP558003, and OP558005, respectively.

Phylogenetic analysis involved 62 reference bacteriophage genomes recommended by the International Committee on Taxonomy of Viruses (ICTV). Phylogenetic trees were constructed in the offline version of the ViPTree server (v. 1.1.2) based on the pairwise genetic distanced between the phage genomes [22]. The closest bacteriophage homologues were

defined using the BLASTn algorithm. BLASTp services were used to compare the sequences of certain proteins.

RESULTS

Isolation, morphology and host range of the *K. pneumoniae* bacteriophages

A total of four *K. pneumoniae* bacteriophages were isolated from the water sample collected from the Likhoborka River (Moscow) by enrichment culture method: vB_KpnM_NDO71, vB_KpnS_MAG26fr, vB_KpnS_MDA2066, and vB_KpnS_PMM-G3. The clinical strains with certain capsular types isolated in 2020 were used as host strains: *K. pneumoniae* Kp71 (capsular type KL45), Kp26f (KL19), Kp2066 (KL107), and KpG3 (KL28).

Bacteriophage vB_KpnM_NDO71 formed small (0.5 mm) plaques surrounded by wide (2–4 mm) halos. The plaques formed by bacteriophage vB_KpnS_PMM-G3 were much larger (1–2 mm) and had wide (4–5 mm) halos. Bacteriophages vB_KpnS_MAG26fr and vB_KpnS_MDA2066 formed small (0.5 mm) plaques surrounded by small (1–2 mm) halos (Fig. 1).

Bacteriophage host ranges were assessed on a collection of 180 *K. pneumoniae* strains with known capsular types based on the *wzi* gene sequence typing. The strains had 31 unique capsular types, among which KL2 (19.4%), KL23 (9.4%), KL39 (8.9%), KL64 (8.9%), and KL20 (6.1%) were the most common.

Bacteriophages vB_KpnM_NDO71, vB_KpnS_MAG26fr, and vB_KpnS_PMM-G3 had a narrow lytic spectrum and lysed all strains with the capsular type of the host strain: KL45 ($n = 4$; 2.2%), KL19 ($n = 6$; 3.3%), and KL28 ($n = 4$; 2.2%), respectively. Bacteriophage vB_KpnS_MDA2066 demonstrated lytic activity against strains with two different capsular types: KL19 and KL107 ($n = 7$; 3.9%).

Bacteriophage whole-genome sequencing and phylogenetic analysis

Genomes of the studied bacteriophages were represented by double-stranded DNA molecules with the length of 49,477–158,414 bps and G+C content of 44.4–56.1% (Table 1). The number of predicted open reading frames (ORFs) varied between 76 and 236. Some tRNA genes were revealed in bacteriophages vB_KpnM_NDO71 and vB_KpnS_MDA2066 (21 and 7, respectively).

A phylogenetic tree was constructed based on the whole-genome sequences of phages recommended by ICTV in order to define the taxonomic status of bacteriophages (Fig. 2). Bacteriophages vB_KpnM_NDO71, vB_KpnS_MAG26fr, vB_KpnS_MDA2066, and vB_KpnS_PMM-G3 belonged to different phyla and were parts of the clusters formed by members of the Mydovirus, Yonseivirus, Taipeivirus, and Webervirus genera, respectively, of the phylogenetic tree.

According to the results of BLASTn analysis, Klebsiella phage vB_KpnM_KB57 (GenBank KT934943.1; 84% query coverage and 96.49% sequence identity) turned out to be the closest homologue of phage vB_KpnM_NDO71, Klebsiella
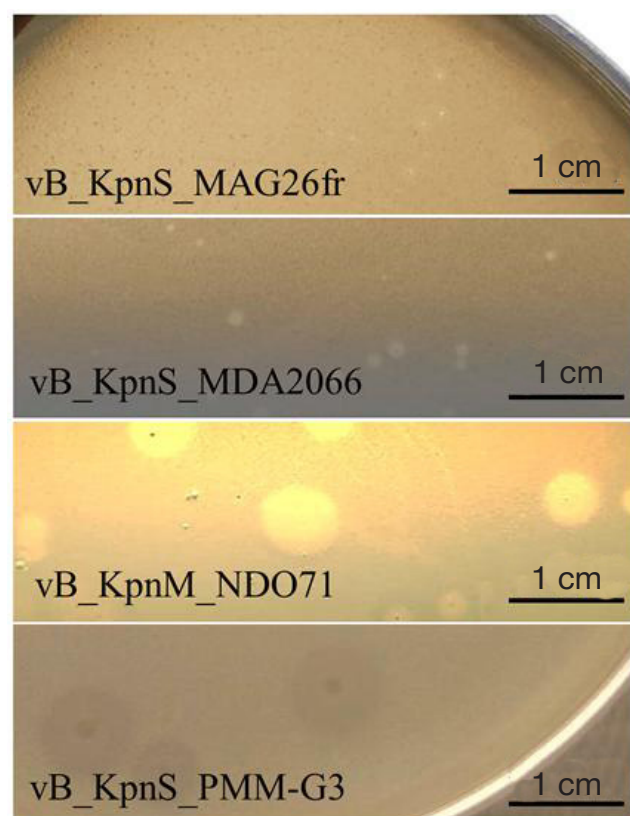
Fig. 1. Morphology of the vB_KpnM_NDO71, vB_KpnS_MAG26fr, vB_KpnS_MDA2066 and vB_KpnS_PMM-G3 phage plaques

phage S9a (GenBank ON623732.1; 71% query coverage and 93.88% sequence identity) was most close to phage vB_KpnS_MAG26fr, Klebsiella virus UPM 2146 (GenBank NC_049472.1; 95% query coverage and 98.98% sequence identity) was most close to phage vB_KpnS_MDA2066, and Klebsiella virus UPM 2146 (GenBank NC_049472.1; 95% query coverage and 98.98% sequence identity) was the closest homologue of phage vB_KpnS_PMM-G3.

Functional analysis of *K. pneumoniae* phages

We successfully predicted the functions of 61 proteins during functional annotation of the vB_KpnM_NDO71 phage genome. The bacteriophage structural organization was typical for rV5-like phages: the phage did not encode RNA polymerase and produced o-spanin as a lytic protein. In contrast to homologue phages Seu621 and VIK251 [23, 24], DNA polymerase gene found in the vB_KpnM_NDO71 phage genome was divided into two reading frames by the gene encoding homing endonuclease.

As for phage vB_KpnS_MAG26fr, the expected functions (structural proteins; enzymes involved in replication, regulation, transcription and translation of DNA; lysis of the host) were attributed to the products of 42 ORFs. Of these 19 were structural proteins of the phages, while the cassette comprising five proteins (o-spanin, component of the inner membrane

Table 1. General characteristics of the genomes of phages vB_KpnM_NDO71, vB_KpnS_MAG26fr, vB_KpnS_MDA2066, and vB_KpnS_PMM-G3

Bacteriophage	Genome size, bp	G+C	ORF	tRNA
vB_KpnM_NDO71	136 566	44,40%	236	21
vB_KpnS_MAG26fr	59 701	56,10%	79	0
vB_KpnS_MDA2066	158 414	46,40%	208	7
vB_KpnS_PMM-G3	49 477	50,10%	76	0
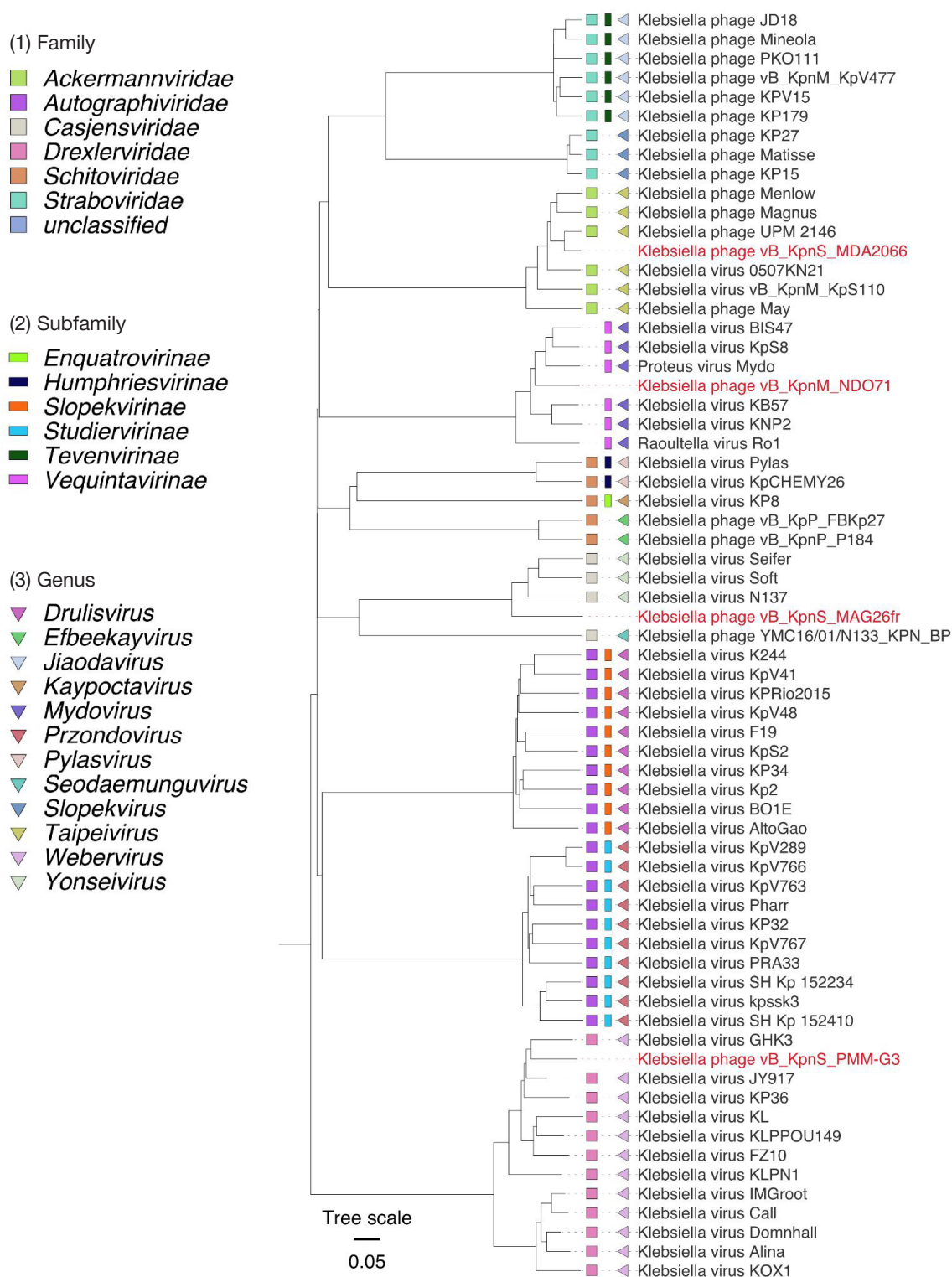
Fig. 2. Phylogeny of the *K. pneumoniae* bacteriophages. The studied bacteriophages are highlighted in red

spanin, endolysin, and two proteins of the choline–anti-choline system) was responsible for the host cell lysis.

Bacteriophage vB_KpnS_MDA2066 encoded 80 proteins assigned the expected functions. Of these 27 were structural proteins, 52 belonged to genes involved in replication, regulation, transcription and translation of DNA. Furthermore, phage encoded one endolysin protein responsible for lysis of the host bacterium.

Of 76 ORFs of the vB_KpnS_PMM-G3 phage, 43 encoded proteins assigned the expected functions, the majority of which were considered structural proteins. The bacteriophage had

genome structural organization typical for T1-like bacteriophages and encoded no genes of DNA and RNA polymerases.

Bacteriophage receptor-binding proteins

Five ORFs of the vB_KpnM_NDO71 bacteriophage were annotated as proteins of the phage tail fibers based on the results of functional analysis. It was later found that NDO71_orf047 carried a depolymerase domain represented by pectate lyase 4 (Table 2). The analysis performed using BLASTp showed that this protein shared a high degree of homology

Table 2. Predicted depolymerase domains of phages vB_KpnM_NDO71, vB_KpnS_MAG26fr, vB_KpnS_MDA2066 and vB_KpnS_PMM-G3

ORF	Depolymerase domain	Protein size, aa	Similarity with the closest homologue, %		
			N-terminal domain	Depolymerase domain	C-terminal domain
vB_KpnM_NDO71					
orf047	Pectate lyase 4	597	0	90,8	57,8
vB_KpnS_MAG26fr					
orf055	Family 48 glycoside hydrolase	941	29,4	41,8	50,8
vB_KpnS_PMM-G3					
orf046	Pectate lyase 3	742	98,5	83,5	99,7
vB_KpnS_MDA2066					
orf130	Pectate lyase 3	960	0	38,2	33,5
orf131	Family 28 glycoside hydrolase	766	6,8	73,4	64,7
orf133	Family 28 glycoside hydrolase	660	100	100	100
orf135	Family 28 glycoside hydrolase	721	31,8	67,2	59,6

with the hypothetical proteins of the *K. pneumoniae* prophages (GenBank WP_180812430.1; 89% query coverage and 68.97% sequence identity).

The vB_KpnS_MDA2066 genome also encoded five proteins annotated as proteins of the phage tail fibers. However, in contrast to vB_KpnM_NDO71, four predicted phage tail fiber proteins out of five carried the polysaccharide depolymerase domains: pectate lyase 3 in MDA2066_orf130 and family 28 glycoside hydrolases in MDA2066_orf131, MDA2066_orf133, and MDA2066_orf135. Two phage tail fiber proteins of bacteriophage vB_KpnS_MDA2066 (orf131 and orf135) demonstrated more than 50% homology with the previously reported tail fibers of Klebsiella phage K64-1 that showed specificity for capsular types K30/K69 and KN4, respectively. The tail fiber protein MDA2066_orf130 shared a certain degree of homology (53% query coverage and 34.87% sequence identity according to BLASTp) with the tail fiber protein of the previously reported phage P929 showing lytic activity against strains with the KL19 capsular type (Table 2). The fourth tail fiber protein MDA2066_orf133 was identical to the tail fiber protein of the Klebsiella virus UPM 2146 phage and shared a high degree of homology with similar proteins of the Taipeivirus genus phages (100% query coverage and 99% sequence identity).

The vB_KpnS_MAG26fr phage genome encoded two proteins annotated as proteins of the phage tail fibers. One of these proteins (MAG26fr_orf055) encoded a depolymerase domain represented by the family 48 glycoside hydrolase (Table 2). The Soft bacteriophage distal tail protein (GenBank YP_009851405.1; 100% query coverage and 46.36% sequence identity) was the closest homologue of this tail fiber protein.

Similar to phage vB_KpnS_MAG26fr, the vB_KpnS_PMM-G3 encoded two tail fiber proteins. A closer analysis made it possible to predict a polysaccharide depolymerase domain represented by pectatlyase 3 for one of these proteins (PMMG3_orf046). This protein shared a high degree of homology with the tail fiber protein of the undescribed Klebsiella phage VLCpiD7c (GenBank UVX29830.1; 100% query coverage and 95.15% sequence identity).

DISCUSSION

A total of four bacteriophages capable of lysing K. pneumoniae strains with the capsular types KL19, KL28, KL45 and KL107 were isolated during the study. It should be noted that

bacteriophages showing activity against three types were reported for the first time, while phages vB_KpnS_MDA2066 and vB_KpnS_MAG26fr showed activity against strains with the KL19 capsular type, just like the previously reported Klebsiella phage P929 [25].

We have used the whole-genome sequencing, that has been increasingly used to define the phage taxonomic status and structural organization in recent years [26], to describe the genetic features of the phages. Phylogenetic analysis has revealed that the studied phages belong to different genera and families. Furthermore, genome alignment using the BLASTn algorithm has revealed significant differences (> 5%) from genomes of the closest phages, thus allowing the researchers to conclude that the studied bacteriophages are members of new species [26].

Functional analysis of the encoded genes showed that the genome structural organization of the phages was typical for the members of appropriate genera. Bacteriophages were strictly virulent and contained no integrase genes, potentially dangerous toxin genes or antibiotic resistance determinants. This makes it possible to use the phages in therapeutic practice.

The receptor-binding proteins represented by polysaccharide depolymerases were predicted in genomes of all four bacteriophages. No homology with the bacteriophages previously reported in literature was revealed in depolymerases of bacteriophages vB_KpnM_NDO71, vB_KpnS_MAG26fr, and vB_KpnS_PMM-G3. This expands the theoretical knowledge and the possibilities of the future development of the broad-spectrum polysaccharide depolymerase-based drugs. Three tail fibers of the vB_KpnS_MDA2066 bacteriophage (orf130, orf131, and orf135) showed a certain degree of homology with the tail fiber proteins with known specificity: KL19, K30/K69, and KN4, respectively. Meanwhile, the main differences were found in the N-terminus that encoded sites of the tail fiber attachment to other phage proteins. By contrast, a high degree of homology was observed in the region of the predicted enzyme domain and in the C-terminus responsible for substrate recognition [27] (Table 2). It is also worth mentioning that there were no samples with the K30/K69 capsular type in the tested collection of *K. pneumoniae* clinical isolates, and the other typing scheme should be used to define the KN4 type.

The lytic spectrum of the studied phages is limited to four capsular types. Despite the fact that there is a small number of strains with capsular types KL19, KL28, KL45, and KL107 in the tested collection (11.7%), isolates with these capsular types

are associated with nosocomial infections resistant to a wide range of antibiotics, including colistin [28]. Furthermore, two phages show activity against strains with the KL19 capsular type (vB_KpnS_MAG26fr and vB_KpnS_MDA2066 have polysaccharide depolymerase domains of different types), which could potentially result in lower frequency of mutation in case of the combined use.

When developing medications, several bacteriophages with various lytic profiles are usually combined into phage cocktails to increase the therapeutic efficiency. Currently, the following requirements are applied to such cocktails: the bacteriophage titer in the preparation should not be below 10^8 PFU/mL, bacteriophages should be strictly virulent and should not contain potentially dangerous genes, bacteriophages should effectively lyse causative agents of infections [29, 30]. Thus, combining these phages with other capsule-specific bacteriophages has the potential to raise the therapeutic cocktail efficiency to 100%.

CONCLUSIONS

The studied bacteriophages vB_KpnM_NDO71, vB_KpnS_MAG26fr, vB_KpnS_MDA2066, and vB_KpnS_PMM-G3 belong to new species of the well-characterized families and subfamilies and are promising candidates for the development of efficient phage cocktails. In turn, the predicted depolymerases showing activity against rare capsular types KL19, KL28, KL45, and KL107 may be the subjects of further study as potential therapeutic agents.

ACKNOWLEDGMENTS

References

1. Paczosa MK, Mecsas J. Klebsiella pneumoniae: Going on the Offense with a Strong Defense. Microbiol Mol Biol Rev. 2016; 80 (3): 629–61.
2. Touati A, Mairi A, Baloul Y, Lalaoui R, Bakour S, Thighilt L et al. First detection of Klebsiella pneumoniae producing OXA-48 in fresh vegetables from Béjaïa city, Algeria J Glob Antimicrob. Resist. 2017; 9: 17–18.
3. Podschun R, Ullmann U. Klebsiella spp. as nosocomial pathogens: Epidemiology, taxonomy, typing methods, and pathogenicity factors. Clin Microbiol Rev. 1998; 11 (4): 589–603.
4. Sukhorukova MV, Edelstein MV, Skleenova EY, Ivanchik NV, Shajdullina ER, Azyzov IS et al. Antimicrobial resistance of nosocomial Enterobacterales isolates in Russia: results of multicenter epidemiological study "MARATHON 2015–2016". 2019; 21 (2): 147–59.
5. Kuzmenkov AY, Vinogradova AG, Trushin IV, Eidelstein MV, Avramenko AA, Dehnich AV et al. AMRmap — ANTIBIOTIC RESISTANCE SURVEILLANCE SYSTEM IN RUSSIA. Kliniceskaa Mikrobiologia i Antimikrobnaa Himioterapia, 2021; 23 (2): 198–204.
6. Murray CJ, Ikuta KS, Sharara F, Swetschinski L, Aguilar GR, Gray A, et al. Global burden of bacterial antimicrobial resistance in 2019: a systematic analysis. Lancet. 2022; 399 (10325): 629–55.
7. Górski A, Międzybrodzki R, Węgrzyn G, Jończyk-Matysiak E, Borysowski J, Weber-Dąbrowska B. Phage therapy: Current status and perspectives. Med Res Rev. 2020; 40 (1): 459–63.
8. Clokie MR, Millard AD, Letarov AV, Heaphy S. Phages in nature. Bacteriophage. 2011; 1 (1): 31.
9. D'Herelle MF. On an invisible microbe antagonistic to dysentery bacilli. Comptes Rendus Acad des Sci Paris. 1917; 165: 373–5.
10. Khatami A, Lin RC, Petrovic-Fabijan A, Alkalay-Oren S, Almuzam S, Britton PN et al. Bacterial lysis, autophagy and innate immune responses during adjunctive phage therapy in a child. EMBO Mol Med. 2021; 13 (9): e13936.
11. Leitner L, Ujmajuridze A, Chanishvili N, Goderdzishvili M, Chkonia I, Rigvava S et al. Intravesical bacteriophages for treating urinary tract infections in patients undergoing transurethral resection of the prostate: a randomised, placebo-controlled, double-blind clinical trial. Lancet Infect Dis. 2021; 21 (3): 427–36.
12. Petrovic Fabijan A, Lin RC, Ho J, Maddocks S, Ben Zakour NL, Iredell JR. Safety of bacteriophage therapy in severe Staphylococcus aureus infection. Nat Microbiol. 2020; 5 (3): 465–72.
13. Verbeken G, Pirnay JP. European regulatory aspects of phage therapy: magistral phage preparations. Curr Opin Virol. 2022; 52 (November): 24–29.
14. Pires DP, Oliveira H, Melo LD, Sillankorva S, Azeredo J. Bacteriophage-encoded depolymerases: their diversity and biotechnological applications. Appl. Microbiol Biotechnol. 2016;

100 (5): 2141–51.
15. Danis-Wlodarczyk KM, Wozniak DJ, Abedon ST. Treating bacterial infections with bacteriophage-based enzybiotics: In vitro, in vivo and clinical application. Antibiotics. 2021; 10 (12): 1–36.
16. Kornienko M, Ilina E, Lubasovskaya L, Priputnevich T, Falova O, Sukhikh G et al. Analysis of nosocomial Staphylococcus haemolyticus by MLST and MALDI-TOF mass spectrometry. Infect. Genet Evol. 2016; 39: 99–105.
17. Brisse S, Passet V, Haugaard AB, Babosan A, Kassis-Chikhani N, Struve C et al. Wzi gene sequencing, a rapid method for determination of capsulartype for klebsiella strains. J Clin Microbiol. 2013; 51 (12): 4073–8.
18. Mazzocco A, Waddell TE, Lingohr E, Johnson RP. Enumeration of Bacteriophages by the Direct Plating Plaque Assay. Methods Mol. Biol. Humana Press. 2009; 501: 77–80.
19. Green MR, Sambrook J. Molecular Cloning: a Laboratory Manual. New York: Cold Spring Harbor Laboratory Press, 2012; 1890 p.
20. Liu B, Zheng D, Jin Q, Chen L, Yang J. VFDB 2019: A comparative pathogenomic platform with an interactive web interface. Nucleic Acids Res. 2019; 47 (D1): D687–D692.
21. Liu B, Pop M. ARDB — Antibiotic resistance genes database. Nucleic Acids Res. 2009; 37 (SUPPL. 1): 443–447.
22. Nishimura Y, Yoshida T, Kuronishi M, Uehara H, Ogata H, Goto S. ViPTree: the viral proteomic tree server. Bioinformatics. 2017; 33 (15): 2379–80.
23. Gorodnichev RB, Volozhantsev NV, Krasilnikova VM, Bodoev IN, Kornienko MA, Kuptsov NS et al. Novel Klebsiella pneumoniae K23-Specific Bacteriophages From Different Families: Similarity of Depolymerases and Their Therapeutic Potential. Front Microbiol. 2021; 12: 669618.
24. Gorodnichev RB, Kornienko MA, Kuptsov NS, Malakhova MV, Bespiatykh DA, Veselovsky VA et al. Molecular Genetic Characterization Of Three New Klebsiella pneumoniae Bacteriophages Suitable For Phage Therapy. Extreme medicine. 2021; 23 (3): 90-97.
25. Chen X, Tang Q, Li X, Zheng X, Li P, Li M et al. Isolation, characterization, and genome analysis of bacteriophage P929 that could specifically lyase the KL19 capsular type of Klebsiella pneumoniae. Virus Res. 2022; 314: 198750.
26. Turner D, Kropinski AM, Adriaenssens EM. A Roadmap for Genome-Based Phage Taxonomy. Viruses. 2021; 13 (3): 506.
27. Squeglia F, Maciejewska B, Łątka A, Ruggiero A, Briers Y, Drulis-Kawa Z et al. Structural and Functional Studies of a Klebsiella Phage Capsule Depolymerase Tailspike: Mechanistic Insights into Capsular Degradation. Structure. 2020; 28 (6): 613–624.e4.
28. Zhao J, Liu C, Liu Y, Zhang Y, Xiong Z, Fan Y et al. Genomic characteristics of clinically important ST11 Klebsiella pneumoniae strains worldwide. J Glob Antimicrob Resist. 2020;

22: 519–6.
29. Petrovic Fabijan A, Khalid A, Maddocks S, Ho J, Gilbey T, Sandaradura I et al. Phage therapy for severe bacterial infections: a narrative review. Med J Aust. 2020; 212 (6): 279–5.

30. Aslanov BI, Zueva LP, Kaftyreva LA, Bojcov AG, Akimkin VG, Dolgij AA. et al. Racional'noe primenenie bakteriofagov v lechebnoj i protivojepidemicheskoj praktike. Izd-vo «Remedium Privolzh'e»; 2014; 54 c.

Литература

1. Paczosa MK, Mecsas J. Klebsiella pneumoniae: Going on the Offense with a Strong Defense. Microbiol Mol Biol Rev. 2016; 80 (3): 629–61.

2. Touati A, Mairi A, Baloul Y, Lalaoui R, Bakour S, Thighilt L et al. First detection of Klebsiella pneumoniae producing OXA-48 in fresh vegetables from Béjaïa city, Algeria J Glob Antimicrob. Resist. 2017; 9: 17–18.

3. Podschun R, Ullmann U. Klebsiella spp. as nosocomial pathogens: Epidemiology, taxonomy, typing methods, and pathogenicity factors. Clin Microbiol Rev. 1998; 11(4): 589–603.

4. Сухорукова, М. В., Эйдельштейн, М. В., Иванчик, Н. В., Склеенова, Е. Ю., Шайдуллина, Э. Р., Азизов, И. С., и др. Антибиотикорезистентность нозокомиальных штаммов Enterobacterales в стационарах России: результаты многоцентрового эпидемиологического исследования «МАРАФОН 2015–2016». Клиническая микробиология и антимикробная химиотерапия. 2019; 21(2): 147–59.

5. Кузьменков, А. Ю., Виноградова, А. Г., Трушин, И. В., Эйдельштейн, М. В., Авраменко, А. А., Дехнич А.В. и др. AMRmap — система мониторинга антибиотикорезистентности в России. Клиническая микробиология и антимикробная химиотерапия. 2021; 23(2): 198–204.

6. Murray CJ, Ikuta KS, Sharara F, Swetschinski L, Aguilar GR, Gray A, et al. Global burden of bacterial antimicrobial resistance in 2019: a systematic analysis. Lancet. 2022; 399(10325): 629–55.

7. Górski A, Międzybrodzki R, Węgrzyn G, Jończyk-Matysiak E, Borysowski J, Weber-Dąbrowska B. Phage therapy: Current status and perspectives. Med Res Rev. 2020; 40(1): 459–463.

8. Clokie MR, Millard AD, Letarov AV, Heaphy S. Phages in nature. Bacteriophage. 2011; 1 (1): 31.

9. D'Herelle MF. On an invisible microbe antagonistic to dysentery bacilli. Comptes Rendus Acad des Sci Paris. 1917; 165: 373–5.

10. Khatami A, Lin RC, Petrovic-Fabijan A, Alkalay-Oren S, Almuzam S, Britton PN et al. Bacterial lysis, autophagy and innate immune responses during adjunctive phage therapy in a child. EMBO Mol Med. 2021; 13 (9): e13936.

11. Leitner L, Ujmajuridze A, Chanishvili N, Goderdzishvili M, Chkonia I, Rigvava S et al. Intravesical bacteriophages for treating urinary tract infections in patients undergoing transurethral resection of the prostate: a randomised, placebo-controlled, double-blind clinical trial. Lancet Infect Dis. 2021; 21 (3): 427–36.

12. Petrovic Fabijan A, Lin RC, Ho J, Maddocks S, Ben Zakour NL, Iredell JR. Safety of bacteriophage therapy in severe Staphylococcus aureus infection. Nat Microbiol. 2020; 5 (3): 465–72.

13. Verbeken G, Pirnay JP. European regulatory aspects of phage therapy: magistral phage preparations. Curr Opin Virol. 2022; 52 (November): 24–29.

14. Pires DP, Oliveira H, Melo LD, Sillankorva S, Azeredo J. Bacteriophage-encoded depolymerases: their diversity and biotechnological applications. Appl. Microbiol Biotechnol. 2016; 100 (5): 2141–51.

15. Danis-Wlodarczyk KM, Wozniak DJ, Abedon ST. Treating bacterial infections with bacteriophage-based enzybiotics: In vitro, in vivo and clinical application. Antibiotics. 2021; 10 (12): 1–36.

16. Kornienko M, Ilina E, Lubasovskaya L, Priputnevich T, Falova O, Sukhikh G et al. Analysis of nosocomial Staphylococcus haemolyticus by MLST and MALDI-TOF mass spectrometry. Infect. Genet Evol. 2016; 39: 99–105.

17. Brisse S, Passet V, Haugaard AB, Babosan A, Kassis-Chikhani N, Struve C et al. Wzi gene sequencing, a rapid method for determination of capsulartype for klebsiella strains. J Clin Microbiol. 2013; 51 (12): 4073–8.

18. Mazzocco A, Waddell TE, Lingohr E, Johnson RP. Enumeration of Bacteriophages by the Direct Plating Plaque Assay. Methods Mol. Biol. Humana Press. 2009; 501: 77–80.

19. Green MR, Sambrook J. Molecular Cloning: a Laboratory Manual. New York: Cold Spring Harbor Laboratory Press, 2012; 1890 p.

20. Liu B, Zheng D, Jin Q, Chen L, Yang J. VFDB 2019: A comparative pathogenomic platform with an interactive web interface. Nucleic Acids Res. 2019; 47 (D1): D687–D692.

21. Liu B, Pop M. ARDB — Antibiotic resistance genes database. Nucleic Acids Res. 2009; 37 (SUPPL. 1): 443–7.

22. Nishimura Y, Yoshida T, Kuronishi M, Uehara H, Ogata H, Goto S. ViPTree: the viral proteomic tree server. Bioinformatics. 2017; 33 (15): 2379–80.

23. Gorodnichev RB, Volozhantsev NV, Krasilnikova VM, Bodoev IN, Kornienko MA, Kuptsov NS et al. Novel Klebsiella pneumoniae K23-Specific Bacteriophages From Different Families: Similarity of Depolymerases and Their Therapeutic Potential. Front Microbiol. 2021; 12: 669618.

24. Городничев Р. Б., Корниенко М. А., Купцов Н. С., Малахова М. В., Беспятых Д. А., Веселовский В. А. и др. Молекулярно-генетическая характеристика трех новых бактериофагов Klebsiella pneumoniae, перспективных для применения в фаговой терапии. Медицина экстремальных ситуаций. 2021; 23 (3): 90–97.

25. Chen X, Tang Q, Li X, Zheng X, Li P, Li M et al. Isolation, characterization, and genome analysis of bacteriophage P929 that could specifically lyase the KL19 capsular type of Klebsiella pneumoniae. Virus Res. 2022; 314: 198750.

26. Turner D, Kropinski AM, Adriaenssens EM. A Roadmap for Genome-Based Phage Taxonomy. Viruses. 2021; 13 (3): 506.

27. Squeglia F, Maciejewska B, Łątka A, Ruggiero A, Briers Y, Drulis-Kawa Z et al. Structural and Functional Studies of a Klebsiella Phage Capsule Depolymerase Tailspike: Mechanistic Insights into Capsular Degradation. Structure. 2020; 28 (6): 613–24.e4.

28. Zhao J, Liu C, Liu Y, Zhang Y, Xiong Z, Fan Y et al. Genomic characteristics of clinically important ST11 Klebsiella pneumoniae strains worldwide. J Glob Antimicrob Resist. 2020; 22: 519–6.

29. Petrovic Fabijan A, Khalid A, Maddocks S, Ho J, Gilbey T, Sandaradura I et al. Phage therapy for severe bacterial infections: a narrative review. Med J Aust. 2020; 212 (6): 279–85.

30. Асланов, Б. И., Зуева, Л. П., Кафтырева, Л. А., Бойцов, А. Г., Акимкин, В. Г., Долгий, А. А. и др. Рациональное применение бактериофагов в лечебной и противоэпидемической практике. Изд-во «Ремедиум Приволжье», 2014; 54 с.

EVALUATION OF METHODS OF AVIAN LEUCOSIS VIRUS INACTIVATION IN PRODUCTION OF INFLUENZA VACCINES

Savina NN[1], Ekimov AA[1] ✉, Shuklina MA[2], Trukhin VP[1], Evtushenko AE[1], Zhirenkina EN[1], Stepanova LA[2]

[1] St. Petersburg Research Institute of Vaccines and Serums and Bacterial Preparations Production Company of the FMBA of Russia, St. Petersburg, Russia

[2] Smorodintsev Research Institute of Influenza, St. Petersburg, Russia

The process of production of inactivated influenza vaccines involves a stage of inactivation of both the influenza virus and the possible viral contaminants that can come from the raw materials (chicken embryos). One of such contaminants is the avian leucosis virus. The minimum viral contaminant load reduction that the inactivating agents should guarantee is by 4 lg/ml; this or higher level of the deactivating ability ensures the finished vaccine is free from viral contaminants. The purpose of this work was to cultivate the leucosis virus to the titer of 5 lg/ml (minimum) and to measure the reduction of the avianleucosis virus titer in influenza vaccine intermediates upon exposure to the inactivating agents. The RAV-1 and RAV-2 leucosis virus strains and influenza vaccine intermediates such as virus-containing allantoic fluid and virus concentrates were used in the study. Avian leucosis virus titers were determined by enzyme immunoassay. We created conditions for cultivation of the RAV-1 and RAV-2 avian leucosis virus strains in the primary culture of chicken embryo fibroblasts (CEF); the inactivating agents considered were the most commonly used β-propiolactone and UV radiation. It was found that after 12 hours of exposure to β-propiolactone, the RAV-1 avian leucosis virus load decreased by 4.61 ± 0.46 lg, and that of RAV-2 strain — by 4.33 ± 0.33 lg, which indicates that β-propiolactone is an effective inactivating agent. Five minutes of exposure to UV radiation reduces the RAV-1 strain viral load by 4.22 ± 0.31 lg and RAV-2 strain viral load by 4.44 ± 0.48 lg.

Keywords: influenza vaccines, inactivation, avian leucosis virus, RAV-1, RAV-2, propiolactone, UV radiation

ОЦЕНКА МЕТОДОВ ИНАКТИВИРОВАНИЯ ВИРУСА ЛЕЙКОЗА ПТИЦ ПРИ ПРОИЗВОДСТВЕ ГРИППОЗНЫХ ВАКЦИН

Н. Н. Савина[1], А. А. Екимов[1] ✉, М. А. Шуклина[2], В. П. Трухин[1], А. Э. Евтушенко[1], Е. Н. Жиренкина[1], Л. А. Степанова[2]

[1] Санкт-Петербургский научно-исследовательский институт вакцин и сывороток и предприятие по производству бактерийных препаратов Федерального медико-биологического агентства, Санкт-Петербург, Россия

[2] Научно-исследовательский институт гриппа имени А. А. Смородинцева Минздрава России, Санкт-Петербург, Россия

При производстве инактивированных гриппозных вакцин на стадии инактивации должен быть инактивирован как вирус гриппа, так и возможные вирусные контаминанты, которые могут попасть в вакцину из сырья (куриных эмбрионов). Одним из возможных контаминантов является вирус лейкоза птиц. Инактиваторы должны обеспечивать гарантированное снижение вирусной нагрузки контаминанта не менее чем на 4 lg/мл, что обеспечит его отсутствие в готовой вакцине. Целью работы было осуществить наработку вируса лейкоза для достижения минимального титра 5 lg/мл, оценить снижение титра вируса лейкоза птиц в полупродуктах гриппозных вакцин при воздействии инактиваторов. В исследовании использовали штаммы вируса лейкоза RAV-1 и RAV-2 и полупродукты гриппозных вакцин, такие как вируссодержащая аллантоисная жидкость и вирусные концентраты. Титры вируса лейкоза птиц определяли методом иммуноферментного анализа. Были подобраны условия наработки вируса лейкоза птиц штаммов RAV-1 и RAV-2 в первичной культуре фибробластов эмбрионов кур (ФЭК); рассмотрены основные используемые инактиваторы — β-пропиолактон и УФ-излучение. Выявлено, что спустя 12 ч инактивации β-пропиолактоном вирус лейкоза птиц штамма RAV-1 показал снижение вирусной нагрузки на 4.61 ± 0.46 lg, а вирус лейкоза птиц штамма RAV-2 — на 4.33 ± 0.33 lg, что указывает на эффективное действие β-пропиолактона при инактивации. Проведение инактивации УФ-излучением позволяет снизить вирусную нагрузку штамма RAV-1 на 4.22 ± 0.31 lg, а штамма RAV-2 на 4.44 ± 0.48 lg за 5 мин.

Ключевые слова: гриппозные вакцины, инактивация, вирус лейкоза птиц, RAV-1, RAV-2, пропиолактон, УФ-излучение

To make the end product safe, the influenza virus should be completely inactivated during production of the inactivated influenza vaccines. This is a recommendation by both the World Health Organization and the European Medical Agency [1, 2]; for vaccines of international quality, it is a requirement. Chicken embryos used in the production of influenza vaccines can potentially carry zoonotic infections, such as the avian leucosis virus, avian adenovirus, mycoplasma. The mentioned recommendation prescribes that the vaccine production technology includes measures aimed at inactivation of the listed contaminants, too.

There are various ways of inactivating viruses in production of vaccines, including those employing UV radiation, formaldehyde or β-propiolactone [3]. The efficacy of these agents against viruses differs.

An earlier research investigated the effect of inactivating agents on avian adenovirus of CELO and Fontes strains [4]: both β-propiolactone and UV radiation were found to be effective in inactivating these strains. It was established that after 10 hours of exposure to β-propiolactone, the viral load associated with the CELO strain adenovirus decreased by 4.12 ± 0.06 lg (PFU)/ml and that by the Fontes strain adenovirus — by 4.20 ± 0.19 lg (PFU)/ml, which indicates that β-propiolactone is an effective solution to the inactivation task. Five minutes of exposure to UV radiation reduces the CELO strain viral load by 4.22 ± 0.31 lg and Fontes strain viral load by 4.44 ± 0.48 lg. It was noted that detergent added at the scission stage also reduces the viral load by 0.93 ± 0.15 lg (PFU)/ml and 1.04 ± 0.12 lg (PFU)/ml in case of CELO and Fontes strains, respectively, when the substance is n-octyl-β-D-glucopyranoside, and by 1.18 ± 0.17 lg (PFU)/ml and 1.12 ± 0.38 lg (PFU)/ml when the substance is tetradecyltrimethylammonium bromide.

In this connection, it became necessary to study in detail the effect of the above agents on another possible contaminant, the avian leucosis virus. The avian leucosis virus belongs to RNA-containing oncornaviruses of the *Retraviridae* family; they cause leucosis and sarcomas in birds and include six antigenic subgroups A, B, C, D, E, J. The viruses of this group are found in tumor tissue, blood, parenchymal organs and in chicken eggs. A team of researchers has investigated the subject of avian leucosis virus in poultry farms of the Russian Federation and found antibodies thereto at 90% of the farms involved in the study [5]. Thus, there is a serious risk of contamination of eggs used in vaccine production with avian leucosis virus. It should also be noted that there is an urgent need to introduce regulations in the Russian Federation prescribing use of hatching eggs free from the avian leucosis virus in vaccine production.

The use of UV radiation to inactivate viruses has been investigated earlier, but there was only one strain considered, RAV-1 [6]. Formaldehyde is one of the potential inactivating agents, but it can jeopardize the stability of the finished influenza vaccine and its immunogenicity, since it is a highly reactive compound; moreover, formaldehyde is capable of chemically modifying the influenza virus hemagglutinin and affecting the antigenic determinants [7, 8]. Another chemical inactivating agent, β-propiolactone, does not have these drawbacks; it effectively inactivates the influenza virus and is hydrolyzed to 3-hydroxypropionic acid, an intermediate metabolite of human lipid metabolism [9], this hydrolysis being a positive factor for the safety of the vaccine.

The purpose of this study was to select an optimal agent to inactivate the contaminant of influenza vaccines, avian leucosis virus, its most common groups RAV-1 (subgroup A) and RAV-2 (subgroup B) in particular. We also aimed to find out the minimum duration of the inactivation stage that guarantees viral load reduction by at least 4 lg infectious units (IU)/ml [10].

METHODS

Materials

For our study, we used:
– avian leucosis virus RAV-1 (ATCC-VR-335) from the ATCC collection (USA);
– avian leucosis virus RAV-2 (ATCC-VR-1828) from the ATCC collection (USA);
– 10-day-old chicken embryos from Sinyavinskaya Poultry Farm (Russia);
– IDEXX ALV Ag Test (IDEXX Laboratoties, Inc., USA).

Virus-containing allantoic fluid

We used 9–11-day-old chicken embryos to cultivate the influenza virus. The embryos were infected with a dose of 0.2 ml, infectious activity 102.0–104.5, and an egg infective dose 50 (EID_{50}). Chicken embryos were incubated at 35 °C for 48 hours for type A influenza virus and for 72 hours in case of type B influenza virus. After incubation, the embryos were cooled and allantoic fluid containing the virus (AF) harvested.

Virus concentrates (VC)

We filtered AF through a cascade of filters with a pore diameter of 10.6 and 1 μm, then concentrated the resulting fluid and put it into the ultrafiltration unit with cutoff at 300 kDa. The concentrated virus-containing allantoic fluid was ultracentrifuged in the sucrose density gradient (60–20%). We harvested fractions of the sucrose gradient in the range of 40–25% of sucrose. The harvested fractions were mixed and stored at –20 °C until the study.

RAV-1 and RAV-2 avian leucosis virus strains cultivation

We used the primary fibroblast cell culture (CEF) prepared from 10-day-old chicken embryos to cultivate the avian leucosis virus strains RAV-1 and RAV-2. Production of the CEF culture followed prescriptions provided in the respective publication [11]; it was done in 75 cm^3 culture flasks.

After formation of the cell culture monolayer, we diluted the virus on a medium as needed (nutrient medium 199, with the addition of TPCK-trypsin to a final concentration of 2 μg/ml and BSA (fraction V) to a final concentration of 0.2%). The resulting virus culture dilution was introduced to the primary cell culture of CE fibroblasts (85–95% monolayer), preliminarily washed twice with PBS, in a volume of 2–3% of the mattress volume (necessary for complete coverage of the monolayer with the virus-containing liquid). Three ml of the virus culture were added to the fibroblast cell culture, the cultures left in contact for 1 hour at +37 °C. Then, we added the maintenance medium (6 ml) and incubated the culture in a CO_2 incubator at +37 °C. The medium was changed on the 5th day of incubation.

The samples (virus-containing culture fluid) were harvested on the 13th (RAV-1) or on the 7th (RAV-2) days. At the end of the incubation, the vials with the virus-containing liquid were frozen at –20 °C and left to thaw at room temperature; the freezing-thawing routine was repeated 2–3 times. Then the virus-containing liquid was taken from the vials, centrifuged at 1159 g for 10 minutes to pellet the cells.

Determination of the RAV-1 and RAV-2 avian leucosis virus titers in the CEF primary cell culture

To determine the titers of RAV-1 and RAV-2 viruses in the AF and VC in the context of modeling their inactivation with β-propiolactone (β-PL) and UV irradiation, we titrated the samples at different periods of inactivation on the CEF primary cell culture and then tested them for p27 in each dilution with the help of ELISA. Each sample was studied in triplicates. We prepared 10-fold dilutions of the samples (from 10^{-1} to 10^{-6}) cultured on the maintenance medium. The dilutions used in modeling the RAV-1 virus inactivation with β-PL or UV irradiation, as well as the negative control culture (AF and VC series free from contaminants) were added to the CEF cell culture, 0.5 ml per well (each dilution studied in triplicate), and
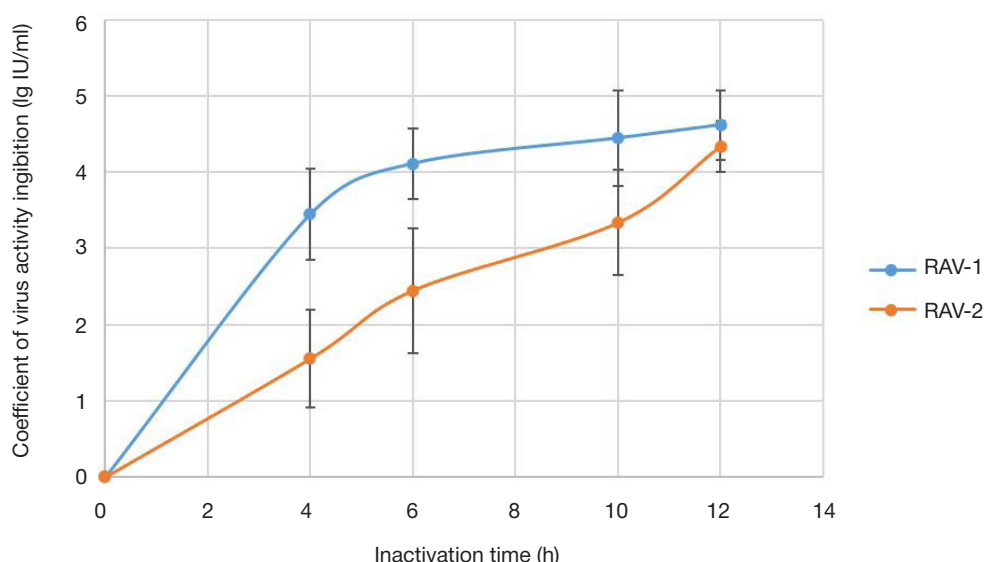
Fig. 1. Dynamics of inactivation of the RAV-1 and RAV-2 avian leucosis virus strains with β-propiolactone

left in contact for 5 hours at the temperature of +37 °C. Then the virus-containing culture fluid was removed and maintenance medium added, 1 ml per well. The plates were incubated in a CO2 incubator at +37 °C, 5% CO_2, for 7 days.

At the end of the incubation, the plates with the CEF primary cell culture were frozen at –20 °C and left to thaw at room temperature; the freezing-thawing routine was repeated 2–3 times. Then culture liquid was harvested from the wells and centrifuged at 3000 rpm to pellet the cells.

The supernatant was further tested for p27 antigen with ELISA, testing enabled by the IDEXX ALV Ag Test (IDEXX Laboratoties, Inc., USA) as per the manufacturer's instructions. We took as a titer the highest dilution of the virus-containing liquid sample that had the the optical densities ratio with the positive control greater than 0.2. The sensitivity limit of the method is 1lg IU/ml. A titer less than 1lg IU/ml was taken as 0.5.

Statistical processing of results

We processed the results with Microsoft Excel 365 (Microsoft corp.; USA) and Minitab 19 (Minitab Inc.; USA). The confidence intervals of the mean value were calculated with a confidence level of 95%.

RESULTS

Investigation of the dynamics of inactivation of avian leucosis virus in virus-containing allantoic fluid by β-propiolactone

The simulation of AF infection with the avian leucosis virus and subsequent inactivation thereof followed the pattern applied in the avian adenovirus inactivation study [4]. We added the preliminarily titrated infectious material containing avian leucosis

virus to the AF samples in a volume equal to 10% of the initial sample volume, so that its final content was at least 5 lg IU/ml. The resulting contaminated samples were supplemented with β-propiolactone to a final concentration of 0.09%, and the avian leucosis virus titer in the samples was determined in accordance with the described method. Figure 1 shows the inactivation dynamics.

According to the data obtained, the viral load decreased by at least 4 lg IU/ml in at least 12 hours after supplementation with β-propiolactone at the temperature of +4 – +8 °C (Table 1).

Investigation of the dynamics of inactivation of avian leucosis virus in virus concentrates with UV radiation

The simulation of VC infection with the avian leucosis virus and subsequent inactivation thereof followed the pattern applied in the avian adenovirus inactivation study [4]. We added the preliminarily titrated infectious material containing avian leucosis virus to the VC samples in a volume equal to 10% of the initial sample volume, so that its final content was at least 5 lg IU/ml. Seven ml of the contaminated VC were placed into 90 mm Petri dishes. The dishes were then irradiated with 60 W UV light from 0, 0.5, 1, 2 and 5 minutes; the source of light was 20 cm away. The inactivation was carried out at the temperature of +18 °C.

After the specified time intervals, we removed the cups from the unit and took samples (1 ml) for further determination of the virus titer as per the described method. Figure 2 shows the inactivation dynamics.

The viral load decreased by at least 4 lg IU/ml in at least 5 minutes under UV light (Table).

DISCUSSION

According to the long-term data collected at the St. Petersburg Research Institute of Vaccines and Serums of the FMBA

Table. Reduction of the viral load by avian leucosis virus under the action of various inactivating agents

Inactivating agent	Strain	
	RAV-1	RAV-2
β-Propiolactone (inactivation time: 12 hours)	4,61 ± 0,46 lg	4,33 ± 0,33 lg
UV radiation (inactivation time: 5 minutes)	4,22 ± 0,31 lg	4,33 ± 0,48 lg
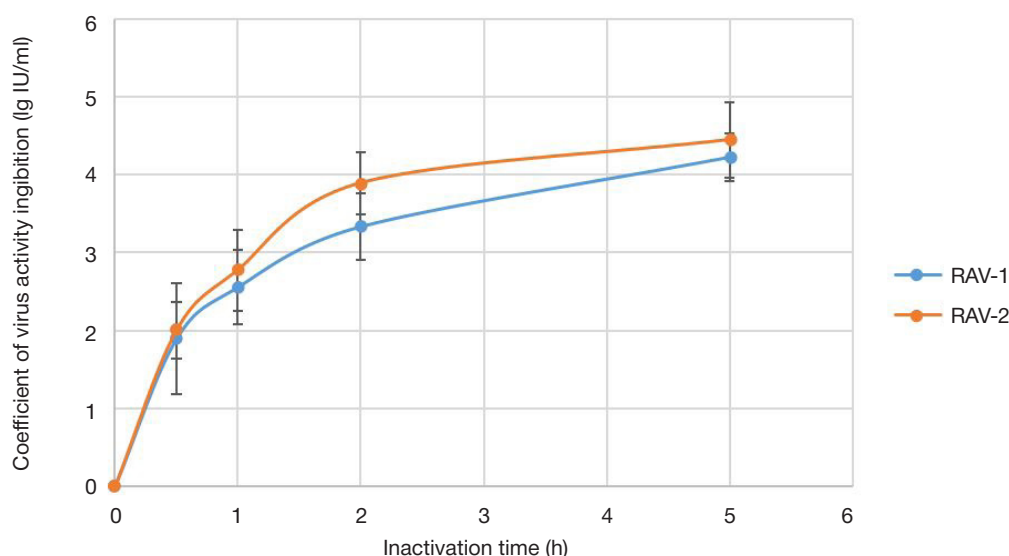
Fig. 2. Dynamics of inactivation of the RAV-1 and RAV-2 avian leucosis virus strains with UV radiation

of Russia, the term of full inactivation of the influenza virus strains that the WHO recommends for inclusion in inactivated influenza vaccines is 4–6 hours in case of β-propiolactone and 3–4 minutes under UV radiation. However, these terms do not guarantee inactivation of the possible contaminants, which makes the risk of producing unsafe vaccines real. In an earlier study [4], we have shown that both β-propiolactone and UV radiation are effective against adenovirus (strains Fontes and CELO), which is a possible a contaminant. The associated viral load decreases by more than 4 lg PFU / ml in at least 10 hours when β-propiolactone is used to inactivate AF (4.12 ± 0.06 lg and 4.20 ± 0.19 lg for CELO and Fontes, respectively) and in at least 5 minutes when the inactivating agent is UV (4.69 ± 0.89 lg and 4.44 ± 1.06 for CELO and Fontes, respectively).

According to the published research, the common inactivating agents used against avian leucosis virus are temperature and formalin (inactivation term of 24 hours) [12, 13], but they are hardly usable in production of the influenza vaccines since both temperature and formalin decrease their immunogenicity and formaldehyde itself is toxic. UV radiation has only been described as an inactivating agent for RAV-1 [6]; the reported viral load decrease was by 2 lg after 10 minutes of irradiation of virus-containing materials from a distance of 40 cm with lamps with a total power of 30 W.

This study has shown that β-propiolactone and UV radiation are also effective against RAV-1 and RAV-2 strains of the avian leucosis virus. However, the avian leucosis virus is inactivated with β-propiolactone in no less than 12 hours, while the term for adenovirus is 10 hours. Therefore, to inactivate both contaminants, the influenza vaccine production process should include the stage of inactivation with β-propiolactone

that lasts at least 12 hours at a temperature of +4–+8 °C. As for the UV radiation, the lower confidence interval (*p* = 0.95) limit for the viral load reduction factor is less than 4 lg, which indicates the need to increase the duration of inactivation to more than 5 minutes.

Thus, inactivation with β-propiolactone ensures greater reproducibility of the results and decreases the viral load by both avian leucosis virus and avian adenovirus by more than 4 lg (guaranteed) in the process of production of influenza vaccines. Subsequently, β-propiolactone minimizes the risks and is used as an inactivating agent as part of the inactivated influenza vaccines production process adopted by various companies, e.g., by the St. Petersburg Research Institute of Vaccines and Serums of the FMBA of Russia, Novartis, GSK, ID Biomedical Corp of Quebec [14–16].

CONCLUSIONS

This study has shown that the minimum time of inactivation of the allantoic fluid containing the avian leucosis virus with β-propiolactone in the context of production of influenza vaccines is 12 hours. Through this term, the load by the avian leucosis virus grows down by 4 lg IE/ml. As for UV, the time of exposure with the aim to inactivate virus concentrates should be no less than 5 minutes, which ensures a decrease of load by the avian leucosis virus by 4 lg IE/ml. Such patterns of inactivation guarantee complete adenovirus inactivation and ensure an adequate level of safety of the produced influenza vaccines in terms of these contaminants. The next stage is to study the kinetics of mycoplasma inactivation by various inactivating agents in the process of production of influenza vaccines.

References

1. EMA/CHMP/BWP/310834/2012 Rev.1 Committee for Medicinal Products for Human use (CHMP) Guideline on Influenza vaccines — Quality module, 2017.
2. Rekomendacii po proizvodstvu i kontrolyu vakciny protiv grippa inaktivirovannoj, Prilozhenie 3 serii texnicheskix dokladov VOZ # 927, 2005. Russian.
3. Sabbaghi A, Miri SM, Keshavarz M, Zargar M, Ghaemi A. Inactivation methods for whole influenza vaccine production. Rev Med Virol. 2019; 29 (6): e2074.
4. Savina NN, Ekimov AA, Trukhin VP, Evtushenko AE, Zhirenkina EN, Sinegubova EO. Evaluation of avian adenovirus inactivation methods used in the production of influenza vaccines. Extreme Medecine. 2021; (3): 84–9.
5. Plotnikov VA, Grebennikova TV, Dudnikova EK, Shulpin MI, Lazareva SP, Nikonova ZB, i dr. O rasprostranenii virusa lejkoza ptic v pticevodcheskix xozyajstvax na territorii Rossii. Sel'skoxozyajstvennaya biologiya. 2013; 6: 36–42. Russian.
6. Bister K, Varmus HE, Stavnezer E, Hunters E, Vogt PK. Biological

and biochemical studies on the inactivation of avian oncoviruses by ultraviolet irradiation. Virology. 1977; 77 (2): 689–704.

7. Herrera-Rodriguez J, Signorazzi A, Holtrop M, de Vries-Idema J, Huckriede A. Inactivated or damaged? Comparing the effect of inactivation methods on influenza virions to optimize vaccine production. Vaccine. 2019; 37 (12): 1630–7.

8. Kap M, Arron GI, Loibner M, Hausleitner A, Siaulyte G, Zatloukal K, Riegman P. Inactivation of Influenza A virus, Adenovirus, and Cytomegalovirus with PAXgene Tissue Fixative and Formalin. Biopreservation and Biobanking. 2013; 11 (4): 229–34.

9. Shuo Lei, Xun Gao, Yang Sun, Xiangyong Yu, Longshan Zhao, Gas chromatography-mass spectrometry method for determination of β-propiolactone in human inactivated rabies vaccine and its hydrolysis analysis, Journal of Pharmaceutical Analysis. 2018; 8 (6): 373–7.

10. Rukovodstvo po issledovaniyu validacii virusnoj ochistki: proektirovanie, vklad i interpretaciya issledovanij, ispol'zuyushhix inaktivaciyu i udalenie virusov, EMA CPMP/BWP/268/95, 1996. Russian.

11. Freshni RYa. Kul'tura zhivotnyx kletok: prakticheskoe rukovodstvo. Per. 5-go angl. izd. M.: BINOM. Laboratoriya znanij, 2018; 691 s. Russian.

12. Li Xue, Dong Xuan, Sun Xiaolong, Li Weihua, Zhao Peng, Cui Zhizhong, Wang Xin. Preparation and immunoprotection of subgroup B avian leukosis virus inactivated vaccine. Vaccine. 2013; 31 (46): 5479–85.

13. Zavala, Guillermo, Sunny Cheng. Detection and Characterization of Avian Leukosis Virus in Marek's Disease Vaccines. Avian Diseases. 2006; 50 (2): 209–15.

14. Haussmann C, Hauschild F, Jobst B, Novartis AG. Improvements in preparation of influenza virus vaccine antigens. Патент США № US6986808P. 18.03.2008.

15. Burt DS, Jones DH, Lowell GH, White GL, Torossian K, Fries LF. ID Biomedical Corp of Quebec. Proteosome influenza vaccine. Патент США № US18247600P. 15.02.2000.

16. Truhin VP, Evtushenko AJe, Krasilnikov IV, Savina NN, Bykov DG, Ujba SV, Vasilev AN, Ryskova EV, Nacharova EP, Arakelov SA, avtory. Federal'noe gosudarstvennoe unitarnoe predpriyatie «Sankt-Peterburgskij nauchno-issledovatel'skij institut vakcin i syvorotok i predpriyatie po proizvodstvu bakterijnyx preparatov» Federal'nogo mediko-biologicheskogo agentstva (FGUP SPbNIIVS FMBA Rossii). Sposob polucheniya antigena ili antigenov dlya proizvodstva protivogrippoznoj vakciny i vakcina na ego osnove. Patent RF # RU2019118695A. 14.06.2019. Russian.

Литература

1. EMA/CHMP/BWP/310834/2012 Rev.1 Committee for Medicinal Products for Human use (CHMP) Guideline on Influenza vaccines — Quality module, 2017.

2. Рекомендации по производству и контролю вакцины против гриппа инактивированной, Приложение 3 серии технических докладов ВОЗ № 927, 2005.

3. Sabbaghi A, Miri SM, Keshavarz M, Zargar M, Ghaemi A. Inactivation methods for whole influenza vaccine production. Rev Med Virol. 2019; 29 (6): e2074.

4. Савина Н. Н., Екимов А. А., Трухин В. П., Евтушенко А. Э., Жиренкина Е. Н., Синегубова Е. О. и др. Оценка методов инактивирования аденовируса птиц при производстве гриппозных вакцин. Медицина экстремальных ситуаций. 2021; (3): 84–9.

5. Плотников В. А., Гребенникова Т. В., Дудникова Е. К., Шульпин М. И., Лазарева С. П., Никонова З. Б., и др. О распространении вируса лейкоза птиц в птицеводческих хозяйствах на территории России. Сельскохозяйственная биология. 2013; 6: 36–42.

6. Bister K, Varmus HE, Stavnezer E, Hunters E, Vogt PK. Biological and biochemical studies on the inactivation of avian oncoviruses by ultraviolet irradiation. Virology. 1977; 77 (2): 689–704.

7. Herrera-Rodriguez J, Signorazzi A, Holtrop M, de Vries-Idema J, Huckriede A. Inactivated or damaged? Comparing the effect of inactivation methods on influenza virions to optimize vaccine production. Vaccine. 2019; 37 (12): 1630–7.

8. Kap M, Arron GI, Loibner M, Hausleitner A, Siaulyte G, Zatloukal K, Riegman P. Inactivation of Influenza A virus, Adenovirus, and Cytomegalovirus with PAXgene Tissue Fixative and Formalin. Biopreservation and Biobanking. 2013; 11 (4): 229–34.

9. Shuo Lei, Xun Gao, Yang Sun, Xiangyong Yu, Longshan Zhao, Gas chromatography-mass spectrometry method for determination of β-propiolactone in human inactivated rabies vaccine and its hydrolysis analysis, Journal of Pharmaceutical Analysis. 2018; 8 (6): 373–7.

10. Руководство по исследованию валидации вирусной очистки: проектирование, вклад и интерпретация исследований, использующих инактивацию и удаление вирусов, EMA CPMP/BWP/268/95, 1996.

11. Фрешни Р. Я. Культура животных клеток: практическое руководство. Пер. 5-го англ. изд. М.: БИНОМ. Лаборатория знаний, 2018; 691 с.

12. Li Xue, Dong Xuan, Sun Xiaolong, Li Weihua, Zhao Peng, Cui Zhizhong, Wang Xin. Preparation and immunoprotection of subgroup B avian leukosis virus inactivated vaccine. Vaccine. 2013; 31 (46): 5479–85.

13. Zavala, Guillermo, Sunny Cheng. Detection and Characterization of Avian Leukosis Virus in Marek's Disease Vaccines. Avian Diseases. 2006; 50 (2): 209–15.

14. Haussmann C, Hauschild F, Jobst B, Novartis AG. Improvements in preparation of influenza virus vaccine antigens. Патент США № US6986808P. 18.03.2008.

15. Burt DS, Jones DH, Lowell GH, White GL, Torossian K, Fries LF. ID Biomedical Corp of Quebec. Proteosome influenza vaccine. Патент США № US18247600P. 15.02.2000.

16. Трухин В. П., Евтушенко А. Э., Красильников И. В., Савина Н. Н., Быков Д. Г., Уйба С. В., Васильев А. Н., Рыськова Е. В., Начарова Е. П., Аракелов С. А., авторы. Федеральное государственное унитарное предприятие «Санкт-Петербургский научно-исследовательский институт вакцин и сывороток и предприятие по производству бактерийных препаратов» Федерального медико-биологического агентства (ФГУП СПбНИИВС ФМБА России). Способ получения антигена или антигенов для производства противогриппозной вакцины и вакцина на его основе. Патент РФ № RU2019118695A. 14.06.2019.

SOLUTION TO THE PROBLEM OF DESIGNING A SAFE CONFIGURATION OF A HUMAN UPPER LIMB ROBOTIC PROSTHESIS

Bureev ASh[1,2], Golobokova EV[1,2], Zhdanov DS[1,2] ✉, Kosteley YaV[1,2], Koshelev RV[2], Seleznev AI[1,2], Fomenko EA[2]

[1] Center for Development of Science, Technology and Education in the Field of Defense and State Security, National Research Tomsk State University, Tomsk, Russia

[2] Federal Research and Clinical Center of Medical Rehabilitation and Balneology of the Federal Medical Biological Agency, Moscow, Russia

This study aimed to develop a method allowing to improve safety of use of robotic medical rehabilitation devices by designing and testing an algorithm for calculation of the angular positions of rehabilitation robotic manipulators or robotic prostheses and allowing to reproduce the natural arc of a human arm under control of a CVS. The Introduction section supports the urgency of development of the methods granting control over positioning of robotic manipulators with the help of a computer vision system (CVS) and thus guarantee safety of patients and medical personnel in the context of work with medical robotic rehabilitation devices. The Materials and Methods section contains a brief description of the robotic arm used in this study, a description of the existing approaches to calculation of angular positions of drives, and a description of the proposed algorithm. The final sections compare application of the proposed algorithm and existing methods of calculation of angular positions of drives of robotic manipulators (robotic prostheses) and outline the possible directions for further improvement.

✉ Correspondence should be addressed: Dmitry S. Zhdanov
Krasnoarmeyskaya, 14, Tomsk, 634029, Russia; D_S_Zhdanov@mail.ru

РЕШЕНИЕ ЗАДАЧИ ФОРМИРОВАНИЯ БЕЗОПАСНОЙ КОНФИГУРАЦИИ РОБОТИЧЕСКОГО ПРОТЕЗА ВЕРХНЕЙ КОНЕЧНОСТИ ЧЕЛОВЕКА

А. Ш. Буреев[1,2], Е. В. Голобокова[1,2], Д. С. Жданов[1,2] ✉, Я. В. Костелей[1,2], Р. В. Кошелев[2], Е. А. Фоменко[2]

[1] Центр развития науки, технологий и образования в области обороны и обеспечения безопасности государства, Национальный исследовательский Томский государственный университет, Томск, Россия

[2] Федеральный научно-клинический центр медицинской реабилитации и курортологии Федерального медико-биологического агентства, Москва, Россия

На сегодняшний день остается актуальной разработка методов контроля позиционирования роботических манипуляторов с помощью систем технического зрения (СТЗ) с целью обеспечения безопасности пациентов и медицинского персонала при работе с медицинскими роботизированными реабилитационными устройствами. Целью исследования было разработать метод повышения безопасности применения роботизированных медицинских реабилитационных устройств путем разработки и апробации алгоритма расчета угловых положений роботизированных манипуляторов или роботических протезов, применяемых в восстановительном лечении и позволяющих воспроизвести естественную траекторию перемещения руки человека под контролем СТЗ. Дано описание роботизированного манипулятора, использованного при проведении исследований, представлены существующие подходы к расчету угловых положений приводов, а также описание предлагаемого алгоритма. Приведены сравнительные результаты работы предлагаемого алгоритма и существующих методов расчета угловых положений приводов роботизированных манипуляторов (роботических протезов) и предполагаемые направления для его доработки.

✉ Для корреспонденции: Дмитрий Сергеевич Жданов
ул. Красноармейская, д. 14, г. Томск, 634029, Россия; d_s_zhdanov@mail.ru

The current worldwide trend around the latest R&D achievements involves active introduction of robotic equipment in all sectors of the economy. A paper by The Boston Consulting Group (BCG) states that by 2030 the total global market of professional robotics will reach $260 billion [1].

Medical robotics is one of the leading segments of professional robotics by the level of technology employed and demand present. As Joseph Engelberger, father of commercial robotics, said, "... hospitals are the ideal place and the ideal environment for use of robots" [2].

Nevertheless, despite the broad introduction of robotic medical systems, the matters of safety of patients and medical staff that use such systems have not been investigated sufficiently. Some of the published studies point to the documents reporting results of operations that employed robots, and the number of subsequent adverse consequences exceeded one and a half thousand [3]. During the period from 2000 through 2013, surgeries done with the help of robots resulted in death of 144 people. Between 2000 and 2013, the equipment ignited or failed on more than 190 cases. Almost 800 other cases of adverse consequences of robotics-enabled operations resulted from systemic errors such as loss of the video feed [3].

According to the authors of the article, robotic rehabilitation implies slightly different risks for patients: robot arms may move incorrectly (along an unacceptable trajectory or at an unacceptable angle) and thus injure the patient or medical personnel. With this in mind, we undertook to make use of medical rehabilitation robots safer for people by developing a method installing an additional control loop for the robot manipulator's movements that relies on a computer vision system (CVS). "Robot arm movement control" in the context of this study means establishing the fact of that arm reaching a preset point within a local coordinate system. Thus, we employed CVS only to confirm the successfully performed movements without assessing the controlled manipulator's final configuration. For the stated purpose, we analyzed the 3D coordinates for each manipulator's structural components.

The subject we tested the developed method of positioning robotic manipulator's components on was an AR-600E anthropomorphic robot (NPO Androidnaya Tekhnika; Russia). The testing sought to confirm the possible way to improve safety of use and accuracy of positioning of anthropomorphic robotic prostheses of human upper limbs. We paid special attention to finding a solution to the problem of establishing the coordinates of individual components of the manipulator to design its configuration to mimic movements of a human arm in the best possible way. The solution allows designing missing or dysfunctional arm replacements with kinematics matching kinematics of a human arm as close as possible, which makes them safer in use.

It should be taken into account that, unlike industrial robot arms, an anthropomorphic robotic rehabilitation manipulator is not fixed on a rigid base. Coupled with mechanical complexity and a large number of interconnected components, this translates into considerably inaccurate positioning values, which, in some cases, can make the robotic prosthesis dangerous to its owner or people around him/her. Under such conditions, the task of accurate and safe positioning is not a trivial one; it largely depends on the method of designing the mechanism itself.

A suggested solution to this task involves a CVS module integrated into the robotic rehabilitation anthropomorphic manipulator's control loop. This module would monitor the position of the manipulator in its field of view and generate commands to interrupt or correct a potentially dangerous movement. The module is supposed to recognize and track both the manipulator's grip and special markers attached to its components [4, 5]. However, even with a CVS enhancing the traditional methods of estimation of the manipulator's position (relative to the elements of the CVS), the absolute mean calibration error between the system [6, 7] and the manipulator's grip is more than ± 5 cm [4].

The traditional approach to determining the current position of the manipulator's components involves requesting their 3D coordinates from the direct kinematics logic. The inputs are the values transmitted by the angular position sensors of the corresponding drives. The logic also contains the current coordinates by the CVS. At the initial stages, the software must search for the target object and calculate its spatial position relative to the elements of the system or the absolute zero of the kinematics logic. This can be done with the help of position-based (PBVS), image-based (IBVS) visual servoing or hybrid methods. In general, the above methods calculate the needed coordinates by analyzing images; they are applicable to both industrial manipulators and anthropomorphic robots and robotic prostheses of the human hand.

Image-based visual servoing allows comparing the calculated needed and current positions of the manipulator or object on a plane. The difference between the needed and the current positions (the error) is used as feedback. The connection between the received information and changes in the position of the components is made through a Jacobi matrix and the direct kinematic logic of the robot [8]. There are a large number of methods to determine this connection [9–11]. It should be taken into account that a single marker on the object (either the manipulated object or the manipulator itself) enables control over only two degrees of freedom. At least four markers are needed to control six degrees of freedom. Greater number of markers also increases the probability of an unambiguous decision supporting the control command [11, 12]. The IBVS method does not allow linear control of the robot components and does not rely on 3D information about position of the manipulated object. This leads to generation of non-optimal or unrealizable trajectories, a problem that can be solved through adjustments by selected visual parameters [13–15].

The PBVS method implies the coordinates of objects inside the manipulator operating space are determined relative to the coordinate system of the camera part of the CVS. The parameters of the geometric model of the tracked object and camera parameters are factored in together for this purpose. The parameters of the tracked manipulator in the operating space are known; the changes of these parameters can be tracked by responses from the robot's kinematics logic. Geometrical parameters of the manipulated object, on the contrary, strongly depend on the CVS parameters and the adopted methods of 3D localization [16–22].

Hybrid visual servo-enabled control involves both the IBVS and PBVS methods. This approach improves the accuracy of the generated commands through separation of control over manipulator's degrees of freedom [23–27]. Systems that rely on such an approach are less dependent on the robot cameras' calibration accuracy and give a more true idea of the objects' geometry. However, such systems harder to build and consume more computing resources. Moreover, they do not eliminate the risk of non-optimal or unrealizable trajectories, which can still impair the process due to positioning errors and/ or incorrect estimation of the 3D coordinates of the tracked objects by the CVS.
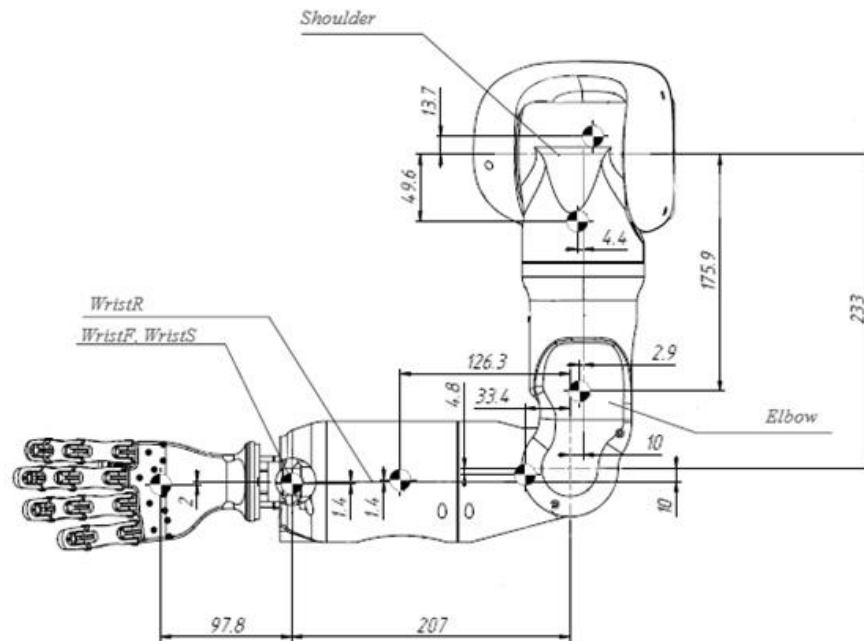
Fig. 1. Structure of the AR-600E manipulator

Calculation of the optimal positions of the manipulator's grip should factor in mechanical limitations of the joints peculiar to both the initial positioning and the subsequent manipulation stages. In addition, since of anthropomorphic prostheses are supposed to be a safer robotic rehabilitation device fir for use in "human" environment, positioning of the manipulator may include stopping before obstacles while moving to target position.

With the current methods of processing data inputs from the CVS, development of the software generating movement trajectories for the AR-600E manipulators does not exclude the possibility of generation of a trajectory (arm to target object) that is either unsafe or unrealizable. In addition, we undertook to enable generation of the trajectories that mimic natural movements of the human arm. In the context of this study, we assessed various options of solutions to the manipulator's inverse kinematics problem and formulated a method that ensures building the movement trajectory as expected.

This study aimed to develop a method making use of robotic medical rehabilitation devices safer by designing and testing an algorithm for calculation of the angular positions of robotic manipulators or robotic prostheses used for rehabilitation purposes and capable of reproducing the natural human.

METHODS

For this study, we developed a number of algorithmic solutions allowing to build a movement trajectory for an anthropomorphic manipulator that closely resembles that of a human arm. The solutions were implemented as software that controls the manipulator of an AR-600E anthropomorphic robot in a simulation environment enabled with quaternion algebra. The manipulator includes the following components (Fig. 1):

1) the Shoulder groups of components moves the Elbow component and the lower components of the manipulator along the frontal (ShoulderS), sagittal (ShoulderF) and vertical axes (ElbowR);

2) the Elbow component moves its child components along the sagittal axis;

3) the WristR component moves its child component along the vertical axis;

4) the WristF and WristS components move the hand along the frontal and sagittal axes, respectively.

The fingers are driven with actuators located on the WristS component.

The Forward and Backward Reaching Inverse Kinematics (FABRIK) method [28] was used to calculate the spatial position of the manipulator's components. This method accounts for the constraints and represents the components of the components, which, combined, allow bringing the hand to the target position in the 3D space.

Two cameras on the head of the anthropomorphic mechanism captured color images within the operating space. Machine learning methods enabled control of the movements of manipulator's grip and tracking thereof, assessment point being whether it has reached the set coordinate in the operating space or not. The main task set before the routines that incorporate machine learning is to detect the grip and assess how it performs a given task within the operating space.

Two approaches to assess correctness of the grip positioning were applied: 1) by requesting responses from the manipulator drives and modeling the current configuration of the manipulator based thereon, and 2) with the CVS of anthropomorphic mechanism. Configuration of the manipulator in its entirety is not controlled, since the CVS' field of view does not cover all of its components. This task is solved after modeling the spatial position of the manipulator, through calculation of angular positions of the drives that bring it to the set 3D coordinates. Below, we consider the possible ways of their calculation on the example of the Shoulder group (Fig. 1) the movements of which affect the spatial position of all other components of the manipulator. The following methods of angular positions calculation were compared:

1) using orthogonal projections of specific points on the manipulator's components. The angle between two points (for example, axis of the Elbow component and the Shoulder group) was calculated by the following formula:

$$angle = 90° - asin\left(\frac{a}{c}\right), \qquad (1)$$

where a is the module of the y coordinate for the corresponding axis of the component, and c is the distance between components in the corresponding orthogonal plane;

2) as angle of rotation of the orthogonal plane between projection of the Elbow component during initialization of the kinematic logic and projection in the analyzed plane of its movement. We used the following formula in this case:

$$cos(\overline{a};\overline{b}) = \frac{(\overline{a};\overline{b})}{|\overline{a}|\cdot|\overline{b}|} = \frac{a_1\cdot b_1 + a_2\cdot b_2 + a_3\cdot b_3}{\sqrt{a_1^2+a_2^2+a_3^2}\cdot\sqrt{b_1^2+b_2^2+b_3^2}}, \qquad (2)$$

where $\bar{a}$ and $\bar{b}$ are the 3D vectors between which the angle is calculated, and a_n, b_n are the corresponding coordinates of 3D vectors after modeling of the orthogonal projections;

3) through the Elbow component's 3D coordinates projection onto the corresponding Shoulder group movement planes:

$$YZ = \left[0; \frac{Elbow.y*dist}{Elbow.x+dist}; \frac{Elbow.z*dist}{Elbow.x+dist}\right],$$

$$XZ = \left[\frac{Elbow.x*dist}{Elbow.y+dist}; 0; \frac{Elbow.z*dist}{Elbow.y+dist}\right], \qquad (3)$$

$$XY = \left[\frac{Elbow.x*dist}{Elbow.z+dist}; \frac{Elbow.y*dist}{Elbow.z+dist}; 0\right],$$

$$dist = \sqrt{(Elbow.x - null.x)^2 + (Elbow.y - null.y)^2 + (Elbow.z - null.z)^2}$$

where *dist* is the distance between the current coordinate on the Elbow component axis and the common axis (null) of ShoulderF, ShoulderS components (Shoulder group). We used both (1) and (2) to calculate the angular positions;

4) with the help of the "Shortest arc" method used by game developers to calculate the shortest arc of movement of connected components of virtual objects from the initial point to a given point in 3D space. Practically, implementation by this method means generation of the rotation quaternion from the double rotation and zero rotation quaternions, with the resulting quaternion being the sum of the double rotation quaternion and the identity quaternion;

5) using the algorithm suggested by the authors of this article.

The angular positions calculation method suggested and tested by the authors makes use of a matrix containing interrelated positions of the manipulator components, i.e., a set of coordinates corresponding to certain angles. The increment between them is set during initialization of the algorithm, which prevents repeated generation of the matrix. The input data for the suggested algorithm is the 3D coordinate of a point (center of the hand; Fig. 1) on the manipulator's grip. Next, application of the FABRIK approach yields a set of coordinates of the axis points of the main components' nodes, which, combined, form configuration of the manipulator in 3D space. After that, inside the generated matrix of interrelated positions, using the principle of minimum distances (dist; formula (3)), the most suitable angular position of the drive is selected between the coordinates of the estimated position of the Elbow component and the coordinates stored in the matrix. If necessary, the angular position is adjusted through generation of a local matrix of interrelated positions with a more accurate increment within a small range of rotation angles. Then the angular position of the Elbow component drive is calculated by formula (1), with a being the y axis value by the orthogonal projection of the target position and c being the length of the component. The ElbowR drive's angular position is calculated relative to the axis of the WristR component (Fig. 1). This step involves a number of iterations: sequentially formed quaternions enable rotation of WristR to a given increment. The procedure stops upon reaching the minimum distance between the coordinates calculated by the FABRIK method and the coordinates extracted from the matrix of interrelated positions.
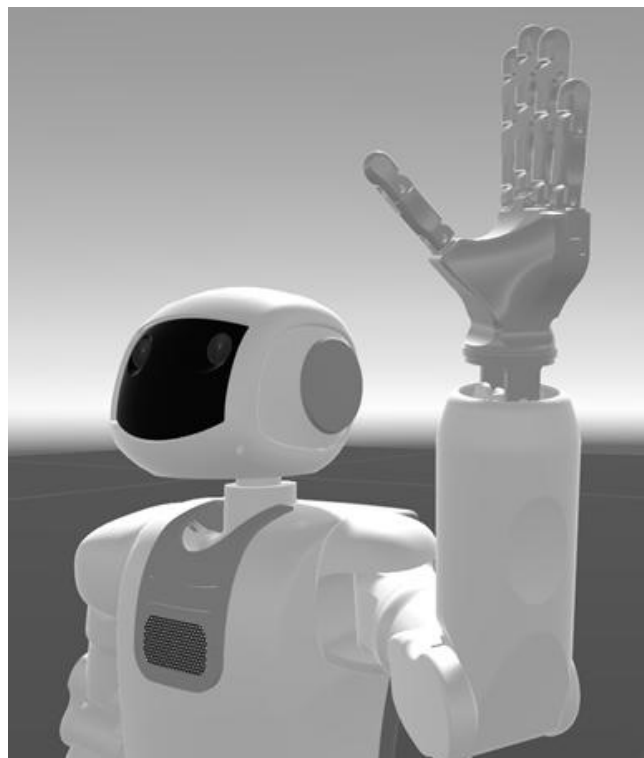
Fig. 2. Example of configuration of the manipulator of AR-600E anthropomorphic mechanism

RESULTS

The experimental part of the study involved application of the considered methods to calculate angular positions of drives of the AR-600E anthropomorphic robot's manipulator in a simulation environment. For this purpose, operator manually set target positions of the components and registered the resulting angular positions of their drives and 3D coordinates of the axes of Elbow and WristS drives. The next step was to compare the results and select the best method by proximity of the resulting coordinates with the coordinates of axes of the components registered by the operator. Figure 2 shows one of the manipulator configurations recorded during the experimental part of the study.

Table 1 shows angular positions of the components of the Shoulder group and Elbow component:

1) 0 — initial position for the anthropomorphic mechanism;

2) 1 — angular positions set by the operator;

3) 2 — angular positions for the configuration calculated by formula (1);

4) 3 – angular positions for the configuration calculated by formula (2);

5) 4 — angular positions for the configuration calculated through the projection of the coordinate onto the respective axis by formula (1);

6) 5 — angular positions for the configuration calculated through the projection of the coordinate onto the respective axis by formula (2);

7) 6 — angular positions calculated by the suggested method.

Elbow and WristS cells of Table 1 contain the 3D coordinates of axes of these components that were discovered through application of the formed angular positions of the drives to them. Cells Elbow and WristR present information about angular positions of the drives (in degrees) that move the respective components to target points in 3D space.

Table 1. Comparison of the results of application of various algorithms enabling calculation of the angular positions of component drives of the anthropomorphic manipulator

	Angular positions of components				Coordinates of components					
Position I										
Method	Elbow		WristS		Elbow			WristS		
	ShF, °	ShS, °	ElR, °	El, °	x, mm	y, mm	z, mm	x, mm	y, mm	z, mm
0	0	0	0	0	191,92	229	3,58	201,85	−14,5	−49,5
1	−26,72	39,16	−3,16	−52,48	321,34	304,77	109,56	394,25	239,27	338,9
2	−27,42	43,16	58,51	−53,52	340,21	318,79	105,39	526	320,28	271,84
3	−27,42	47,72	52,23	−53,52	353,67	330,78	101,59	544,74	347,27	261,05
4	−27,42	43,16	58,51	−53,52	340,25	318,85	105,42	525,96	320,33	271,87
5	−27,42	60,97	52,23	−53,52	586,38	432,61	223,53	387,28	370,68	86,67
6	−26,73	39,15	−2,90	−52,53	321,31	304,78	109,6	394,77	239,73	338,92
Position II										
Method	Elbow		WristS		Elbow			WristS		
	ShF, °	ShS, °	ElR, °	El, °	x, mm	y, mm	z, mm	x, mm	y, mm	z, mm
0	0	0	0	0	191,92	229	3,58	201,85	−14,50	−49,50
1	10,45	2,54	11,73	−84,81	211,85	231,44	−35,88	222,95	116,65	185,26
2	10,52	3,07	20,71	−85,86	215,97	231,91	−36,70	264,48	124,16	182,92
3	10,52	8,61	20,71	−85,86	238,42	234,61	−31,99	292,75	135,74	190,43
4	10,52	3,07	20,71	−85,86	215,97	231,91	−36,70	264,48	124,16	182,92
5	10,52	8,61	20,71	−85,86	238,42	234,61	−31,99	292,75	135,74	190,43
6	10,51	3,04	11,15	−84,89	213,77	231,59	−35,70	223,09	117,25	185,78
Position III										
Method	Elbow		WristS		Elbow			WristS		
	ShF, °	ShS, °	ElR, °	El, °	x, mm	y, mm	z, mm	x, mm	y, mm	z, mm
0	0	0	0	0	191,92	229	3,58	201,85	−14,50	−49,50
1	−70,09	69,21	9,7	−31,31	393,83	443,58	112,32	598,23	493,83	246,09
2	−74,57	85,2	69,97	−32,36	419,98	465,41	50,68	658,75	533,46	72,92
3	−76,68	85,49	68,62	−32,36	421,26	467,23	45,12	660,52	535,69	59,34
4	−74,57	85,2	69,97	−32,36	419,98	465,41	50,68	58,75	533,46	72,92
5	−76,68	86,64	68,62	−32,36	421,5	467,5	44,02	660,75	536,27	57,02
6	−70,00	69,64	8,2	−31,41	394,33	444,03	111,57	598,59	494,73	245,3

Table 2 below illustrates the absolute difference between the coordinates of the Elbow and WristR axes, i.e., the difference between the coordinates resulting from operator's actions (manual movement of the components) and coordinates discovered through application of each of the considered method to calculate angular positions to which the drives moved. Table 2 does not include information on positions 0 and 1.

DISCUSSION

Analysis of the results given in Tables 1 and 2 allows deducing that the suggested drive angular position calculation method ensures generation of the target configuration of the manipulator and movement of its components to the target points. There are also visible differences between the manipulator components' position coordinates calculated by the suggested algorithm and learned as a result of manual movements by the operator. Axis coordinate of the WristS component presents the greatest discrepancy between the obtained results and the reference values. To compensate for this error, we applied an algorithm that, like the one discussed above, uses a matrix of interrelated positions. The WristS component should be moved to its

initial position for this purpose. Then, the matrix of interrelated positions is scanned for the drive's angular position value that fits the minimum distances condition. To speed up performance of the algorithm, we decided to calculate the initial value of the WristF drive's angular position:

$$angle = -\left(nullWristF - \left(\pi - acos\left(\frac{a^2 + b^2 - c^2}{2 * a * b}\right)\right)\right), \quad (4)$$

where *angle* is a precalculated rotation angle of the WristS drive along the sagittal axis; *nullWristF* is the static angle of rotation of WristS relative to WristF, calculated during the initialization of the anthropomorphic robot's software; *a* is the length of the forearm of the anthropomorphic robot; *b* is the distance from the WristF axis to the WristS axis; *c* is the distance from the axis of WristS to the axis of WristR.

We calculated the angular position of the WristR drive in a similar way to the respective calculation for ElbowR. Table 3 presents adjustments of the manipulator configurations shown in Table 1.

The "Difference between deviations" line in Table 3 reflects the magnitude and direction of changes of distances (in millimeters) between the target 3D coordinates of the manipulator components and their values calculated before

Table 2. Absolute difference between the coordinates of the axes of Elbow and WristR components discovered through application of the considered methods to calculate their drives' angular positions

	Position I									
	Angular positions of components				Coordinates of components					
Method	Elbow		WristS		Elbow			WristS		
	ShF, °	ShS, °	EIR, °	El, °	x, mm	y, mm	z, mm	x, mm	y, mm	z, mm
2	0,7	4	61,67	1,04	18,87	14,01	4,17	131,75	81,01	67,06
3	0,7	8,56	55,39	1,04	32,33	26	7,97	150,49	108	77,85
4	0,7	4	61,67	1,04	18,91	14,08	4,14	131,71	81,06	67,03
5	0,7	21,81	55,39	1,04	265,04	127,84	113,97	6,98	131,41	252,23
6	0,01	0,01	0,26	0,05	0,03	0,01	0,04	0,52	0,46	0,02
	Position II									
Method	Elbow		WristS		Elbow			WristS		
	ShF, °	ShS, °	EIR, °	El, °	x, mm	y, mm	z, mm	x, mm	y, mm	z, mm
2	0,07	0,53	8,98	1,05	4,12	0,47	0,82	41,53	7,51	2,34
3	0,07	6,07	8,98	1,05	26,57	3,17	3,89	69,8	19,09	5,17
4	0,07	0,53	8,98	1,05	4,12	0,47	0,82	41,53	7,51	2,34
5	0,07	6,07	8,98	1,05	26,57	3,17	3,89	69,8	19,09	5,17
6	0,06	0,5	0,58	0,08	1,92	0,15	0,18	0,14	0,6	0,52
	Position III									
Method	Elbow		WristS		Elbow			WristS		
	ShF, °	ShS, °	EIR, °	El, °	x, mm	y, mm	z, mm	x, mm	y, mm	z, mm
2	4,48	15,99	60,27	1,05	26,15	21,83	61,64	60,52	39,63	173,17
3	6,59	16,28	58,92	1,05	27,43	23,65	67,2	62,29	41,86	186,75
4	4,48	15,99	60,27	1,05	26,15	21,83	61,64	539,48	39,63	173,17
5	6,59	17,43	58,92	1,05	27,67	23,92	68,3	62,52	42,44	189,07
6	0,09	0,43	1,5	0,1	0,5	0,45	0,75	0,36	0,9	0,79

and after adjustment for the angular positions of the WristS drive. The analysis of the presented data allows deducing that an additional stage of adjustment of the coordinates makes manipulator movements more accurate. In such a case, the movement error does not exceed 0.5 mm. This mechanism can be used when setting a large search increment in generation of the interrelated positions matrices. A more accurate adjustment of the configuration is undertaken at an additional adjustment stage, which ultimately speeds up the suggested algorithm.

CONCLUSIONS

We developed an algorithm for calculation of angular positions of the manipulator components' drives that produces the most accurate and predictable result (Tables 2, 3), which ultimately allows forming the configuration designed by the operator. The algorithm also minimizes the probability of an unpredictable

result and robot arm movements along a trajectory unsafe for human beings. It should be noted separately that the accuracy of calculation of the coordinates with the help of the suggested algorithm depends directly on the search increment value (in degrees) set for the interrelated positions matrices generation stage. The algorithm was coded and optimized in C++. Its execution time on a personal computer (Intel Core i7–4770 3.40 GHz, RAM 16 Gb) ranged from 5 to 8 ms, which is sufficient for the purpose of controlling the manipulator of an anthropomorphic robot and a robotic prosthesis. The accuracy of the drives' angular position calculations can be improved by reducing the increment used at interrelated positions matrices generation stage. This, however, would require more RAM capacity for the control software and slow down execution of the algorithm. The way to mitigate this problem is to add a modified version of the suggested algorithm to the control software, i.e. a version that would

Table 3. Results of adjustment of the angular position of WristS drive

Position	Position I			Position II			Position III		
Angular positions, °	WristF	WristS	WristR	WristF	WristS	WristR	WristF	WristS	WristR
	0	0,25	−0,04	0,25	−0,25	0,21	0,25	−1,5	−0,01
Coordinate axis, mm	x	y	z	x	y	z	x	y	z
Target coordinate	394,25	239,27	338,9	222,95	116,65	185,25	598,23	493,83	246,09
Before adjustment	394,77	239,73	338,92	223,09	117,25	185,78	598,59	494,73	245,3
After adjustment	394,93	239,8	338,88	222,08	117,03	185,45	598	494,15	246,13
Deviation along the coordinate axis, mm	x	y	z	x	y	z	x	y	z
Before adjustment	0,52	0,46	0,02	0,14	0,6	0,53	0,36	0,9	0,79
After adjustment	0,68	0,53	0,02	0,15	0,38	0,2	0,23	0,32	0,04
Difference between deviations	−0,16	−0,07	0	−0,01	0,22	0,33	0,13	0,58	0,75

calculate angular positions of the manipulator drives factoring in its previous configuration. In this case, the search in the matrices of interrelated positions will be significantly more narrow, which will speed up generation of the move command by the manipulator/robotic prosthesis control software while also improving the accuracy of its positioning. In the context of application of the suggested algorithm, CVS will be used

only to control the correctness of execution of an action by the manipulator, which greatly simplifies the algorithmic part, reduces the computational load and time to generate a command. This approach will increase the safety of medical rehabilitation robotic devices for which the key performance criteria are speed of reaction and accuracy of execution of actions.

References

1. Lassig R, Lorenz M, Sissimators E, Wicker I, Buchner T. Robotics Outlook 2030: How intelligence and mobility will shape the future. 2021. The Boston Consulting Group.
2. Joseph F. Robotics in Service. Engelberger, 1989; 248 p.
3. Alemzadeh H, Raman J, Leveson N, Kalbarczyk Z, Iyer RK. Adverse Events in Robotic Surgery: A Retrospective Study of 14 Years of FDA Data. PLOS ONE. 2016; 11 (4): e0151470. DOI: 10.1371/journal.pone.0151470.
4. Taylor GR, Kleeman L. Grasping unknown objects with a humanoid robot. 2002.
5. Kragic D, Christensen HA. Survey on Visual Servoing for Manipulation. Comput Vis Act Percept Lab. 2002; 15 p.
6. Dong G, Zhu ZH. Position-based visual servo control of autonomous robotic manipulators. Acta Astronautica. 2015; 115: 291–302. DOI: 10.1016/j.actaastro.2015.05.036.
7. Vahrenkamp N, Wieland S, Azad P, Gonzalez D, Asfour T, Dillmann R. Visual servoing for humanoid grasping and manipulation tasks. Humanoids 2008 — 8th IEEE-RAS International Conference on Humanoid Robots. 2000. DOI: 10.1109/ichr.2008.4755985.
8. Chaumette F, Hutchinson S. Visual servo control, Part I: Basic approaches. IEEE Robotics and Automation Magazine. 2006; 13 (4): 82–90.
9. Espiau B, Chaumette F, Rives P. A new approach to visual servoing in robotics. IEEE Transactions on Robotics and Automation. 1992; 8 (3): 313–26. DOI: 10.1109/70.143350.
10. Chaumette F. Potential problems of stability and convergence in image-based and position-based visual servoing. Lecture Notes in Control and Information Sciences. 66–78. DOI: 10.1007/bfb0109663.
11. Michel H, Rives P. Singularities in the determination of the situation of a robot efector from the perspective view of 3 points. Technical Report 1850, INRIA Research, 1993.
12. Chaumette F. 2004. Image Moments: A General and Useful Set of Features for Visual Servoing. IEEE Transactions on Robotics. 20 (4): 713–23. DOI: 10.1109/tro.2004.829463.
13. Tahri O, Chaumette F. Point-based and region-based image moments for visual servoing of planar objects. IEEE Transactions on Robotics. 2005; 21 (6): 1116–27. DOI: 10.1109/TRO.2005.853500.
14. Tahri O, Mezouar Y, Chaumette F, Corke P. Decoupled Image-Based Visual Servoing for Cameras Obeying the Unified Projection Model. Robotics, IEEE Transactions on. 2010; 26: 684–97. DOI: 10.1109/TRO.2010.2051593.
15. Dementhon DF, Davis LS. Model-based object pose in 25 lines of code. International Journal of Computer Vision. 1995; 15 (1–2):

123–41. DOI: 10.1007/bf01450852.
16. Lowe DG. Three-dimensional object recognition from single two-dimensional images. Artif Intell. 1987; 31: 355–95.
17. Malis E, Chaumette F, Boudet S. 2-1/2D visual servoing. IEEE Transactions on Robotics and Automation. 1999; 15 (2): 238–50.
18. Wilson WJ, Hulls CCW, Bell GS. Relative end-effector control using Cartesian position based visual servoing. IEEE Transactions on Robotics and Automation. 1996; 12 (5): 684–96. DOI: 10.1109/70.538974.
19. Corke PI. Visual control of robot manipulators — a review. Visual Servoing: Real-Time Control of Robot Manipulators Based on Visual Sensory Feedback. 1993; pp. 1–31.
20. Corke PI, Hutchinson SA. A new partitioned approach to image-based visual servo control. IEEE Transactions on Robotics and Automation. 2001; 17 (4): 507–15. DOI: 10.1109/70.954764.
21. Deguchi K. Optimal motion control for image-based visual servoing by decoupling translation and rotation. Proceedings. 1998 IEEE/RSJ International Conference on Intelligent Robots and Systems. Innovations in Theory, Practice and Applications (Cat. #. 98CH36190). DOI: 10.1109/iros.1998.727274.
22. Gans NR, Hutchinson SA. Stable Visual Servoing Through Hybrid Switched-System Control. IEEE Transactions on Robotics. 2007; 23 (3): 530–40. DOI: 10.1109/tro.2007.895067.
23. Kermorgant O, Chaumette F. Combining IBVS and PBVS to ensure the visibility constraint. 2011 IEEE/RSJ International Conference on Intelligent Robots and Systems. 2011. DOI: 10.1109/iros.2011.6048254.
24. Pang Y, Huang Q, Jia D, Tian Y, Gao J, Zhang W. Object manipulation of a humanoid robot based on visual Servoing. 2007 IEEE/RSJ International Conference on Intelligent Robots and Systems. 2007. DOI: 10.1109/iros.2007.4399445.
25. Moughlbay AA, Cervera E, Martinet P. Real-time model based visual servoing tasks on a humanoid robot. Intelligent Autonomous Systems 12. Berlin, Heidelberg: Springer, 2013; c. 321–333.
26. Agravante DJ, Cherubini A, Bussy A, Kheddar A. Human-humanoid joint haptic table carrying task with height stabilization using vision. 2013 IEEE/RSJ International Conference on Intelligent Robots and Systems. 2013. DOI: 10.1109/iros.2013.6697019.
27. Hogan N. Impedance Control: An Approach to Manipulation. American Control Conference. 1984; pp. 304–313. DOI: 10.23919/ACC.1984.4788393.
28. Aristidou A, Lasenby J. FABRIK: A fast, iterative solver for the Inverse Kinematics problem. Graphical Models. 2011; 73 (5): 243–60. DOI: 10.1016/j.gmod.2011.05.003.

Литература

1. Lassig R, Lorenz M, Sissimators E, Wicker I, Buchner T. Robotics Outlook 2030: How intelligence and mobility will shape the future. 2021. The Boston Consulting Group.
2. Joseph F. Robotics in Service. Engelberger, 1989; 248 p.
3. Alemzadeh H, Raman J, Leveson N, Kalbarczyk Z, Iyer RK. Adverse Events in Robotic Surgery: A Retrospective Study of 14 Years of FDA Data. PLOS ONE. 2016; 11 (4): e0151470. DOI: 10.1371/journal.pone.0151470.
4. Taylor GR, Kleeman L. Grasping unknown objects with a humanoid robot. 2002.
5. Kragic D, Christensen HA. Survey on Visual Servoing for

Manipulation. Comput Vis Act Percept Lab. 2002; 15 p.
6. Dong G, Zhu ZH. Position-based visual servo control of autonomous robotic manipulators. Acta Astronautica. 2015; 115: 291–302. DOI: 10.1016/j.actaastro.2015.05.036.
7. Vahrenkamp N, Wieland S, Azad P, Gonzalez D, Asfour T, Dillmann R. Visual servoing for humanoid grasping and manipulation tasks. Humanoids 2008 — 8th IEEE-RAS International Conference on Humanoid Robots. 2000. DOI: 10.1109/ichr.2008.4755985.
8. Chaumette F, Hutchinson S. Visual servo control, Part I: Basic approaches. IEEE Robotics and Automation Magazine. 2006; 13 (4): 82–90.

9. Espiau B, Chaumette F, Rives P. A new approach to visual servoing in robotics. IEEE Transactions on Robotics and Automation. 1992; 8 (3): 313–26. DOI: 10.1109/70.143350.

10. Chaumette F. Potential problems of stability and convergence in image-based and position-based visual servoing. Lecture Notes in Control and Information Sciences. 66–78. DOI: 10.1007/bfb0109663.

11. Michel H, Rives P. Singularities in the determination of the situation of a robot efector from the perspective view of 3 points. Technical Report 1850, INRIA Research, 1993.

12. Chaumette F. 2004. Image Moments: A General and Useful Set of Features for Visual Servoing. IEEE Transactions on Robotics. 20 (4): 713–23. DOI: 10.1109/tro.2004.829463.

13. Tahri O, Chaumette F. Point-based and region-based image moments for visual servoing of planar objects. IEEE Transactions on Robotics. 2005; 21 (6): 1116–27. DOI: 10.1109/TRO.2005.853500.

14. Tahri O, Mezouar Y, Chaumette F, Corke P. Decoupled Image-Based Visual Servoing for Cameras Obeying the Unified Projection Model. Robotics, IEEE Transactions on. 2010; 26: 684–97. DOI: 10.1109/TRO.2010.2051593.

15. Dementhon DF, Davis LS. Model-based object pose in 25 lines of code. International Journal of Computer Vision. 1995; 15 (1–2): 123–41. DOI: 10.1007/bf01450852.

16. Lowe DG. Three-dimensional object recognition from single two-dimensional images. Artif Intell. 1987; 31: 355–95.

17. Malis E, Chaumette F, Boudet S. 2-1/2D visual servoing. IEEE Transactions on Robotics and Automation. 1999; 15 (2): 238–50.

18. Wilson WJ, Hulls CCW, Bell GS. Relative end-effector control using Cartesian position based visual servoing. IEEE Transactions on Robotics and Automation. 1996; 12 (5): 684–96. DOI: 10.1109/70.538974.

19. Corke PI. Visual control of robot manipulators — a review. Visual Servoing: Real-Time Control of Robot Manipulators Based on Visual Sensory Feedback. 1993; pp. 1–31.

20. Corke PI, Hutchinson SA. A new partitioned approach to image-based visual servo control. IEEE Transactions on Robotics and Automation. 2001; 17 (4): 507–15. DOI: 10.1109/70.954764.

21. Deguchi K. Optimal motion control for image-based visual servoing by decoupling translation and rotation. Proceedings. 1998 IEEE/RSJ International Conference on Intelligent Robots and Systems. Innovations in Theory, Practice and Applications (Cat. #. 98CH36190). DOI: 10.1109/iros.1998.727274.

22. Gans NR, Hutchinson SA. Stable Visual Servoing Through Hybrid Switched-System Control. IEEE Transactions on Robotics. 2007; 23 (3): 530–40. DOI: 10.1109/tro.2007.895067.

23. Kermorgant O, Chaumette F. Combining IBVS and PBVS to ensure the visibility constraint. 2011 IEEE/RSJ International Conference on Intelligent Robots and Systems. 2011. DOI: 10.1109/iros.2011.6048254.

24. Pang Y, Huang Q, Jia D, Tian Y, Gao J, Zhang W. Object manipulation of a humanoid robot based on visual Servoing. 2007 IEEE/RSJ International Conference on Intelligent Robots and Systems. 2007. DOI: 10.1109/iros.2007.4399445.

25. Moughlbay AA, Cervera E, Martinet P. Real-time model based visual servoing tasks on a humanoid robot. Intelligent Autonomous Systems 12. Berlin, Heidelberg: Springer, 2013; c. 321–333.

26. Agravante DJ, Cherubini A, Bussy A, Kheddar A. Human-humanoid joint haptic table carrying task with height stabilization using vision. 2013 IEEE/RSJ International Conference on Intelligent Robots and Systems. 2013. DOI: 10.1109/iros.2013.6697019.

27. Hogan N. Impedance Control: An Approach to Manipulation. American Control Conference. 1984; pp. 304–313. DOI: 10.23919/ACC.1984.4788393.

28. Aristidou A, Lasenby J. FABRIK: A fast, iterative solver for the Inverse Kinematics problem. Graphical Models. 2011; 73 (5): 243–60. DOI: 10.1016/j.gmod.2011.05.003.

COMPUTATIONAL PHANTOM FOR RED BONE MARROW DOSIMETRY FROM INCORPORATED BETA EMITTERS IN A NEWBORN BABY

Sharagin PA[1] ✉, Shishkina EA[1,2], Tolstykh EI[1]

[1] Urals Research Center for Radiation Medicine of the Federal Medical-Biological Agency, Chelyabinsk, Russia

[2] Chelyabinsk State University, Chelyabinsk, Russia

Active (red) bone marrow (AM) exposure due to ingested bone-seeking radionuclides can lead to grave medical consequences. For example, a radioactive contamination of the Techa River in the 1950s caused exposure to AM for riverside residents and led to chronic radioactive exposure syndrome in some of them, with higher risk of leukemia. The main sources of the marrow exposure were the bone-seeking beta emitters [89,90]Sr. Improving the dosimetry of AM internal exposure is an important step in clarifying the risks of chronic radiation exposure for riverside residents. To evaluate the energy absorbed by AM from incorporated ^{90}Sr it is customary to use computational phantoms where radiation transport can be emulated. A phantom is a representative digital representation of skeletal bone geometry and AM The goal of this work was to develop a computational phantom of a newborn skeleton for dosimetry of AM from incorporated [90]Sr. The researchers have used the Stochastic Parametric Skeletal Dosimetry method (SPSD), where hematopoietic sites were modeled as a set of phantoms of simple geometric shape describing individual skeletal bone areas. The AM content in the skeleton as well as the phantom parameters were evaluated on the basis of published measurements of real bones. As a result, a computational phantom of the main skeletal hematopoietic sites was generated for a newborn baby, including 34 phantoms of bone areas. The simulated phantom simulates the bone structure as well as the variability of skeletal parameters within the population and corresponds well to measurements of real bones.

Keywords: active bone marrow, trabecular bone, cortical bone, bone marrow dosimetry, computational phantoms, [90]Sr

ВЫЧИСЛИТЕЛЬНЫЙ ФАНТОМ ДЛЯ ДОЗИМЕТРИИ КРАСНОГО КОСТНОГО МОЗГА НОВОРОЖДЕННОГО РЕБЕНКА ОТ ИНКОРПОРИРОВАННЫХ БЕТА-ИЗЛУЧАТЕЛЕЙ

П. А. Шарагин[1] ✉, Е. А. Шишкина[1,2], Е. И. Толстых[1]

[1] Уральский научно-практический центр радиационной медицины Федерального медико-биологического агентства России, Челябинск, Россия

[2] Челябинский государственный университет, Челябинск, Россия

Внутреннее облучение красного костного мозга (ККМ), обусловленное техногенными остеотропными радионуклидами, может приводить к серьезным медицинским последствиям. Так, радиоактивное загрязнение реки Течи в 1950-е годы стало причиной облучения ККМ у жителей прибрежных территорий, что привело к возникновению хронического лучевого синдрома у некоторых из них, а также повысило риск развития лейкозов в когорте этих жителей. Основными источниками внутреннего облучения ККМ были остеотропные бета-излучатели [89,90]Sr. Усовершенствование дозиметрии внутреннего облучения ККМ является важным этапом уточнения рисков хронического радиационного воздействия для жителей прибрежных территорий. Для оценки поглощенной энергии в ККМ от инкорпорированного [90]Sr используют вычислительные фантомы, в которых можно имитировать транспорт излучений. Фантом — это репрезентативное цифровое представление геометрии костей скелета и ККМ. Целью работы было разработать вычислительный фантом скелета новорожденного ребенка для дозиметрии ККМ от инкорпорированного [90]Sr. Для моделирования скелета использовали оригинальную методику SPSD (Stochastic parametric skeletal dosimetry): участки скелета с активным гемопоэзом моделировали как набор фантомов простой геометрической формы, описывающих отдельные участки костей скелета. Содержание ККМ в скелете, а также параметры фантомов оценивали на основе опубликованных результатов измерений реальных костей. В результате был сгенерирован вычислительный фантом основных участков скелета с активным гемопоэзом для новорожденного ребенка, включающий 34 фантома участков костей. Смоделированный фантом имитирует структуру костной ткани, а также вариабельность параметров скелета внутри популяции и хорошо соответствует измерениям реальных костей.

Ключевые слова: красный костный мозг, трабекулярная кость, кортикальная кость, дозиметрия костного мозга, вычислительные фантомы, [90]Sr

Active marrow (AM) exposure due to internal radiation from man-made bone-seeking radionuclides can lead to grave medical consequences. Such exposure can occur both as part of radionuclide therapy and due to radionuclides have been released into the environment as a result of nuclear weapons testing or radiation accidents. Radioactive contamination of the Techa River in the 1950s led to exposure AM of riverside village residents to doses of about 0.35 Gy, which caused chronic radiation syndrome [1–4] and an increased risk of leukemia. The main sources of AM internal exposure were the bone-seeking beta emitters [89,90]Sr [2]. This demonstrates that improvement of AM dosimetry from incorporated ^{90}Sr is an urgent task of radiobiology and radiation protection. [90]Sr dosimetry includes biokinetic modeling to estimate its distribution in body tissues and calculate the specific activity of ^{90}Sr in the source tissues, as well as dosimetric modeling of energy transfer from the source tissue (bone) to the target tissue (AM). The results of dosimetric modeling are dose factors (DF), which allow converting the specific activity of the incorporated radiation source into the absorbed dose rate in the target tissue. An important step in dosimetric modeling is the development of computational phantoms, i.e., a representative digital representation of source and target tissue geometries in which researchers can model the radiation transport. The bone is an object of modelling when constructing phantoms for AM dosimetry. The dosimetric bone model is a simplified representation of a real bone; it consists of a solid cortical bone layer that covers the phantom from the outside, whereas the spongiosa fills the model from the inside. Spongiosa is a set of trabecular bone, which modeled as a network of rod-like trabeculae and the AM located between them. Currently, there are several approaches for modeling the shape and structure of bone, based on the analysis of computed tomography (CT) images [5–9]. These methods require pathoanatomic material and do not allow taking into account the individual variability of the size of human bones. Instead, in the Urals Research Centre for Radiation Medicine" was developed an original parametric method for stochastic modeling of bone structures, known as SPSD modeling (stochastic parametric skeletal dosimetry) [10]. This method is based on the use of published averaged measurements of bone structures as phantom parameters, thus avoiding using of autopsy material, and assessing uncertainties associated with skeletal variability in different individuals.

The aim of this study is to develop a computational phantom of newborn skeleton for AM dosimetry from incorporated [90]Sr.

METHODS

The original SPSD technique was used for the skeleton modeling. In the frame of this approach, only skeletal areas with active hematopoiesis, i.e., those containing AM (hematopoietic sites), are modeled. The SPSD phantom of skeletal hematopoietic sites consist of a set of smaller phantoms — the Bone Phantom Segments (BPS) of a simple geometric shape, describing individual skeletal bone sites. Each phantom includes a description of the simulated media and a description of the source and target tissue geometries.

The modeled skeletal sites with active hemopoiesis (hemopoietic sites) were identified according to published data on AM distribution.

Each BPS consists of mineralized bone tissue and AM. To simulate the transport of energy in these two medias, we determined their chemical composition and density according to published data. These characteristics were used as parameters for all phantoms.

We evaluated parameters characterizing irradiation geometry for each BPS: linear bone dimensions, cortical layer thickness (*Ct.Th*), trabecular thickness (*Tb.Th*), trabecular separation (*Tb.Sp.*), bone fraction in spongiosa volume (*BV/TV*). We evaluated the listed parameters based on published data. To assess the characteristics of bone geometry, articles in peer-reviewed publications, atlases, manuals, monographs and theses were considered. Also, we analyzed electronic resources containing collections of X-rays. The results of measurements of people/samples, which the authors identified as healthy and without diseases leading to bone deformation, were taken for analysis. Ethnically people/samples belonged to Caucasians and Mongolians due to the fact that these groups are characteristic of the population of the Ural region. We considered data from measurements of skeletal bones using various techniques: micrometers, anatomical boxes, ultrasound and radiological studies, CT (for linear dimensions and *Ct.Th*), histomorphometry and micro-CT — for microarchitecture parameters (*Tb.Th, Tb.Sp, BV/TV*). Averaged estimates of bone characteristics were taken as parameters of digital phantoms. If published data on individual measurements were available, we combined them and calculated arithmetic means and standard deviations (*SDs*). In the case of averaging the results of studies of groups of people, we would introduce a weighting coefficient (*Wn*), which took into account the number (*n*) of the studied subjects: $Wn = 1$, if $n \geq 25$; $Wn = n/25$ if $n < 25$. Methods for the selection and analysis of literature data are described in detail [11–14].

Based on the average values of the selected parameters for each bone segment, using the original Trabecula software [15] a computational phantom in voxel form — Bone Phantom Segment (BPS) was generated. BPS is a model of a simple geometric shape (rectangular parallelepiped, cylinder, prism, etc.), filled inside with spongiosa and on the outside covered with a cortical layer, as shown by the example of the phantom of the iliac bone of a newborn (Fig. 1).

Each phantom element (AM, trabecula, cortical layer) was imitated by a set of three-dimensional elements – voxels – from which simulated structures were composed. Each voxel imitate either mineralized bone or bone marrow (BM), depending on the location of the voxel center in the phantom. As source tissues, the dosimetric model considers trabecular bone (TB) and cortical bone (CB) separately, and bone marrow is considered as a target tissue, assuming that AM is uniformly distributed inside the BPS. The voxel size differed between phantoms, did not exceed 70% of the trabecula thickness [15, 16], and varied from 50 to 200 µm. Volumes of source and target tissues were automatically calculated in Trabecula software for each voxel phantom.

Fig. 1. Newborn's iliac phantom section (trabeculae's and cortical bone are shown in *black*, red bone marrow is shown in *white*)

Table 1. Mass fraction of AM (% of the total mass of AM in the skeleton) in the main hematopoietic sites of the skeleton of a newborn baby [17]

№	Hematopoietic site	AM mass fraction, %
1	Femur	6,7
2	Humeri	4,5
3	Sacrum	4,4
4	Tibia bones	7,1
5	Pelvic bones	11,4
6	Skull	28,2
7	Clavicle	0,7
8	Scapula	2,3
9	Ribs	7,1
10	Radius and ulna	2,4
11	Hand and foot bones	10,8
12	Cervical vertebrae	1,7
13	Thoracic vertebrae	7,2
14	Lumbar vertebrae	5,5

To simulate population variability of size and microstructure characteristics, 12 Supplementary Phantom Segments (SPS) were created with parameters randomly selected within the range of their population variability (within the limits of minimum and maximum measured values) for each BPS.

RESULTS

The main hematopoietic sites of a newborn's skeleton and the mass fraction of AM in them were determined according to the data of MRI studies [17] and are presented in Table 1.

The phantom of skeletal hematopoietic sites of a newborn baby includes 14 hematopoietic sites. AM content of these varies from 1.7 to 28.2%.

Hematopoietic sites include bone regions that were not modeled in the SPSD approach. So, epiphyses of long bones were not modeled, since they are mostly composed of cartilage tissue [18–22]. We did not model the bones of the facial skull, since its share compared to the brain is about 13%, and a significant part of the body of the maxilla and mandibula is occupied by developing teeth [33–35]. Besides, vertebral processes were not modeled, since only small ossification centers are observed in newborns [23].

The chemical composition of the simulated medias was selected based on ICRP data for adults [19]. The chemical composition of bone tissue and the AM used for all BPS is presented in Table 2.

The density of mineralized bone tissue was estimated based on the results of measurements of the cortical bone density of newborns [24] and is 1.65 g/cm³. The density of the red bone marrow was taken equal to the density of water (1 g/cm³) [25].

We estimated the parameters of the spongiosa microarchitecture based on published data already described in detail [14]. The linear dimensions and thickness of the cortical layer as BPS parameters are presented in Table 3.

Thus, the phantom of skeletal hematopoietic sites of a newborn consist of 34 BPSs. Depending on the form of the simulated hematopoietic site, it may include 1 (ribs) to 5 (sacrum) BPSs. Most of the BPSs are cylinders and rectangular parallelepipeds. The sizes of phantoms vary widely: from 2 to 33 mm. As shown in Table 3, not all phantoms are covered with a cortical layer, which is associated with an incomplete process of ossification of the spine and skull bones. The highest *Ct.Th* value for a newborn is characteristic of the diaphysis of the femur (1.7 mm).

DISCUSSION

To test the adequacy of the SPSD approach, we performed a comparison of simulated phantoms and real bones. There are unique data on the mass of wet mineralized bones obtained during the study of 40 full-term newborns [68]. Masses corresponding to the sizes of phantoms were calculated as the sum of the volumes of simulated medias (BM, TB, CB) multiplied by their density.

Table 2. Chemical composition of simulated media adopted for all BPS

Chemical composition, rel. unit		
Chemical element	Bone	Active marrow
H	0,035	0,105
C	0,16	0,414
N	0,042	0,034
O	0,445	0,439
Na	0,003	0,001
Mg	0,002	0,002
P	0,095	0,002
S	0,003	0,002
Ca	0,215	–

Table 3. Linear dimensions and cortical thickness accepted for BPS of a newborn baby

Hematopoietic site	Segment	Shape[1]	Phantom parameters, mm (CV, % is in parentheses)[2]						References
			h	*a*	*b*	*c*	*d*	*Ct.Th.*	
Femur	Diaphysis[4]	c	30	7.2 (11)	7.2 (11)	–	–	1.7 (24)	26–32
	Proximal end	dc	19 (5)	26 (9)	12 (12)	7.2 (11)	7.2 (11)	0.5 (24)	
	Distal end	dc	19 (5)	26 (9)	12 (12)	7.2 (11)	7.2 (11)	0.4 (24)	
Humeri	Diaphysis tube[4]	c	30	6 (12)	6 (12)	–	–	1.3 (15)	26–31, 33
	Proximal end	dc	13 (10)	13 (12)	13 (12)	6 (12)	6 (11)	0.4 (15)	
	Distal end	dc	13 (10)	17 (13)	6 (12)	6 (12)	6 (11)	0.3 (19)	
Ribs	Ribs[4]	p	5.7 (38)	30	3.2 (12)	–	–	0.4 (37)	34, 35
Sacrum	Body of the 1st vertebra	p	6.3 (21)	15 (10)	7.5 (10)	–	–	–	36–39
	Body of the 2nd vertebra	p	6.3 (21)	12 (10)	6 (10)	–	–	–	
	Body of the 3rd vertebra	p	5.7 (19)	8.9 (10)	5.3 (9)	–	–	–	
	Body of the 4th vertebra	p	3.8 (21)	8.9 (10)	5.3 (9)	–	–	–	
	Body of the 5th vertebra	p	3.8 (21)	7.5 (10)	3.8 (11)	–	–	–	
Tibia bones	Fibula [4]	c	30	2.9 (7)	2.9 (7)	–	–	0.7 (14)	26, 30, 40
	Tibia diaphysis.[4]	c	30	6.9 (28)	6.9 (28)	–	–	1.4 (14)	26–29, 32, 41, 42
	Tibia proximal end	dc	19 (9)	21 (9)	13 (18)	6.9 (28)	6.9 (28)	0.3 (17)	
	Tibia distal end	dc	15 (9)	15 (23)	15 (23)	6.9 (28)	6.9 (28)	0.3 (17)	
Pelvic bones	Iliac bone part 1	p	4 (23)	24 (3)	24 (3)	–	–	1.2 (33) 0.5 (47)3	23, 43–47
	Iliac bone part 2	p	4 (23)	20 (3)	20 (3)	–	–	0.2 (25)	
	Pubic bone	c	16 (13)	7.5 (16)	7.5 (16)	–	–	0.4 (9)	
	Ischial bone	c	7.5 (16)	18 (11)	12 (8)	–	–	0.4 (9)	
Skull	Flat bones[4]	p	2 (25)	30	30	–	–	–	49–52
Clavicle	Body	c	33 (15)	4.3 (23)	5.9 (25)	–	–	0.8 (25)	53–58
	Sternum end	dc	5.9 (15)	12 (24)	10 (24)	5.9 (25)	4.3 (23)	0.3 (24)	
	Acromial end	dc	5.9 (15)	10 (24)	5.9 (49)	5.9 (25)	4.3 (23)	0.3 (24)	
Radius and ulna	Diaphysis[4]	c	30	3.9 (8)	3.9 (8)	–	–	0.9 (13)	26, 27, 29, 30, 41
	End	dc	12 (6)	5.8 (7)	5.8 (7)	3.9 (8)	3.9 (8)	0.3 (29)	
Hand and foot bones	Tubular bones	c	8.9 (43)	3.8 (42)	3.8 (42)	–	–	0.2 (25)	23, 53, 59,
	The talus and calcaneus	e	–	7.8 (14)	12 (11)	7.8 (14)	–	0.2 (25)	
Scapula	Glenoid	c	5.4 (4)	10 (21)	7.6 (18)	–	–	0.5 (29)	53, 60–63
	Acromion	p	7 (19)	16 (14)	13 (25)	–	–	0.4 (13)	
	Body[4]	p	2.7 (13)	30	30	–	–	0.4 (17)	
Cervical vertebrae	Vertebral body	c	4.1 (1)	6.9 (1)	6.5 (1)	–	–	–	64–66
Thoracic vertebrae	Vertebral body	c	5.1 (2)	7.6 (2)	11 (2)	–	–	–	66, 67
Lumbar vertebrae	Vertebral body	c	7.1 (1)	7.7 (1)	15 (1)	–	–	–	37, 66, 67

Note: [1] — the shape of the phantom was designated as follows: c — cylinder, dc — deformed cylinder, p-rectangular parallelepiped, e — ellipsoid; [2] — the dimensions of the BPS were designated as follows: *h* — height; *a* — major axis (c), major axis for a larger base (dc), or side *a* (p); *b* — minor axis (c), minor axis for a larger base (dc), or side b (*n*); *c* — major axis for a smaller base (dc); *d* — minor axis for a smaller base (dc); for an ellipsoid (e), *a*, *b*, *c* denote the axes of the ellipsoid; [3] — the thickness of the cortical layer was taken to be different for the inner (medial) and outer (gluteal) surfaces of this segment of the iliac bone (Fig. 1); [4] — the BPS imitated only a part of the simulated bone segment, if the dimensions of the bone segment significantly exceeded 30 mm, since in such cases, from the point of view of dosimetry, it does not have it makes no sense to model the entire bone section as a whole [11, 12].

A comparison of the measured bone masses and masses of SPSD phantoms (calculated as the sum of the masses of the segments describing the bone) is shown in Fig. 2.

As can be seen from the comparison, the masses corresponding to the sizes of SPSD phantoms in most cases fall within the range of standard deviation of the values obtained by the author of the compared work [68], that is, they correspond well to the masses of real bones.

A feature of the SPSD phantom is the generation by the BPS of a simple geometric shape, that is, a simplified representation of the real shape of the bone site. A simplified representation can result in biased estimates of simulation results. As mentioned earlier, BPS is modeled with mean population parameter values, and SPS parameters were randomly selected within their population variability range. As a result, the simulated bone segment is "inside" a set of SPSs
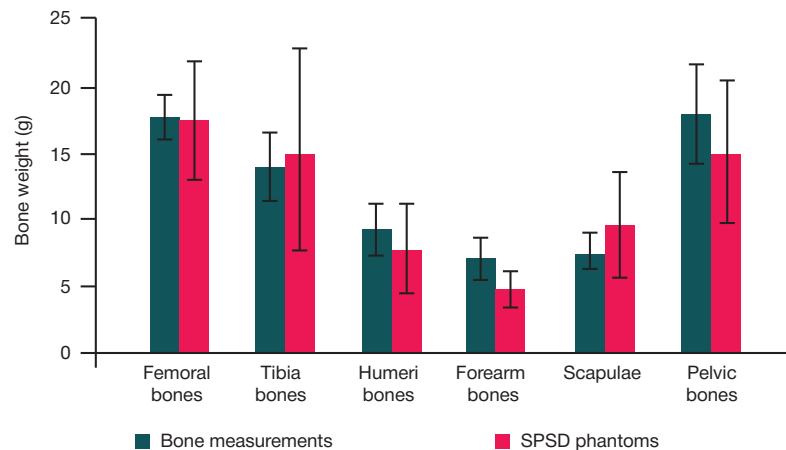
Fig. 2. Comparison of measured bone masses [68], and masses corresponding to the sizes of SPSD phantoms estimated as the sum of masses of all segments describing specific bones (left + right) of newborns, taking into account repeating and paired segments. Error bars showed the standard deviations."

geometric shapes. The variance of the DF set calculated for SPS reflects the effect of variability in bone size, shape, and microstructure.

CONCLUSIONS

As a result of the work, computational phantoms of the main skeletal sites with active hematopoiesis for a newborn were generated. The simulated phantom imitate the structure of bone tissue as well as the variability of skeletal parameters within a population. The phantom fits well with measurements of the newborn's real bones. The phantom is used to improve the the Techa River dosimetry system. In the future, SPSD phantoms will be created for other age groups: 1 year, 5 years, 10 years, 15 years, adults and for the human fetus at 24 weeks of pregnancy. SPSD phantoms can be used for dosimetry of other bone-seeking beta emitters including used in radionuclide therapy such as ^{89}Sr, ^{32}P, ^{186}Re, ^{188}Re, ^{117m}Sm.

References

1. Degteva MO, Shagina NB, Vorobiova MI, Shishkina EA, Tolstykh EI, Akleyev AV. Contemporary Understanding of Radioactive Contamination of the Techa River in 1949–1956. Radiats Biol Radioecol. 2016; 56 (5): 523–34. English, Russian. PMID: 30703313.
2. Krestinina LY, Epifanova S, Silkin S, Mikryukova L, Degteva M, Shagina N, Akleyev A. Chronic low-dose exposure in the Techa River Cohort: risk of mortality from circulatory diseases. Radiat Environ Biophys. 2013; 52 (1): 47–57. DOI: 10.1007/s00411-012-0438-5. Epub 2012 Nov 4.
3. Akleev AV. Xronicheskij luchevoj sindrom u zhitelej pribrezhnyx sel reki Techa. Chelyabinsk: Kniga, 2012; 464 s. Russian.
4. Preston DL, Sokolnikov ME, Krestinina LY, Stram DO. Estimates of Radiation Effects on Cancer Risks in the Mayak Worker, Techa River and Atomic Bomb Survivor Studies. Radiat Prot Dosimetry. 2017; 173 (1–3): 26–31. DOI: 10.1093/rpd/ncw316.
5. O'Reilly SE, DeWeese LS, Maynard MR, Rajon DA, Wayson MB, Marshall EL, et al. An 13 image-based skeletal dosimetry model for the ICRP reference adult female-internal electron 14 sources. Phys Med Biol. 2016; 61 (24): 8794–8824. Epub 2016 Nov 29.
6. Xu XG, Chao TC, Bozkurt A. VIP-Man: an image-based whole-body adult male model constructed from color photographs of the Visible Human Project for multi-particle Monte Carlo calculations. Health Phys. 2000; 78 (5): 476–86. DOI: 10.1097/00004032-200005000-00003. PMID: 10772019.
7. Shah AP, Bolch WE, Rajon DA, Patton PW, Jokisch DW. A paired-image radiation transport model for skeletal dosimetry. J Nucl Med. 2005; 46 (2): 344–53. PMID: 15695796.
8. Pafundi D. Image-based skeletal tissues and electron dosimetry models for the ICRP reference pediatric age series. A dissertation presented to the graduate schools of the University of Florida in partial fulfillment of the requirements for the degree of doctor of the philosophy. University of Florida, 2009.
9. Hough M, Johnson P, Rajon D, Jokisch D, Lee C, Bolch W. An image-based skeletal dosimetry model for the ICRP reference adult male–internal electron sources. Phys Med Biol. 2011; 56 (8):

2309–46. DOI: 10.1088/0031-9155/56/8/001. Epub 2011 Mar 22.
10. Degteva MO, Tolstykh EI, Shishkina EA, Sharagin PA, Zalyapin VI, Volchkova AYu, et al. Stochastic Parametric Skeletal Dosimetry model for humans: General description. PlosOne; 2021 (submitted).
11. Sharagin PA, Shishkina EA, Tolstykh EI, Volchkova AYu, Smith MA, Degteva MO. Segmentation of hematopoietic sites of human skeleton for calculations of dose to active marrow exposed to bone-seeking radionuclides. In: RAD Conference Proceedings, 2018; (3): 154–8. DOI: 10.21175/RadProc.2018.33.
12. Sharagin PA, Tolstykh EI, Shishkina EA, Degteva MO. Dozimetricheskoe modelirovanie kosti dlya osteotropnyx beta-izluchayushhix radionuklidov: razmernye parametry i segmentaciya. V sbornike: Materialy mezhdunarodnoj nauchnoj konferencii «Sovremennye problemy radiobiologii». Belarus', Gomel', 23–24 sentyabrya 2021. 2021; s. 200–204. Russian.
13. Tolstykh EI, Sharagin PA, Shishkina EA, Degteva MO. Formirovanie doz oblucheniya krasnogo kostnogo mozga cheloveka ot 89,90Sr, ocenka parametrov trabekulyarnoj kosti dlya dozimetricheskogo modelirovaniya. V sbornike: Materialy mezhdunarodnoj nauchnoj konferencii «Sovremennye problemy radiobiologii». Belarus', Gomel', 23–24 sentyabrya 2021. 2021; s. 176–179. Russian.
14. Tolstykh EI, Sharagin PA, Shishkina EA, Volchkova AYu. Degteva MO. Anatomo-morfologicheskij bazis dlya dozimetricheskogo modelirovaniya trabekulyarnoj kosti cheloveka s ispol'zovaniem stoxasticheskogo parametricheskogo podxoda. Klinicheskij vestnik GNC FMBC im.A. I. Burnazyana. 2022; 3: 25–40. Russian.
15. Shishkina EA, Timofeev YS, Volchkova AY, Sharagin PA, Zalyapin VI, Degteva MO, et al. Trabecula: A Random Generator of Computational Phantoms for Bone Marrow Dosimetry. Health Phys. 2020; 118 (1): 53–59. DOI: 10.1097/HP.0000000000001127.
16. Zalyapin VI, Timofeev YuS, Shishkina EA. A parametric stochastic model of bone geometry. Bulletin of Southern Urals State University, Issue «Mathematical Modelling. Programming & Computer Software» (SUSU MMCS). 2018; 11 (2): 44–57. DOI: 10.14529/mmp180204.

17. Cristy M. Active bone marrow distribution as a function of age in humans. Phys Med Biol. 1981; 26 (3): 389–400.

18. Vogler JB 3rd, Murphy WA. Bone marrow imaging. Radiology. 1988; 168 (3): 679–93.

19. Vande Berg BC, Malghem J, Lecouvet FE, Maldague B. Magnetic resonance imaging of the normal bone marrow. Skeletal Radiology. 1998; 27: 471–83.

20. Vande Berg BC, Malghem J, Lecouvet FE, Maldague B. Magnetic resonance imaging of normal bone marrow. Eur Radiol. 1998; 8 (8): 1327–34.

21. Taccone A, Oddone M, Dell'Acqua AD, Occhi M, Ciccone MA. MRI "road-map" of normal age-related bone marrow. II. Thorax, pelvis and extremities. Pediatr Radiol. 1995; 25 (8): 596–606; PubMed PMID: 8570312.

22. Taccone A, Oddone M, Occhi M, Dell'Acqua AD, Ciccone MA. MRI "road-map" of normal age-related bone marrow. I. Cranial bone and spine. Pediatr Radiol. 1995; 25 (8): 588–95; PubMed PMID: 8570311.

23. Cunningham C, Scheuer L, Black S. Developmental Juvenile Osteology. Elsevier Academic Press, 2016.

24. Robinson RA. Chemical analysis and electron microscopy of bone. In: Bone as a tissue, ed. by Rodahl K, Nicholson JT, Brown EM. New York: McGraw-Hill, 1960; p. 186–250.

25. Valentin J. Basic anatomical and physiological data for use in radiological protection: reference values. Annals of the ICRP. Annals of the ICRP. 32 (3–4): 1–277. 2002.

26. Medvedev MV. Ul'trazvukovaya fetometriya: spravochnye tablicy i nomogrammy. M.: Real'noe vremya, 2009; 19–24. Russian.

27. Florence JL. Linear and cortical bone dimensions as indicators of health status in subadults from the Milwaukee County Poor Farm Cemetery. M.A., University of Colorado at Denver, 2007.

28. Miles AEW. Growth Curves of Immature Bones from a Scottish Island Population of Sixteenth to mid-Nineteenth Century: Limb-bone Diaphyses and Some Bones of the Hand and Foot. International Journal of Osteoarcheology. 1994; 4: 121–36.

29. Maresh MM. Measurements from roentgenograms. In: Human Growth and Development (R.W. McCammon, Ed.). Springfield, IL: Charles C. Thomas, 1970; p. 157–200.

30. Jeanty P. Fetal limb biometry. Radiology. 1983; 147 (2): 601–2. DOI: 10.1148/radiology.147.2.6836145. PMID: 6836145.

31. Svadovsky VS. Age-related bone remodeling. Moscow, 1961.

32. Dhavale N, Halcrow SE, Buckley HR, Tayles N, Domett KM, Gray AR. Linear and appositional growth in infants and children from the prehistoric settlement of Ban Non Wat, Northeast Thailand: Evaluating biological responses to agricultural intensification in Southeast Asia, Journal of Archaeological Science: Reports. 2017; V11: 435–46.

33. Danforth ME, Wrobel GD, Armstrong CW, Swanson D. Juvenile age estimation using diaphyseal long bone lengths among ancient Maya populations. Latin American Antiquity. 2017; 20 (1): 3–13.

34. Beresheim AC, Pfeiffer S, Grynpas M. Ontogenetic changes to bone microstructure in an archaeologically derived sample of human ribs. J Anat. 2019. DOI: 10.1111/joa.13116.

35. Pfeiffer S. Cortical Bone Histology in Juveniles. Available from: https://www.researchgate.net/publication/303179375_Cortical_bone_histology_in_Juveniles

36. Hresko AM, Hinchcliff EM, Deckey DG, Hresko MT. Developmental sacral morphology: MR study from infancy to skeletal maturity. Eur Spine J. 2020. Available from: https://doi.org/10.1007/s00586-020-06350-6.

37. Mavrych V, Bolgova O, Ganguly P and Kashchenko S. Age-Related Changes of Lumbar Vertebral Body Morphometry. Austin J Anat. 2014; 1 (3): 7.

38. Dimeglio A, Bonnel F, Canavese F. The Growing Spine. In: Spinal Anatomy. Modern Concepts. Springer. 2020; 25–52.

39. Andronesky A. Anatomiya rebenka. Buxarest: Meridian, 1970. Russian.

40. Bernert Zs, Évinger S, Hajdu T. New data on the biological age estimation of children using bone measurements based on historical populations from the Carpathian Basin. Annales Historico-Naturales Musei Nationalis Hungarici. 2007; 99: 199–206.

41. Gindhart PS. Growth Standards for the Tibia and Radius in Children Aged One Month through Eighteen Years. Am J Phys Anthrop. 1973; 39: 41–48.

42. Suominen PK, Nurmi E, Lauerma K. Intraosseous access in neonates and infants: risk of severe complications - a case report. Acta Anaesthesiol Scand. 2015; 59 (10): 1389–93. DOI: 10.1111/aas.12602. Epub 2015 Aug 24. PubMed PMID: 26300243.

43. Blake KAS. An investigation of sex determination from the subadult pelvis: A morphometric analysis. Doctoral Dissertation, University of Pittsburgh. 2011.

44. Cunningham CA, Black SM. Iliac cortical thickness in the neonate — the gradient effect. J Anat. 2009; 215 (3): 364–70. DOI: 10.1111/j.1469-7580.2009.01112.x.

45. Cunningham CA, Black SM. Anticipating bipedalism: trabecular organization in the newborn ilium. J Anat. 2009; 214 (6): 817–29. DOI: 10.1111/j.1469-7580.2009.01073.x.

46. Corron L, Marchal F, Condemi S, Chaumoître K, Adalian P. A New Approach of Juvenile Age Estimation using Measurements of the Ilium and Multivariate Adaptive Regression Splines (MARS) Models for Better Age Prediction. Forensic Sci. 2017; 62 (1): 18–29. DOI: 10.1111/1556-4029.13224.

47. Yusof NA, Soames RW, Cunningham CA, Black SM. Anat Rec (Hoboken). Growth of the human ilium: the anomalous sacroiliac junction 2013; 296 (11): 1688–94. DOI: 10.1002/ar.22785.

48. Schnitzler CM, Mesquita JM, Pettifor JM. Cortical bone development in black and white South African children: iliac crest histomorphometry. Bone. 2009; 44 (4): 603–11. DOI: 10.1016/j.bone.2008.12.009.

49. De Boer HH, Van der Merwe AE, Soerdjbalie-Maikoe VV. Human cranial vault thickness in a contemporary sample of 1097 autopsy cases: relation to body weight, stature, age, sex and ancestry. Int J Legal Med. 2016; 130 (5): 1371–7. DOI: 10.1007/s00414-016-1324-5.

50. Margulies S, Coats B. Experimental Injury Biomechanics of the Pediatric Head and Brain. In: Pediatric Injury Biomechanics. New York: Springer Science + Business Media, 2013; 157–190.

51. Li Z, Park BK, Liu W, Zhang J, Reed MP, Rupp JD, et al. A statistical skull geometry model for children 0–3 years old. PLoS One. 2015; 10 (5): e0127322. DOI: 10.1371/journal.pone.0127322. eCollection 2015.

52. Rodriguez-Florez N, Ibrahim A, Hutchinson JC, Borghi A, James G, Arthurs OJ, et al. Cranial bone structure in children with sagittal craniosynostosis: Relationship with surgical outcomes. J Plast Reconstr Aesthet Surg. 2017; 70 (11): 1589–97. DOI: 10.1016/j.bjps.2017.06.017.

53. Fazekas IGy. and Kósa F. Forensic Fetal Osteology. Budapest: Akadémiai Kiadó, 1978.

54. Sherer D, Sokolovski M, Dalloul M, Khoury-Collado F, Osho J, Lamarque M, et al. Fetal clavicle length throughout gestation: a nomogram. Ultrasound in Obstetrics and Gynecology. 2006; 27: 306–10.

55. McGraw MA, Mehlman CT, Lindsell CJ, Kirby CL. Postnatal growth of the clavicle: birth to eighteen years of age. Journal of Pediatric Orthopedics. 2009; 29: 937.

56. Black SM. and Scheuer JL. Age changes in the clavicle: from the early neonatal period to skeletal maturity. International Journal of Osteoarchaeology. 1996; 6: 425–34.

57. Bernat A, Huysmans T, Van Glabbeek F, Sijbers J, Gielen J, Van Tongel A. The anatomy of the clavicle: a three-dimensional cadaveric study. Clin Anat. 2014; 27 (5): 712–90.

58. Fujita T, Orimo H, Ohata M, Yoshikawa M. Changes in the cortical thickness of the clavicle according to age. J Am Geriatr Soc. 1968; 16 (4): 458–62.

59. Raziye D, Ceren U, Kadir D, Osman S, Mehmed Ali M. A Radiological Investigation on the Hand Development in Human Fetuses Throughout the Fetal Period and an Evaluation Performed in Terms of its Clinical Importance Hand Development. International Journal of Morphology. International Journal of Morphology. 2016; 34: 1539–52. DOI: 10.4067/s0717-95022016000400057.

60. Corrigan GE. The neonatal scapula. Biol Neonat. 1960; 2: 159–67. PubMed PMID: 13695677.

61. Hrdlicka A. The scapula: visual observations. Am J Phys Anthropol. 1942; 29: 73–94.

62. Vallois HV. L'omoplate humaine. Bulletin de la Sociétié d'Anthropolgie de Paris. 1946; 7: 16–99.

63. Saunders S, Hoppa R, Southern R. Diaphyseal growth in a nineteenth-century skeletal sample of subadults from St Thomas' Church, Belleville, Ontario. International Journal of Osteoarchaeology. 1993; 3: 265–81.

64. Xomutova E. Yu. Anatomiya shejnogo otdela pozvonochnika novorozhdennyx pri luchevyx metodax issledovaniya [dissertaciya]. Sankt-Peterburg, 2005. Russian.

65. Sharma N, Jain SK, Singh PK, Rohin Garg. A morphometric study of predictors for sexual dimorphism of cervical part of vertebral column in human fetuses. Journal of the Anatomical Society of India. 2017; 66: 135–39.

66. Kneissel M, Roschger P, Steiner W, Schamall D, Kalchhauser G, Boyde A, et al. Cancellous Bone Structure in the Growing and Aging Lumbar Spine in a Historic Nubian Population. Calcif Tissue Int. 1997; 61: 95–100.

67. Ponrartana S, Aggabao PC, Dharmavaram NL, Fisher CL, Friedlich P, Devaskar SU, et al. Sexual Dimorphism in Newborn Vertebrae and its Potential Implications. J Pediatr. 2015; 167: 416–21.

68. Borisov BK. Vesovye pokazateli razvitiya skeleta ploda cheloveka i soderzhanie v nem stronciya i kal'ciya. M.: Gosudarstvennyj komitet po ispol'zovaniyu atomnoj ehnergii SSSR, 1973; 14 s. Russian.

Литература

1. Degteva MO, Shagina NB, Vorobiova MI, Shishkina EA, Tolstykh EI, Akleyev AV. Contemporary Understanding of Radioactive Contamination of the Techa River in 1949–1956. Radiats Biol Radioecol. 2016; 56 (5): 523–34. English, Russian. PMID: 30703313.

2. Krestinina LY, Epifanova S, Silkin S, Mikryukova L, Degteva M, Shagina N, Akleyev A. Chronic low-dose exposure in the Techa River Cohort: risk of mortality from circulatory diseases. Radiat Environ Biophys. 2013; 52 (1): 47–57. DOI: 10.1007/s00411-012-0438-5. Epub 2012 Nov 4.

3. Аклеев А. В. Хронический лучевой синдром у жителей прибрежных сел реки Теча. Челябинск: Книга, 2012; 464 с.

4. Preston DL, Sokolnikov ME, Krestinina LY, Stram DO. Estimates of Radiation Effects on Cancer Risks in the Mayak Worker, Techa River and Atomic Bomb Survivor Studies. Radiat Prot Dosimetry. 2017; 173 (1–3): 26–31. DOI: 10.1093/rpd/ncw316.

5. O'Reilly SE, DeWeese LS, Maynard MR, Rajon DA, Wayson MB, Marshall EL, et al. An 13 image-based skeletal dosimetry model for the ICRP reference adult female-internal electron 14 sources. Phys Med Biol. 2016; 61 (24): 8794–8824. Epub 2016 Nov 29.

6. Xu XG, Chao TC, Bozkurt A. VIP-Man: an image-based whole-body adult male model constructed from color photographs of the Visible Human Project for multi-particle Monte Carlo calculations. Health Phys. 2000; 78 (5): 476–86. DOI: 10.1097/00004032-200005000-00003. PMID: 10772019.

7. Shah AP, Bolch WE, Rajon DA, Patton PW, Jokisch DW. A paired-image radiation transport model for skeletal dosimetry. J Nucl Med. 2005; 46 (2): 344–53. PMID: 15695796.

8. Pafundi D. Image-based skeletal tissues and electron dosimetry models for the ICRP reference pediatric age series. A dissertation presented to the graduate schools of the University of Florida in partial fulfillment of the requirements for the degree of doctor of the philosophy. University of Florida, 2009.

9. Hough M, Johnson P, Rajon D, Jokisch D, Lee C, Bolch W. An image-based skeletal dosimetry model for the ICRP reference adult male–internal electron sources. Phys Med Biol. 2011; 56 (8): 2309–46. DOI: 10.1088/0031-9155/56/8/001. Epub 2011 Mar 22.

10. Degteva MO, Tolstykh EI, Shishkina EA, Sharagin PA, Zalyapin VI, Volchkova AYu, et al. Stochastic Parametric Skeletal Dosimetry model for humans: General description. PlosOne; 2021 (submitted).

11. Sharagin PA, Shishkina EA, Tolstykh EI, Volchkova AYu, Smith MA, Degteva MO. Segmentation of hematopoietic sites of human skeleton for calculations of dose to active marrow exposed to bone-seeking radionuclides. In: RAD Conference Proceedings, 2018; (3): 154–8. DOI: 10.21175/RadProc.2018.33.

12. Шарагин П. А., Толстых Е. И., Шишкина Е. А., Дегтева М. О. Дозиметрическое моделирование кости для остеотропных бета-излучающих радионуклидов: размерные параметры и сегментация. В сборнике: Материалы международной научной конференции «Современные проблемы радиобиологии». Беларусь, Гомель, 23–24 сентября 2021. 2021; с. 200–204.

13. Толстых Е. И., Шарагин П. А., Шишкина Е. А., Дегтева М. О. Формирование доз облучения красного костного мозга человека от 89,90Sr, оценка параметров трабекулярной кости для дозиметрического моделирования. В сборнике: Материалы международной научной конференции «Современные проблемы радиобиологии». Беларусь, Гомель, 23–24 сентября 2021. 2021; с. 176–179.

14. Толстых Е. И., Шарагин П. А., Шишкина Е. А., Волчкова А. Ю. Дегтева М. О. Анатомо-морфологический базис для дозиметрического моделирования трабекулярной кости человека с использованием стохастического параметрического подхода. Клинический вестник ГНЦ ФМБЦ им. А. И. Бурназяна. 2022; 3: 25–40.

15. Shishkina EA, Timofeev YS, Volchkova AY, Sharagin PA, Zalyapin VI, Degteva MO, et al. Trabecula: A Random Generator of Computational Phantoms for Bone Marrow Dosimetry. Health Phys. 2020; 118 (1): 53–59. DOI: 10.1097/HP.0000000000001127.

16. Zalyapin VI, Timofeev YuS, Shishkina EA. A parametric stochastic model of bone geometry. Bulletin of Southern Urals State University, Issue «Mathematical Modelling. Programming & Computer Software» (SUSU MMCS). 2018; 11 (2): 44–57. DOI: 10.14529/mmp180204.

17. Cristy M. Active bone marrow distribution as a function of age in humans. Phys Med Biol. 1981; 26 (3): 389–400.

18. Vogler JB 3rd, Murphy WA. Bone marrow imaging. Radiology. 1988; 168 (3): 679–93.

19. Vande Berg BC, Malghem J, Lecouvet FE, Maldague B. Magnetic resonance imaging of the normal bone marrow. Skeletal Radiology. 1998; 27: 471–83.

20. Vande Berg BC, Malghem J, Lecouvet FE, Maldague B. Magnetic resonance imaging of normal bone marrow. Eur Radiol. 1998; 8 (8): 1327–34.

21. Taccone A, Oddone M, Dell'Acqua AD, Occhi M, Ciccone MA. MRI "road-map" of normal age-related bone marrow. II. Thorax, pelvis and extremities. Pediatr Radiol. 1995; 25 (8): 596–606; PubMed PMID: 8570312.

22. Taccone A, Oddone M, Occhi M, Dell'Acqua AD, Ciccone MA. MRI "road-map" of normal age-related bone marrow. I. Cranial bone and spine. Pediatr Radiol. 1995; 25 (8): 588–95; PubMed PMID: 8570311.

23. Cunningham C, Scheuer L, Black S. Developmental Juvenile Osteology. Elsevier Academic Press, 2016.

24. Robinson RA. Chemical analysis and electron microscopy of bone. In: Bone as a tissue, ed. by Rodahl K, Nicholson JT, Brown EM. New York: McGraw-Hill, 1960; p. 186–250.

25. Valentin J. Basic anatomical and physiological data for use in radiological protection: reference values. Annals of the ICRP. Annals of the ICRP. 32 (3–4): 1–277. 2002.

26. Медведев М. В. Ультразвуковая фетометрия: справочные таблицы и номограммы. М.: Реальное время, 2009; 19–24.

27. Florence JL. Linear and cortical bone dimensions as indicators of health status in subadults from the Milwaukee County Poor Farm Cemetery. M.A., University of Colorado at Denver, 2007.

28. Miles AEW. Growth Curves of Immature Bones from a Scottish Island Population of Sixteenth to mid-Nineteenth Century: Limb-bone Diaphyses and Some Bones of the Hand and Foot. International Journal of Osteoarcheology. 1994; 4: 121–36.

29. Maresh MM. Measurements from roentgenograms. In: Human Growth and Development (R.W. McCammon, Ed.). Springfield, IL: Charles C. Thomas, 1970; p. 157–200.

30. Jeanty P. Fetal limb biometry. Radiology. 1983; 147 (2): 601–2. DOI: 10.1148/radiology.147.2.6836145. PMID: 6836145.

31. Svadovsky VS. Age-related bone remodeling. Moscow, 1961.
32. Dhavale N, Halcrow SE, Buckley HR, Tayles N, Domett KM, Gray AR. Linear and appositional growth in infants and children from the prehistoric settlement of Ban Non Wat, Northeast Thailand: Evaluating biological responses to agricultural intensification in Southeast Asia, Journal of Archaeological Science: Reports. 2017; V11: 435–46.
33. Danforth ME, Wrobel GD, Armstrong CW, Swanson D. Juvenile age estimation using diaphyseal long bone lengths among ancient Maya populations. Latin American Antiquity. 2017; 20 (1): 3–13.
34. Beresheim AC, Pfeiffer S, Grynpas M. Ontogenetic changes to bone microstructure in an archaeologically derived sample of human ribs. J Anat. 2019. DOI: 10.1111/joa.13116.
35. Pfeiffer S. Cortical Bone Histology in Juveniles. Available from: https://www.researchgate.net/publication/303179375_Cortical_bone_histology_in_Juveniles
36. Hresko AM, Hinchcliff EM, Deckey DG, Hresko MT. Developmental sacral morphology: MR study from infancy to skeletal maturity. Eur Spine J. 2020. Available from: https://doi.org/10.1007/s00586-020-06350-6.
37. Mavrych V, Bolgova O, Ganguly P and Kashchenko S. Age-Related Changes of Lumbar Vertebral Body Morphometry. Austin J Anat. 2014; 1 (3): 7.
38. Dimeglio A, Bonnel F, Canavese F. The Growing Spine. In: Spinal Anatomy. Modern Concepts. Springer. 2020; 25–52.
39. Андронеску А. Анатомия ребенка. Бухарест: Меридиан, 1970.
40. Bernert Zs, Évinger S, Hajdu T. New data on the biological age estimation of children using bone measurements based on historical populations from the Carpathian Basin. Annales Historico-Naturales Musei Nationalis Hungarici. 2007; 99: 199–206.
41. Gindhart PS. Growth Standards for the Tibia and Radius in Children Aged One Month through Eighteen Years. Am J Phys Anthrop. 1973; 39: 41–48.
42. Suominen PK, Nurmi E, Lauerma K. Intraosseous access in neonates and infants: risk of severe complications - a case report. Acta Anaesthesiol Scand. 2015; 59 (10): 1389–93. DOI: 10.1111/aas.12602. Epub 2015 Aug 24. PubMed PMID: 26300243.
43. Blake KAS. An investigation of sex determination from the subadult pelvis: A morphometric analysis. Doctoral Dissertation, University of Pittsburgh. 2011.
44. Cunningham CA, Black SM. Iliac cortical thickness in the neonate — the gradient effect. J Anat. 2009; 215 (3): 364–70. DOI: 10.1111/j.1469-7580.2009.01112.x.
45. Cunningham CA, Black SM. Anticipating bipedalism: trabecular organization in the newborn ilium. J Anat. 2009; 214 (6): 817–29. DOI: 10.1111/j.1469-7580.2009.01073.x.
46. Corron L, Marchal F, Condemi S, Chaumoître K, Adalian P. A New Approach of Juvenile Age Estimation using Measurements of the Ilium and Multivariate Adaptive Regression Splines (MARS) Models for Better Age Prediction. Forensic Sci. 2017; 62 (1): 18–29. DOI: 10.1111/1556-4029.13224.
47. Yusof NA, Soames RW, Cunningham CA, Black SM. Anat Rec (Hoboken). Growth of the human ilium: the anomalous sacroiliac junction 2013; 296 (11): 1688–94. DOI: 10.1002/ar.22785.
48. Schnitzler CM, Mesquita JM, Pettifor JM. Cortical bone development in black and white South African children: iliac crest histomorphometry. Bone. 2009; 44 (4): 603–11. DOI: 10.1016/j.bone.2008.12.009.
49. De Boer HH, Van der Merwe AE, Soerdjbalie-Maikoe VV. Human cranial vault thickness in a contemporary sample of 1097 autopsy cases: relation to body weight, stature, age, sex and ancestry. Int J Legal Med. 2016; 130 (5): 1371–7. DOI: 10.1007/s00414-016-1324-5.
50. Margulies S, Coats B. Experimental Injury Biomechanics of the Pediatric Head and Brain. In: Pediatric Injury Biomechanics. New York: Springer Science + Business Media, 2013; 157–190.
51. Li Z, Park BK, Liu W, Zhang J, Reed MP, Rupp JD, et al. A statistical skull geometry model for children 0–3 years old. PLoS One. 2015; 10 (5): e0127322. DOI: 10.1371/journal.pone.0127322. eCollection 2015.
52. Rodriguez-Florez N, Ibrahim A, Hutchinson JC, Borghi A, James G, Arthurs OJ, et al. Cranial bone structure in children with sagittal craniosynostosis: Relationship with surgical outcomes. J Plast Reconstr Aesthet Surg. 2017; 70 (11): 1589–97. DOI: 10.1016/j.bjps.2017.06.017.
53. Fazekas IGy. and Kósa F. Forensic Fetal Osteology. Budapest: Akadémiai Kiadó, 1978.
54. Sherer D, Sokolovski M, Dalloul M, Khoury-Collado F, Osho J, Lamarque M, et al. Fetal clavicle length throughout gestation: a nomogram. Ultrasound in Obstetrics and Gynecology. 2006; 27: 306–10.
55. McGraw MA, Mehlman CT, Lindsell CJ, Kirby CL. Postnatal growth of the clavicle: birth to eighteen years of age. Journal of Pediatric Orthopedics. 2009; 29: 937.
56. Black SM. and Scheuer JL. Age changes in the clavicle: from the early neonatal period to skeletal maturity. International Journal of Osteoarchaeology. 1996; 6: 425–34.
57. Bernat A, Huysmans T, Van Glabbeek F, Sijbers J, Gielen J, Van Tongel A. The anatomy of the clavicle: a three-dimensional cadaveric study. Clin Anat. 2014; 27 (5): 712–23.
58. Fujita T, Orimo H, Ohata M, Yoshikawa M. Changes in the cortical thickness of the clavicle according to age. J Am Geriatr Soc. 1968; 16 (4): 458–62.
59. Raziye D, Ceren U, Kadir D, Osman S, Mehmed Ali M. A Radiological Investigation on the Hand Development in Human Fetuses Throughout the Fetal Period and an Evaluation Performed in Terms of its Clinical Importance Hand Development. International Journal of Morphology. International Journal of Morphology. 2016; 34: 1539–52. DOI: 10.4067/s0717-95022016000400057.
60. Corrigan GE. The neonatal scapula. Biol Neonat. 1960; 2: 159–67. PubMed PMID: 13695677.
61. Hrdlicka A. The scapula: visual observations. Am J Phys Anthropol. 1942; 29: 73–94.
62. Vallois HV. L'omoplate humaine. Bulletin de la Sociétié d'Anthropolgie de Paris. 1946; 7: 16–99.
63. Saunders S, Hoppa R, Southern R. Diaphyseal growth in a nineteenth-century skeletal sample of subadults from St Thomas' Church, Belleville, Ontario. International Journal of Osteoarchaeology. 1993; 3: 265–81.
64. Хомутова Е. Ю. Анатомия шейного отдела позвоночника новорожденных при лучевых методах исследования [диссертация]. Санкт-Петербург, 2005.
65. Sharma N, Jain SK, Singh PK, Rohin Garg. A morphometric study of predictors for sexual dimorphism of cervical part of vertebral column in human fetuses. Journal of the Anatomical Society of India. 2017; 66: 135–39.
66. Kneissel M, Roschger P, Steiner W, Schamall D, Kalchhauser G, Boyde A, et al. Cancellous Bone Structure in the Growing and Aging Lumbar Spine in a Historic Nubian Population. Calcif Tissue Int. 1997; 61: 95–100.
67. Ponrartana S, Aggabao PC, Dharmavaram NL, Fisher CL, Friedlich P, Devaskar SU, et al. Sexual Dimorphism in Newborn Vertebrae and its Potential Implications. J Pediatr. 2015; 167: 416–21.
68. Борисов Б. К. Весовые показатели развития скелета плода человека и содержание в нем стронция и кальция. М.: Государственный комитет по использованию атомной энергии СССР, 1973; 14 с.

METHODOLOGICAL SUPPORT OF ACTIVITIES ON DECOMMISSIONING THE NUCLEAR FACILITIES

Kalinkin DE[1,2] ✉, Takhauov AR[1], Takhauova LR[1,2], Milto IV[1,2], Takhauov RM[1,2]

[1] Seversk Biophysical Research Center of the Federal Medical Biological Agency, Seversk, Russia

[2] Siberian State Medical University, Tomsk, Russia

Personnel safety is a priority when decommissioning obsolete nuclear facilities. The study was aimed to develop the methodological basis for the medical and sanitary support of the nuclear industry enterprise personnel radiation safety during the nuclear legacy elimination on the example of Siberian Chemical Plant (SCP, Seversk). The study involved the data of the SCP employees' medical and dosimetric register containing information about all cases of death (with an indication of the cause) of former and current employees of the enterprise. The study results were used to justify selection of the area for development of scientific and methodological support of activities in the field of medical and sanitary support of radiation safety during the nuclear legacy elimination. Death rates and the risk of dying from cancer of certain localizations (trachea, bronchi, lung, skin, stomach, colon, lymphoid, hematopoietic and related tissues, breast and prostate glands) in the nuclear industry enterprise employees were assessed. The directions for improving the medical support of the nuclear enterprise employees and the population of the surveillance zones during the nuclear legacy elimination were defined. The findings will make it possible to adjust the medical support of the nuclear industry enterprise employees in order to extend their working longevity, as well as to reduce the adverse radiation-induced health effects in people engaged in the nuclear legacy elimination.

Keywords: nuclear legacy, radiation safety, nuclear industry enterprise, personnel

✉ Correspondence should be addressed: Dmitry E. Kalinkin
P.O. box 130, Seversk-13, Closed Administrative-Territorial Unit Seversk, Tomsk Region, Russia, 636013; kalinkin750@gmail.com

МЕТОДИЧЕСКОЕ СОПРОВОЖДЕНИЕ РАБОТ ПО ВЫВОДУ ИЗ ЭКСПЛУАТАЦИИ ОБЪЕКТОВ АТОМНОЙ ОТРАСЛИ

Д. Е. Калинкин[1,2] ✉, А. Р. Тахауов[1], Л. Р. Тахауова[1,2], И. В. Мильто[1,2], Р. М. Тахауов[1,2]

[1] Северский биофизический научный центр Федерального медико-биологического агентства, Северск, Россия

[2] Сибирский государственный медицинский университет, Томск, Россия

Безопасность персонала является приоритетом при выводе из эксплуатации устаревших объектов атомной отрасли. Целью исследования было разработать методические основы медико-санитарного обеспечения радиационной безопасности персонала предприятия атомной отрасли при ликвидации ядерного наследия на примере Сибирского химического комбината (СХК) г. Северск. Исследование проведено на основании сведений медико-дозиметрического регистра персонала СХК, содержащего информацию обо всех случаях смерти (с указанием причины) бывших и действующих работников предприятия. В результате работы обоснован выбор территории для разработки научно-методического сопровождения работ в области медико-санитарного обеспечения радиационной безопасности при ликвидации объектов ядерного наследия. Проанализированы показатели смертности населения выбранной территории и риски смертности персонала предприятия атомной индустрии вследствие злокачественных новообразований некоторых локализаций (трахея, бронхи, легкое, кожа, желудок, толстая кишка, лимфоидной, кроветворной и родственных им тканей, молочная и предстательная железы). Определены направления совершенствования медицинского обеспечения персонала предприятия атомной индустрии и населения зон наблюдения при ликвидации ядерного наследия. Полученные данные позволят скорректировать медицинское сопровождение персонала предприятия атомной отрасли с целью продления трудового долголетия работников, а также снизить негативные радиационно обусловленные последствия на здоровье людей, задействованных в ликвидации объектов ядерного наследия.

Ключевые слова: ядерное наследие, радиационная безопасность, предприятие атомной индустрии, персонал

✉ Для корреспонденции: Дмитрий Евгеньевич Калинкин
а/я № 130, г. Северск-13, ЗАТО Северск, Томская область, Россия, 636013; kalinkin750@gmail.com

Over the past few decades, the issue of decommissioning obsolete factories and nuclear facilities that have reached the end of their service life is becoming more and more urgent due to rapid development of nuclear industry in Russia. When doing such work, ensuring the safety of personnel working at these enterprises, as well as ensuring the safety of the population and environment in the areas where the enterprises are located is one of the priorities declared by the Rosatom State Corporation [1].

Some enterprises of the Russian nuclear industry have been functioning for more than 60 years, these move closer to inevitable scheduled decommissioning. Over more than 75 years of the development of domestic nuclear power, the

technologies, equipment and types of fuel have changed considerably, that is why modernization of the existing nuclear enterprises is sometimes impossible. In this regard, the problem arises of the sheduled elimination of the nuclear legacy created at various stages of the nuclear industry development, including elimination with the possibility to reuse these territories for construction of new infrastructure nuclear facilities. This challenging task can be accomplished only through bringing together specialists from various fields (engineers, ecologists, biologists, etc.) and through preliminary development of the evidence-based methodological support taking into account the features of the nuclear legacy to be eliminated [1, 2].

Medical and sanitary support of radiation safety of the eliminated nuclear industry enterprise employees and the population of the surveillance zones is one of the most important activities preceding safe decommissioning of nuclear facilities [1].

Scientific and methodological support of activities aimed at ensuring radiation safety during decomissioning of nuclear facilities requires the assessment of the ionizing radiation (IR) exposure biomedical effects on the personnel of nuclear enterprises, as well as the estimation of radiogenic risks in employees of these enterprises. Scientific and methodological support should be developed based on the production features (technology type, radionuclide spectrum, radiation type, etc.) [2, 3].

In each specific case, the Medical Dosimetric Registry (MDR) of the nucler enterprise employees and the population of adjacent areas together with the data of organizations engaged in monitoring of the conditions of manufacturing process in the main facilities of the enterprise and the employees' health should be used as a source of specific information for such studies [4].

Scientific and methodological support of activities on the nuclear legacy elimination will make it possible to define the major biomedical health effects in the employees engaged in decommissioning of nuclear facilities and to determine a set of measures for extension of their working longevity [3].

At the current phase of the Russian nuclear industry development, given the good progress in radiation safety that had been achieved over the recent years, the focus should be placed on assessing the effects of IR (for example, risk of cancer) involving accumulation of the total external dose (TED) of no more than 100 mSv [1].

The results of numerous epidemiology studies do not allow an unambiguous conclusion about the increased risk of cancer or death from cancer in people who are exposed to IR from man-made sources at work. Some researchers have managed to reveal the increased risk of dying from cancer in the nuclear facility employees [2–4], while other researchers point out that there is no increase in the relative risk of cancer or dying from cancer in employees of such production facilities [5–7].

Methodological support of activities aimed at nuclear legacy elimination requires implementation of the high-tech methods for continuous public health monitoring aimed at identification of the radiation exposure health effects in employees engaged in the nuclear legacy decommissioning, for example, implementation of the automated health monitoring system for the registered population, creation and management of the decommissioned nuclear facility employees' MDR.

The study was aimed to develop the methodological basis for the medical and sanitary suport of the nuclear industry enterprise personnel radiation safety during the nuclear legacy elimination on the example of Siberian Chemical Plant (SCP, Seversk).

METHODS

It is impossible to obtain the evidence-based study results without the use of appropriate research method, i.e. without the correct selection of the objects and methods of research. While the research methods and interim mathematical tools are generally well known and easy to choose (in most cases, these are epidemiologic methods used to assess the risk of the stochastic effects induced by the radiation hazardous facility personnel exposure to IR, primarily of the malignant neoplasms), the selection of object and, therefore, the research territory, is a challenging practical task. The research object and the area where the object is located should meet the following requirements.

1. The research object (nuclear industry enterprise) should have the longest possible history of trouble-free operation; decommissioning of such objects that should be performed on a scheduled basis requires appropriate scientific and methodological support. In case the object has a history of accidents associated with the release of radionuclides into the environment, "accidental" exposure of the personnel and the population of adjacent areas, it is necessary to develop the qualitatively different scientific and methodological support.

2. The development of the mentioned above scientific and methodological support is not possible without using the MDR of the enterprise employees and the population of the surveillance zone taking into account the occupational doses and all cases of cancer. In turn, full maintenance of MDR is possible only in the administratively closed territories, where only one medical institution provides a centralized medical support to the radiation hazardous facility personnel and the population of the surveillance zones.

Based on the above, the Closed Administrative-Territorial Unit (CATU) Seversk is the optimal platform for the development of methodological support for the scheduled decommissioning of nuclear legacy. CATU Seversk is formed around the city of Seversk, where SCP is a city-forming enterprise. The first facilities of SCP (for example, sublimation plant and separation plant) were commissioned in 1953. Over more than 60 years of SCP operation no major accidents resulting in the radionuclide release into the environment were reported. The most notable radiation accident occurred in 1993 at the SCP radiochemical plant. The accident was assigned level three according to the seven-point international radiological event scale.

Medical support of the CATU Seversk population (105,238 people as of 2022), including the SCP employees, is provided by one large medical institution, the Federal Siberian Research Clinical Centre of FMBA of Russia (FSRCC).

The SCP employees' MDR was created by the Seversk Biophysical Research Center of FMBA of Russia (SBRC). The MDR database contains up-to-date information about all employees who ever worked at the SCP, the data about all cases of death (with an indication of the cause) of the former and current SCP employees in CATU Seversk, and the data about the major socially significant non-communicable diseases in SCP employees.

The cohort of SCP employees included all employees (regardless of the type of production) who were hired between 1 January 1950 and 31 December 2020 and worked at the SCP for at least one year.

The SCP structure includes the main and auxiliary production facilities (MP and AP, respectively).

The MP facilities of SCP include the reactor (RF), radiochemistry (RCF), plutonium (PF), separation (SF) facilities, and sublimation plant (SP).

Table 1. Characteristics of the cohort of SCP employees hired between 01 January 1950 and 31 December 2019

Indicator	Gender	RF	RCF	PF	SF	SP	AP
Total number of employees	M	6651	5272	7569	4935	3581	21,373
	F	1323	1115	2267	1492	1101	8766
Number of employees with the defined vital status	M	5493	4454	6561	3389	2477	13,343
	F	1165	1019	2120	1143	865	6643
Number of employees who died from cancer	M	418	286	456	300	226	1312
	F	101	80	171	103	79	579
Number of employees who were provided personal dosimetry due to external exposure	M	5171	4632	3 254	1113	1935	2043
	F	710	802	832	309	487	847
Number of employees who were provided personal dosimetry due to internal exposure	M	86	1990	3 491	534	1039	163
	F	14	441	1 100	270	322	121

The employees of four production facilities (RCF, PF, SF, and SP) are exposed mainly to the combination radiation, while the RF employees are exposed to external radiation only and can be used as a control group when assessing the contribution of internal exposure to radiation-induced effects.

Currently, the MDR database contains the following information about the SCC employees:

– total number of the SCP employees hired since 1950 in accordance with the production type (it should be emphasized that information about all the SCP employees registered by the enterprise Human Resources departments for the whole period of the combine activity has been added to the database since the moment of the MDR creation; this approach makes it possible to form various control groups in accordance with the broad spectrum of scientific tasks);

– personal radiation doses and doses accumulated over time;

– number of deceased SCP employees;

– SCP employees who developed cancer.

All available data is stored electronically and in the form of the archived hard copies.

Table 1 contains information about the employees hired by the SCP MP facilities in 1950–2019.

Tables 2 and 3 present the demographic characteristics of the CATU Seversk population for the period of 1970–2019.

In 1970–2019, the total population (all age groups) of CATU Seversk increased, along with the adult population. Most notably, the number of people over the age of 60 dramatically increased. At the same time, the share of the child population significantly decreased: from 29.5% in 1970–1974 гг. To 15.8% in 2015–2019. The share of males in the population decreased from 48.6% in 1970–1974 to 46.3% in 2015–2019.

Birth rate significantly decreased and mortality increased during the observation period. This resulted in the natural population decline. Changes in the demographic structure of

the population, in particular, population ageing, was the cause of the above processes. At the same time, the population life expectancy significantly increased.

Indicators that have been used in the study and information sources for calculation of these indicators are provided in Table 4.

The risk of dying from cancer in the SCP employees was calculated based on the standardized relative risk (SRR).

SRR was calculated in accordance with the following formula:

$$SRR = \frac{A}{E}$$

where A was the actual number of the disease cases or deaths; E was the expected number of the disease cases or deaths .

The lower and upper limits of the SRR 95% confidence interval were calculated in accordance with the following formulae:

$$LL = SRR \times \left(1 - \frac{1,96}{2 \times \sqrt{A}}\right)^2$$

$$UL = SRR \times \left(1 - \frac{1,96}{2 \times \sqrt{A+1}}\right)^2 \times \frac{A+1}{A}$$

where UL was the upper limit and LL was the lower limit.

It was believed that the incidence in the studied group was significantly higher than that in the comparison group when the lower limit of the SRR confidence interval exceeded 1.

To estimate the relationship between the SSR and the increase in TED, we devided the employees into subgroups with various TED values. The indicators of incidence (or mortality) among the SCP employees with no reported exposure doses or employees who never contacted with the man-made radiation sources at work were used as a comparison group (standard). The direct standardization method was used, age stratification was not applied. The calculations were performed twice: first for the dose ranges with the clearly defined lower and upper TED limits (0–20 mSv, 20–50 mSv, 50–100 mSv, 100–150 mSv,

Table 2. Demographic characteristic of the CATU Seversk adult population in the years 1970–2019

Category of the population	Range within the studied period, years							
	1970–1974	1980–1984	1990–1994	1995–1999	2000–2004	2005–2009	2010–2014	2015–2019
Overall population	87 121 ± 2302.0	97 763.2 ± 1310.1	109 230.0 ± 1580.6	111 701.4 ± 344.2	110 816.4 ± 1732.9	109 949.7 ± 3500.7	115 511.1 ± 750.0	113 728.8 ± 861.5
Adults	57 019.3 ± 1792.0	68 548.4 ± 965.9	78 609.4 ± 2048.1	84 024.0 ± 1667.0	88 255.6 ± 695.8	91 036.6 ± 3313.3	95 679.0 ± 674.1	92 716.8 ± 909.1
People over the age of 60	4140.1 ± 268.9	5 724.3 ± 254.9	11 402.4 ± 1117.8	15 462.8 ± 1592.5	19 223.0 ± 486.3	20 021.3 ± 1236.4	21 335.7 ± 5821.3	26 783.8 ± 1207.7
Men of working age	27 252.9 ± 775.9	30 946.1 ± 882.1	33 790.4 ± 661.9	35 095.2 ± 320.0	35 282.6 ± 208.0	35 919.0 ± 996.5	36 210.6 ± 512.1	33 599.9 ± 754.1
Women of working age	27 480.3 ± 551.9	29 670.0 ± 877.1	32 743.2 ± 224.3	33 029.4 ± 697.1	34 487.2 ± 557.2	33 709.9 ± 816.6	33 207.0 ±1006.2	29 699.6 ± 862.9

Table 3. Major demographic characteristics of the CATU Seversk population in 1970–2019 (per 1000 population)

Indicator	Range within the studied period, years							
	1970–1974	1980–1984	1990–1994	1995–1999	2000–2004	2005–2009	2010–2014	2015–2019
Birth rate	18.7 ± 1.7	16.9 ± 0.9	10.6 ± 2.1	8.1 ± 0.4	8.5 ± 0.2	9.6 ± 1.0	10.9 ± 0.3	9.4 ± 1.5
Mortality	3.8 ± 0.1	5.7 ± 0.3	8.9 ± 2.1	10.2 ± 0.4	12.1 ± 0.9	12.2 ± 0.6	11.9 ± 0.4	12.5 ± 0.2
Natural increase	14.9 ± 1.8	11.2 ± 0.7	1.8 ± 4.2	-2.1 ± 0.5	-3.6 ± 0.8	-2.6 ± 1.1	-1.1 ± 0.4	-3.1 ± 0.2
Life expectancy, years	72.46 ± 0.48	71.18 ± 0.55	68.67 ± 2.89	68.60 ± 1.36	68.44 ± 0.88	70.89 ± 0.38	73.25 ± 0.60	74.25 ± 0.63

150–200 mSv, 200–300 mSv, 300–500 mSv, and 500–1000 mSv), then for broader ranges in which only the lower limit was defined (> 0 mSv, > 100 mSv, > 200 mSv, > 300 mSv, > 500 mSv), since the range expansion (and, therefore, the increase of person years of observation) increased the statistical significance of the results.

RESULTS

Information about the death rates caused by cancer affecting bronchi, trachea, lungs, stomach, colon, lymphoid, hematopoietic and related tissues, breast and prostate glands, skin among male and female populations of CATU Seversk in 1970–2019 is provided in Tables 5 and 6.

The increase in death rates caused by malignant neoplasms of the stomach, colon, bronchi, lung, and prostate gland among male population of CATU Seversk was observed during the studied period (Table 5).

The same trend was observed among females (including death rates caused by breast cancer); the exception were the death rates caused by malignant neoplasms of the stomach that surpassed the high recorded in 2005–2009 and dropped to 25.4 cases per 100,000 population by 2015–2019 (Table 6).

Tables 7 and 8 show the SRR of dying from cancer affecting trachea, bronchi, lungs, skin, stomach, colon, lymphoid, hematopoietic and related tissues, breast and prostate glands, in relation to the TED values of the SCP employees for the period between 01 January 1970 and 31 December 2019. TED means the external effective dose absorbed by the employee during the entire period of working at the nuclear industry enterprise.

The analysis did not take into account the employees' age and the calendar time of observation due to the relatively small sample size.

The cases of cancer affecting the digestive organs (stomach and colon), respiratory organs (trachea, bronchi, lung), skin, organs of the male reproductive system (prostate gland), lymphoid, hematopoietic and related tissues among male SCP employees were analyzed. Malignant neoplasms of these organs and tissues were selected because of the fact that these cancer localizations were most common among male population of CATU Seversk not exposed to the man-made IR.

The assessed range covers "low" IR doses (< 100 mSv) that are typical for normal working conditions at modern nuclear enterprises and "medium" IR doses (< 1 Sv) that become possible during radiation emergencies at the nuclear industry enterprises.

Male SCP employees who have been exposed to IR at work with the TED values of 200–1000 mSv have a higher SRR of dying from prostate cancer (Table 4).

The cases of cancer affecting breast, digestive organs (stomach and colon), respiratory organs (trachea, bronchi, lung), skin, lymphoid, hematopoietic and related tissues among female SCP employees were also assessed. Malignant neoplasms of these organs and tissues were selected because of the fact that these cancer localizations were most common among female population of CATU Seversk not exposed to the man-made IR.

Statistical accuracy of the data on female employees is lower than that of the data on male employees due to small sample size resulting from the significantly lower number of women engaged with the IR sources.

The lack of data on some cancer localizations (for example, trachea, bronchi, lung, skin, lymphoid, hematopoietic and related tissues) in female employees exposed to "medium" IR doses is due to the extremely small sample size that is insuffucient for statistical analysis.

Female SCP employees with the TED values reaching 100–150 mSv have the increased SRR of dying from malignant neoplasms of trachea, bronchi, lung, stomach, colon, skin, breast, and lymphoid, hematopoietic and related tissues.

It is especially worth noting that the SRR of dying from malignant neoplasms of trachea, bronchi, lung, and breast is increased among female employees with the TED values of 0–20 mSv (Table 8).

Medical support of employees during elimination of nuclear legacy should involve three phases.

Phase one: defining health risk factors for the described population.

Identification of the set of risk factors includes the following:
– assessment of demographics (birth rate, mortality, rate of natural increase), life expectancy, and disability rate in the studied population;
– assessment of morbidity patterns in the studied population and identification of the most prevalent disorders;

Table 4. Indicators and information sources used during the study

Studied indicator	Information source
Cancer mortality in the CATU Seversk population in 1970–2019	Information obtained from: – Territorial unit of the Federal State Statistics Service, Tomsk Region (Tomskstat); – Federal Siberian Research Clinical Centre of FMBA of Russia; – database of the regional MDR of the CATU Seversk population and SCP employees containing the up-to-date information about all cases of death from cancers of the main localizations (trachea, bronchi, lung, skin, stomach, colon, lymphoid, hematopoietic and related tissues, breast and prostate glands) in CATU Seversk in 1970–2019
Risk of dying from cancer in the nuclear industry enterprise employees between 01 January 1970 and 31 December 2019	The data obtained from the database of the regional MDR of the CATU Seversk population and SCC employees containing the up-to-date information about all cases of death from cancers of the main localizations (trachea, bronchi, lung, skin, stomach, colon, lymphoid, hematopoietic and related tissues, breast and prostate glands) in SCP employees in 1970–2019

Table 5. Death rates caused by cancer among adult male population of CATU Seversk in 1970–2019 (per 100,000 population; group average)

Cancer localization (ICD-10 code)	Range within the studied period, years									
	1970–1974	1975–1979	1980–1984	1985–1989	1990–1994	1995–1999	2000–2004	2005–2009	2010–2014	2015–2019
Stomach (C16)	19	22.4	20.5	19	18.4	25.9	38.3	44	43.1	24.6
Colon (C18)	0	0	2.2	10.2	14.9	12.2	14.3	22.4	26	26.3
Trachea (C33)	0	0	0	0	0.7	1.5	0.8	1.9	1.9	0.8
Bronchi and lung (C34)	11.2	10.2	36.1	50.8	65.7	80	75.6	80.1	70	99
Skin (C43–44)	0	0	1	2	0.8	2.6	2.8	2.9	3.7	2.8
Prostate gland (C61)	2.3	1.7	0.5	0.7	6	8.7	14.3	19.8	24.6	29.3
Lymphoid, hematopoietic and related tissues (C81–96)	5.3	6	9.2	8.4	11	13.2	20.8	9.5	18.3	25.2

– identification of the risk factors and determination of the potentially modifiable risk factors, such as social-economic, behavioral, medical-organizational, and technogenic factors.

Phase two: formulation of proposals to manage the most common disorders and risk factors identified in the population. Thus, our findings show that the main focus should be on cancer prevention and treatment when developing the strategy for medical support of employees engaged in the activities on the nuclear legacy decommissioning.

Phase three: development of the strategy for medical support of employees engaged in the activities on the nuclear legacy decommissioning by adjustment of the existing strategy based on the new information about the health status of the studied population (demographics, data on morbidity and disability rates) and risk factors in the population.

According to the study, male SCP employees have a high SRR of dying from prostate cancer, while female employees have a high SRR of dying from malignant neoplasms of trachea, bronchi, lung, stomach, colon, skin, breast, lymphoid, hematopoietic and related tissues.

The strategy for medical support of employees engaged in the activities on the nuclear legacy decommissioning should be developed based on the above data in accordance with the goals and outputs of the Healthcare national project and the Fight Against Oncological Diseases federal project. In particular, it is necessary to define the list of additional instrumental and laboratory tests for diagnosis of cancer to be used during the routine medical check-ups in employees engaged in the nuclear legacy elimination (primarily based on the cancer localizations identified).

According to the Fight Against Oncological Diseases federal project, the death rate caused by cancer in the population should not exceed 185 cases per 100,000 population by the year 2024. It is appropriate to consider these values as the target indicators when developing the strategy for health protection of employees engaged in the activities on the nuclear legacy decommissioning.

DISCUSSION

Organizing activities on decommissioning the nuclear facilities that have reached the end of their service life is one of the areas of nuclear safety. In turn, safe decommissioning of the nuclear facility is impossible without medical and sanitary support [1].

In this regard, the study was aimed to develop the methodological basis for the medical and sanitary support of the nuclear industry enterprise personnel radiation safety during the nuclear legacy elimination on the example of SCP (CATU Seversk). For that the following tasks were accomplished: selection of the area for the development of methodological support of activities on ensuring radiation safety during elimination of nuclear legacy was substantiated; death rates caused by cancers of most common localizations were defined; the risk of dying from cancers of most common localization in employees engaged in decommissioning the nuclear industry enterprise (nuclear legacy) was assessed; directions for improvement of the medical support of employees engaged in the nuclear legacy elimination were determined.

During the study we managed to justify the use of CATU Seversk as a platform for the development of methodological support of activities on the scheduled nuclear legacy decommissioning. The analysis of death rates caused by malignant neoplasms of bronchi, trachea, lung, stomach, colon, lymphoid, hematopoietic and related tissues, breast and prostate glands, and skin among male and female SCC employees in 1970–2019 made it possible to reveal the increase in the studied indicators, except for the malignant neoplasms of the stomach in women. It is clear that the increase in cancer mortality observed in the studied population is mainly due to the population ageing. This is clearly illustrated

Table 6. Death rates caused by cancer among adult female population of CATU Seversk in 1970–2019 (per 100,000 population; group average)

Cancer localization (ICD-10 code)	Range within the studied period, years									
	1970–1974	1975–1979	1980–1984	1985–1989	1990–1994	1995–1999	2000–2004	2005–2009	2010–2014	2015–2019
Stomach (C16)	31.3	15.9	24.7	27.2	18.9	21.7	19.6	38.8	15.9	25.4
Colon (C18)	4.5	4.3	7.7	7.4	16.3	6.8	23.5	18	19.5	22.5
Trachea (C33)	0	0	0	0	0	0	0	0	0	0
Bronchi and lung (C34)	6.8	2.3	9.7	7.6	12.4	3.5	15.5	9.8	11.4	24.5
Skin (C43–44)	0.3	2.2	0.4	0.6	1.9	3.6	13.8	8.4	3.4	4.5
Breast (C50))	4.8	12.9	15	18.9	19.1	25.9	30.2	36.5	38.4	30.6
Lymphoid, hematopoietic and related tissues (C81–96)	4.9	12.9	9.5	5.3	17.4	22.3	19.9	8.1	9.1	15.9

Table 7. SRR of dying from cancer in male nuclear industry enterprise employees based on TED (95% confidence interval)

Cancer localization	TED, mSv							
	0–20	> 20–50	> 50–100	> 100–150	> 150–200	> 200–300	> 300–500	> 500–1 000
Stomach and colon	0.68 (−0.11–5.18)	0.70 (−0.10–0.94)	1.06 (0.04–1.34)	0.49 (−0.16–0.69)	0.73 (−0.09–0.97)	0.74 (−0.09–0.98)	0.98 (0.01–1.25)	1.25 (0.14–1.56)
Trachea, bronchi, and lung	0.52 (−0.15–4.90)	0.48 (−0.16–0.70)	0.66 (−0.11–0.92)	0.54 (−0.15–0.77)	1.24 (0.13–1.58)	1.09 (0.06–1.41)	0.49 (−0.16–0.72)	2.29 (0.73–2.73)
Skin	–	1.59 (0.15–4.99)	2.08 (0.32–5.72)	–	–	–	2.21 (0.37–5.91)	–
Prostate gland	0.69 (−0.06–5.20)	0.24 (−0.04–1.13)	1.26 (0.10–2.61)	0.57 (−0.08–1.65)	0.85 (−0.03–2.05)	3.08 (1.03–4.93)	3.96 (2.18–6.61)	3.16 (1.60–5.60)
Lymphoid, hematopoietic and related tissues	0.77 (−0.06–5.34)	0.73 (−0.07–1.45)	0.96 (0.00–1.75)	0.58 (−0.10–1.25)	0.86 (−0.06–1.62)	1.25 (0.11–2.12)	1.36 (0.16–2.25)	0.53 (−0.11–1.18)

Table 8. SRR of dying from cancer in female nuclear industry enterprise employees based on TED (95% confidence interval)

Cancer localization	TED, mSv					
	0–20	> 20–50	> 50–100	> 100–150	> 150–200	> 200–300
Stomach and colon	0.6 (0.45–5.13)	1.07 (0.82–5.86)	0.48 (0.32–4.83)	1.78 (1.42–6.97)	0.56 (0.38–4.97)	1.07 (0.82–5.86)
Trachea, bronchi, and lung	1.93 (1.20–7.25)	0.49 (0.16–4.83)	0.80 (0.36–5.39)	1.75 (1.05–6.96)	–	–
Skin	–	1.65 (0.55–6.80)	–	5.94 (3.59–13.06)	–	–
Breast	1.66 (1.18–6.81)	0.66 (0.38–5.15)	0.36 (0.16–4.61)	1.58 (1.12–6.69)	1.27 (0.86–6.18)	–
Lymphoid, hematopoietic and related tissues	0.18 (0.02–4.27)	0.83 (0.41–5.43)	0.69 (0.30–5.18)	2.97 (2.11–8.83)	–	–

by the above population dynamics of the major age groups. The analysis of the SCP employees' SRR of dying from cancer of key localizations has made it possible to reveal the significant increase (compared to non-exposed employees) in the studied indicators for prostate cancer in males and malignant neoplasms of trachea, bronchi, lung, stomach, colon, skin, breast, lymphoid, hematopoietic and related tissues in females. The findings are generally consistent with the results obtained by other authors [2–4]. However, we believe that our findings cannot form the basis for definitive conclusions about the impact of ionizing radiation on cancer in employees of the nuclear industry enterprises. That is why further research is required involving larger samples of employees.

In our study we defined the main phases of improving the medical support of employees during elimination of nuclear legacy (identification of the set of risk factors, formulation of proposals to manage the major risk factors, development of the strategy for medical support of employees engaged in the activities on the nuclear legacy decommissioning).

CONCLUSIONS

During the study, information about the SRR of dying from the most common cancer types and the dynamic changes in cancer mortality in the nuclear industry enterprise employees was obtained. This data makes it possible to adjust medical support of the nuclear industry enterprise employees in order to extend their working longevity, as well as to reduce the adverse rediation-induced health effects in people engaged in the nuclear legacy elimination. The findings will provide the basis for the information and methodological documents to be used in the practice of scientific and medical institutions that provide medical support of the activities at the nuclear facilities and are responsible for health monitoring in employees of these facilities and the population of the adjacent areas.

References

1. Ilyin LA, redaktor. Texnogennoe obluchenie i bezopasnost' cheloveka. M.: IzdAT, 2006; 304 s. Russian.
2. Shilnikova NS, Preston DL, Ron E, Gilbert ES, Vassilenko EK, Romanov SA, et al. Cancer mortality risk among workers at the Mayak nuclear complex. Radiat Res. 2003; 159 (6): 787–98. DOI: 10.1667/0033-7587(2003)159[0787:cmrawa]2.0.co;2.
3. Zablotska LB, Ashmore JP, Howe GR. Analysis of mortality among Canadian nuclear power industry workers after chronic low-dose exposure to ionizing radiation. Radiat Res. 2004; 161 (6): 633–41. DOI: 10.1667/rr3170.
4. Gilbert ES, Koshurnikova NA, Sokolnikov ME, Shilnikova NS, Preston DL, Ron E, et al. Lung cancer in Mayak workers. Radiat Res. 2004; 162 (5): 505–16. DOI: 10.1667/rr3259.
5. Auvinen A, Pukkala E, Hyvönen H, Hakama M, Rytömaa T. Cancer incidence among Finnish nuclear reactor workers. J Occup Environ Med. 2002; 44 (7): 634–8. DOI: 10.1097/00043764-200207000-00008.
6. Cardis E, Vrijheid M, Blettner M, Gilbert E, Hakama M, Hill C, et al. Risk of cancer after low doses of ionising radiation: retrospective cohort study in 15 countries. BMJ. 2005; 331 (7508): 77. DOI: 10.1136/bmj.38499.599861.E0.
7. Jeong M, Jin YW, Yang KH, Ahn Y-O, Chaet C-Y. Radiation exposure and cancer incidence in a cohort of nuclear power industry workers in the Republic of Korea, 1992–2005. Radiat Environ Biophys. 2010; 49 (1): 47–55. DOI: 10.1007/s00411-009-0247-7.

Литература

1. Ильин Л. А., редактор. Техногенное облучение и безопасность человека. М.: ИздАТ, 2006; 304 с.
2. Shilnikova NS, Preston DL, Ron E, Gilbert ES, Vassilenko EK, Romanov SA, et al. Cancer mortality risk among workers at the Mayak nuclear complex. Radiat Res. 2003; 159 (6): 787–98. DOI: 10.1667/0033-7587(2003)159[0787:cmrawa]2.0.co;2.
3. Zablotska LB, Ashmore JP, Howe GR. Analysis of mortality among Canadian nuclear power industry workers after chronic low-dose exposure to ionizing radiation. Radiat Res. 2004; 161 (6): 633–41. DOI: 10.1667/rr3170.
4. Gilbert ES, Koshurnikova NA, Sokolnikov ME, Shilnikova NS, Preston DL, Ron E, et al. Lung cancer in Mayak workers. Radiat Res. 2004; 162 (5): 505–16. DOI: 10.1667/rr3259.
5. Auvinen A, Pukkala E, Hyvönen H, Hakama M, Rytömaa T. Cancer incidence among Finnish nuclear reactor workers. J Occup Environ Med. 2002; 44 (7): 634–8. DOI: 10.1097/00043764-200207000-00008.
6. Cardis E, Vrijheid M, Blettner M, Gilbert E, Hakama M, Hill C, et al. Risk of cancer after low doses of ionising radiation: retrospective cohort study in 15 countries. BMJ. 2005; 331 (7508): 77. DOI: 10.1136/bmj.38499.599861.E0.
7. Jeong M, Jin YW, Yang KH, Ahn Y-O, Chaet C-Y. Radiation exposure and cancer incidence in a cohort of nuclear power industry workers in the Republic of Korea, 1992–2005. Radiat Environ Biophys. 2010; 49 (1): 47–55. DOI: 10.1007/s00411-009-0247-7.

PROBLEMS OF MORTALITY ANALYSIS IN TOWNS OF THE RUSSIAN FEDERATION

Saltykova MM ✉, Antipina UI, Balakaeva AV

Centre for Strategic Planning and Management of Biomedical Health Risks of the Federal Medical Biological Agency, Moscow, Russia

Mortality rate is one of the main indicators of how healthy a population is, and planning and implementing measures aimed at reducing morbidity and increasing life expectancy in the population is impossible without an adequate analysis and interpretation of mortality data. At the same time, as pointed out by many researchers, there are factors external to a human body being that can have a significant effect on the mortality rate in a population. This study aimed to assess the impact of one of these factors, the number of beds in hospitals (per 10,000 people) of cities with population exceeding 100,000 people. The analysis included data from Rosstat (Russian statistics service) on the population size, mortality, number of hospital beds, average monthly wages in 12 cities within the period from 2017 through 2019. Five cities from these 12 were selected as a more homogeneous subgroup in terms of socio-economic conditions. We found a positive correlation between mortality rate per 1000 inhabitants ($R > 0.7$; $p < 0.009$) and the number of hospital beds per 10,000 people in the sample of 12 cities. This correlation was higher ($R \geq 0.9$; $p < 0.037$) in the more homogeneous subgroup. A factor that may condition this correlation may be that of deaths of people from other regions in hospitals of the cities in question, which are counted when estimating the mortality rate and have a significant effect on that estimation. The results of the study point to the need to differentiate between people registered in a city and those living there permanently when assessing mortality rate therein.

✉ **Correspondence should be addressed:** Marina M. Saltykova
Pogodinskaya st., 10, building 1, Moscow, 119121, Russia; saltykova@cspmz.ru

ПРОБЛЕМЫ АНАЛИЗА СМЕРТНОСТИ В ГОРОДАХ РОССИЙСКОЙ ФЕДЕРАЦИИ

М. М. Салтыкова ✉, У. И. Антипина, А. В. Балакаева

Центр стратегического планирования и управления медико-биологическими рисками здоровью Федерального медико-биологического агентства, Москва, Россия

Уровень смертности является одним из основных индикаторов здоровья населения, поэтому планирование и проведение мероприятий, направленных на снижение заболеваемости и увеличение продолжительности жизни населения, невозможны без адекватного анализа и интерпретации данных о смертности. Вместе с тем, как отмечают многие исследователи, существуют внешние для организма человека факторы, которые могут существенно влиять на показатели смертности населения. Целью работы было оценить значимость влияния одного из таких факторов — размера коечного фонда больничных организаций (на 10 тыс. населения) — в городах с населением более 100 тыс. человек на показатели смертности населения в этих городах. В анализ были включены данные Росстата за 2017–2019 гг. о количестве населения, смертности, количестве больничных коек, среднемесячной заработной плате в 12 городах. Из этих городов была сформирована более однородная по социально-экономическим условиям подгруппа, включающая 5 городов. Выявлено, что показатель смертности населения на 1000 жителей положительно коррелировал ($R > 0,7$; $p < 0,009$) с числом больничных коек на 10 тыс. населения в группе из 12 городов и корреляция была выше ($R \geq 0,9$; $p < 0,037$) в более однородной подгруппе. Указанная закономерность может быть обусловлена тем, что при оценке показателей смертности населения значимым оказывается вклад количества умерших в городских стационарах жителей других регионов. Полученные результаты указывают на необходимость при изучении смертности населения в городах анализировать число смертей, не только зарегистрированных в городе, но и постоянно проживающих в нем жителей.

✉ **Для корреспонденции:** Марина Михайловна Салтыкова
ул. Погодинская, д. 10, стр. 1, г. Москва, 119121, Россия; saltykova@cspmz.ru

Since mortality rate is one of the main indicators of how healthy a population is, adequate analysis and interpretation of the data on mortality are mandatory prerequisites for measures aimed at reducing morbidity and increasing life expectancy in a population.

As of 2019, there were over 1100 cities in Russia. Most of them (about 1000) are cities with a population of less than 100,000 people, i.e. medium and small towns [1]. Most of the restricted administrative-territorial entities and territories serviced by the Federal Medical Biological Agency (FMBA) of Russia also fall into this category [2]. Relatively small population in such localities considerably impedes statistical analysis of

data on mortality of the population stratified by sex, age and cause of death [3].

In addition, it should be noted that such factors as the rules of death registration and indication of the cause thereof, which are essentially external to the human body, have an effect on the mortality data [4, 5]. Throughout the world, it is common practice to keep track of morbidity and causes of death relying on the 10th revision of the International Classification of Diseases (ICD 10). Many researchers note that in the Russian Federation there is a relatively high percentage of fatalities the conditions of which are recorded in an obscure way: "injuries with uncertain intentions", "ill-defined and unspecified causes of

death", "unspecified cardiomyopathy", "old age" [6–10]. These causes of death can be used to underrate contribution of the so-called "socially significant causes of death" (alcohol and drug poisoning, murder and suicide) and causes that were targeted with a mitigation and reduction plan (diseases of the circulatory system) [7]. Some causes of death that were registered as belonging to the circulatory system diseases category before 2013 have been attributed to other categories thereafter, which significantly distorts the real structure of mortality in a population [6]. High losses from ill-defined conditions disallow adequate assessment of the potential for reducing mortality and development of the effective prevention measures.

Another factor that significantly distorts mortality statistics is the following one. Currently, in addition to the deaths of city residents, indicators of mortality in a given city incorporate deaths of persons who permanently lived in another place but died and were registered dead (Civil Registry Office) in that given city [7, 11]. This problem has been analyzed in greatest detail for Moscow [11, 12]. The large population of the metropolis allows obtaining the most reliable and reproducible results; they clearly show the significance of this problem. In addition, at any given moment there is a significant population of migrants in Moscow that includes both citizens of other countries and Russian nationals from other regions of the country. In 2003, migrants that died from neoplasms in Moscow made up 5.3% (men) and 6.3% (women) of the respective mortality rate for the entire population of the city, and the shares of migrants in the category of deaths from circulatory system diseases were 8.4% (for men) and 6.0% (for women) [11]. At the same time, the contribution of this population group to mortality from infections, injuries and poisoning, as well as inaccurately described conditions, was over 33% for men and more than 25% for women; from a quarter to a third of all deaths from all major causes at a young working age also happened in this group. The revealed patterns persisted through 2013. The authors of this study conclude that if only the residents of Moscow were factored in, the mortality rate there would have been lower than what is recorded by the statistics currently, and the structure of causes of death would be closer to that seen in European countries due to lower mortality from external causes. Similar patterns were also registered in other regions of the Russian Federation [13].

In addition, city hospitals throughout the Russian Federation set up primary vascular departments, and there are also dedicated regional vascular centers established. In a centralized manner, these medical facilities receive patients with the most severe cardiovascular pathologies, and these patients come not only from the city where such center/hospital department operates but also from other cities, towns and villages. On the one hand, the said centers/hospital departments improve accessibility of qualified medical care for the population, and on the other hand, they contribute to the city's mortality rates because deaths of patients from outside the city are factored in when calculating the respective indicators. This factor has the greatest impact on mortality rates in cities with relatively small populations. Another factor that significantly affects a small town's mortality rates but bears no relation to the state of health of its population is the presence of penitentiary facilities therein, which show high mortality from socially significant diseases [14].

It should be noted that a complete and detailed analysis of the death rate of residents of a given city is required in order to implement targeted measures that account for the specifics of that city, such analysis factoring in all possible statistical artifacts. Small sample size makes conducting such an analysis in small towns most difficult. It seems appropriate to target larger cities with analytical studies in order to identify the possible

statistical artifacts. Such studies should include cities with similar natural-climatic and socio-economic conditions, since this approach allows excluding the impact of factors of natural conditions (how favorable they are) and living standards, which are significant for public health. As noted above, one of the possible statistical artifacts that can affect the mortality rates in a city is the presence of a large hospital therein, including a dedicated regional vascular center, since this would mean that the overall number of the deceased recorded in the that city will include deaths of people from other cities and regions [7, 11]. This allows hypothesizing that the number of hospital beds (per 10,000 people of population) can affect the mortality rate (the number of deaths per 100,000 residents) in cities with a population of up to 500,000 people. It is obvious that this factor will be of smaller significance in the largest cities and cities with over a million residents.

The purpose of this study was to assess the significance of impact of the number of hospital beds (per 10,000 people of population) on the mortality rates in the cities of the Moscow region with a population ranging from 100,000 to 500,000 people.

METHODS

The study included 2017–2019 Rosstat [15] data on the number of deaths per 1000 people, the average monthly nominal accrued salaries, the number of hospital beds in round-the-clock hospitals (per 10,000 people), as well as the population of 12 cities of the Moscow region (range from 100,000 to 500,000 people). The study included: 1) only the cities that have the all the indicators considered in the study published in freely available press; 2) only the cities of the Moscow region, which nullifies the effect differences in natural and climatic conditions have on mortality rates (the entire Moscow region is in the same climatic zone) and reduces the impact of socio-economic conditions. To improve accuracy of the assessment of possible impact of living standard on the mortality in a population, the analysis included data on the average monthly nominal accrued wages.

Table 1 presents data on the main group (12 cities, G_12) population in 2017 and shows the proportion of people outside the working age.

Spearman's rank correlation coefficient (R) was used to assess the statistical dependence between the studied indicators. Descriptive statistics data are presented in the tables as a median (Med) and an interquartile range (Q_1; Q_3). To assess reproducibility of the identified patterns, we analyzed the statistical relationship separately for each year (2017, 2018, 2019). The study analyzed statistical relationship between the mortality rate (the number of deaths from all causes per 1000 people), the average monthly nominal accrued wages of employees and the number of hospital beds in round-the-clock hospitals (per 10,000 people of population). Additionally, we analyzed such indicators as the share of residents over the working age (according to Rosstat [15]) and distance from the considered city to the center of Moscow. These indicators were included in the analysis to form a more homogeneous subgroup and thus eliminate the influence of the following factors: transport accessibility of medical institutions located in the regional center and share of older age people.

Since a relatively small sample size disallowed multivariate analysis, we formed a relatively homogeneous group of cities (G_5) lying within 30 kilometers from the center of Moscow (Balashikha, Khimki, Reutov, Mytishchi, Korolev) where the average monthly nominal accrued wages of exceeded 50,000 RUB in 2017.

Table 1. Population in the studied cities in 2017

	Population at the end of 2017, thousand human	Share of residents over the working age, %
Domodedovo	127.9	20
Balashikha	468.2	20
Reutov	103.8	23
Khimki	250.7	23
Mytishchi	211.6	22
Elektrostal	158.2	28
Korolev	223	27
Serpukhov	125.8	27
Zhukovsky	108.2	29
Podolsk	302.8	24
Kolomna	142.7	29
Orekhovo-Zuevo	118.8	27

Table 2. Statistical characteristics (median, lower and upper quartiles) of the studied indicators in the G_12 group

	Med (Q$_1$;Q$_3$)		
	2017	2018	2019
Mortality (per 1000 people)	12.25 (10.8; 13.7)	12.1 (10.6; 14.1)	11.65 (10.2; 13.7)
Number of hospital beds (per 10,000 people)	48.2 (35.0; 58.7)	47.4 (33.0; 55.8)	47.45 (32.6; 54.3)
Average salary	52,133 (44,795; 58,443)	57,551 (48,286; 65,401)	62,727 (51,390; 69,294)

RESULTS

Table 2 presents the statistical characteristics of such studied indicators as the population mortality rate (per 1000 people), the number of hospital beds in round-the-clock hospitals (per 10,000 people) and the average monthly salary in 12 cities (G_12) in 2017–2019.

At the first stage, we analyzed the dependence of population mortality rates on the number of hospital beds and the level of wages, as well as on such factors as the share of people above working age (in 2017) and distance to the center of Moscow.

Table 3 presents Spearman's correlation coefficients between population mortality rates, number of hospital beds and the level of salary in the G_12 group.

The mortality rates per 1000 residents correlated ($R > 0.7$) with the number of hospital beds per 10,000 people. This dependence is highly significant; it was registered every year. The correlation coefficient between wage and mortality rates was negative, smaller in absolute value and also differing significantly from 0 every year.

We have analyzed the values of Spearman's correlation coefficients between the mortality rates and the share of population over working age in 2017, as well as between the mortality rates and the distance to the center of Moscow. The former was 0.675 ($p < 0.016$) and the latter 0.904 ($p < 0.0001$).

Thus, there is a strong statistical relationship between mortality rates in the population, number of hospital beds and distance from the considered city to the center of Moscow (positive relationship). The relationships with wages (negative) and the share of population over the working age (positive relationship) are not as strong.

Having identified these patterns, we additionally analyzed the values of Spearman's rank correlation coefficients between the distance to the center of Moscow and wages, as well as the distance to the center of Moscow and the share of population over the working age. All the correlation coefficient values differed from 0 significantly ($p < 0.04$) and amounted to –0.601, –0.629, –0.625 for wages in 2017, 2018 and 2019, respectively, and 0.615 for the share of population over the working age in 2017. To a large extent, the identified dependencies on the distance to the center of Moscow are conditioned by the specifics of the cities of Orekhovo-Zuevo, Kolomna, Serpukhov, Elektrostal, which are 60–115 km away from Moscow. There, the wages were lowest (in 2017 — 42,000–45,000 RUB), the proportion of residents over the working age was 27–29% and the number of hospital beds per 10,000 people was largest (from 13 to 16.7).

The identified significant patterns, on the one hand, and the small sample size, on the other hand, necessitated formation of a more homogeneous group of cities. This group consisted of five cities (G_5) located within a 30-kilometer radius from the center of Moscow: Balashikha, Khimki, Reutov, Mytishchi, Korolev. The average monthly nominal accrued wages therein exceeded 50,000 RUB in 2017. Table 4 presents the statistical features of the studied indicators in this group, which show that on average, both the mortality rate and the number of hospital beds are smaller in this subgroup.

Table 5 shows the G_5 Spearman's rank correlation coefficient values of the population mortality rates, wages and the number of hospital beds in 2017, 2018 and 2019. In a subgroup of cities relatively homogeneous in terms of socio-economic conditions, an even stronger positive statistical relationship was registered between the population mortality

Table 3. Spearman's correlation coefficients (R) between population mortality rates, salary and the number of hospital beds in 2017, 2018 and 2019, group G_12

	2017		2018		2019	
	R	p	R	p	R	p
Number of hospital beds (per 10,000 people)	0.828	0.001	0.727	0.007	0.709	0.009
Average salary	–0.585	0.046	–0.594	0.042	–0.628	0.029

Table 4. Statistical characteristics (median, lower and upper quartiles) of the studied indicators in the G_5 group

	Med (Q1;Q3)		
	2017	2018	2019
Mortality (per 1000 people)	9.5 (8.7; 11.2)	9.4 (8.4; 11)	9.3 (8.0; 10.5)
Number of hospital beds (per 10,000 people)	35.8 (32.4; 42.0)	34.3 (29.2; 39.8)	33.3 (30.5; 37.7)
Average salary	52,602 (51,664; 60,621)	60,349 (58,106; 66,172)	65,233 (63,066; 69,031)

Table 5. Spearman's correlation coefficients (R) between population mortality rates, salary and the number of hospital beds in 2017, 2018 and 2019, group G_5

	2017 г.		2018 г.		2019 г.	
	R	p	R	p	R	p
Number of hospital beds (per 10,000 people)	0.975	0.005	0.9	0.037	0.975	0.005
Average salary	0.5	0.391	0.7	0.188	0.668	0.219

rate and the number of hospital beds ($R \geq 0.9$), while there was no significant dependence on salary recorded.

We identified no significant dependence of the G_5 population mortality rate on the distance to the center of Moscow and the share of people over the working age in 2017. The respective correlation coefficients amounted to 0.4 ($p = 0.505$) and 0.7 ($p = 0.188$).

DISCUSSION

The results of this study, which considered 12 cities of the Moscow region, confirmed the well-known negative correlation between population mortality rate and standard of living [8, 12, 16, 17] (in this study — between mortality and the average monthly nominal accrued salary).

This study has also revealed a positive correlation between the number of deaths per 1000 people of population, a widely used indicator in healthcare, and the number of hospital beds in round-the-clock hospitals (per 10,000 people of population), another widely used indicator. The latter indicator (number of beds) also characterizes availability of medical care [18]. The apparent contradiction — mortality is higher with greater availability of medical care in a hospital setting - has the following reasons behind it. Hospitals, especially in regional centers, admit not only residents of the city where they are located but also residents of the neighboring towns and villages, as well as people from other regions. When a patient dies, the death can be registered in the city of the hospital [7, 11]. This applies, first of all, to the residents of other subjects of the Russian Federation and foreign countries. It should be noted that in the largest cities and cities with over a million residents there is no effect from large medical institutions on the overall death rate assessment, since residents of these cities constitute the majority in the number of deaths per 1000 people of population

in these cities. In small towns, on the contrary, deaths of non-residents in hospitals have had a greater distorting effect on mortality rates therein. This is of particular importance in cities located in the territories served by the FMBA of Russia. A significant part of the nuclear industry workers are exposed to low doses of ionizing radiation throughout their professional life, which potentially contributes to the development of malignant neoplasms and diseases of the circulatory system, the two main causes of death of the population [19–21]. At the same time, as shown by this study, presence of a regional vascular center, for example, in the city of Severodvinsk (population 180000 people, there are shipyards repairing nuclear submarines therein), can, to some extent, condition the increased mortality from the circulatory system diseases in this city [22].

The results of this study are consistent with the results of other researchers who have identified statistical artifacts in assessing a city's mortality rates, such artifacts resulting from the presence of a significant number of labor migrants therein, which translates into the increased number of deaths from infectious diseases and external causes [11–13].

The results published in this article indicate that studying population mortality rates of relatively small cities it is necessary to analyze not only the number of deaths registered in the city but also the number of deaths of permanent residents of this city.

CONCLUSIONS

Medical care availability indicators have an ambiguous association with health status indicators in cities. An adequate assessment of the mortality rate in small towns requires accounting for the possible contribution of deaths of residents of other regions to the overall number number of deaths therein. This contribution is directly related to the number of hospital beds in round-the-clock hospitals.

References

1. Svod pravil SP 42.13330.2016 Gradostroitel'stvo. Planirovka i zastrojka gorodskix i sel'skix poselenij Aktualizirovannaya redakciya SNiP 2.07.01-89. Russian.

2. Ob utverzhdenii perechnya organizacij i perechnya territorij, podlezhashhix obsluzhivaniyu FMBA Rossii: Rasporyazhenie Pravitel'stva Rossijskoj Federacii ot 21 avgusta 2006 g. N 1156-r (s izmeneniyami na 2 oktyabrya 2021 g.). Russian.

3. Shaposhnikov DA, Revich BA. O nekotoryx podxodax k vychisleniyu riskov temperaturnyx voln dlya zdorov'ya. Analiz riska zdorov'yu. 2018; 1: 22–31. Russian.

4. Drapkina OM, Samorodskaya IV, Semyonov VYu, Zajratyanc OV. Sravnitel'nyj analiz variabel'nosti pokazatelej smertnosti ot

razlichnyx prichin v sub"ektax Rossijskoj Federacii. Arxiv patologii. 2020; 82 (3): 31–37. Russian.

5. Ivanova AE, Sabgajda TP, Semenova VG, Zaporozhchenko VG, Zemlyanova EV, Nikitina SYu. Faktory iskazheniya struktury prichin smerti trudosposobnogo naseleniya Rossii. Social'nye aspekty zdorov'ya naseleniya. 2013; 14 (4). Russian.

6. Sabgajda TP, Semenova VG. Svyaz' snizheniya serdechno-sosudistoj smertnosti 2013–2015 godov s izmeneniem smertnosti ot drugix prichin. Social'nye aspekty zdorov'ya naseleniya. 2017; 57 (5). Russian.

7. Yumaguzin VV, Vinnik MV. Problemy kachestva statistiki smertnosti v Rossii. EhKO. 2019; 10: 54–77. Russian.

8. Semenova VG, Golovenkin SE, Evdokushkina GN, Sabgajda TP. Poteri ot boleznej sistemy krovoobrashheniya v kontekste programmy po snizheniyu serdechno-sosudistoj smertnosti v Rossii. Zdravooxranenie Rossijskoj Federacii. 2016; 60 (1): 4–9. Russian.

9. Sabgajda TP, Semenova VG, Evdokushkina GN, Sekrieru EM, Nikitina SYu. Modifikaciya prichiny smerti pri statisticheskom uchete smertnosti. Social'nye aspekty zdorov'ya naseleniya. 2017; 57 (5). Russian.

10. Sabgajda TP, Tarasov NA, Evdokushkina GN. Smertnost' ot saxarnogo diabeta v rakurse mnozhestvennyx prichin smerti: problemy kodirovaniya. Problemy social'noj gigieny, zdravooxraneniya i istorii mediciny. 2019; 27 (6): 1043–8. Russian.

11. Ivanova AE, Ryazancev SV. Vklad migrantov v smertnost' naseleniya g. Moskvy. Seriya 1. Ehkonomika i pravo, 2015; 3: 174–84. Russian.

12. Ivanova AE, Ryazancev SV, Semenova VG. Vklad migracii v smertnost' rossijskogo naseleniya trudosposobnogo vozrasta. Nauchnoe obozrenie. Seriya 2. Gumanitarnye nauki. 2016; 6: 47–60. Russian.

13. Mixajlova YuV, Nechaeva OB, Shikina IB, Sorokin VN. Vliyanie migracionnyx faktorov na ehpidemicheskuyu situaciyu po tuberkulyozu i VICh infekcii v Rossii. Social'nye aspekty zdorov'ya naseleniya. 2018; 62 (4). Russian.

14. Tulenkov AM, Dyuzheva EV, Romanov KA. Mediko-demograficheskaya situaciya v penitenciarnyx uchrezhdeniyax Privolzhskogo federal'nogo okruga v period reformirovaniya ugolovno-ispolnitel'noj sistemy. Kazanskij medicinskij zhurnal.

15. Regiony Rossii. Osnovnye social'no-ehkonomicheskie pokazateli gorodov. 2020: Stat. sb. / Rosstat. M., 2020; 456 s. Russian.

16. Samorodskaya IV, Barabash OL, Kondrtkova NV, Bojcov SA. Vzaimosvyaz' social'no-ehkonomicheskix faktorov i pokazatelej smertnosti naseleniya. Profilakticheskaya medicina. 2017; 1: 10–14. Russian.

17. Kossova T. Ehkonomicheskie faktory smertnosti ot infekcionnyx boleznej v regionax Rossii. Ehkonomicheskaya politika. 2020; 15 (6): 90–109. Russian.

18. Rukovodstvo po analizu deyatel'nosti uchrezhdenij zdravooxraneniya municipal'nogo urovnya. M.: CNIIOIZ, 2008; 97 s. Russian.

19. Leuraud K, Richardson DB, Cardis E, Daniels RD, Gillies M, O'Hagan JA, et al. Ionising radiation and risk of death from leukaemia and lymphoma in radiation-monitored workers (INWORKS): an international cohort study. Lancet Haematol. 2015; 2 (7): 276–81.

20. Daniels RD, Bertke SJ, Richardson DB, Cardis E, Gillies M, O'Hagan JA, et al. Examining temporal effects on cancer risk in the international nuclear workers' study. Int J Cancer. 2017; 140 (6): 1260–9.

21. Kamiya K, Ozasa K, Akiba S, Niwa O, Kodama K, Takamura N, et al. Long-term effects of radiation exposure on health. Lancet. 2015; 386 (9992): 469–78.

22. Saltykova MM, Bobrovnickij IP, Balakaeva AV. Sravnitel'nyj analiz smertnosti naseleniya v gorodax Severodvinske i Arxangel'ske. Medicina ehkstremal'nyx situacij. 2021; 4: 17–22. Russian.

Литература

1. Свод правил СП 42.13330.2016 Градостроительство. Планировка и застройка городских и сельских поселений Актуализированная редакция СНиП 2.07.01-89.

2. Об утверждении перечня организаций и перечня территорий, подлежащих обслуживанию ФМБА России: Распоряжение Правительства Российской Федерации от 21 августа 2006 г. N 1156-р (с изменениями на 2 октября 2021 г.).

3. Шапошников Д. А., Ревич Б. А. О некоторых подходах к вычислению рисков температурных волн для здоровья. Анализ риска здоровью. 2018; 1: 22–31.

4. Драпкина О. М., Самородская И. В., Семёнов В. Ю., Зайратьянц О. В. Сравнительный анализ вариабельности показателей смертности от различных причин в субъектах Российской Федерации. Архив патологии. 2020; 82 (3): 31–37.

5. Иванова А. Е., Сабгайда Т. П., Семенова В. Г., Запорожченко В. Г., Землянова Е. В., Никитина С. Ю. Факторы искажения структуры причин смерти трудоспособного населения России. Социальные аспекты здоровья населения. 2013; 14 (4).

6. Сабгайда Т. П., Семенова В. Г. Связь снижения сердечно-сосудистой смертности 2013–2015 годов с изменением смертности от других причин. Социальные аспекты здоровья населения. 2017; 57 (5).

7. Юмагузин В. В., Винник М. В. Проблемы качества статистики смертности в России. ЭКО. 2019; 10: 54–77.

8. Семенова В. Г., Головенкин С. Е., Евдокушкина Г. Н., Сабгайда Т. П. Потери от болезней системы кровообращения в контексте программы по снижению сердечно-сосудистой смертности в России. Здравоохранение Российской Федерации. 2016; 60 (1): 4–9.

9. Сабгайда Т. П., Семенова В. Г., Евдокушкина Г. Н., Секриеру Е. М., Никитина С. Ю. Модификация причины смерти при статистическом учете смертности. Социальные аспекты здоровья населения. 2017; 57 (5).

10. Сабгайда Т. П., Тарасов Н. А., Евдокушкина Г. Н. Смертность от сахарного диабета в ракурсе множественных причин смерти: проблемы кодирования. Проблемы социальной гигиены, здравоохранения и истории медицины. 2019; 27 (6): 1043–8.

11. Иванова А. Е., Рязанцев С. В. Вклад мигрантов в смертность населения г. Москвы. Серия 1. Экономика и право. 2015; 3: 174–84.

12. Иванова А. Е., Рязанцев С. В., Семенова В. Г. Вклад миграции в смертность российского населения трудоспособного возраста. Научное обозрение. Серия 2. Гуманитарные науки. 2016; 6: 47–60.

13. Михайлова Ю. В., Нечаева О. Б., Шикина И. Б., Сорокин В. Н. Влияние миграционных факторов на эпидемическую ситуацию по туберкулезу и ВИЧ инфекции в России. Социальные аспекты здоровья населения. 2018; 62 (4).

14. Туленков А. М., Дюжева Е. В., Романов К. А. Медико-демографическая ситуация в пенитенциарных учреждениях Приволжского федерального округа в период реформирования уголовно-исполнительной системы. Казанский медицинский журнал. 2016; 97 (1): 124–30.

15. Регионы России. Основные социально-экономические показатели городов. 2020: Стат. сб. / Росстат. М., 2020; 456 с.

16. Самородская И. В., Барабаш О. Л., Кондрткова Н. В., Бойцов С. А. Взаимосвязь социально-экономических факторов и показателей смертности населения. Профилактическая медицина. 2017; 1: 10–14.

17. Коссова Т. Экономические факторы смертности от инфекционных болезней в регионах России. Экономическая политика. 2020; 15 (6): 90–109.

18. Руководство по анализу деятельности учреждений здравоохранения муниципального уровня. М.: ЦНИИОИЗ, 2008; 97 с.

19. Leuraud K, Richardson DB, Cardis E, Daniels RD, Gillies M, O'Hagan JA, et al. Ionising radiation and risk of death from leukaemia and lymphoma in radiation-monitored workers (INWORKS): an international cohort study. Lancet Haematol. 2015; 2 (7): 276–81.

20. Daniels RD, Bertke SJ, Richardson DB, Cardis E, Gillies M, O'Hagan JA, et al. Examining temporal effects on cancer risk in the international nuclear workers' study. Int J Cancer. 2017; 140 (6): 1260–9.

21. Kamiya K, Ozasa K, Akiba S, Niwa O, Kodama K, Takamura N, et al. Long-term effects of radiation exposure on health. Lancet. 2015; 386 (9992): 469–78.

22. Салтыкова М. М., Бобровницкий И. П., Балакаева А. В. Сравнительный анализ смертности населения в городах Северодвинске и Архангельске. Медицина экстремальных ситуаций. 2021; 4: 17–22.

ATTENTION INDICATORS AS MARKERS OF FATIGUE IN AMBULANCE WORKERS

Bolobonkina TA ✉, Dementiev AA, Minaeva NV

Pavlov Ryazan State Medical University, Ryazan, Russia

Medical care at the pre-hospital stage requires concentration of attention from ambulance workers and induces stress on the functional systems of their bodies. The spread of COVID-19 has increased the workload on mobile ambulance teams and worsened functional state of the team members' central nervous systems. This study aimed to investigate the impact of professional activity on changes in the indicators reflecting attention capacity, allocation and switching in mobile ambulance healthcare workers in the context of the COVID-19 pandemic. We used the Number Square method to assess these indicators. The participants were divided into groups with the help of standard tens, through standardization of the number of digital symbols, correct answers, mistakes made and time spent. The clear signs of fatigue by the end of the work shift are the decreased attention capacity, registered in 40.48% ($p < 0.0001$) of participants, and deteriorating attention allocation, registered in 64.29% ($p < 0.05$). The dynamics of the indicators were revealed to be associated (negative trends) with length of service and age. The registered values did not decrease at each subsequent shift, which proves the rest period between the shifts ensures a sufficient recovery. Decreased attention capacity and allocation by the end of the shift, as objective signs of fatigue, depend on age and length of service. Lack of negative dynamics shift-to-shift shows that the functional resources of the body are restored during the prescribed rest period even in the intense conditions of mobile ambulance teams' work during the COVID-19 pandemic.

Keywords: medical worker, ambulance, fatigue, functional state, COVID-19

✉ Correspondence should be addressed: Tatyana Alexandrovna Bolobonkina
8 Marta, 8, Ryazan, 390027, Russia; bolobonkina@bk.ru

ПОКАЗАТЕЛИ ВНИМАНИЯ КАК ИНДИКАТОРЫ УТОМЛЕНИЯ МЕДИЦИНСКИХ РАБОТНИКОВ СКОРОЙ МЕДИЦИНСКОЙ ПОМОЩИ

Т. А. Болобонкина ✉, А. А. Дементьев, Н. В. Минаева

Рязанский государственный медицинский университет имени И. П. Павлова, Рязань, Россия

Оказание медицинской помощи на догоспитальном этапе требует концентрации внимания и напряжения функциональных систем организма сотрудников скорой медицинской помощи. Распространение COVID-19 увеличило нагрузку на выездные бригады и привело к негативным изменениям функционального состояния центральной нервной системы работников. Целью исследования было изучить влияние профессиональной деятельности на изменение показателей объема, распределения и переключения внимания медицинских работников выездных бригад скорой медицинской помощи в условиях пандемии COVID-19. Для оценки объема, распределения и переключения внимания использовали методику «Числовой квадрат». Разделение обследуемых на группы проводили по индексам стенов путем стандартизации показателей количества цифровых символов, правильных ответов, допущенных ошибок и затраченного времени. Снижение объема внимания у 40,48% ($p < 0,0001$) обследованных и снижение его распределения у 64,29% ($p < 0,05$) свидетельствуют об утомлении к концу рабочей смены. Выявлены негативные тенденции динамики показателей с увеличением стажа работы и возраста. Отсутствие отрицательной динамики показателей между соседними сменами свидетельствует о достаточном восстановлении за период отдыха. Уменьшение объема и распределения внимания к концу смены как объективные признаки утомления имеют зависимость от возраста и стажа. Отсутствие негативной динамики у работников между сменами является признаком восстановления функциональных ресурсов за период регламентированного отдыха в условиях напряженной работы выездных бригад скорой медицинской помощи в период пандемии COVID-19.

Ключевые слова: медицинские работники, скорая помощь, утомление, функциональное состояние, коронавирусная инфекция

✉ Для корреспонденции: Татьяна Александровна Болобонкина
ул. 8-го Марта, д. 8, г. Рязань, 390027, Россия; bolobonkina@bk.ru

The work of healthcare professionals implies extensive reliance on memory, concentration of attention, need to make complex decisions in non-standard situations, often based on insufficient information and pressed for time, with high personal responsibility for the result [1, 2]. These factors explain the high intensity associated with their work, which is especially true about medical workers providing emergency care [3]. Such conditions lead to professional burnout, which, according to the published research papers, develops more often among healthcare professionals helping patients in emergency

situations, when diagnosing and treatment become a complex tactical task that sometimes requires knowledge and skill beyond the competence of these specialists [4, 5]. The work schedule has a significant impact on the overstrain of functional systems of emergency responders. Medical personnel working in shifts or at night are especially susceptible to the negative effects of the respective factors on the functional state of the central nervous system (CNS), which directly affects the occurrence of dangerous health consequences [6]. Shift work can negatively affect awareness and performance due to lack of sleep and disruption of biological rhythms [7].

Attention is a dynamic characteristic of the psyche; it represents the orientation and concentration of consciousness. The ability to activate attention enables clear understanding of the situation [8, 9].

The levels of attention allocation and switching reflect the degree of mobility of nervous processes in the cortical parts of the CNS and determine the ability to quickly navigate a complex and changing situation. The latter quality is one of the most important components of a successful discharge of professional duty by mobile ambulance medics. The high intensity of work associated with their professional activity adversely affects the functioning of various body systems, translates into the growth of inhibition processes in the CNS and development of fatigue, the severity of which largely depends on gender, age, length of service and schedule (shift) [10].

The COVID-19 pandemic has significantly increased the load on the primary care system and further boosted the persistent fatigue processes evident among medical workers, including ambulance personnel [11]. Intensification of work at the pre-hospital stage exacerbated the negative dynamics of the professional burnout syndrome prevalence among workers. The main reasons for this were the limitedness of the healthcare system resources, the threat of viral contamination as an additional professional risk, increased time spent with a single patient because of the epidemic prevention steps made before and after contact with the patient, sleep disturbance, work-life balance, neglect of personal and family needs with increased workload in the background and lack of information about the methods of treatment and prevention of COVID-19 [12].

The above factors determined the relevance of this study, the purpose of which was to investigate the impact of professional activity on changes in the indicators reflecting attention capacity, allocation and switching among mobile ambulance healthcare workers in the context of the COVID-19 pandemic.

METHODS

City clinical ambulance station of Ryazan was the base facility for the study. Sample size sufficiency was calculated with the help of the standard resampling formula using the small population size correction technique. The inclusion criteria were: employment with Ryazan city clinical ambulance station as a member of a mobile ambulance team, shift-based: 24-hour work shift and a rest period of 72 hours; age up to 65 years (inclusive); length of service as a mobile ambulance medic — over a year; absence of medical contraindications to 24-hour shifts and hazardous working conditions.

Because of the severe epidemic situation and the pronounced ambulance staff shortage in the region, the teams of all specialties were literally devoid of breaks between calls, and the specifics of patient conditions became similar throughout the practice. Data from the Ambulance automated information system: the number of calls responded to by a single team through a shift ranged from 15 to 26 (average 19.45 ± 3.37), the

total time of one call averaged at 45.46 ± 15.98 minutes. The participants were exposed to similar occupational factors and characteristics of the work process.

The sample was formed from May to October 2021. It included 42 medical workers (11 male and 31 female); 10 of them occupied positions of doctors, 32 — positions of paramedics. The mean age of the participants was 35.77 ± 3.39. NS-PsychoTest hardware and software complex (Neurosoft; Russia) was used for the study. Attention capacity (AC), attention allocation (AA) and attention switching were assessed with the help of the Number Square [13]. The examinations were done three times, during the time period from 7.00 to 8.00 AM, in accordance with the daily schedule of work shifts as follows: first examination — at the beginning of the daily work shift, second examination — 24 hours later at the end of the same shift, third examination — after 72 hours of rest (recovery period as per the applicable regulations), at the beginning of the next shift. The time allocated to the participants for the test was limited to 90 s. A single examination did not last longer than 3 minutes, including the methodology explanation and equipment set up stages.

The participants were divided into groups depending on the attention capacity and allocation levels, with the help of standard tens, which are normalized and centered assessments resulting from standardization of the number of digital symbols, correct answers, mistakes made and time spent.

The normality of the distribution of variables was checked with the help of Kolmogorov–Smirnov test. The Wilson's test (Wilson, 1927) was used to establish the confidence intervals for the stage of distribution of the examined into groups depending on the dynamics of the indicators; the significance of differences registered among the subgroups exhibiting oppositely directed trends was checked with the Pearson's chi-squared test; mean values of quantitative variables with a normal distribution are presented as $M \pm tm$ (M is the arithmetic mean of the indicator, expressed in absolute figures; m is the standard error, t is the test of validity with the given sample size).

We analyzed significant individual changes in functional indicators as registered during the work shift, when they fluctuate dynamically, and between adjacent shifts. Depending on the trend of indicator value changes, the participants were divided into three groups: group 1 — indicator value increased, group 2 — indicator value decreased, group 3 — indicator value did not change. Then we calculated the percentage of workers showing different dynamics of the studied functional changes, after that — compared groups of workers (occupation, age, length of service) by the percentage of participants exhibiting different trends of the considered indicators. The final exercise was to conduct a comparative assessment of the group means. To assess the significance of the average indicator value dynamics (mean difference between raises and falls) as registered considering the dynamics of the work shifts, we used the paired Student's t-test (the data obtained had a normal distribution). The statistical significance of the hypothesis was accepted at $p < 0.05$.

Statistical processing of the data was done with the help of Microsoft Excel 2007 (Microsoft; USA) with the Data Analysis add-on.

RESULTS

Table 1 shows the distribution of workers into groups by the nature of changes in AC through the work shift.

The physiological study revealed that by the end of the shift 40.48% of workers had the AC falling by 3.61 units on average

Table 1. Structure of workers with different individual dynamics of the attention capacity indicator against the shift-based schedule

Groups of workers	Groups with increasing AC		Groups with decreasing AC		Groups with unchanging AC
	Share, % ДИ, $p < 0,05$	Average growth of AC t-test	Share, % CI, $p < 0,05$	Average fall of AC t-test	Share, % CI, $p < 0,05$
Total $n = 42$	11,9	3,57 ± 1,04*	40,48	3,61 ± 0,98***	47,62
	[5,19; 25,0]	3,42	[27,04; 55,51]	7,33	[33,36; 62,28]
Sex distribution					
Women $n = 31$	12,9	3,16 ± 3,20	41,94	3,07 ± 1,04***	45,16
	[5,13; 28,85]	–	[26,42; 59,23]	5,87	[29,16; 62,23]
Men $n = 11$	9,09	4,66 ± 4,04	36,36	5,0 ± 1,90***	54,55
	[1,62; 37,74]	–	[15,17; 64,62]	5,27	[28,01; 78,83]
Age distribution					
Up to 30 y.o. $n = 16$	18,75	2,5 ± 1,73	50	3,00 ± 1,51*	31,25
	[6,59; 43,01]	–	[28,0; 72,0]	3,97	[14,16; 55,6]
30–39 y.o. $n = 14$	14,29	4,25 ± 3,3	14,29	6,00 ± 0,00	71,43
	[4,01; 39,94]	–	[4,01; 39,94]	–	[45,35; 88,28]
40 years and older $n = 12$	0	–	58,33	3,62 ± 1,41***	41,67
			[31,95; 80,67]	5,14	[19,33; 68,05]
Distribution by length of service					
0–5 years $n = 13$	23,08	2,50 ± 1,73	30,77	2,0 ± 1,15	46,15
	[8,18; 50,26]	–	[12,68; 57,63]	–	[23,21; 70,76]
6–10 years $n = 12$	8,33	1,00 ± 0,00	41,67	3,6 ± 2,15*	50
	[1,49; 35,39]		[19,33; 68,05]	3,34	[25,38; 74,62]
11 years and over $n = 17$	5,88	7,00 ± 0,00	47,06	4,33 ± 1,33***	47,06
	[1,05; 26,98]	–	[26,17; 69,04]	7,33	[26,17; 69,04]

Note: * — $p < 0.05$; ** — $p < 0.01$; *** — $p < 0.001$ — degree of significance using paired Student's t-test; CI, $p < 0.05$ — 95% confidence interval.

($p < 0.0001$). The share of participants whose AC increased was 3.4 times smaller; this indicator value did not change in the remaining participants throughout the working shift. It should be noted that the average AC decrease for men was 5.00 units ($p < 0.0001$), which is 1.6 times greater than that for women ($p > 0.05$). In 58.33% of the participants aged 40 years and older, we registered a significant mean AC decrease by 3.62 units ($p < 0.001$), and the remaining 41.77% of this age group's participants had this indicator unchanged.

We revealed an AC decrease trend associated with the length of service: from the 0-5 years mark to 11 and more years in service, the share of persons whose AC has deteriorated changed from 30.77 to 47.06%.

Table 2 shows the distribution of workers with different AA dynamics through a shift.

Most of the participants (64.29%; $p < 0.05$) had their AA decreasing by the end of the shift by an average of 3.0 units ($p < 0.0001$), with no pronounced gender differences registered in the choice behavior in the context of the work schedule's phase.

We have identified significant oppositely directed trends in the AA dynamics that depended on the age of workers ($\chi^2 = 11.407$; $p = 0.023$). In particular, half of the workers aged 30 and below exhibited a positive AA trend by an average of 2.62 units ($p = 0.0013$) and only 37.5% had the value of this indicator decreasing by an average of 3.28 units ($p = 0.0001$). On the contrary, in the age groups of 30–39 years and 40 years and older, the majority of participants (78.57 and 83.33%, respectively) had their AA value decreasing by the end of the work shift by an average of 3.60 and 3.45 units ($p < 0,0001$).

We have registered that the number of people whose AA value decreases tends to grow larger with the length of service.

Thus, 82.35% of medical workers with an experience of 11 years or more have had their AA decreasing by an average of 3.71 units during the shift ($p < 0.0001$ — confidence level using Student's paired t-test), while those whose length of service ranged from 0–5 years to 6–10 years, lost in their AA capability 2.1 and 1.2 times less, respectively.

Physiological test have shown that, by the beginning of the next shift, 62.5% of the participants had their AA value changing to the better by an average of 2.2 units ($p < 0.0001$). This inter-shift AA improvement dynamics were registered in both men and women, the percentage of participants exhibiting the pattern — 55.56% (value increased by 2.33 on average) and 83.33% (value increased by 1.8 on average), respectively ($p < 0.0001$).

DISCUSSION

The significant deterioration of AA registered in most of the participants of the study signals of the fatigue-induced negative changes in the functional state of the CNS by the end of the work shift. A possible reason behind these processes is hard work with frequent calls and longer visit durations, as well as the need for additional anti-epidemic measures when coming in contact with infected patients. During the COVID-19 pandemic, the use of personal protection equipment contributed to the number and severity of fatigue symptoms, which resulted from the changes in the ergonomics of the work process ultimately compromising functional state and efficiency [14]. It is also known that emergency medical personnel performs better on day shifts than on night shifts [15]. The actual lack of sleep breaks with a continuous stream of calls from patients was

Table 2. Structure of workers with different individual dynamics of the attention allocation indicator against the shift-based schedule

Groups of workers	Groups with increasing AA		Groups with decreasing AA		Groups with unchanging AA
	Share, % CI, *p* < 0,05	Average growth of AA *t*-test	Share, % CI, *p* < 0,05	Average fall of AA *t*-test	Share, % CI, *p* < 0,05
Total *n* = 42	23,81*	3,98 ± 1,46***	64,29*	3,46 ± 0,78***	11,9
	[13,48; 38,53]	4,47	[49,17; 77,01]	8,81	[5,19; 25,0]
Sex distribution					
Women *n* = 31	25,81*	2,89 ± 1,51**	61,29*	2,95 ± 1,13***	12,9
	[13,7; 43,25]	3,83	[43,82; 76,27]	7,7	[5,13; 28,85]
Men *n* = 11	18,18*	5,5	72,73*	4,00 ± 3,05***	9,09
	[5,14; 42,70]	–	[43,44; 90,25]	8,1	[1,62; 37,74]
Age distribution					
Up to 30 y.o. *n* = 16	50	2,62 ± 1,41**	37,5	3,28 ± 0,84***	12,5
	[28,0; 72,0]	3,72	[18,48; 61,36]	7,81	[3,5; 36,02]
30–39 y.o. *n* = 14	14,29	5,33 ± 2,08	78,57	3,60 ± 1,37***	7,14
	[4,01; 39,94]	–	[52,41; 92,43]	5,24	[1,27; 31,47]
40 years and older *n* = 12	0	–	83,33	3,45 ± 1,56***	16,67
			[55,2; 95,3]	4,43	[4,7; 44,8]
Distribution by length of service					
0–5 years *n* = 13	46,15	2,50 ± 1,61*	38,46	3,16 ± 0,95***	15,38
	[23,21; 70,76]	3,1	[17,71; 64,48]	6,63	[4,33; 42,23]
6–10 years *n* = 12	25	4,00 ± 2,64	66,67	6,25 ± 1,29**	8,33
	[8,89; 53,23]	–	[39,06; 86,19]	4,08	[1,49; 35,39]
11 years and over *n* = 17	5,88	5,00 ± 2,82	82,35	3,71 ± 1,26***	17,65
	[1,05; 26,98]		[58,97; 93,81]	5,87	[6,19; 41,03]

Note: * — *p* < 0.05; ** — *p* < 0.01; *** — *p* < 0.001 — degree of significance using paired Student's *t*-test; CI, *p* < 0.05 — 95% confidence interval.

one of the important factors in the development of fatigue. There was also established a correlation between shift-based schedule, prevalence of drowsiness and a higher risk of workplace injury among ambulance workers [16, 17]. In this connection, monitoring attention indicators among providers of emergency medical services in order to reduce the number of occupational injuries is a task of practical importance.

The significant multidirectional trends seen in the dynamics of AA depending on the age of workers, as well as a pronounced increase of the proportion of workers with deteriorating AA in older age groups, indicate that the reserves a body has for adaptation to the specifics of work grow smaller with age, which leads to a more rapid development of fatigue [18]. The respective changes are caused by natural processes: aging disrupts the finely tuned balance of excitation and inhibition in the cerebral cortex and translates into functional disorders [8, 19].

We have found that the percentage of participants whose AC and AA tend to decrease through the shift as their length of service grows indicates its adverse effect on the development of fatigue processes in the higher parts of the CNS [20]. Long and hard work in the ambulance service leads to disruption of the processes of excitation and inhibition in the cortical parts of the CNS, which compromises attention allocation and switching.

Significant improvement of the AA indicator value registered in most workers at the beginning of their next shift (compared to the state recorded during the previous one) signals of a fairly complete restoration of the functional state of the CNS during the rest period prescribed by the applicable regulations, which is a positive factor.

Prolonged work implying continuous strain on the regulatory systems can lead to the development of various pathological conditions in a worker, as well as cause professional burnout [4, 5, 21]. Potentially, schedules without night shifts for the most maladjusted groups of workers combined with elimination of the shortage of teams (by employing reserve personnel) when the incidence is rising will help solve the problem.

CONCLUSIONS

The significant decrease of the AA indicator value registered in the majority of ambulance medics by the end of the work shift can be viewed as one of the objective signs of fatigue. The share of medical workers suffering deterioration of the functional capabilities of CNS in terms of AA tends to grow with age, which is an adverse trend. Comparison of the attention-related indicators registered at the beginning of adjacent shifts reveals no negative trends, which means the rest period, as prescribed by the applicable regulations, ensures sufficient restoration of the functional state of CNS. Tailored work schedules combined with elimination of the shortage of teams when the incidence is rising can help solve the stated problem. The next study dedicated to this subject, as planned, will rely on the similar algorithm and seek to evaluate effectiveness of the recommended preventive measures, as well as compare the attention-related indicators during the highest and lowest workload periods.

References

1. Deng S, Yang N, Li S, et al. Doctors' job satisfaction and its relationships with doctor-patient relationship and work-family conflict in China: A Structural Equation Modeling. Inquiry. 2018; 55: 46958018790831. DOI: 10.1177/0046958018790831.
2. Bi J, Yin X, Li H, et al. Effects of monitor alarm management training on nurses' alarm fatigue: A randomised controlled trial. J Clin Nurs. 2020; 29 (21–22): 4203–16. DOI:10.1111/jocn.15452.
3. Bolobonkina TA, Dementev AA, Shatrova NV. Tyazhest' i napryazhennost' trudovogo processa medicinskix rabotnikov vyezdnyx brigad skoroj medicinskoj pomoshhi v usloviyax modernizacii zdravooxraneniya. Nauka molodyx (Eruditio Juvenium). 2019; 7 (4): 501–08. DOI: 10.23888/HMJ201974501-508. Russian.
4. Milas GP, Issaris V, Zareifopoulos N. Burnout for medical professionals during the COVID-19 pandemic in Greece; the role of primary care. Hosp Pract (1995). 2022; 50 (2): 102–3. DOI: 10.1080/21548331.2022.2045133.
5. Moukarzel A, Michelet P, Durand AC, et al. Burnout syndrome among emergency department staff: prevalence and associated factors. Biomed Res Int. 2019; 2019: 6462472. Published 2019 Jan 21. DOI: 10.1155/2019/6462472.
6. Knap M, Maciąg D, Trzeciak-Bereza E, et al. Sleep disturbances and health consequences induced by the specificity of nurses' work. Int J Environ Res Public Health. 2022; 19 (16): 9802. DOI: 10.3390/ijerph19169802.
7. Ganesan S, Magee M, Stone JE, et al. The impact of shift work on sleep, alertness and performance in healthcare workers. Sci Rep. 2019; 9 (1): 4635. DOI: 10.1038/s41598-019-40914-x.
8. Kupcova SV, Ivanova MV, Petrushevskij AG, Fedina ON, Zhavoronkova LA. FMRT-issledovanie pereklyucheniya zritel'nogo vnimaniya u zdorovyx lyudej. Zhurnal vysshej nervnoj deyatel'nosti. 2015; 65 (1): 61–71. Russian.
9. Poysophon P, Rao AL. Neurocognitive deficits associated with ADHD in athletes: a systematic review. Sports Health. 2018; 10 (4): 317– 26.
10. Il'yasova SD, Kulikov RF. Psixoehmocional'noe vygoranie rabotnikov skoroj medicinskoj pomoshhi. Colloquium-journal. 2019; 10–3 (34): 35–37. Russian.
11. Zhan YX, Zhao SY, Yuan J, et al. Prevalence and influencing factors on fatigue of first-line nurses combating with COVID-19 in China: A Descriptive Cross-Sectional Study. Curr Med Sci. 2020; 40 (4): 625–35. DOI: 10.1007/s11596-020-2226-9
12. Raudenská J, Steinerová V, Javůrková A, et al. Occupational burnout syndrome and post-traumatic stress among healthcare professionals during the novel coronavirus disease 2019 (COVID-19) pandemic. Best Pract Res Clin Anaesthesiol. 2020; 34 (3): 553–60. DOI: 10.1016/j.bpa.2020.07.008.
13. Shapar VB, Timchenko AV, Shvydchenko VN. Prakticheskaya psixologiya. Instrumentarij. Rostov-na-Donu: Feniks, 2002; 688 s. Russian.
14. Zelenko AV, Tolkach SN, Sinyakova OK, i dr. Sub"ektivnaya ocenka sostoyaniya organizma kak ehlement profilaktiki narusheniya professional'nogo zdorov'ya medicinskix rabotnikov. V sbornike: Analiz riska zdorov'yu — 2021. Vneshnesredovye, social'nye, medicinskie i povedencheskie aspekty. Sovmestno s mezhdunarodnoj vstrechej po okruzhayushhej srede i zdorov'yu RISE-2021. Materialy XI Vserossijskoj nauchno-prakticheskoj konferencii s mezhdunarodnym uchastiem: v 2 t. Perm', 2021; c. 153–61. Russian.
15. Patterson PD, Weaver MD, Markosyan MA, et al. Impact of shift duration on alertness among air-medical emergency care clinician shift workers. Am J Ind Med. 2019; 62 (4): 325–36. DOI: 10.1002/ajim.22956.
16. Lin MH, Huang YC, Chen WK, Wang JY. Sleepiness and injury risk in emergency medical service workers in Taiwan. PLoS One. 2020; 15 (2): e0229202. Published 2020 Feb 24. DOI: 10.1371/journal.pone.0229202.
17. Mansukhani MP, Kolla BP, Surani S, et al. Sleep deprivation in resident physicians, work hour limitations, and related outcomes: a systematic review of the literature. Postgrad Med. 2012; 124 (4): 241–9. DOI: 10.3810/pgm.2012.07.2583.
18. Violanti JM, Owens SL, Fekedulegn D, et al. An Exploration of Shift Work, Fatigue, and Gender Among Police Officers: The BCOPS Study. Workplace Health Saf. 2018; 66 (11): 530–7. DOI: 10.1177/2165079918754586.
19. Petitet P, Spitz G, Emir UE, et al. Age-related decline in cortical inhibitory tone strengthens motor memory. Neuroimage. 2021; 245: 118681. DOI: 10.1016/j.neuroimage.2021.118681.
20. Gubareva LI, Ponomareva TYu, Ermolova LS. Osobennosti funkcionirovaniya central'noj nervnoj sistemy u rabotnikov gazotransportnoj sistemy s raznoj stepen'yu adaptacii k usloviyam professional'noj sredy. Medicinskij vestnik Severnogo Kavkaza. 2016; 11 (4): 573–6. Russian.
21. Rabinerson D, Markovitch L, Gabbay-Ben-Ziv R. Harefuah. 2016; 155 (7): 394–7.

Литература

1. Deng S, Yang N, Li S, et al. Doctors' job satisfaction and its relationships with doctor-patient relationship and work-family conflict in China: A Structural Equation Modeling. Inquiry. 2018; 55: 46958018790831. DOI: 10.1177/0046958018790831.
2. Bi J, Yin X, Li H, et al. Effects of monitor alarm management training on nurses' alarm fatigue: A randomised controlled trial. J Clin Nurs. 2020; 29 (21–22): 4203–16. DOI:10.1111/jocn.15452.
3. Болобонкина Т. А., Дементьев А. А., Шатрова Н. В. Тяжесть и напряженность трудового процесса медицинских работников выездных бригад скорой медицинской помощи в условиях модернизации здравоохранения. Наука молодых (Eruditio Juvenium). 2019; 7 (4): 501–08. DOI: 10.23888/HMJ201974501-508.
4. Milas GP, Issaris V, Zareifopoulos N. Burnout for medical professionals during the COVID-19 pandemic in Greece; the role of primary care. Hosp Pract (1995). 2022; 50 (2): 102–3. DOI: 10.1080/21548331.2022.2045133.
5. Moukarzel A, Michelet P, Durand AC, et al. Burnout syndrome among emergency department staff: prevalence and associated factors. Biomed Res Int. 2019; 2019: 6462472. Published 2019 Jan 21. DOI: 10.1155/2019/6462472.
6. Knap M, Maciąg D, Trzeciak-Bereza E, et al. Sleep disturbances and health consequences induced by the specificity of nurses' work. Int J Environ Res Public Health. 2022; 19 (16): 9802. DOI: 10.3390/ijerph19169802.
7. Ganesan S, Magee M, Stone JE, et al. The impact of shift work on sleep, alertness and performance in healthcare workers. Sci Rep. 2019; 9 (1): 4635. DOI: 10.1038/s41598-019-40914-x.
8. Купцова С. В., Иванова М. В., Петрушевский А. Г., Федина О. Н., Жаворонкова Л. А. ФМРТ-исследование переключения зрительного внимания у здоровых людей. Журнал высшей нервной деятельности. 2015; 65 (1): 61–71.
9. Poysophon P, Rao AL. Neurocognitive deficits associated with ADHD in athletes: a systematic review. Sports Health. 2018; 10 (4): 317– 26.
10. Ильясова С. Д., Куликов Р. Ф. Психоэмоциональное выгорание работников скорой медицинской помощи. Colloquium-journal. 2019; 10–3 (34): 35– 37.
11. Zhan YX, Zhao SY, Yuan J, et al. Prevalence and influencing factors on fatigue of first-line nurses combating with COVID-19 in China: A Descriptive Cross-Sectional Study. Curr Med Sci. 2020; 40 (4): 625–35. DOI: 10.1007/s11596-020-2226-9.
12. Raudenská J, Steinerová V, Javůrková A, et al. Occupational burnout syndrome and post-traumatic stress among healthcare professionals during the novel coronavirus disease 2019 (COVID-19) pandemic. Best Pract Res Clin Anaesthesiol. 2020; 34 (3): 553–60. DOI: 10.1016/j.bpa.2020.07.008.
13. Шапарь В. Б., Тимченко А. В., Швыдченко В. Н. Практическая психология. Инструментарий. Ростов-на-Дону: Феникс, 2002; 688 с.
14. Зеленко А. В., Толкач С. Н., Синякова О. К., и др. Субъективная

оценка состояния организма как элемент профилактики нарушения профессионального здоровья медицинских работников. В сборнике: Анализ риска здоровью — 2021. Внешнесредовые, социальные, медицинские и поведенческие аспекты. Совместно с международной встречей по окружающей среде и здоровью RISE-2021. Материалы XI Всероссийской научно-практической конференции с международным участием: в 2 т. Пермь, 2021; с. 153–61.

15. Patterson PD, Weaver MD, Markosyan MA, et al. Impact of shift duration on alertness among air-medical emergency care clinician shift workers. Am J Ind Med. 2019; 62 (4): 325–36. DOI: 10.1002/ajim.22956.

16. Lin MH, Huang YC, Chen WK, Wang JY. Sleepiness and injury risk in emergency medical service workers in Taiwan. PLoS One. 2020; 15 (2): e0229202. Published 2020 Feb 24. DOI: 10.1371/journal.pone.0229202.

17. Mansukhani MP, Kolla BP, Surani S, et al. Sleep deprivation in resident physicians, work hour limitations, and related outcomes: a systematic review of the literature. Postgrad Med. 2012; 124 (4): 241–9. DOI: 10.3810/pgm.2012.07.2583.

18. Violanti JM, Owens SL, Fekedulegn D, et al. An Exploration of Shift Work, Fatigue, and Gender Among Police Officers: The BCOPS Study. Workplace Health Saf. 2018; 66 (11): 530–7. DOI: 10.1177/2165079918754586.

19. Petitet P, Spitz G, Emir UE, et al. Age-related decline in cortical inhibitory tone strengthens motor memory. Neuroimage. 2021; 245: 118681. DOI: 10.1016/j.neuroimage.2021.118681.

20. Губарева Л. И., Пономарева Т. Ю., Ермолова Л. С. Особенности функционирования центральной нервной системы у работников газотранспортной системы с разной степенью адаптации к условиям профессиональной среды. Медицинский вестник Северного Кавказа. 2016; 11 (4): 573–6.

21. Rabinerson D, Markovitch L, Gabbay-Ben-Ziv R. Harefuah. 2016; 155 (7): 394–7.

METABOLIC ACTIVITY OF IMMUNOCOMPETENT CELLS IN ASSESSMENT OF INDIVIDUAL COLD SENSITIVITY

Patrakeeva VP ✉, Schtaborov VA

N. Laverov Federal Center for Integrated Arctic Research of the Ural Branch of the Russian Academy of Sciences, Arkhangelsk, Russia

The rapid switch on of the transient short-term responses involved in adjustment of homeostasis plays a key role in human adaptation to low temperatures that is essential for adjustment to low-temperature environment. The network of signaling pathways together with metabolic regulators provide sufficient plasticity of the cells of immune system, the normal function of which is extremely important for successful human adaptation. Sufficient energy supply to immunocompetent cells makes it possible to form an adequate immune response to any negative factor and to ensure adaptive functional rearrangements. The study was aimed to assess the variants of the immunocompetent cell metabolic pathways involved in acquiring individual cold sensitivity. A total of 180 people aged 25–55 (130 females, 50 males) were assessed before and after the short-term whole body cooling. Enzyme immunoassay was used to define the levels of IL10, IL6, TNFα, irisin, transferrin, sTfR, HIF-1α, Sirt3 in peripheral blood and cell lysate. The levels of glycogen (cytochemical methods) and ATP (luciferin-luciferase assay) in lymphocytes were defined. The decrease in peripheral blood lymphocyte levels after cooling was indicative of the formation of immediate adaptive response and activation of glycolysis amid less intense inflammatory response. The increase in the levels of circulating lymphocytes after the cold esposure was associated with activation of inflammatory responses. The lower ratio of HIF-1α/SIRT3 metabolic regulators was found in the surveyed volunteers who showed no changes in the levels of lymphocytes. This indicated predominance of mitochondrial activity in adaptation to low temperatures.

Keywords: cold, metabolic activity, glycogen, irisin, ATP, oxygen saturation

✉ Correspondence should be addressed: Veronika P. Patrakeeva
Naberezhnaya Severnoi Dviny, 23, Arkhangelsk, 163000, Russia; patrakeewa.veronika@yandex.ru

МЕТАБОЛИЧЕСКАЯ АКТИВНОСТЬ ИММУНОКОМПЕТЕНТНЫХ КЛЕТОК В ОЦЕНКЕ ИНДИВИДУАЛЬНОЙ ХОЛОДОВОЙ ЧУВСТВИТЕЛЬНОСТИ

В. П. Патракеева ✉, В. А. Штаборов

Институт физиологии природных адаптаций Федеральный исследовательский центр комплексного изучения Арктики имени Н. П. Лавёрова Уральского отделения Российской академии наук, Архангельск, Россия

Центральную роль в адаптации организма человека к холоду играет быстрое включение переходных краткосрочных реакций, которые участвуют в корректировке гомеостаза, необходимой для приспособления к низкотемпературной среде. Сеть сигнальных путей и регуляторы метаболизма обеспечивают достаточную пластичность работы клеток иммунной системы, нормальное функционирование которой крайне важно для успешной адаптации организма человека. Энергообеспеченность иммунокомпетентных клеток дает возможность формирования адекватного иммунного ответа на воздействие любого негативного фактора, обеспечения адаптационных функциональных перестроек. Целью работы было изучить варианты путей метаболической активности иммунокомпетентных клеток в формировании индивидуальной холодовой чувствительности. Проведено обследование 180 человек в возрасте 25–55 лет (130 женщин, 50 мужчин) до и после кратковременного общего охлаждения. В периферической крови и лизате клеток иммуноферментным анализом определяли уровни IL10, IL6, TNFα, иризина, трансферрина, sTfR, HIF-1α, Sirt3. В лимфоцитах определяли содержание гликогена (цитохимически) и АТФ (люциферин-люциферазный метод). Снижение уровня лимфоцитов в периферической крови после охлаждения свидетельствует о формировании срочной адаптивной реакции и активации гликолитических процессов в клетке на фоне более низкого уровня воспалительной реакции. Повышение уровня лимфоцитов в циркуляции после воздействия холода происходит на фоне активации воспалительных реакций. Для обследованных волонтеров, у которых не было зарегистрировано изменений в уровне лимфоцитов, выявлено более низкое соотношение регуляторов метаболизма HIF-1α/SIRT3, что свидетельствует о преобладании митохондриальной активности при адаптации к холоду.

Ключевые слова: холод, метаболическая активность, гликоген, иризин, АТФ, сатурация кислорода

✉ Для корреспонденции: Вероника Павловна Патракеева
наб. Северной Двины, д. 23, г. Архангельск, 163000, Россия; patrakeewa.veronika@yandex.ru

Adaptation to the Northern environment is associatied with the body's ability to adapt to low temperatures, which results in the need for metabolic rearrangements. Glycolysis, that is used by cells during proliferation or when exposed to extreme loads, is the quickest way to acquire energy [1]. Mitochondria slower but more effectively facilitate ATP production, however, mitochondrial oxidative metabolism sensitizes cells to apoptosis [2]. Sirt3 is one of the key mitochondrial metabolic regulators [3–6]. The Sirt3 downregulation can be observed in individuals with cardiovascular disorders, diabetes mellitus, cancer and metabolic disorders, it is also involved in regulation of oxidative stress via the Sirt3-AMPK-α-PGC-1α pathway [7–11]. Hypoxia-inducible factor HIF-1α that increases glycolysis and suppresses mitochondrial activity is the other factor involved in regulation of cellular metabolism [12]. Evaluation of the relationship between these two regulators would make it possible to assess the direction of cellular metabolic activity. Our previous studies showed that people living in the North respond differently to the short-term whole body cooling, which was evident in altered peripheral blood lymphocyte levels (decreased levels, increased levels or no response) [13, 14]. Thus, it would be interesting to assess the role of the immunocompetent cell metabolic activity pathways in acquiring individual cold sensitivity. This consideration has become the aim of the study.

METHODS

Examination of 180 people (among them 130 females and 50 males) aged 25–55 before and after the short-term whole body cooling in the cooling chamber at –25 °C for 5 min was performed. Blood was collected from the cubital vein before and immediately after cooling. Inclusion criteria: healthy working-age people with no chronic and/or recurrent diseases at the time of examination. The leukogram patterns were defined with the XS-1000i haematology analyser (Sysmex; Japan). Concentrations of cytokines IL10, IL6, TNFα, irisin, transferrin, sTfR, HIF-1α, Sirt3 were measured by enzyme immunoassay using the Evolis (Bio-Rad; France) and Multiscan MS (Finland) enzyme immunoassay analyzers. Glycogen levels were assessed by cytochemical method (Abris+; Russia). Adenosine triphosphate (ATP) was quantified by luciferin-luciferase assay. The results of chemical reaction were assessed in the LUM-1 luminometer (Lumtek; Russia) using the Lumtek standard reagent kits. Oxygen saturation levels were defined with the pulse oximeter (Armed YX300; China). Body weight (kg), body length (cm) were measured and body mass index (kg/m^2) was calculated in all the surveyed individuals. Subcutaneous and visceral fat assessment was performed with the portable device by Omron (Japan). In accordance with the manufacturer's guidelines, visceral fat percentage of 1–9% was considered normal, the percentage of 10–14% was considered high, and the percentage of 15–30% was considered very high.

The study results obtained were assessed in three groups based on alterations in peripheral blood lymphocyte counts after the short-term whole body cooling. In group 1, lymphocyte counts decreased by 1.5–2 times from 2.1 (1.77–2.44) to 1.69 (0.95–2.16) $\times$ 10^9 cells/L ($p < 0.001$); in group 2, lymphocyte counts increased from 1.49 (1.26–1.74) to 2.22 (1.48–2.61) $\times$ $\times$ 10^9 cells/L ($p < 0,01$); no significant changes were observed in group 3 (1.88 (1.46–2.17) and 1.82 (1.46–2.56) $\times$ 10^9 cells/L). There were no differences in age between groups; the average age was 33 years in group 1, 2–31 years in group 2, 32 years in group 3. Statistical processing of the results was performed using the Statistica 10 software package (USA). Trait distribution was non-normal (Shapiro–Wilk test), that is why the data were expressed as median and 25th-75th percentile (Me (25–75)). Multiple data samples (of three groups) were compared using the Kruscal–Wallis test ($p < 0.05$). Mann–Whitney U-test was used for pairwise comparison ($p < 0.017$).

RESULTS

There were no significant differences in body mass index between groups: it was 23.50 kg/m^2 in group 1, 24.16 kg/m^2 in group 2, and 24.78 kg/m^2 in group 3. Comparison of bio-impedancemetry data showed that higher visceral fat percentage of 12.1% (group 1 — 7.2%, group 2 — 5.3%; p^{1-2}, 1–3 < 0.01) was typical for people whose peripheral blood lymphocyte counts decreased in response to the short-term whole body cooling. However, there were no significant differences in the percentage of subcutaneous adipose tissue between the surveyed people: it was 31.8% in group 1, 30% in group 2, and 30.1% in group 3. High visceral fat percentage increases the risk of cardiovascular and metabolic disorders, and positively correlates with elevated fasting levels of triglycerides and glucose, as well as with the decreased levels of high density lipoproteins (HDL) [15–17]. It is known that dysfunctional visceral fat contributes to hypoxia [18]. This was reflected in lower oxygen saturation that made up 97% (min — 94%, max — 99%) in group 1, 98% (min — 97%, max — 99%) in group 2, and 99% (min — 98%, max — 99%) in group 3. After the short-term whole body cooling, oxygen saturation in group 1 actually equaled the values obtained on other two groups and rose to 98% (min — 97%, max — 99%). The combined effects of hypoxia and low temperatures resulted in activation of gene that encoded transferrin and transferrin accumulation in plasma (Table 1). The relatively high levels of soluble sTfR transferrin receptor and transferrin were detected in all groups: the concentrations exceeded 340 mg/dL in 75% of surveyed people in group 1, 77.8% in group 2, and 90.9% in group 3.

Such an increase in the levels of transferrin and sTfR is indicative of iron deficiency affecting tissues and hypoxia. Furthermore, high transferrin levels are a risk factor of cardiovascular disorders, since these facilitate activation of blood clotting factors and hypercoagulation [19, 20].

Table 1. Concentrations of transferrin and sTfR in peripheral blood, Me (25–75)

		Transferrin, mg/dL	sTfR, µg/mL
Group 1	Before cooling	455.9 (306.5–846.7)	27.1 (1.5–53.4)
	After cooling	430.3 (333.1–480.0)	35.9 (17.4–344.6)*
Group 2	Before cooling	371.4 (341.4–543.4)	20.0 (18.46–22.60)
	After cooling	573.8 (434.20–640.2)**	22.6 (21.54–46.2)
Group 3	Before cooling	434.2 (363.8–517.0)	22.3 (20.0–126.2)
	After cooling	434.2 (324.2–663.2)	25.6 (18.72–130.8)

Note: * — $p_{gr.\ 1}$ < 0,01; ** — $p_{gr.\ 2}$ < 0,01.

Таблица 2. Concentrations of HIF-1α of SIRT-3 in peripheral blood lymphocytes, Me (25–75)

Indicator	Group 1	Group 2	Group 3
HIF-1α, 10^6 cells/mL	1.3 (0.9–1.8)	1.8 (1.48–2.1)	1.3 (1.13–2.0)
SIRT-3, 10^6 cells/mL	0.2 (0.1–0.2)	0.3 (0.12–0.5)	0.3 (0.19–0.5)

Alterations in cellular metabolic activity determine the capability of adaptation to changing environment. For cells, glycolysis is the fastest way to acquire energy, and ATP synthesis takes an average of 2–4 min. The decrease in peripheral blood lymphocyte levels after the short-term cooling was associated with the decrease in lymphocyte glycogen levels from 4 to 2.83% ($p = 0.0056$); in other two groups, glycogen levels in lymphocytes did not change, these were 5.8 and 6.2% in group 2, and 3.6 and 4.8% in group 3, respectively. The decrease in glycogen levels results in the increased ATP production by lymphocytes (from 0.98 (0.42–2.87) to 3.16 (0.55–4.19) μmol/bn cells); cells are unable to deposit ATP for prolonged use due to the lack of specific mechanism, that is why such an increase in ATP levels is indicative of cell activation. The increase in the HIF-1α/SIRT3 ratio observed in the cells during the increased ATP production testifies in favor of the increased glycolytic activity, since HIF-1α has a predominantly inhibiting effect on the oxidative phosphorylation pathways and stimulates glycolysis, thus inducing both glucose uptake and expression of glycolytic enzymes (Table 2) [21–23].

Irisin, the member of myokine family, the receptors to which are found in all cells of the body, is involved in regulation of adaptation to low temperatures [24, 25]. Irisin enables thermoregulation processes due to activation of thermogenin (UCP1) and increases energy expenditure. Moreover, irisin exerts anti-inflammatory effects and protects cell junctions against damage due to interaction with Src tyrosine kinase and AMPK phosphorylation [26–28]. The highest levels of this myokine, 6.29 (3.04–7.98) μg/mL, were observed in group 1. The levels observed in other two groups were lower: 3.06 (1.59–6.70) μg/mL in group 2, and 4.32 (3.11–8.08) μg/mL in group 3 ($p^{1–2} = 0,005$). After exposure to low temperatures, irisin levels in group 1 significantly decreased to 3.17 (1.349–6.64) μg/mL ($p < 0.01$). Such a decrease in irisin levels after cooling could enhance endothelial permeability and increase cellular adhesion and migration. This was associated with the decrease in the levels of circulating lymphocytes in this group of surveyed people. Higher background levels of irisin increase the concentration of anti-inflammatory cytokine IL10 in peripheral blood amid lower concentrations of pro-inflammatory cytokines L6 and TNFα (see Fig.).

DISCUSSION

It is known that the early period of acclimatization to low temperatures (within 7 days) is associated with the increase in the levels of HIF-1α protein that facilitates activation of glycolysis and β-oxidation [29, 30]. Our study showed that even the short-term exposure to low temperatures for 5 min contributes to adaptive responses, as determined by the background immune defenses and regulatory mechanisms that underlie cellular metabolic activity. The combined effects of hypoxia and low temperatures are associated with the elevated levels of transferrin and soluble transferrin receptor, that are the risk factors of cardiovascular disorders prevalent among residents of the Northern territories, in almost all the surveyed volunteers. Transferrin is a principal carrier of the iron ions involved in various metabolic pathways [31, 32], which have a direct impact on the response to cold exposure due to immediate or long-term adaptive responses. Thus, the determined decrease in peripheral blood lymphocyte levels in response to the short-term whole body cooling is indicative of the establishment of immediate adaptive response associated with activation of glycolysis in the cells that ensures rapid boosting of the energy reserve essential for lymphocyte activation. Higher background levels of irisin found in group 1 of the surveyed people ensure regulation of inflammatory response due to stimulation of the higher anti-inflammatory cytokine levels. The increased levels of circulating lymphocytes found in group 2 of the surveyed people are associated with the more intense inflammatory response reflected in the levels of pro-inflammatory cytokines. Furthermore, this group is characterized by the higher visceral fat percentage that is also capable of promoting more severe inflammation. No activation of immediate adaptive response has been found in the surveyed individuals who have shown no changes in lymphocyte levels (group 3). This group shows lower ratio of the HIF-1α/SIRT3 metabolic regulators, which indicates predominance of mitochondrial activity in adaptation to low temperatures.
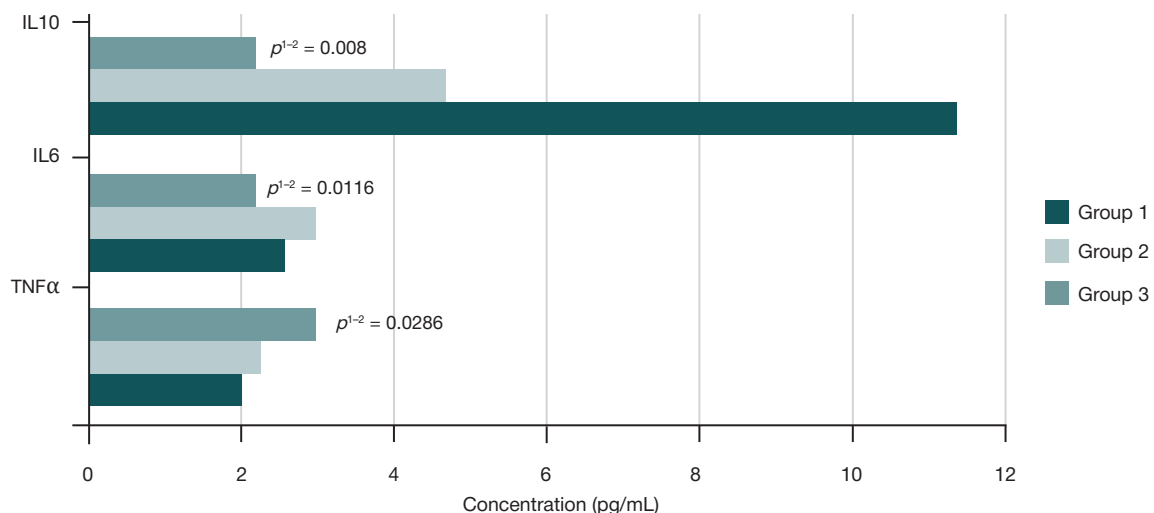

Fig. Cytokine levels in peripheral blood

CONCLUSIONS

Background immune defense and the concentrations of pro- and anti-inflammatory factors are associated with immediate and long-term adaptive responses to the cold exposure. Assessment of changes in the levels of circulating lymphocytes is a simple and affordable method for prediction of human adaptive capabilities ensured by regulation of the cellular metabolic pathway activation.

References

1. Zhu J, Thompson CB. Metabolic regulation of cell growth and proliferation. Nat Rev Mol Cell Biol. 2019; 20 (7): 436–50.
2. Ferranti CS, Cheng J, Thompson C, Zhang J, Rotolo JA, Buddaseth S, et al. Fusion of lysosomes to plasma membrane initiates radiation-induced apoptosis. J Cell Biol. 2020; 219 (4): e201903176.
3. Newman JC, He W, Verdin E. Mitochondrial protein acylation and intermediary metabolism: regulation by sirtuins and implications for metabolic disease. J Biol Chem. 2012; 287 (51): 42436–43.
4. Zhang J, Xiang H, Liu J, Chen Y, He R-R, Liu B. Mitochondrial sirtuin 3: new emerging biological function and therapeutic target. Theranostics. 2020; 10 (18): 8315–42.
5. Reverdy C, Gitton G, Guan X, Adhya I, Krishna Dumpati R, Roy S, et al. Discovery of novel compounds as potent activators of Sirt3. Bioorganic & Medicinal Chemistry. 2022; 73: 116999.
6. Anderson KA, Hirschey MD. Mitochondrial protein acetylation regulates metabolism. Essays Biochem. 2012; 52: 23–35.
7. Bagul PK, Katare PB, Bugga P, Dinda AK, Banerjee SK. SIRT-3 modulation by resveratrol improves mitochondrial oxidative phosphorylation in diabetic heart through deacetylation of TFAM. Cells. 2018; 7 (12): 235.
8. Kincaid B, Bossy-Wetzel E. Forever young: SIRT3 a shield against mitochondrial meltdown, aging, and neurodegeneration. Front Aging Neurosci. 2013; 5: 48.
9. Anderson KA, Hirschey MD. Mitochondrial protein acetylation regulates metabolism. Essays Biochem. 2012; 52: 23–35.
10. Porter GA, Urciuoli WR, Brookes PS, Nadtochiy SM. SIRT3 deficiency exacerbates ischemia-reperfusion injury: implication for aged hearts. Am J Phys Heart Circ Phys. 2014; 306: H1602–H1609.
11. Bugga P, Alam J, Kumar R, Pal S, Chattopadyay N, Banerjee SK. Sirt3 ameliorates mitochondrial dysfunction and oxidative stress through regulating mitochondrial biogenesis and dynamics in cardiomyoblast. Cellular Signalling. 2022; 94: 110309.
12. Denko NC. Hypoxia, HIF1 and glucose metabolism in the solid tumour. Nature Reviews Cancer. 2008; 8: 705–13.
13. Patrakeeva VP, Samodova AV. Vlijanie kratkovremennogo obshhego ohlazhdenija na migraciju, recirkuljaciju i jenergeticheskij resurs immunokompetentnyh kletok pericheskoj krovi cheloveka. Vestnik Ural'skoj medicinskoj akademicheskoj nauki. 2017; 14 (4): 362–8. Russian.
14. Patrakeeva VP. Izmenenie urovnja limfocitov pericheskoj venoznoj krovi kak metod ocenki individual'noj holodovoj chuvstvitel'nosti. V sbornike: Jekologicheskij monitoring: metody i podhody. Materialy Mezhdunarodnoj satellitnoj konferencii «Jekologicheskij monitoring: metody i podhody» i HH Mezhdunarodnogo simpoziuma «Slozhnye sistemy v jekstremal'nyh uslovijah». 20–24 sentjabrja 2021 g.; Krasnojarsk, 2021: 170–3. Russian.
15. Piché M-E, Tchernof A, Després J-P. Obesity phenotypes, diabetes, and cardiovascular diseases. Circ Res. 2020; 126 (11): 1477–500.
16. Després J-P. Body fat distribution and risk of cardiovascular disease. Circulation. 2012; 126 (10): 1301–13.
17. Sukkriang N, Chanprasertpinyo W, Wattanapisit A, Punsawad C, Thamrongrat N, Sangpoom S. Correlation of body visceral fat rating with serum lipid profile and fasting blood sugar in obese adults using a noninvasive machine. Heliyon. 2021; 7 (2): e06264.
18. Gugliucci A. Biomarkers of dysfunctional visceral fat. Advances in Clinical Chemistry. 2022; 109: 1–30.
19. Addo OY, Mei Z, Hod EA, Jefferds ME, Sharma AJ, Flores-Ayala RS, et al. Physiologically based serum ferritin thresholds for iron deficiency in women of reproductive age who are blood donors. Blood Advances. 2022; 6 (12): 3661–5.
20. Li M, Tang X, Liao Z, Shen C, Cheng R, Fanget M. Hypoxia and low temperature up-regulate transferrin to induce hypercoagulability at high altitude. Blood. 2022; 2022016410.
21. Kierans SJ, Taylor CT. Regulation of glycolysis by the hypoxia-inducible factor (HIF): implications for cellular physiology. J Physiol. 2021; 599 (1): 23–37.
22. Singh D, Arora R, Kaur P, Singh B, Mannan R, Arora S. Overexpression of hypoxia-inducible factor and metabolic pathways: possible targets of cancer. Cell Biosci. 2017; 7: 62.
23. Sautchuk Jr R, Eliseev RA. Cell energy metabolism and bone formation. Bone Reports. 2022; 16: 101594.
24. Kim H, Wrann CD, Jedrychowski M, Vidoni S, Kitase Y, Nagano K. et al Irisin mediates effects on bone and fat via αV integrin receptors. Cell. 2019; 178 (2): 507–8.
25. Fu T, Li C, Sun Z, Yan B, Wu Y, Huang Z, et al Integrin αV mediates the effects of irisin on human mature adipocytes. Obes Facts. 2022; 15 (3): 442–50.
26. Bi J, Zhang J, Ren Y, Du Z, Li T, Wang T, et al Irisin reverses intestinal epithelial barrier dysfunction during intestinal injury via binding to the integrin αVβ5 receptor. J Cell Mol Med. 2020; 24 (1): 996–1009.
27. Drewlo S, Johnson E, Kilburn BA, Kadam L, Armistead B, Kohan-Ghadr H-R. Irisin induces trophoblast differentiation via AMPK activation in the human placenta. J Cell Physiol. 2020; 235 (10): 7146–58.
28. Slate-Romano JJ, Yano N, Zhao TC. Irisin reduces inflammatory signaling pathways in inflammation-mediated metabolic syndrome. Molecular and Cellular Endocrinology. 2022; 552: 111676.
29. Pescador N, Villar D, Cifuentes D, Garcia-Rocha M, Ortiz-Barahona A, Vazquez S, et al. Hypoxia promotes glycogen accumulation through hypoxia inducible factor (HIF)-mediated induction of glycogen synthase 1. PLoS One. 2010; 5: e9644.
30. Vucetic M, Otasevic V, Korac A, Stancic A, Jankovic A, Markelic M, et al. Interscapular brown adipose tissue metabolic reprogramming during cold acclimation: Interplay of HIF-1α and AMPKα. Biochimica et Biophysica Acta (BBA) — General Subjects. 2011; 1810 (12): 1252–61.
31. Xu Y, Alfaro–Magallanes VM, Babitt JL. Physiological and pathophysiological mechanisms of hepcidin regulation: clinical implications for iron disorders. Br J Haematol. 2021; 193 (5): 882–93.
32. Kawabata H. Transferrin and transferrin receptors update. Free Radic Biol Med. 2019; 133: 46–54.

Литература

1. Zhu J, Thompson CB. Metabolic regulation of cell growth and proliferation. Nat Rev Mol Cell Biol. 2019; 20 (7): 436–50.
2. Ferranti CS, Cheng J, Thompson C, Zhang J, Rotolo JA, Buddaseth S, et al. Fusion of lysosomes to plasma membrane initiates radiation-induced apoptosis. J Cell Biol. 2020; 219 (4): e201903176.
3. Newman JC, He W, Verdin E. Mitochondrial protein acylation and intermediary metabolism: regulation by sirtuins and implications

for metabolic disease. J Biol Chem. 2012; 287 (51): 42436–43.

4. Zhang J, Xiang H, Liu J, Chen Y, He R-R, Liu B. Mitochondrial sirtuin 3: new emerging biological function and therapeutic target. Theranostics. 2020; 10 (18): 8315–42.

5. Reverdy C, Gitton G, Guan X, Adhya I, Krishna Dumpati R, Roy S, et al. Discovery of novel compounds as potent activators of Sirt3. Bioorganic & Medicinal Chemistry. 2022; 73: 116999.

6. Anderson KA, Hirschey MD. Mitochondrial protein acetylation regulates metabolism. Essays Biochem. 2012; 52: 23–35.

7. Bagul PK, Katare PB, Bugga P, Dinda AK, Banerjee SK. SIRT-3 modulation by resveratrol improves mitochondrial oxidative phosphorylation in diabetic heart through deacetylation of TFAM. Cells. 2018; 7 (12): 235.

8. Kincaid B, Bossy-Wetzel E. Forever young: SIRT3 a shield against mitochondrial meltdown, aging, and neurodegeneration. Front Aging Neurosci. 2013; 5: 48.

9. Anderson KA, Hirschey MD. Mitochondrial protein acetylation regulates metabolism. Essays Biochem. 2012; 52: 23–35.

10. Porter GA, Urciuoli WR, Brookes PS, Nadtochiy SM. SIRT3 deficiency exacerbates ischemia-reperfusion injury: implication for aged hearts. Am J Phys Heart Circ Phys. 2014; 306: H1602–H1609.

11. Bugga P, Alam J, Kumar R, Pal S, Chattopadyay N, Banerjee SK. Sirt3 ameliorates mitochondrial dysfunction and oxidative stress through regulating mitochondrial biogenesis and dynamics in cardiomyoblast. Cellular Signalling. 2022; 94: 110309.

12. Denko NC. Hypoxia, HIF1 and glucose metabolism in the solid tumour. Nature Reviews Cancer. 2008; 8: 705–13.

13. Патракеева В. П., Самодова А. В. Влияние кратковременного общего охлаждения на миграцию, рециркуляцию и энергетический ресурс иммунокомпетентных клеток периферической крови человека. Вестник Уральской медицинской академической науки. 2017; 14 (4): 362–8.

14. Патракеева В. П. Изменение уровня лимфоцитов периферической венозной крови как метод оценки индивидуальной холодовой чувствительности. В сборнике: Экологический мониторинг: методы и подходы. Материалы Международной сателлитной конференции «Экологический мониторинг: методы и подходы» и XX Международного симпозиума «Сложные системы в экстремальных условиях». 20–24 сентября 2021 г.; Красноярск, 2021: 170–3.

15. Piché M-E, Tchernof A, Després J-P. Obesity phenotypes, diabetes, and cardiovascular diseases. Circ Res. 2020; 126 (11): 1477–500.

16. Després J-P. Body fat distribution and risk of cardiovascular disease. Circulation. 2012; 126 (10): 1301–13.

17. Sukkriang N, Chanprasertpinyo W, Wattanapisit A, Punsawad C, Thamrongrat N, Sangpoom S. Correlation of body visceral fat rating with serum lipid profile and fasting blood sugar in obese adults using a noninvasive machine. Heliyon. 2021; 7 (2): e06264.

18. Gugliucci A. Biomarkers of dysfunctional visceral fat. Advances in Clinical Chemistry. 2022; 109: 1–30.

19. Addo OY, Mei Z, Hod EA, Jefferds ME, Sharma AJ, Flores-Ayala RS, et al. Physiologically based serum ferritin thresholds for iron deficiency in women of reproductive age who are blood donors. Blood Advances. 2022; 6 (12): 3661–5.

20. Li M, Tang X, Liao Z, Shen C, Cheng R, Fanget M. Hypoxia and low temperature up-regulate transferrin to induce hypercoagulability at high altitude. Blood. 2022; 2022016410.

21. Kierans SJ, Taylor CT. Regulation of glycolysis by the hypoxia-inducible factor (HIF): implications for cellular physiology. J Physiol. 2021; 599 (1): 23–37.

22. Singh D, Arora R, Kaur P, Singh B, Mannan R, Arora S. Overexpression of hypoxia-inducible factor and metabolic pathways: possible targets of cancer. Cell Biosci. 2017; 7: 62.

23. Sautchuk Jr R, Eliseev RA. Cell energy metabolism and bone formation. Bone Reports. 2022; 16: 101594.

24. Kim H, Wrann CD, Jedrychowski M, Vidoni S, Kitase Y, Nagano K. et al Irisin mediates effects on bone and fat via αV integrin receptors. Cell. 2019; 178 (2): 507–8.

25. Fu T, Li C, Sun Z, Yan B, Wu Y, Huang Z, et al Integrin αV mediates the effects of irisin on human mature adipocytes. Obes Facts. 2022; 15 (3): 442–50.

26. Bi J, Zhang J, Ren Y, Du Z, Li T, Wang T, et al Irisin reverses intestinal epithelial barrier dysfunction during intestinal injury via binding to the integrin αVβ5 receptor. J Cell Mol Med. 2020; 24 (1): 996–1009.

27. Drewlo S, Johnson E, Kilburn BA, Kadam L, Armistead B, Kohan-Ghadr H-R. Irisin induces trophoblast differentiation via AMPK activation in the human placenta. J Cell Physiol. 2020; 235 (10): 7146–58.

28. Slate-Romano JJ, Yano N, Zhao TC. Irisin reduces inflammatory signaling pathways in inflammation-mediated metabolic syndrome. Molecular and Cellular Endocrinology. 2022; 552: 111676.

29. Pescador N, Villar D, Cifuentes D, Garcia-Rocha M, Ortiz-Barahona A, Vazquez S, et al. Hypoxia promotes glycogen accumulation through hypoxia inducible factor (HIF)-mediated induction of glycogen synthase 1. PLoS One. 2010; 5: e9644.

30. Vucetic M, Otasevic V, Korac A, Stancic A, Jankovic A, Markelic M, et al. Interscapular brown adipose tissue metabolic reprogramming during cold acclimation: Interplay of HIF-1α and AMPKα. Biochimica et Biophysica Acta (BBA) — General Subjects. 2011; 1810 (12): 1252–61.

31. Xu Y, Alfaro–Magallanes VM, Babitt JL. Physiological and pathophysiological mechanisms of hepcidin regulation: clinical implications for iron disorders. Br J Haematol. 2021; 193 (5): 882–93.

32. Kawabata H. Transferrin and transferrin receptors update. Free Radic Biol Med. 2019; 133: 46–54.

COMPARATIVE ASSESSMENT OF THE IMPACT OF WEATHER AND CLIMATE CONDITIONS IN THE ARCTIC REGION BY BIOCLIMATIC INDICES

Rakhmanov RS[1] ✉, Narutdinov DA[2], Bogomolova ES[1], Razgulin SA[1]

[1] Privolzhsky Research Medical University, Nizhny Novgorod, Russia

[2] Medical service of military unit 73633, Krasnoyarsk, Russia

There are single and multi parameter bioclimatic indices that enable assessment of the impact of weather and climatic conditions on health of a human being. This study aimed to comparatively assess health risks in the Arctic's open area using the bioclimatic indices. Relying on the data from the Central Siberian Department for Hydrometeorology and Environmental Monitoring (Krasnoyarsk) that describe the weather on Cape Chelyuskin in 2010–2022, we assessed the temperature, the integral indicator of body cooling conditions (IIBCC), the wind chill factor (WCF), the effective (ET) and the net effective temperature (NET), and the universal thermal climate index (UTCI). It was found that the WCF temperature can characterize the degree of frost risk as established by the IIBCC: the indicator has the critical frost risk period lasting November through April, and the respective risk level by WCF is "discomfort" (coolness) and "very cold", that by UTCI — "extreme stress", by ET — "caution — frostbite of exposed skin" (shorter), by NET — "threat of frostbite" (longer). The IIBCC and the UTCI show that the risk of cold injury in the conditions of Cape Chelyuskin is year-round: according to the IIBCC, its level changes between moderate (4–6 months) and critical (4–6 months), and according to UTCI, it may be very strong (4 months), and very strong and extreme (8 months). We have proven the advantages of UTCI over other integral indicators in assessment of the cold-related health risk and updated the basis for the hygienic requirements regulating practice of work in the open or in unheated enclosed spaces during the cold season.

Keywords: Cape Chelyuskin, bioclimatic indices, cold injury risk

Author contribution: RS Rakhmanov — study design and concept, article authoring; ES Bogomolova — editing, approval of the final version of the article; DA Narutdinov — collection of the material, participation in its statistical processing; SA Razgulin — selection of the reference data sources, participation in the statistical processing of the material.

✉ **Correspondence should be addressed:** Rofail Salykhovich Rakhmanov
ploschad Minina i Pozharskog, 10/1, Nizhny Novgorod, Russia; raf53@mail.ru

Received: 31.10.2022 **Accepted:** 08.12.2022 **Published online:** 22.12.2022

DOI: 10.47183/mes.2022.041

СРАВНИТЕЛЬНАЯ ОЦЕНКА ВЛИЯНИЯ ПОГОДНО-КЛИМАТИЧЕСКИХ УСЛОВИЙ В АРКТИКЕ ПО БИОКЛИМАТИЧЕСКИМ ИНДЕКСАМ

Р. С. Рахманов[1] ✉, Д. А. Нарутдинов[2], Е. С. Богомолова[1], С. А. Разгулин[1]

[1] Приволжский исследовательский медицинский университет, Нижний Новгород, Россия

[2] Медицинская служба войсковой части 73633, Красноярск, Россия

Влияние на здоровье погодно-климатических условий определяют по одно- или многопараметрическим биоклиматическим индексам. Целью работы было провести сравнительную оценку риска для здоровья на открытой территории в Арктике по биоклиматическим индексам. По данным метеорологического центра "Среднесибирское управление по гидрометеорологии и мониторингу окружающей среды» (г. Красноярск) за 2010–2022 гг. на мысе Челюскин оценили температуру, интегральный показатель условий охлаждения организма (ИПУОО), ветро-холодовой индекс (ВХИ), эффективную (ЭТ) и эквивалентно-эффективную температуры (ЭЭТ), интегральный индекс теплового комфорта (UTCI). Определено, что температура ВХИ может характеризовать степень холодового риска, установленную по ИПУОО. Периоду критического холодового риска по ИПУОО (ноябрь–апрель) соответствует риск по ВХИ, оцениваемый как «дискомфорт» (прохлада) и «очень холодно», по UTCI — «экстремальный стресс»; по ЭТ — «осторожно — обморожение открытых участков кожи» (более короткий); по ЭЭТ — «угроза обморожения» (более длительный).   ИПУОО и UTCI указывают на круглогодичный риск холодовой травмы в условиях мыса Челюскин: по ИПУОО — умеренный (4–6 месяцев) и критический (4–6 месяцев), по UTCI очень сильный (4 месяца), а также очень сильный и экстремальный (8 месяцев). Доказано преимущество использования UTCI для оценки холодового риска для здоровья. Актуализируется вопрос нормирования гигиенических требований к режиму работ на открытой территории или в неотапливаемых помещениях в холодный период года.

Ключевые слова: мыс Челюскин, биоклиматические индексы, риск холодовой травмы

Вклад авторов: Р. С. Рахманов — разработка дизайна и концепции исследования, написание статьи; Е. С. Богомолова — редактирование, утверждение окончательного варианта статьи; Д. А. Нарутдинов — сбор материала, участие в статистической обработке материала; С. А. Разгулин — подбор литературных данных, участие в статистической обработке материала.

✉ **Для корреспонденции:** Рофаиль Салыхович Рахманов
пл. Минина и Пожарского, д. 10/1, г. Нижний Новгород, Россия; raf53@mail.ru

Статья получена: 31.10.2022 **Статья принята к печати:** 08.12.2022 **Опубликована онлайн:** 22.12.2022

DOI: 10.47183/mes.2022.041

The meteorological factors of the environment can have a pathological, sanogenic, stable and unstable, direct and indirect effect on an individual [1–3]. Therefore, the approach practiced to determine their significance for human health involves assessment of one factor or multicomponent physical quantities (expressed as bioclimatic indices), which allows establishing health risks related to morbidity, mortality, injuries, as well as describe meteorologically conditioned sensations in zones of comfort and discomfort and under extreme conditions [4–9].

Studies by various researchers prove that it is air temperature and wind speed that influence safety of work outdoors or the risk of frostbite associated therewith when the weather conditions are severe [10–12].

At the same time, air humidity or radiation temperature are two other major factors determining how safe it is to work in the open. For example, when the air temperature is extremely low and wind speed and humidity are high, clothing loses its heat insulation properties, which dramatically increases the

risk to human health [13, 14]. Radiation temperature (average temperature of radiation, including short-wave and long-wave radiation of the atmosphere) is one of the key components shaping the pattern of heat exchange between a person's body and the environment [15–16].

The purpose of this study is to comparatively assess weather and climatic conditions in the Arctic by bioclimatic indices, factoring in various combinations of air temperature, radiation temperature, air humidity and movement speed.

METHODS

The basis for the study were the weather and climatic conditions at Cape Chelyuskin (77.717,104.300). Using the data reflecting physical factors (temperature, relative air humidity, air speed (wind), all registered on a daily basis) collected by the Central Siberian Department for Hydrometeorology and Environmental Monitoring in 2010–2020, we calculated the daily average monthly indicators describing the conditions in the open:

– temperature;

– two parameter indicators (factor in temperature and wind speed), which are the integral indicator of body cooling conditions (IIBCC) and the wind chill factor (WCF);

– three parameter indicators (also factor in relative air humidity), which are the net effective temperature (NET) as per the Missenard's formula and the effective temperature (ET) under the Robert Steadman's formula;

– four parameter indicator (factors in radiation temperature), which is the universal thermal climate index (UTCI).

The IIBCC score was calculated as prescribed by the regulations (MR 2.2.7.2129-06). The health risk criteria levels are as follows: ≤ 34 — no risk; < 34 – ≤ 47 — moderate risk; < 47 – ≤ 57 — critical risk; > 57 — catastrophic risk. The IIBCC score allows determining the safe duration of work in the open: when the level of risk is moderate, it is safe to work outdoors for 60 minutes, when it is critical - for 1 minute only, and catastrophic risk level means it is safe to work outdoors for no more than half a minute.

The wind chill factor (°C) reflects the time of onset of hypothermia (without frostbite) in uncovered parts of a human body in cold environments. An environment is considered to be cold when the temperature there is +10 °C and below. For work that involves light physical exertion an environment with the temperature of +10 °C or below is a cold one. The pattern of establishing the health risk by WCF is as follows: from –10 to –24 °C — uncomfortable, chilly; from –25 to –34 °C — very cold, skin surface hypothermia; from –35 to –59 °C — extremely cold, possible hypothermia of the exposed parts of the body in 10 minutes; from –60 °C down — extremely cold, possible hypothermia of the exposed parts of the body in 2 minutes.

NET (°C) is used to establish thermal comfort/discomfort zones: from –24 °C and below (threat of frostbite); from –18 °C through –24 °C (very cold); from –12 °C through –18 °C (cold); from –6 °C through –12 °C (moderately cold); from –6 °C through 0 °C (very cool); from 0 °C to +6 °C (moderately cool) [17, 18].

We used the Steadman's formula to calculate the effective temperature (ET, °C). Subzero temperatures indicate the likelihood of frostbite (below –50°C — possibly in less than 5 minutes; from –38 °C to –50 °C — possible in 10–15 minutes; from –28 —C to –38 °C — possible after 20–30 minutes of exposure; from -28 °C to –27 °C — no danger for a properly dressed person) [19].

Using UTCI, we assessed the risk to health associated with the cold by stress, which can be weak (from 0 to +9.0 °C), moderate (from –13 to 0 °C), severe (from –27 to –13 °C), very

severe (from –40 to –27 °C), extreme (below –40 °C) [15, 20] and non-existent (from +9.0 to +18.0 °C). The UTCI values were calculated with the help of BioKlima 2.6 software [21].

To calculate the indicators, it was necessary to determine the daily average wind speed by months, which was done using the Beaufort scale (0 to 12 points), and the average daily relative humidity of the air, which could be dry (55.0% and below), moderately dry (56.0–70.0%), moderately humid (71.0–85.0%) and highly humid (85.0% and above) [22, 23].

We used the Statistica 6.1 software (StatSoft; USA) to statistically process the database. The mean values and standard errors (M ± m) were determined and Student's t-test employed. The differences were considered significant at p < 0.05.

RESULTS

The air in December through April (5 months) was moderately humid, and in May through October (6 months) — highly humid. In November, the air humidity level fluctuated between "moderately humid" and "highly humid" marks (Table 1). Compared to April, the relative humidity in May was greater (p = 0.001), same as for October and November (p = 0.001), which provoked special interest. Relative humidity reached its maximum in July and was decreasing afterwards.

The wind was moderate (4 points) throughout the year. There were no statistically significant differences identified by months of the year.

By average monthly temperatures, weather conditions in the Arctic allowed labeling it as "cold environment" throughout the year. The temperature in the open was above zero only in July and August; in June and September, it fluctuated between above zero subzero values (Table 2).

Temperature calculations factoring in the complex influence of various physical factors led to a conclusion that all the values obtained were below the outdoor temperatures considered.

All bioclimatic indices shared a distinctive feature: the temperature difference was decreasing January through August and then increasing again towards January (Table 3). Another feature was the dynamics of differences between WCF and ET values and temperature in the open. If the former follow a clear "decrease-increase" pattern, the latter's dynamics relative to the former fluctuates noticeably: in January–April, the temperatures were higher than those accepted for the former, in May and October they were equal to each other, and in June–September the values were lower.

As for the health risk criteria, the data were as follows: IIBCC signaled of the year-round risk of frostbite in exposed parts of the human body, with the values of this index reaching the top of the "moderate risk" span in April and November (Table 4); according to the WCF, hypothermia is a possibility 8 months in a year, with the most severe period ("extremely cold") lasting for 2-4 months; ET alarmed of a risk of frostbite during the winter months and in March, and NET cautioned of the risk of frostbite during 8 months of a year; the UTCI, same as IIBCC, indicated a year-round health risk associated with the cold.

DISCUSSION

According to regulations documents, the duration of warm and cold periods of the year is determined by the outdoor temperature, same as patterns of work in the open and work management conditions for cold environments. It also affects the body's energy expenditure and the need for proteins, fats and carbohydrates, as well as morbidity [13]. Extreme weather

Table 1. Average monthly wind speed and relative humidity at Cape Chelyuskin

Month of the year	Assessed indicators, M ± *m*	
	Relative humidity, %	Wind speed, m/s
January	81.1 ± 0.5	6.4 ± 0.5
February	81.6 ± 0.4	6.5 ± 0.4
March	81.6 ± 0.4	5.9 ± 0.4
April	81.5 ± 0.5	5.8 ± 0.3
May	88.5 ± 0.7	5.7 ± 0.2
June	89.2 ± 0.9	5.8 ± 0.2
July	90.5 ± 0.9	6.1 ± 0.2
August	89.6 ± 1.0	5.9 ± 0.3
September	88.5 ± 0.6	6.0 ± 0.3
October	85.1 ± 0.6	6.2 ± 0.3
November	81.1 ± 0.3	6.4 ± 0.4
December	82.1 ± 0.3	5.8 ± 0.3

conditions, including "cold waves", modify morbidity, mental health and mortality [24–26].

Some researchers believe that for cold conditions, it is best to rely on IIBCC and WCF in establishing the impact of bioclimatic factors of weather on a body [27]. Regression models of frostbite risk built on the values of temperature, wind speed and air humidity indicate that, for work done outdoors, the key factors are temperature and wind speed [10]. It is likely the reason behind the recommendation to rely on IIBCC and WCF for any practical purpose.

However, the "cold indices" do not allow establishing the degree of bioclimatic comfort peculiar to an environment. For this purpose, ET and NET can be used [17, 18].

Our data show that air humidity matters in assessing severity of the weather. For example, the ET value depends thereon: with the air moderately humid, the ET was higher than the temperature according to the WCF, and it decreases as the humidity increases. The NET indicator, which also accounts for air humidity, shows temperatures lower than those by WCF: the difference between them was 6.8 °C only in January, and during the remaining months it ranged from 10.4 °C to 11.7 °C.

However, all three indices (WCF, ET and NET) give different assessments of the impact of outdoor weather conditions on health of a human being. The WCF shows that for 8 months a year the conditions range from "discomfort" to "extremely cold", while 4 months present no risks. This index is a recommended basis for the work conditions management routines, including

work outdoors, in cold environment, with temperatures below +10 °C. But such conditions are already uncomfortable, which translates into the need for protection from the cold.

According to the Steadman's ET formula, there is a risk of cold injury only 4 months in a year. The comfort zone range considered in the context of this indicator is 17.2 to 21.7 °C [28], so it can be assumed that during the remaining months, when the temperature fluctuates between –4.1 and –25.0 °C, the conditions are also not comfortable for a person and can cause cooling of the body.

According to the Missenard's NET index, the period of cold in the considered area lasts longer, with its conditions more severe: it is significantly cold there for 8 months of a year, and the remaining 4 months are not warm but also cold.

The effect of cold and the pathogenesis associated therewith are based of body cooling. The related changes can be both functional and pathological. Compensatory reactions to local cooling cause reflex-driven shifts in the work of cardiovascular, respiratory and endocrine systems, with the gravity of such shifts depending on the body part undergoing cooling (more for face, less for hands). When the cold affects face, respiratory organs, arterial vessels shrink in the limb circulatory and coronary systems, which leads to the elevation of blood pressure. Chronic exposure to cold impairs motor activity, coordination and the ability to perform precise operations; the inhibitory processes in the cerebral cortex intensify and, following respiratory failure and oxygen deficiency,

Table 2. Annual temperature indicators, outdoor and by bioclimatic indices

Month of the year	Evaluation criteria					
	T, °C	IIBCC, points	WCF, °C	ET, °C	NET, °C	UTCI, °C
January	−26.0 ± 1.1	50.8 ± 0.8	−38.9 ± 1.7	−34.5 ± 0.4	−45.7 ± 1.3	−48.8 ± 1.4
February	−24.5 ± 1.0	50.2 ± 0.7	−37.0 ± 2.1	−33.1 ± 0.3	−49.2 ± 1.1	−49.7 ± 1.3
March	−22.9 ± 1.2	49.1 ± 0.8	−34.5 ± 2.3	−31.0 ± 0.3	−46.1 ± 1.2	−46.7 ± 0.9
April	−16.3 ± 0.4	45.9 ± 0.4	−26.0 ± 2.0	−24.1 ± 0.4	−37.3 ± 0.9	−41.0 ± 1.1
May	−8.0 ± 0.5	42.0 ± 0.4	−15.4 ± 2.8	−15.2 ± 0.4	−26.9 ± 0.6	−32.0 ± 0.6
June	−0.3 ± 0.2	38.5 ± 0.2	−5.8 ± 2.5	−6.8 ± 0.4	−16.5 ± 0.5	−23.1 ± 0.8
July	1.4 ± 0.2	37.9 ± 0.2	−3.7 ± 2.5	−5.0 ± 0.4	−14.5 ± 0.3	−21.7 ± 0.6
August	2.1 ± 0.4	37.4 ± 0.4	−2.8 ± 2.0	−4.1 ± 0.4	−13.2 ± 0.5	−20.2 ± 0.7
September	−0.05 ± 0.4	38.5 ± 0.4	−5.5 ± 2.0	−6.6 ± 0.4	−16.1 ± 0.7	−23.1 ± 1.1
October	−6.8 ± 0.6	41.8 ± 0.5	−14.3 ± 2.2	−14.3 ± 0.4	−25.4 ± 0.9	−32.3 ± 1.2
November	−17.0 ± 0.8	45.9 ± 0.6	−27.1 ± 1.9	−25.0 ± 0.4	−38.4 ± 1.1	−42.0 ± 1.3
December	−22.3 ± 0.7	48.7 ± 0.5	−33.6 ± 2.3	−30.3 ± 0.4	−45.3 ± 0.7	−45.8 ± 0.9

Table 3. Fluctuations of temperature by bioclimatic indices relative to the temperature registered in the open

Month of the year	Absolute values of bioclimatic temperature fluctuations			
	WCF, °C	ET, °C	NET, °C	UTCI, °C
January	–12.9	–8.5	–19.7	–22.8
February	–12.3	–8.4	–24.7	–25.0
March	–11.6	–8.1	–23.2	–23.8
April	–9.7	–7.8	–21.0	–24.7
May	–7.4	–7.2	–18.9	–24.0
June	–5.5	–6.5	–16.2	–22.8
July	–2.3	–3.6	–13.1	–20.3
August	–0.7	–2.0	–11.1	–18.1
September	–5.5	–6.6	–16.1	–23.1
October	–7.5	–7.5	–18.6	–25.5
November	–10.1	–8.0	–21.4	–25.0
December	–11.3	–8.0	–23.0	–23.5

"polar hypoxia syndrome", "chronic hypoxic syndrome" or "cold hypoxia" may develop [11, 12, 23, 29–31] . Cold violates nutrient metabolism, which increases the risk of diseases and disorders [14].

According to two bioclimatic indices (IIBCC and UTCI), the risk associated with cold is real all the year round, i.e., frostbite can develop in uncovered areas of the body. But, on the one hand, the first bioclimatic index does not produce the equivalent temperature value determined based on temperature and wind speed. This value is taken from the table given in Appendix 6 to MR 2.2.7.2129-06 approved by the Chief Sanitary Officer of the Russian Federation. However, this table presents a fairly wide range of equivalent temperatures, which complicates selection of specific values. On the other hand, it does not account for the influence of air humidity and radiation temperature. Our data suggests that it corresponds to the equivalent temperatures determined with the help of the WCF formula.

The universal thermal climate index has given the lowest equivalent temperature values and shown a longer period of severe ambient conditions at Cape Chelyuskin. Against the temperature by WCF, the minimum difference therewith was 9.9°C (in January), the maximum — 18.0 °C (July and October). In general, the average annual temperature by WCF was 2.1 times lower than that by UTCI: –20.4 ± 4.0 °C versus –42.8 ± 3.3 °C ($p = 0.008$).

It looked interesting that the temperature values according to UTCI and Missenard's NET in December — March were almost equal.

Thus, based on the data describing Cape Chelyuskin, we have shown the advantages of using UTCI to assess the risk to human health associated with cold; this index can be used to predict the risk considering the severity of weather and climatic conditions. In addition, we generated the data in the context of assessment of the average values of physical indicators describing the conditions outdoors. A combination of maximum/minimum air humidity, extreme physical factor values (in this case, minimum temperature, maximum wind speed) and radiation temperature make the negative effect on the body much more pronounced. Probably, it is necessary to evaluate the influence of weather factors by extreme (unfavorable) values, as pointed out by other researchers [32].

This study updates the basis for the hygienic requirements regulating practice of work in the open or in unheated enclosed spaces during the cold season.

CONCLUSIONS

The temperature determined by the WCF formula (in degrees Celsius) can reflect the degree of cold risk established by the IIBCC in points. The latter indicator has the critical frost risk period lasting November through April, and the respective risk

Table 4. Characteristics of the risk criteria as factored by various bioclimatic indices

№	Index	Type of risk	Months of the year / number of month
1	IIBCC	Moderate	IV–XI (8–6)
		Critical	XII–III (4–6)
2	WCF	lacking	VI–IX (4)
		Discomfort, chill	V, X (2)
		Very cool	III–IV, XI–XII (4–2)
		Extremely cold	I–II (2–4)
3	ET	Lacking	IV–XI (8)
		Be careful — frostbite of exposed skin is possible after 20–30 minutes	XII–III (4)
4	NET	Cold	VI–IX (4)
		Very cold	Нет
		Threat of frostbite	X–V (8)
5	UTCI	Strong	VI–IX (4)
		Very strong	V, X (2)
		Extreme	XI–IV (6)

level by WCF is "discomfort" (coolness) and "very cold", that by UTCI — "extreme stress", by ET — "caution — frostbite of exposed skin" (shorter), by NET — "threat of frostbite" (longer). The IIBCC and the UTCI show that the risk of cold injury in the conditions of Cape Chelyuskin is year-round: according to the IIBCC, its level changes between moderate (4–6 months) and critical (4–6 months), and according to UTCI, it may be very strong (4 months), and very strong and extreme (8 months).

References

1. Veremchuk LV, Chelnokova BI. Vliyanie prirodno-ehkologicheskix uslovij na kachestvo sredy obitaniya cheloveka v Primorskom krae. Zdorov'e naseleniya i sreda obitaniya. 2013; 2 (239): 4–6. Russian.

2. Uyanaeva AI, Tupicyna YuYu, Rassulova MA, Turova EA, Lvova NV, Ajrapetova NS. Vliyanie klimata i pogody na mexanizmy formirovaniya povyshennoj meteochuvstvitel'nosti. Voprosy kurortologii, fizioterapii i lechebnoj fizicheskoj kul'tury. 2016; 93 (5): 52–57. Russian.

3. Grigoreva EA, Xristoforova NK. Bioklimat Dal'nego Vostoka Rossii i zdorov'e naseleniya. Ehkologiya cheloveka. 2019; 5: 4–10. DOI: 10.33396 / 1728-0869-2019-5-4-10. Russian.

4. Revich BA, Shaposhnikov DA. Osobennosti vozdejstviya voln xoloda i zhary na smertnost' v gorodax s rezko-kontinental'nym klimatom. Sibirskoe medicinskoe obozrenie. 2017; (2): 84–90. DOI: 10.20333/2500136-2017-2-84-90. Russian.

5. Shaposhnikov DA, Revich BA. O nekotoryx podxodax k vychisleniyu riskov temperaturnyx voln dlya zdorov'ya. Analiz riska zdorov'yu. 2018; 1: 22–31. DOI: 10.21668/health.risk/2018.1.03. Russian.

6. Shatrova NV, Shaposhnikov DA, Konstantinov PI, Revich BA. Opredelenie porogov temperaturno-zavisimoj smertnosti na osnove universal'nogo indeksa teplovogo komforta — UTCI. Analiz riska zdorov'yu. 2019; 3: 83–93. DOI: 10.21668/health.risk/2019.3.10. Russian.

7. Knaub RV, Ignateva AV. Ocenka ehnergeticheskix posledstvij zabolevaemosti i smertnosti lyudej ot klimaticheskix izmenenij na territorii Tomskoj oblasti Rossii. Sovremennye issledovaniya social'nyx problem. 2015; 4 (48): 466–87. Russian.

8. Sinicyn IS, Georgica IM, Ivanova TG. Bioklimaticheskaya xarakteristika territorii v mediko-geograficheskix celyax. Yaroslavskij pedagogicheskij vestnik. 2013; 3 (4): 279–83. Russian.

9. Chernyx DA, Tasejko OV. Ocenka riska ot temperaturnyx voln, vliyayushhix na povyshenie urovnya smertnosti naseleniya g. Krasnoyarska. Ehkologiya cheloveka. 2018; 2: 3–8. Russian.

10. Shipko YuV Shuvakin EV, Shuvaev MA. Regressionnye modeli ocenki bezopasnosti rabot personala na otkrytoj territorii v zhestkix pogodnyx usloviyax. Vozdushno-kosmicheskie sily. Teoriya i praktika. 2017; 1: 131–40. Russian.

11. Wenz J. What Is Wind Chill, and How Does It Affect the Human Body? Smithsonian Magazine. 2019; 30. Avalable from:https://www.smithsonianmag.com/science-nature/what-wind-chill-and-how-does-it-affect-human-body-180971376.

12. Vankov A. Explainer: What is Wind Chill? What are Its Effects? Posted on January 31, 2019. Avalable from: https://www.profolus.com/topics/explainer-what-is-wind-chill-what-are-its-effects.

13. Chashhin VP, Gudkov AB, Chashhin MV, i dr. Prediktivnaya ocenka individual'noj vospriimchivosti organizma cheloveka k opasnomu vozdejstviyu xoloda. Ehkologiya cheloveka. 2017; 5: 3–13. Russian.

14. Polyakova EM, Melcer AV. Sravnitel'nyj analiz sostoyaniya zdorov'ya rabotnikov, vypolnyayushhix trudovye operacii na otkrytoj territorii v xolodnyj period goda, po rezul'tatam anketirovaniya. Profilakticheskaya medicina. 2019; 4 (73): 35–44. Russian.

15. Fiala D, Havenith G, Brode P, Kampmann B, Jendritzky G. UTCI-Fiala multi-node model of human heat transfer and temperature regulation. Int J Biometeorol. 2012; 56 (3): 429–41.

16. Potchter O, Cohen P, Lin T-P, Matzarakis A, Total S. Environ Outdoor human thermal perception in various climates: A comprehensive review of approaches, methods and quantification. 2018; 631–2: 390–406. DOI: 10.1016/j.scitotenv.2018.02.276.

17. Tkachuk SV. Obzor indeksov stepeni komfortnosti pogodnyx uslovij i ix svyaz' s pokazatelyami smertnosti. Trudy gidrometeorologicheskogo nauchno-issledovatel'skogo centra RF. 2012; 347: 223–45. Russian.

18. Latysheva IV, Loshhenko KA, Potemkin VL, Potemkina TG, Astafeva NV. Integral'nye bioklimatologicheskie pokazateli v issledovaniyax klimata Irkutskoj oblasti za period 1970–2010 gg. Mezhdisciplinarnyj nauchnyj i prikladnoj zhurnal «Biosfera». 2014; 6 (3): 265–74. Russian.

19. Karandeev DYu. Ehffektivnaya temperatura kak faktor, vliyayushhij na ehlektropotreblenie goroda. Sovremennaya texnika i texnologii. 2015; 2. Avalable from (data obrashheniya: 01.11.2022): http://technology. snauka.ru/2015/02/5728. Russian.

20. Di Napoli C, Pappenberger F, Hannah LC. Assessingheat-related health risk in Europe via the Universal Thermal Climate Index (UTCI). Int J Biometeorol. 2018; 62 (7): 1155–65.

21. BioKlima 2.6, software package. Avalable from: www.igipz.pan.pl/ geoekoklimat/blaz/bioklima.htm.

22. Monmonier M. Defining the Wind: The Beaufort Scale, and How a 19th Century Admiral Turned Science into Poetry. Published online: 29 Feb 2008. Pages 474–5. DOI: https://doi.org/10.1111/j.0033-0124.2005.493_1.x.

23. Alenikova AEh, Tepisova EV. Analiz izmenenij gormonal'nogo profilya muzhchin g. Arxangel'ska v zavisimosti ot faktorov pogody. Vestnik Severnogo (Arkticheskogo) federal'nogo universiteta. Seriya: Mediko-biologicheskie nauki. 2014; 3: 5–15. Russian.

24. Pascal M. [Adaptation to extreme weather event is key to protection of human health]. Rev Mal Respir. 2022; 39 (8): 719–25. DOI: 10.1016/j.rmr.2022.08.003. Epub 2022 Sep 8.

25. Weilnhammer V, Schmid J, Mittermeier I, Schreiber F, Jiang L, Pastuhovic V, et al. Extreme weather events in Europe and their health consequences — A systematic review. Jnt J Hyg Environ Health. 2021; 233: 113688. DOI: 10.1016/j.ijheh.2021.113688. Epub 2021 Jan 30.

26. Ebi KL, Vanos J, Baldwin JW, Bell JE, Hondula DM, Errett NA, et al. Extreme Weather and Climate Change: Population Health and Health System Implications. Annu Rev Public Health. 2021; 42: 293–315. DOI: 10.1146/annurev-publhealth-012420-105026. Epub 2021 Jan 6.

27. Shipko YuV, Shuvakin EV, Ivanov AV. Obobshhennyj bioklimaticheskij pokazatel' bezopasnosti rabot na otkrytom vozduxe v surovyx pogodnyx usloviyax. Vestnik KVGU, Seriya: geografiya. Geoehkologiya. 2015; 3: 33–39. Russian.

28. Bol'shaya medicinskaya ehnciklopediya: Ehffektivnaya temperatura. Avalable from: http://bigmeden.ru/article/Ehffektivnaya_Temperatura. Russian.

29. Afanasev RF, Burmistrova OV, Bobrov AF. Xolod, kriterii ocenki i prognozirovanie riska oxlazhdeniya cheloveka. Byulleten' VSNC SO RAMN. 2006; 3 (49):13–18. Russian.

30. Bocharov MI. Termoregulyaciya organizma pri xolodovyx vozdejstviyax (obzor). Soobshhenie 1. Vestnik Severnogo (Arkticheskogo) federal'nogo universiteta. Seriya «Mediko-biologicheskie nauki». 2015; 1: 5–15. Russian.

31. Bocharov MI. Termoregulyaciya organizma pri xolodovyx vozdejstviyax (obzor). Soobshhenie II. Vestnik Severnogo (Arkticheskogo) Federal'nogo universiteta. Seriya «Mediko-biologicheskie nauki». 2015; 2: 5–17. Russian.

32. Mastryukov SI, Chervyakova IV Obzor sovremennyx otechestvennyx i zarubezhnyx metodov ocenki vetrovogo oxlazhdeniya cheloveka. Navigaciya i gidrografiya. 2014; 38: 83–90. Russian.

Epub 2018 Mar 16.

Литература

1. Веремчук Л. В., Челнокова Б. И. Влияние природно-экологических условий на качество среды обитания человека в Приморском крае. Здоровье населения и среда обитания. 2013; 2 (239): 4–6.
2. Уянаева А. И., Тупицына Ю. Ю., Рассулова М. А., Турова Е. А., Львова Н. В., Айрапетова Н. С. Влияние климата и погоды на механизмы формирования повышенной метеочувствительности. Вопросы курортологии, физиотерапии и лечебной физической культуры. 2016; 93 (5): 52–57.
3. Григорьева Е. А., Христофорова Н. К. Биоклимат Дальнего Востока России и здоровье населения. Экология человека. 2019; 5: 4–10. DOI: 10.33396 / 1728-0869-2019-5-4-10.
4. Ревич Б. А., Шапошников Д. А. Особенности воздействия волн холода и жары на смертность в городах с резко-континентальным климатом. Сибирское медицинское обозрение. 2017; (2): 84–90. DOI: 10.20333/2500136-2017-2-84–90.
5. Шапошников Д. А., Ревич Б. А. О некоторых подходах к вычислению рисков температурных волн для здоровья. Анализ риска здоровью. 2018; 1: 22–31. DOI: 10.21668/health.risk/2018.1.03.
6. Шатрова Н. В., Шапошников Д. А., Константинов П. И., Ревич Б. А. Определение порогов температурно-зависимой смертности на основе универсального индекса теплового комфорта – UTCI. Анализ риска здоровью. 2019; 3: 83–93. DOI: 10.21668/health.risk/2019.3.10.
7. Кнауб Р. В., Игнатьева А. В. Оценка энергетических последствий заболеваемости и смертности людей от климатических изменений на территории Томской области России. Современные исследования социальных проблем. 2015; 4 (48): 466–87.
8. Синицын И. С., Георгица И. М., Иванова Т. Г. Биоклиматическая характеристика территории в медико-географических целях. Ярославский педагогический вестник. 2013; 3 (4): 279–83.
9. Черных Д. А., Тасейко О. В. Оценка риска от температурных волн, влияющих на повышение уровня смертности населения г. Красноярска. Экология человека. 2018; 2: 3–8.
10. Шипко Ю. В. Шувакин Е. В., Шуваев М. А. Регрессионные модели оценки безопасности работ персонала на открытой территории в жестких погодных условиях. Воздушно-космические силы. Теория и практика. 2017; 1: 131–40.
11. Wenz J. What Is Wind Chill, and How Does It Affect the Human Body? Smithsonian Magazine. 2019; 30. Avalable from:https://www.smithsonianmag.com/science-nature/what-wind-chill-and-how-does-it-affect-human-body-180971376.
12. Vankov A. Explainer: What is Wind Chill? What are Its Effects? Posted on January 31, 2019. Avalable from: https://www.profolus.com/topics/explainer-what-is-wind-chill-what-are-its-effects.
13. Чащин В. П., А. Б. Гудков А. Б., Чащин М. В, и др. Предиктивная оценка индивидуальной восприимчивости организма человека к опасному воздействию холода. Экология человека. 2017; 5: 3–13.
14. Полякова Е. М., Мельцер А. В. Сравнительный анализ состояния здоровья работников, выполняющих трудовые операции на открытой территории в холодный период года, по результатам анкетирования. Профилактическая медицина. 2019; 4 (73): 35–44.
15. Fiala D, Havenith G, Brode P, Kampmann B, Jendritzky G. UTCI-Fiala multi-node model of human heat transfer and temperature regulation. Int J Biometeorol. 2012; 56 (3): 429–41.
16. Potchter O, Cohen P, Lin T-P, Matzarakis A, Total S. Environ Outdoor human thermal perception in various climates: A comprehensive review of approaches, methods and quantification.

17. 2018; 631–2: 390–406. DOI: 10.1016/j.scitotenv.2018.02.276. Epub 2018 Mar 16.
17. Ткачук С. В. Обзор индексов степени комфортности погодных условий и их связь с показателями смертности. Труды гидрометеорологического научно-исследовательского центра РФ. 2012; 347: 223–45.
18. Латышева И. В., Лощенко К. А., Потемкин В. Л., Потемкина Т. Г., Астафьева Н. В. Интегральные биоклиматологические показатели в исследованиях климата Иркутской области за период 1970–2010 гг. Междисциплинарный научный и прикладной журнал «Биосфера». 2014; 6 (3): 265–74.
19. Карандеев Д. Ю. Эффективная температура как фактор, влияющий на электропотребление города. Современная техника и технологии. 2015; 2. Avalable from (дата обращения: 01.11.2022): http://technology. snauka.ru/2015/02/5728.
20. Di Napoli C, Pappenberger F, Hannah LC. Assessingheat-related health risk in Europe via the Universal Thermal Climate Index (UTCI). Int J Biometeorol. 2018; 62 (7): 1155–65.
21. BioKlima 2.6, software package. Avalable from: www.igipz.pan.pl/ geoekoklimat/blaz/bioklima.htm.
22. Monmonier M. Defining the Wind: The Beaufort Scale, and How a 19th Century Admiral Turned Science into Poetry. Published online: 29 Feb 2008. Pages 474–5. DOI: https://doi.org/10.1111/j.0033-0124.2005.493_1.x.
23. Аленикова А. Э., Теписова Е. В. Анализ изменений гормонального профиля мужчин г. Архангельска в зависимости от факторов погоды. Вестник Северного (Арктического) федерального университета. Серия: Медико-биологические науки. 2014; 3: 5–15.
24. Pascal M. [Adaptation to extreme weather event is key to protection of human health]. Rev Mal Respir. 2022; 39 (8): 719–25. DOI: 10.1016/j.rmr.2022.08.003. Epub 2022 Sep 8.
25. Weilnhammer V, Schmid J, Mittermeier I, Schreiber F, Jiang L, Pastuhovic V, et al. Extreme weather events in Europe and their health consequences — A systematic review. Jnt J Hyg Environ Health. 2021; 233: 113688. DOI: 10.1016/j.ijheh.2021.113688. Epub 2021 Jan 30.
26. Ebi KL, Vanos J, Baldwin JW, Bell JE, Hondula DM, Errett NA, et al. Extreme Weather and Climate Change: Population Health and Health System Implications. Annu Rev Public Health. 2021; 42: 293–315. DOI: 10.1146/annurev-publhealth-012420-105026. Epub 2021 Jan 6.
27. Шипко Ю. В., Шувакин Е. В., Иванов А. В. Обобщенный биоклиматический показатель безопасности работ на открытом воздухе в суровых погодных условиях. Вестник КВГУ, Серия: география. Геоэкология. 2015; 3: 33–39.
28. Большая медицинская энциклопедия: Эффективная температура. Avalable from: http://bigmeden.ru/article/Эффективная_Температура.
29. Афанасьев Р. Ф., Бурмистрова О. В., Бобров А. Ф. Холод, критерии оценки и прогнозирование риска охлаждения человека. Бюллетень ВСНЦ СО РАМН. 2006; 3 (49):13–18.
30. Бочаров М. И. Терморегуляция организма при холодовых воздействиях (обзор). Сообщение 1. Вестник Северного (Арктического) федерального университета. Серия «Медико-биологические науки». 2015; 1: 5–15.
31. Бочаров М. И. Терморегуляция организма при холодовых воздействиях (обзор). Сообщение II. Вестник Северного (Арктического) Федерального университета. Серия «Медико-биологические науки». 2015; 2: 5–17.
32. Мастрюков С. И., Червякова И. В. Обзор современных отечественных и зарубежных методов оценки ветрового охлаждения человека. Навигация и гидрография. 2014; 38: 83–90.

SWOT ANALYSIS OF ORGANIZATION OF ANTI-DOPING MEASURES IN THE CONTEXT OF MEDICAL AND BIOLOGICAL SUPPORT OF ATHLETES

Derevoedov AA[1], Zholinsky AV[1], Feshchenko VS[1,2], Vykhodets IT[2], Stashchuk KA[1], Pavlova AA[1] ✉

[1] Federal Research and Clinical Center of Sports Medicine and Rehabilitation of Federal Medical Biological Agency, Moscow, Russia

[2] Pirogov Russian National Research Medical University, Moscow, Russia

The anti-doping efforts on the part of medics should be constantly improved, which means the exploration and analysis of ways to increase the effectiveness of such efforts should be constant. SWOT analysis (Strengths, Weaknesses, Opportunities, Threats) is one of such ways. It investigates internal problems and resources of an organization and the influence of external factors. This study aimed to improve the anti-doping efforts based on the analysis of their strengths and weaknesses, taking into account external threats and directions of development. We have conducted an express SWOT analysis of anti-doping work in medical organizations of the Federal Medical Biological Agency of Russia and compiled a simple matrix. The factors under consideration are internal, which can be controlled, and external, which are often uncontrollable but should be accounted for. We identified the most significant factors influencing organization of this line of work, compiled the SWOT matrix that allows assessing the possible resources for intensifying the anti-doping work, determined its strengths and weaknesses, threats and opportunities imposed by the environment in this activity takes place in. The express SWOT analysis enabled evaluation of the factors that have the greatest impact on the organization of anti-doping work. Informational and educational programs, including workshops for medics and monitoring of their level of knowledge, can be the key line of activity in the context of such efforts.

SWOT-АНАЛИЗ ОРГАНИЗАЦИИ АНТИДОПИНГОВЫХ МЕРОПРИЯТИЙ ПРИ ПРОВЕДЕНИИ МЕДИКО-БИОЛОГИЧЕСКОГО ОБЕСПЕЧЕНИЯ СПОРТСМЕНОВ

А. А. Деревоедов[1], А. В. Жолинский[1], В. С. Фещенко[1,2], И. Т. Выходец[2], К. А. Стащук[1], А. А. Павлова[1] ✉

[1] Федеральный научно-клинический центр спортивной медицины и реабилитации Федерального медико-биологического агентства, Москва, Россия

[2] Российский национальный исследовательский медицинский университет имени Н. И. Пирогова, Москва, Россия

В связи с необходимостью совершенствования антидопинговой работы врачей требуется постоянный анализ и поиск путей повышения ее эффективности. Одним из таких направлений является SWOT-анализ (от англ. strengths, weaknesses, opportunities, threats), основанный на изучении внутренних проблем и ресурсов организации и влияния внешних факторов. Целью исследования было совершенствование антидопинговой работы на основе анализа сильных и слабых ее сторон с учетом внешних угроз и направлений развития. Проведен экспресс SWOT-анализ антидопинговой работы в медицинских организациях Федерального медико-биологического агентства России с составлением простой матрицы. Рассмотрены внутренние факторы, модификация которых возможна, а также внешние факторы, влияние на которые зачастую невозможно, но они должны быть приняты во внимание. Выделены наиболее значимые факторы, влияющие на организацию этого раздела работы, составлена матрица SWOT, позволяющая оценить возможные ресурсы активизации антидопинговой работы, ее сильные и слабые стороны, а также угрозы и возможности, выявленные в результате анализа среды, в которой осуществляется эта деятельность. Экспресс SWOT-анализ позволил оценить факторы, оказывающие наибольшее влияние на организацию антидопинговой работы. Основным направлением этой работы могут быть информационно-образовательные программы, включая проведение семинаров и контроль уровня знаний врачей.

In medical organizations operating under the Federal Medical Biological Agency (FMBA of Russia), the activities aimed at prevention of use of doping in sports (anti-doping activities) are a constant part of work performed on an ongoing basis, as prescribed by the regulations.

Since 2017, these activities have been structured with the aim of creating a system helping clinicians to prepare Therapeutic Use Exemption (TUE) applications as the main component of anti-doping work. A number of regulatory documents were developed [1, 2], organizational events conducted, regular publication of reference, information and educational materials set up, and most importantly, from then on, clinicians can request and receive assistance at any stage of preparing the said TUE applications.

The effectiveness of anti-doping activities was constantly analyzed; a number of weaknesses therein were identified and eliminated, and some sections improved. The quality of the TUE application documents prepared by medics of FMBA's medical organizations was also controlled on a regular basis.

Whenever possible, the identified deficiencies were remedied immediately, for those that could not be addressed without delay there were developed remedial action suggestions. The risks of violations of anti-doping rules by an athlete or his/her supporting staff cannot be completely and permanently eliminated.

Seeking to further improve anti-doping work, we analyzed its strengths and weaknesses, external threats and directions of development, i.e., did a SWOT (strengths, weaknesses, opportunities, threats) analysis.

There are various approaches to the analysis of effectiveness of anti-doping measures taken by medical professionals. SWOT analysis is a universal matrix that allows not only listing the key resources of an organization and outside threats but also grouping them in an understandable way as the basis for continuous effective planning.

Division of external factors into those that can be predicted and addressed with organizational measures and those that are unpredictable allows identifying the main risks and ways to overcome or mitigate them.

In general, SWOT analysis is one of the components of a comprehensive approach to improving the counter-doping measures as practiced by medical professionals in sports; it enables assessment of the dynamics and evaluation of individual changes in this work.

This study aimed to evaluate various aspects of activities of an organization from the viewpoint of effectiveness of anti-doping measures in the context of biomedical support (BMS) of the Russian Federation national team athletes while factoring in internal resources, external threats and risks subject to constant monitoring and mitigation and ultimately seeking to improve the results of this work.

METHODS

SWOT is a list of an organization's strengths and weaknesses based on the examination of its resources, as well as a register of threats and opportunities identified through analysis of the environment it operates in [3]. Planning based on SWOT should build on strengths and existing opportunities, account for threats and overcome weaknesses (figure).

According to some researchers, SWOT analysis is one of the most popular strategy tools among managers [4].

The analysis may yield various SWOT matrices; its main purpose is to assess the current state of the company or important lines of its business and, based of this assessment, develop a strategy and an action plan aimed at improving work efficiency.

Applied in a broader sense, the SWOT method allows structuring a subject matter into a clear matrix that makes positive and negative sides easily seen from the first sight (instead of making a list of advantages and disadvantages) [5]. Strengths and weaknesses reflect whether an organization has internal resources needed to achieve the set goals (improved effectiveness of anti-doping activities, in this case) or not.

RESULTS

As prescribed by the SWOT analysis structure, we identified and analyzed the following aspects of anti-doping work.

Strengths (S) of organization and implementation of anti-doping measures in the context of BMS activities

In recent years, the patterns of anti-doping work as done by FMBA's medical specialists have changed significantly.

The strengths include, first of all, availability of highly professional personnel, organizational structure and documentary support of the anti-doping efforts:

Professional personnel

In a daily basis, medics rendering the BMS have to decide on prescribing substances, methods, dietary supplements while taking into account their anti-doping status. Most of them have the necessary experience and motivation for further improvement.

The developed programs of postgraduate education and programs designed for doctors of national teams

Recently, sections of the postgraduate programs covering the anti-doping issues have been updated. A special program for doctors of national teams was designed to help them in organizing the main sections of anti-doping work.

Availability of anti-doping regulatory documents by the Ministry of Health of Russia, FMBA of Russia and the Federal Research and Clinical Center of Sports Medicine and Rehabilitation

Since 2018, the main documents that regulate medical assistance to athletes of various levels (released by the Ministry of Health of Russia) have been updated. The entire system of anti-doping activities in medical organizations under the FMBA was structured by orders issued by the FMBA and the Federal Research and Clinical Center of Sports Medicine and Rehabilitation [1, 2].

Allocation of responsibility for anti-doping efforts in the FMBA's medical organizations

The order #49 of April 05, 2016 by FMBA of Russia prescribes selection of persons responsible for anti-doping activities in a medical organization, outlines their rights and obligations and states the procedure of interaction with other participants of the process [6].

Organization and development of a system designed to assist medics in their anti-doping efforts and, as part of that system, active interaction between a medic professional as a person responsible for counter-doping activities in a medical organization (a physician in a Russian national team) and a specialist in anti-doping measures from the Federal Research and Clinical Center of Sports Medicine and Rehabilitation under FMBA of Russia.

Constant updating of the information on anti-doping issues as relevant to medical professionals (comments to the Prohibited List [7], Permitted List [8], translations of articles covering anti-doping matters).

Two key documents to help medics have been published since 2018, Comments to the Prohibited List and Permitted List. In addition, on a regular basis, medical professionals receive translated articles and materials published to the websites of anti-doping organizations and medical journals.
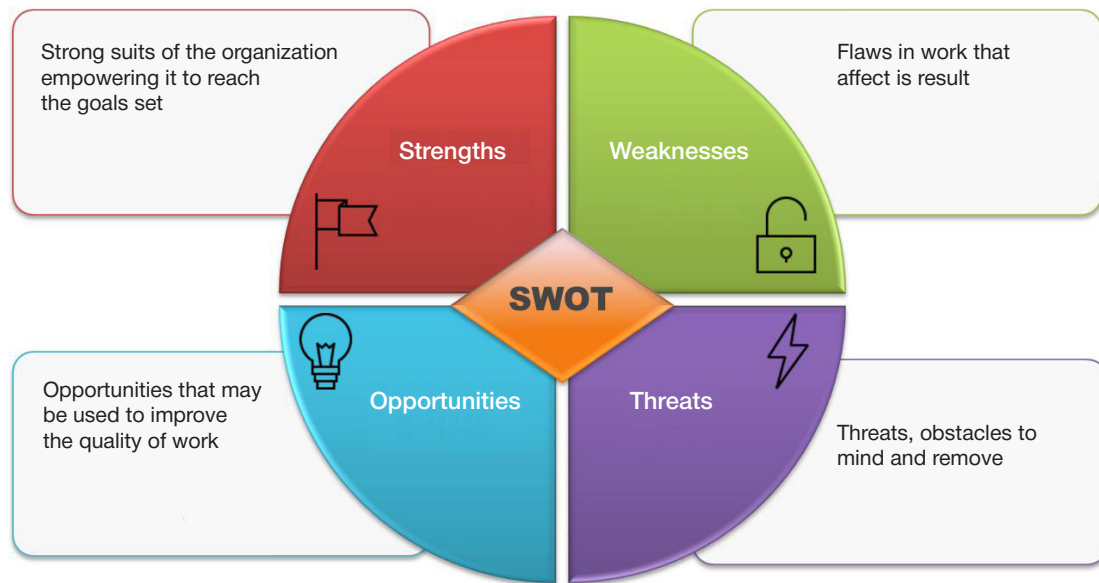
Fig. Key components investigated as part of the SWOT analysis

Weaknesses (W)

As a rule, weaknesses reflect problems and shortcomings in the ways of work the organization has adopted, and largely shape the options of their improvement. This section can be conditionally divided into main blocks: outdated documentation, personnel problems, behavioral (psychological) problems. Currently, it is possible to single out a number of weaknesses in anti-doping work.

Outdated regulatory documentation

A number of regulatory documents should be revised because they were put in force over 5 years ago and the governing anti-doping documentation is amended almost every year [6]. Not all of the amendments require modification of the regulatory documents, but some of them must be accounted for in the work organization process.

Lack of an anti-doping section in the Federal State Medical Informational and Analytical System

Anti-doping work was not factored into the Medical Informational and Analytical System enabling functioning and keeping of the electronic register of health status of the Russian national team athletes (MIAS) when it was developed. Systematization of the respective information in the database could significantly support organization of the efforts aimed at countering doping in sports. There were developed amendment and modification suggestions for the Sports Medicine Physician services part of the MIAS.

Lack of information about TU in outpatient records

Standard medical papers contain no sections related to the anti-doping activities. In particular, they include no records about TU applications. Therefore, any analysis of the said papers does not allow assessing quality of the anti-doping work.

Personnel

1) *staff turnover (doctors). As a rule, medical professionals starting in sports medicine, although experienced in other areas* *of medicine, have not previously dealt with doping problems in general and TU in particular.* The situation calls for appropriate educational activities with subsequent control of the knowledge acquired;

2) graduates without experience and basic knowledge entering the field. This point is similar to the one above, although young doctors have a chance to learn at the continued education cycles covering anti-doping measures (developed for various medical specialties). In any case, young specialists have no experience of such work;

3) long trips with the national teams that prevent the involved medics from continuing their education. Doctors of the national teams can spend most of the year at training camps, which disallows their participation in educational and knowledge control activities. This raises the importance of printed and electronic materials on anti-doping topics, on the one hand, and the capabilities enabling remote consultations on the other hand;

4) *doctors do not track the outcomes of applications they helped prepare.* Following up on applications to the final decisions by the anti-doping agency is an important resource for improvement of the anti-doping work done by medical professionals and the respective educational activities.

Psychological problems

Often, medics perceive doping and the related issues as something secondary, optional, interfering with their main work. The list of problems of this kind includes the following points:

1) *lack of interest on the part of doctors in learning more about the anti-doping measures, coupled with superficial attitude towards this subject*. A doctor starts looking for the relevant information and thus acquire new knowledge only when the matter at hand concerns him/her directly. This approach can translate into unprofessional decisions and increases the risk of possible sanctions from anti-doping agencies;

2) *lack of understanding on the part of healthcare professionals of the risks associated with the possible violations of anti-doping rules.* Poor awareness leads to underestimation of risks (sometimes, on the contrary, to a panic-driven avoidance of the problem), which may also be associated with inaptitude and unwillingness to use reference programs, with the habit of asking colleagues and coaches and not seeking answers in

Table. The SWOT analysis matrix

	Useful factors (S–O)	Threatening factors (W–T)
Internal factors (S–W)	Strengths – Professional personnel – Programs of postgraduate education and programs designed for doctors of national teams – Availability of anti-doping regulatory documents by the Ministry of Health of Russia, FMBA of Russia and the Federal Research and – Clinical Center of Sports Medicine and Rehabilitation – The system of assistance to physicians in anti-doping matters – Current anti-doping information for physicians"	Weaknesses – Staff turnover (doctors). – The doctors are not interested in learning more about the anti-doping measures, coupled with superficial attitude towards this subject. – Outdated individual regulations – Lack of information about TU in medical records and MIAS – Popularization of DS
External factors (O–T)	Opportunities – Constant monitoring of updates of documents made by anti-doping organizations – Introduction of amendments to the current regulatory documents – Improvement of educational programs for doctors – Introduction of amendments to the MIAS and outpatient card to incorporate the sports-related anti-doping efforts – Implementation of a system to control the anti-doping knowledge of doctors on a regular basis	Threats – Regular, not always announced changes in the documents released by anti-doping organizations – Reliance on European standards by anti-doping organizations developing materials for the physicians – Progressive accusatory bias in anti-doping legislation – Anti-doping organizations are not interested in cooperation – Risks associated with falsification of DS

documents or with persons responsible for countering doping in a medical organization. The situation is continually improving, more and more doctors realize the need for deeper knowledge of anti-doping matters, but the risks remain;

3) *the established opinion that the athlete is responsible for everything.* The recent anti-doping documents and new/updated Russian laws have made the doctor's responsibility for doping rule violations significantly more expanded, yet it is still a prevailing point of view that the responsibility for all violations lies solely with the athlete;

4) *unrestrained interest in dietary supplements (DS).* Some medical professionals have developed a dependence on fashionable, advertised and widely used, but far from always effective dietary supplements. The risks associated with poor control over their composition and possible falsification of such products are not taken into account;

5) *poor command of English on the part of the doctors.* This is a serious problem that limits the ability to work with professional publications most often released in English. The problem is not only psychological but also structural, and it requires a solution at the level of educational institutions.

Opportunities (O)

Opportunities reflect the dynamics of external factors and the effect they have on the organization of work. In some cases, opportunities can turn into threats and vice versa, depending on the situation and the availability of resources needed to use or counter them.

The two components that are affected by external factors as pertains the process of improvement of anti-doping activities are the documents adopted by anti-doping organizations or federal executive bodies and the status of medical professionals, specifically, their knowledge and skills they have acquired while learning and working.

Improvement of educational programs for doctors

Effective and regularly organized anti-doping education is the key prerequisite to prevention of violations of anti-doping rules and the main resource enabling anti-doping efforts in medical organizations. Implementation of the respective educational programs allows doctors to stay up-to-date with their knowledge, receive the necessary recommendations and materials covering the key areas of anti-doping work. This point was placed among the external factors because the

documents regulating educational activities and the content of such programs are approved outside the professional community and require quick and effective adaptation.

Introduction of amendments to the regulatory documents

Regular revisions of the main documents of anti-doping organizations (the Russian National Anti-Doping Rules, the Code of the World Anti-Doping Agency (WADA), the Prohibited List and other WADA international standards) require prompt introduction of amendments to the existing departmental documents.

Introduction of amendments to the MIAS and outpatient card to incorporate the sports-related anti-doping efforts

From the point of view of training, analysis of errors and medical care provision continuity, the introduction of these amendments is one of the key tasks. Solving it would also mean automation of registration of TU applications and their analysis by various parameters.

Implementation of a system to control the anti-doping knowledge of doctors on a regular basis

This approach is a continuation and a mandatory integral part of the educational process.

Threats (T)

The concept of threats in this case is a rather arbitrary one, since in some cases, with the right approach, they can also be a resource used in development of the organization.

This section includes the threats that cannot be mitigated on the level of medical practice and thus require actions influencing organization of work.

Regular changes in the documents of anti-doping organizations that should be incorporated into the regulations governing operations of the medical personnel

The frequency of introduction of amendments into the documents released by anti-doping organizations differs: the WADA Code is reviewed every 5 years, the Prohibited List — at least once a year, International Standards are amended, as a rule, once every 5 years (can be done more often), the

WADA guidelines and other advisory documents are changed regularly, and the changes often remain unannounced. It is necessary to monitor the anti-doping documents on a regular basis to prevent missing significant changes thereof.

Progressive accusatory bias in anti-doping legislation

As experience shows, each subsequent edition of the WADA Code has expanded list of anti-doping rule violations, and the sanctions against athlete's support personnel grow more and more strict. This is also true about internal Russian regulatory documents. Recently, the Criminal Code and the Code of Administrative Offenses have been supplemented with the relevant articles, and already there are cases of their real-life application.

In the case of anti-doping organizations, their desire to make the penalties more severe, including those applied to the athlete's support staff, does not correlate with the wish to increase the effectiveness of the main anti-doping tool, i.e., laboratory tests that return positive as a result of compilation of an effective test distribution plan.

Reliance on European standards by anti-doping organizations developing materials for doctors, the resulting presence of diseases and conditions there that are neither diagnosed nor treated in the Russian Federation or diagnosed and treated extremely rarely

The TUE Physician Guidelines developed by WADA [9] provide models of best practices that do not always coincide with the requirements of the Clinical Guidelines of the Russian Ministry of Health. Often, substances and methods from the Prohibited List are used to treat diseases that are not covered in the TUE Physician Guidelines. In such cases, the doctor must follow the national regulations and attach extracts therefrom to the TUE applications. These are some of the significant risks that require attention and competence from the doctor.

The WADA's TUE Physician Guidelines includes 18 diseases and conditions, some of which are practically not applied in the Russian clinical practice. Such diseases and conditions are ADHD, congenital sleep disorders, transgender athletes, neuropathic pain. Treatment of some of them involves substances prohibited in the Russian Federation, which must be taken into account when conducting therapy.

Discrepancies between Clinical Guidelines of the Russian Ministry of Health and the TUE Physician Guidelines

For example, according to the Clinical Guidelines by the Ministry of Health of Russia, the diagnostic sign of diabetes mellitus is the fasting glucose level of over 6.1 mmol/l [10]. According to the European criteria, the minimum level is 7 mmol/l [11]. There may be more discrepancies of this type in the regulations, but finding them would require a detailed analysis of the documents.

Secrecy in the work of anti-doping organizations

As a rule, anti-doping organizations do not employ medical professionals with practical experience, which affects the quality of the advisory services they provide. Doctors are not allowed to attend the TU conferences held annually by WADA and its structures, and information on the issues discussed is not readily available. Thus, the risks are growing up and the effectiveness of implementation of the results of such discussion (and decisions taken) grows down.

The SWOT matrix

There are several ways to summarize the results of a SWOT analysis. The most common approach is to create a so-called matrix, which allows bringing all sections of the SWOT analysis into a table that groups the key features by the selected criteria.

To form the matrix, we selected the approach that highlights useful and threatening factors and accounts for them being external or internal [4]. The most significant factors in each group were selected for the analysis.

According to the table, the organization has all the necessary resources to remedy the shortcomings (weaknesses) and mitigate the possible threats. Such resources include, first of all, active informational and educational work, as well as constant monitoring of changes in the documents released by the anti-doping organizations.

DISCUSSION

The main directions of a SWOT analysis applied to a medical organizations include investigation of its activities in general, analysis of the effectiveness of implementation of various preventive programs among different groups of population, introduction of various diagnostic and treatment methods, use of drugs etc. [3]. The available literature offers no information on application of a SWOT analysis to assess the effectiveness and planning of anti-doping activities in sport.

The anti-doping work of medical professionals, as an integral part of the BMS, is a small section thereof. At the same time, this work is important because of the urgency attached to it and the possible negative consequences associated with the risks of violations of anti-doping rules.

A key task, as it seems, is to bring the relevant sections of the MIAS and outpatient records in line with the anti-doping measures taken. The emergence of a digital component of anti-doping work can bring it to a new level with the possibility of analyzing documents and developing educational programs based thereon.

Essentially, amending the current regulatory documents is a technical task that also requires monitoring of changes introduced to the relevant documents by anti-doping organizations [1, 2, 6].

It is necessary to provide doctors with information when TUE Physicians Guidelines do not cover the case at hand and it is necessary to follow the Clinical Guidelines by the Ministry of Health of Russia. Some reference materials may have to be published, although this task is hampered by the constant changes in the documents by anti-doping organizations.

A number of threats (risks) cannot be compensated, eliminated or predicted. One of them is the desire of all parties involved in the anti-doping process to expand the responsibility of the medical personnel. Only once the regulatory documents are available will it be possible to understand the goals, the mechanism, and the risks themselves.

This approach, in fact, transfers the blame from ineffective doping control to specialists providing professional assistance to the athlete. A physician under constant pressure and control tries to avoid prescribing prohibited substances even when they should be prescribed, which can affect the efficacy of medical care. This is one possible reason for the relatively low number of TUEs that athletes apply for but that are usually initiated by a physician.

CONCLUSIONS

The analysis conducted as part of this study confirms the expediency of selection of the key anti-doping work improvement

directions, the first of which is the effective assistance to physicians in preparing TUE applications and development of information and educational programs and materials that factor in the changes made to the WADA documents and Russian regulations.

References

1. Prikaz FMBA Rossii ot 25.09.2020 № 262 «Ob utverzhdenii Poryadka oformleniya medicinskih dokumentov dlya zaprosa na terapevticheskoe ispol'zovanie zapreshhennoj substancii i (ili) metoda». Dostupno po ssylke: http://www.consultant.ru/document/cons_doc_LAW_428933/ (data obrashheniya 23.12.2022). Russian.
2. Prikaz FGBU FNKCSM FMBA Rossii # 157 ot 28.10.2020 «Poryadok oformleniya medicinskix dokumentov dlya zaprosa na terapevticheskoe ispol'zovanie zapreshhennoj substancii i (ili) zapreshhennogo metoda» (data obrashheniya 23.12.2022). Russian.
3. Stacey R. Strategic Management and Organisational Dynamics. London: Pitman, 1993; 538 p.
4. Überall M, Werner-Felmayer G. Integrative Biology and Big-Data-Centrism: Mapping out a Bioscience Ethics Perspective with a S.W.O.T. Matrix. OMICS 2019; 23 (8): 371–9. DOI: 10.1089/omi.2019.0043.
5. Madsen DØ, SWOT Analysis: A Management Fashion Perspective (March 21, 2016). International Journal of Business Research. 2016; 16 (1): 39–56. DOI: 10.18374/ijbr-16-1.3.
6. Prikaz Ministerstva zdravoohraneniya Rossijskoj Federacii i Federal'nogo mediko-biologicheskogo agentstva ot 05.04.2016 goda № 49 «O protivodejstvii primeneniyu dopinga v sporte i bor'be s nim». Dostupno po ssylke: http://www.consultant.ru/document/cons_doc_LAW_255161/ (data obrashheniya 23.12.2022). Russian.
7. Derevoedov AA, Vykhodets IEh, Vykhodets IT, Zholinsky AV, Pushkina TA, Feshchenko VS. Aktual'nye voprosy protivodejstviya dopingu v sporte v praktike vracha. Kommentarii k zapreshhennomu spisku — 2023. Rukovodstvo dlya vrachej po sportivnoj medicine. 2022; 28 s. Russian.
8. Derevoedov AA, Vykhodets IEh, Vykhodets IT, Zholinsky AV, Ovsyannikov IV, Pavlova AA, i dr. Aktual'nye voprosy protivodejstviya dopingu v sporte v praktike vracha. Broshyura Razreshennyj spisok. Versiya 5.0. Rukovodstvo dlya vrachej po sportivnoj medicine. 2022; 38 s. Russian.
9. TUE Physician Guidelines. Available from: https://www.wada-ama.org/en/search?q=TUE%20Physician%20Guidelines&filters%5Bcontent_type%5D%5B%5D=%22resource%22 (дата обращения 23.12.2022).
10. Dedov II, Shestakova MV, Majorov AYu, redaktory. Algoritmy specializirovannoj medicinskoj pomoshhi bol'nym saharnym diabetom. M., 2021. Dostupno po ssylke: https://doi.org/10.14341/DM12802. Russian.
11. Harreiter J, Roden M. Diabetes mellitus-Definition, classification, diagnosis, screening and prevention Wien Klin Wochenschr. 2019; 131 (Suppl 1): 6–15. DOI: 10.1007/s00508-019-1450-4.

Литература

1. Приказ ФМБА России от 25.09.2020 № 262 «Об утверждении Порядка оформления медицинских документов для запроса на терапевтическое использование запрещенной субстанции и (или) метода». Доступно по ссылке: http://www.consultant.ru/document/cons_doc_LAW_428933/ (дата обращения 23.12.2022).
2. Приказ ФГБУ ФНКЦСМ ФМБА России № 157 от 28.10.2020 «Порядок оформления медицинских документов для запроса на терапевтическое использование запрещенной субстанции и (или) запрещенного метода» (дата обращения 23.12.2022).
3. Stacey R. Strategic Management and Organisational Dynamics. London: Pitman, 1993; 538 p.
4. Überall M, Werner-Felmayer G. Integrative Biology and Big-Data-Centrism: Mapping out a Bioscience Ethics Perspective with a S.W.O.T. Matrix. OMICS 2019; 23 (8): 371–9. DOI: 10.1089/omi.2019.0043.
5. Madsen DØ, SWOT Analysis: A Management Fashion Perspective (March 21, 2016). International Journal of Business Research. 2016; 16 (1): 39–56. DOI: 10.18374/ijbr-16-1.3.
6. Приказ Министерства здравоохранения Российской Федерации и Федерального медико-биологического агентства от 05.04.2016 года № 49 «О противодействии применению допинга в спорте и борьбе с ним». Доступно по ссылке: http://www.consultant.ru/document/cons_doc_LAW_255161/ (дата обращения 23.12.2022).
7. Деревоедов А. А., Высотский И. Э., Выходец И. Т., Жолинский А. В., Пушкина Т. А., Фещенко В. С. Актуальные вопросы противодействия допингу в спорте в практике врача. Комментарии к запрещенному списку — 2023. Руководство для врачей по спортивной медицине. 2022; 28 с.
8. Деревоедов А. А., Высотский И. Э., Выходец И. Т., Жолинский А. В., Овсянников И. В., Павлова А. А., и др. Актуальные вопросы противодействия допингу в спорте в практике врача. Брошюра Разрешенный список. Версия 5.0. Руководство для врачей по спортивной медицине. 2022; 38 с.
9. TUE Physician Guidelines. Available from: https://www.wada-ama.org/en/search?q=TUE%20Physician%20Guidelines&filters%5Bcontent_type%5D%5B%5D=%22resource%22 (дата обращения 23.12.2022).
10. Дедов И. И., Шестакова М. В., Майоров А. Ю., редакторы. Алгоритмы специализированной медицинской помощи больным сахарным диабетом. М., 2021. Доступно по ссылке: https://doi.org/10.14341/DM12802.
11. Harreiter J, Roden M. Diabetes mellitus-Definition, classification, diagnosis, screening and prevention Wien Klin Wochenschr. 2019; 131 (Suppl 1): 6–15. DOI: 10.1007/s00508-019-1450-4.

EFFECTS OF THE SOCIAL MEDIA INTERFERENCE FACTOR ON MEMORY CONSOLIDATION IN ADOLESCENTS

Petrash EA[1] ✉, Nikishina VB[1], Razuvaeva TN[2], Sokolyskaya MV[1], Kuznetsova AA[3], Zapesotskaya IV[1]

[1] Pirogov Russian National Research Medical University, Moscow, Russia

[2] Belgorod State University, Belgorod, Russia

[3] Kursk State Medical University, Kursk, Russia

The relevance of this study is due to the need to answer the question of how the factors of digital medium affect the development of mental functions in the younder generation. The study was aimed to assess the effects of the social media interference factor on memory (auditory-speech and visual-figurative) consolidation in adolescents. The sample was 130 adolescents aged 11–17. The groups were formed based on the age stages (11–12, 13–14, 15–17 years). The study involved the use of the method for the diagnosis of the short-term auditory-speech and visual-figurative memory span. Viewing video content and reading the fragment of the fiction book were used as interference. A significant decrease in the short-term auditory-speech and visual-figurative memory span was observed in adolescents. The short-term memory span is reduced in the context of social media interference (prolonged continuous viewing the heterogenous visual-acoustic and visual-speech content). The high risk of the long-term memory loss due to the impact of the social media interference factor on memory consolidation in adolescents is empirically proven. The more the duration of the maximum continuous video stream and the total time the adolescents spend on Internet (including social media), the larger is the loss of information.

Keywords: short-term memory, auditory-speech memory, visual-figurative memory, interference, visual-acoustic content, visual-speech content

ВЛИЯНИЕ ФАКТОРА ИНТЕРФЕРЕНЦИИ СОЦИАЛЬНЫХ СЕТЕЙ НА ПРОЦЕССЫ КОНСОЛИДАЦИИ ПАМЯТИ У ПОДРОСТКОВ

Е. А. Петраш[1] ✉, В. Б. Никишина[1], Т. Н. Разуваева[2], М. В. Сокольская[1], А. А. Кузнецова[3], И. В. Запесоцкая[1]

[1] Российский национальный исследовательский медицинский университет имени Н. И. Пирогова, Москва, Россия

[2] Белгородский государственный национальный исследовательский университет, Белгород, Россия

[3] Курский государственный медицинский университет, Курск, Россия

Актуальность настоящего исследования обусловлена необходимостью поиска ответа на вопрос о том, как факторы цифровой среды оказывают влияние на формирование психических функций подрастающего поколения. Целью работы было изучение влияния фактора интерференции социальных сетей на процессы консолидации памяти (слухоречевой и зрительно-образной) у подростков. Объем выборки составил 130 подростков в возрасте 11–17 лет. Формирование групп осуществляли по возрастным этапам (11–12, 13–14, 15–17 лет). Исследование осуществляли с использованием методик диагностики объема кратковременной слухоречевой и зрительно-образной памяти. В качестве интерферирующего воздействия выступали просмотр видеоконтента и прочтение фрагмента художественного произведения. Установлено значимое снижение объема кратковременной слухоречевой и зрительно-образной памяти у подростков. В условиях интерферирующего воздействия социальных сетей (длительного непрерывного просмотра визуально-акустического и визуально-речевого контента гетерогенного содержания) происходит снижение объема кратковременной памяти. Эмпирически доказан высокий риск потери долговременной памяти под влиянием фактора интерференции социальных сетей на процессы консолидации памяти у подростков. Чем больше длина максимального непрерывного видеопотока, а также общая длительность нахождения подростков в интернете (в том числе в социальных сетях), тем больше объем потери информации.

Ключевые слова: кратковременная память, слухоречевая память, зрительно-образная память, интерференция, визуально-акустический контент, визуально-речевой контент

For the first time in the history of civilization, the current generation of adolescents lives in two realities, the one mediated by technical devices (digital reality) and another one not mediated by technical devices. The micro- and macrocharacteristics of both realities affect the younger generation mental development. Modern psychologists must now start raising specific questions of how the factors of digital environment affect the development of mental functions in the younger generation.

One of the popular theses on the theories of memory is the thesis that we are our memory. The issue of the impact of the factors of digital environment on memory processes in the younger generation is a specific research issue [1–8].

More than four and a half billion people all over the world (57.6% of the world's population) are active users of social media. Internet users on average spend 6 h 54 min a day online and are on 6–7 various social media (according to the Digital Global Statshot Report in partnership with We Are Social and Hootsuite, 2021).

Regardless of the legal and regulatory framework [9] (the children's use of Internet and social media is regulated by the the letter of the Ministry of Education and Science of the Russian Federation), as well as of the existing age limitations imposed by the social media and/or providers (for example, the TikTok user minimum age is 13 years), children find ways to bypass the established limitations. This significantly expands their access to the shared content with no age-restricted content.

The fundamental process of long-term memory formation referred to as consolidation occurs in many different types of memories, species and memory systems [2, 10, 11].

Initially, the memory is unstable and can be disturbed by several types of interference, including behavioral and pharmacological. Over time, the memory acquires resistance to these forms of interference due to consolidation [2]. Memory formation is a two-stage process. The first stage is a phase of short-term memory that lasts up to several tens of minutes. During this stage the memory is vulnerable to environmental influences: interference from new learning or alterations in gene expression. The phase of long-term memory, being a more stable structure formed 24 h after the engram emergence, constitutes the second stage of memory formation. A number of studies [10, 11] have shown that the consolidated memories that have passed the phase of long-term memory can also become labile, if a conditioned stimulus is applied after memory formation and stabilization. This reflects the process of memory reconsolidation [3, 5, 13].

Experimental studies of memory consolidation were focused on the time window of several hours after learning. Empirical evidence about the fact that memory consolidation in humans may take weeks, months or possibly years suggests that memory consolidation consists of various stages. The proof that different stages of consolidation depend on different cellular mechanisms and brain systems is represented by the findings of human and animal studies showing that hippocampal lesions usually disturb the recently acquired memories. However, the ability to recall past information is preserved.

System consolidation represents the changes associated with memory storage. Memory consolidation and storage involve activity in the hippocampus followed by such cortical areas as entorhinal cortex (CA1–CA3) and posterior parietal cortex [11]. A memory trace (engram) is formed in the hippocampus as a result of encoding information received from various sensory modalities. The incoming information is transformed into the integrated internal representation of the disparate elements of environmental perception that is interpreted and conceptualized by involving elements of past experience linked to actual experiences. Thus, internal representation is transformed into engram subsequently passing the stage of consolidation.

The method used in the study reported was developed based on the concept of working memory by B. B. Velichkovsky [4, 13] and the concept by K. V. Anokhin [14]. Memory, the higher mental function, is characterized by processuality and is implemented through memorizing. Memorizing ensures preservation of information content that goes through two stages (phases). The short-term stage is characterized by retaining the information stored in its fullest form (without losses or distortions of the content) over a short time. This is

a labile memory phase to which there corresponds retention of information trace in the form of the nerve impulse reverberation. The long-term stage of memorizing is characterized by reduction of the amount of information during the long-term storage without modification.

Consolidation that ensures the information content transition from the short-term to the long-term stage also involves further transformation of the information stored in accordance with the existing experience and addition of this information to the already existing information (incorporation into the system of long-term storage). The long-term memory involves preservation of the trace through consolidation and subsequent structural changes.

Working memory is a system of those cognitive processes that ensure rapid storage and processing of information. The working memory stores information using the mechanisms of short-term and long-term storage. Information is retrieved (this process is referred to as reconsolidation) from the long-term memory (that includes the system of images, system of symbols and signs, and the semantic system organized into holistic experience). Furthermore, information consolidated in prior experience is initially reconsolidated. Active reconstruction of information occurs during retrieval in case of memory reactivation that ensures information retrieval. Reconstruction is, in turn, accompanied by recategorization. Each round of recategorization is followed by reconsolidation (re-storing information). Each round of memory retrieval involves replacement of the old trace with the new content (the content could be partially or fully modified).

The interfering information (in our study this information is represented by the visual-acoustic and visual-speech content) occupies the short-term memory. This, in turn, results in consolidation of the initially limited information content.

The study was aimed to study the effects of the social media interference factor on memory consolidation in adolescents.

METHODS

The total sample was 130 in-school adolescents aged 11–17. Three study groups were formed based on age. The first one included 44 adolescents aged 11–12 (23 boys and 21 girls); the second one included 41 adolescents aged 13–14 (20 boys and 21 girls); the third one included 45 adolescents aged 15–17 (23 boys and 22 girls). The control groups also included adolescents of the specified age ranges: 46 people aged 11–12 (26 girls and 20 boys); 42 adolescents aged 13–14 (20 girls and 22 boys); 42 people aged 15–17 (23 girls and 19 boys). Inclusion criteria: screen time, i.e. the time spent on Internet, including social media, had to be at least 6 hrs a day.

The study was performed in three steps (Fig. 1).

Step one

The short-term auditory-speech and visual-figurative memory span was assessed together with the long-term memory span (delayed recall after 40 min); the experimental study of memory consolidation-reconsolidation during storage of figurative-symbolic information was performed. The short-term auditory-speech and visual-figurative memory span was assessed by the method of memorizing ten words proposed by A. R. Luria and the methods "Two Groups of Three Words", "Five Figures That are Hard to Verbalize".

The visual-figurative working memory span was assessed using the Block Span method [15].

Step two

The experimental study of interference in the form of viewing video content on the TikTok social media platform (experimental groups) or in the form of reading the fragment of the children's picture book (control groups) was carried out. Subjects in the experimental groups were offered to watch two series of videos. The first series consisted of 18 videos lasting up to 10 s or longer (the total length of this video content was 5 min). The videos for this series were selected based on the visual-acoustic features. The videos featured video content with some background music or other rhythmic melodic accompaniment, but no background speech. The second series was represented by 22 videos lasting 10–20 s (the total length was 5 min). These videos were selected based on the visual-speech features. The videos featured video content with the direct speech production.

After watching both series of videos (visual-acoustic and visual-speech ones) the subjects were offered to answer the following questions about the video: ordinal number of the video, semantic content, details, impression (in the like/dislike format).

Subjects in the control groups were offered to read several pages of text with pictures (the fragment of the book "Naksitrallid" by Eno Raud) silently (not aloud) within 10 minutes. After reading, the subjects had to retell the piece of text they had read as detailed as possible. Assessment was performed based on the following parameters: number of characters; sequence of actions committed by the main characters; number of semantic units in the retelling.

Step three

The process of auditory-speech and visual-figurative memory reconsolidation in the context of interference was assessed: such parameters as span, pace, precision, and duration of memory trace storage within the framework of auditory and visual modalities were reassessed using the method of memorizing ten words by A. R. Luria, and the methods "Two Groups of Three Words", "Five Figures That are Hard to Verbalize".

The methods of descriptive (mean and standard deviation) and comparative (nonparametric Mann–Whitney U test,

Wilcoxon signed-rank test, $p < 0.05$) statistics were used for quantitative data processing. The studied groups were compared based on the quantitative indicators obtained before (memory consolidation) and after (memory reconsolidation) the interference exposure.

RESULTS

Step one

When completing the task of assessing the short-term and long-term memory span and memory consolidation and reconsolidation in adolescents during the first phase of the study, we revealed the reduced memory span for all memory types in the groups of subjects. The maximum reduction of the short-term auditory-speech and visual-figurative memory span was observed in the groups of adolescents aged 11–12 (Fig. 2).

The maximum short-term memory span (for both auditory-speech and visual-figurative memory) was revealed in the experimental group of adolescents aged 15–17. Significant differences between three experimental groups of adolescents were observed. As for the short-term auditory-speech memory span, there were no significant differences only between the experimental groups of adolescents aged 13–14 and 15–17 in the fourth series to be recalled (immediate recall after the stimulus words) repeated for the fourth time ($p = 0.137$). The same results were obtained in the control groups. There were no significant differences in the short-term auditory-speech memory span between the control groups of adolescents aged 13–14 and 15–17 in the fourth series to be recall ($p = 0.132$).

When recalling two groups of three words, the decrease in the short-term auditory-speech memory span was observed in the group of adolescents. After the fourth series, two groups of three words were not available for recall in full. In the control and experimental groups of adolescents aged 11–12 one word per series (the last one) was available for recall. The other words named were the inflicted ones that are semantically similar to the stimulus words. Adolescents aged 13–14 in both groups recall two words of each group. The grouping principle was not followed: adolescents named together those two words that had been named in different groups during presentation. It should be noted that there was no substitution of words with
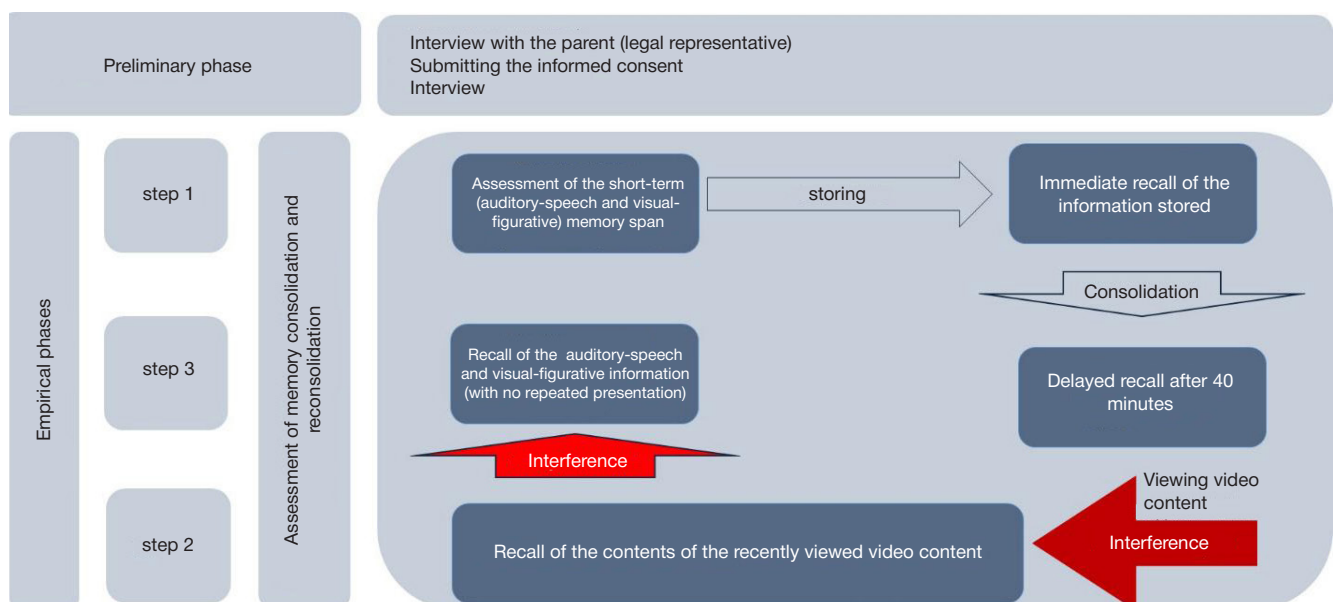

Fig. 1. Design of the study aimed at assessing the effects of the social media interference factor on memory consolidation in adolescents
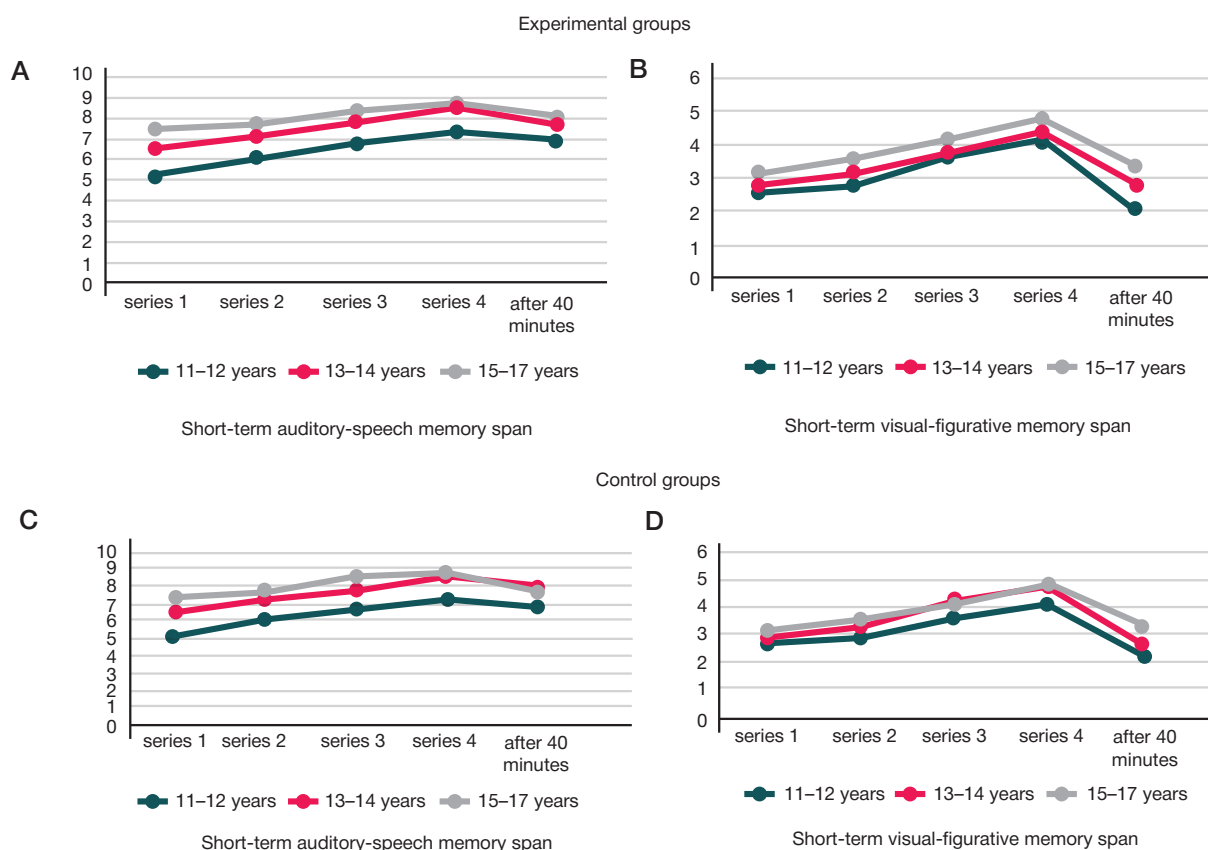
Fig. 2. Parameters of the short-term auditory-speech and visual-figurative memory span in adolescents

the semantically similar ones (typical for adolescents aged 11–12). As for adolescents aged 15–17, the subjects recalled correctly two words of the first group (the first and the last one) and all three words of the second group (out-of-order) after presentation of the fourth series.

A pairwise comparison of experimental and control groups in accordance with age ranges (adolescents aged 11–12 with the control groups of adolescents aged 11–12; adolescents aged 13–14 with the control groups of adolescents aged 13–14; adolescents aged 15–17 with the control groups of adolescents aged 15–17) performed when assessing the short-term auditory-speech and visual-figurative memory span revealed no significant differences.

The findings are also confirmed by the results of using the Block Span instrumental method. Thus, the initial decrease in the short-term memory span can be observed in adolescents who spend at least 6 hrs a day on Internet and social media. The maximum decrease in the short-term (both auditory-speech

and visual-figurative) memory span has been revealed in the groups (both experimental and control) of adolescents aged 11–12. The reduced span leads to the fact that the information content is simplified and reduced during the stage of storing, which, in turn, results in consolidation of the initially distorted information content. Distortions are reflected in simplification and reduction of the information stored. The average loss of original information is 44.16% of the total information content in the experimental group and 44.89% in the control group. The decrease in the short-term memory span in also typical for adolescents aged 13–14. However, in contrast to adolescents aged 11–12, the loss of semantic content is 32.56% in the experimental group and 33.04% in the control group. The form is substituted with equivalent or similar semantic content at the stage of consolidation. When recording auditory-speech information, adolescents of this group replace the stimulus words with semantically similar words or synonyms. The minimum decrease in the short-term memory span has been

Table. The average values of such parameters as idea, details, and impression for video content presented to the groups of adolescents

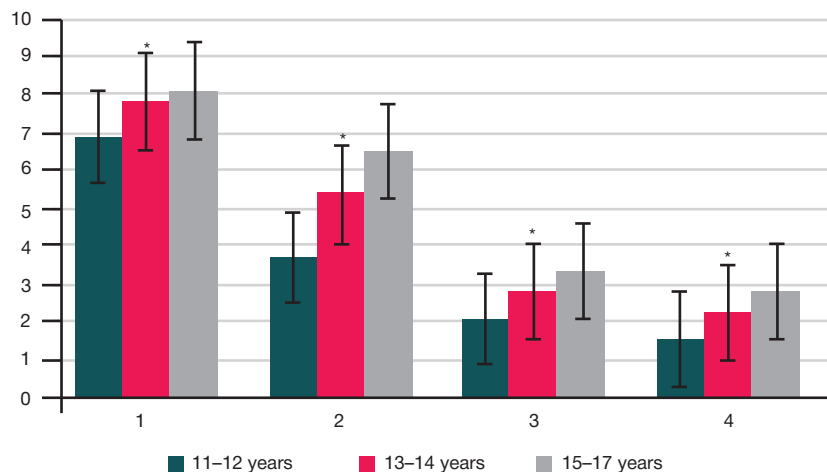| Groups of subjects	Parameters				
	Idea (number of semantic units)	Details		Impression	
		Number of characters	Number of objects	Like	Dislike
Visual-acoustic content (18 videos)					
11–12 years	11	8	6	15	2
13–14 years	16	14	12	10	8
15–17 years	24	18	16	9	9
Visual-speech content (22 videos)					
11–12 years	14	10	7	18	4
13–14 years	19	14	9	14	8
15–17 years	26	18	12	12	10

Fig. 3. Bar graph showing the average values of the auditory-speech and visual-figurative memory span obtained in the experimental groups after exposure to interference

revealed in the groups of adolescents aged 15–17. Furthermore, the distortion of information at the stage of storing is minimal. The loss errors are reported more often than in other groups: adolescents recall only a part of information content, with no distortions or substitution with semantically similar information.

Step two

The factor of interference was analyzed during the second phase.

The consolidated interfering content was assessed in the experimental groups of adolescents after viewing the 10-minute video content based on three parameters: idea (number of semantic units), details (number of characters, humans and animals, as well as the number of objects in the video), impression (whether the subject likes or dislikes the video). These parameters were assessed for each video constituting the video sequence (Table).

Imagine the qualitative structure of the consolidated content of the recently watched video content for two series (visual-acoustic and visual-speech content).

When watching both visual-acoustic and visual-speech content, adolescents of all groups show the loss of semantic content of the videos. When describing the resently watched pieces of video the subjects disrupt the video sequence (all the asolescents enrolled used the sequence that was different from the presented sequence when describing the contents and the characters of the video fragments). The contents of various video fragments is "mixed": when describing semantic content of the video fragment, adolescents specify the characters and other objects from the other videos, either previous or subsequent ones. It is worth mentioning that adolescents most often describe the characters from the first two or three video fragments of the content, or from the last ones in the sequence demonstrated. This is a regular feature that corresponds to the edge effect.

In the experimental group of adolescents aged 11–12, the idea of single video fragment is formilated as a simple sentence or a phrase "noun + adjective". Only 15% of video fragments (six videos) are available for description. The subjects usually specify the character of the video (human or animal), its action or trait. Furthermore, if the adolescent specifies the character, he/she does not specify the objects present in the video. And, vice versa, if the adolescent specifies the objects present in the video, he/she is unable to specify and describe the character. As for the impression criterion, the adolescents like 90% of

video fragments constituting both visual-acoustic and visual-speech content and note these as "interesting", "funny", "curious", "zany", "cool", etc. The authentically established fact is that not the original content, but the emotional response to the content is recorded during consolidation or reconsolidation of video content. Adolescents do not identify information that have made certain impression. The subjects aged 13–14 in the experimental group use enlarged simple sentences that characterize the relationships between the characters of the video and external objects when describing the ideas of the recently watched video fragments, constituting both visual-acoustic and visual-speech content. Only 32% of videos (13) are available for description that constitute mainly the visual-acoustic content. Positive impressions predominate over negative ones by a ratio of 60/40. Adolescents conserve their impressions without recalling the semantic content and details of the video. In the subjects aged 15–17, the percentage of videos available for description increases to 48% (19 video fragments). This age group is characterized by the more precise and detailed description of videos. In contrast to other age group, these adolescents describe the details (characters and other objects) as precisely as possible.

Assessment of the social media interference impact on memory consolidation in adolescents shows loss of the significant amounts of information in the form of missing (the content of the part of videos is recorded only via impression with no semantic content or details) or distorted information (mixing the content of several viewed video fragments). The maximum losses of both visual-figurative and auditory-speech information due to interfering effects of social media are observed in the group of adolescents aged 10–12.

The content consolidated after reading the text was assessed in the control groups of adolescents based on the following parameters: number of characters; main characters' sequence of actions; number of semantic units in the retelling.

The consolidated content qualitative structure allows stating the semantic content distortion manifested in the disruption of the main characters' sequence of actions; actions of one character are attributed to another one; minor characters are lost. The details are missing in the description of events during retelling. The figurative-graphic information represented by the pictures seen when reading the fragment of the book is also modified. When describing the pictures, adolescents correctly specify the main characters. However, they make mistakes when describing actions committed by main characters or their location.
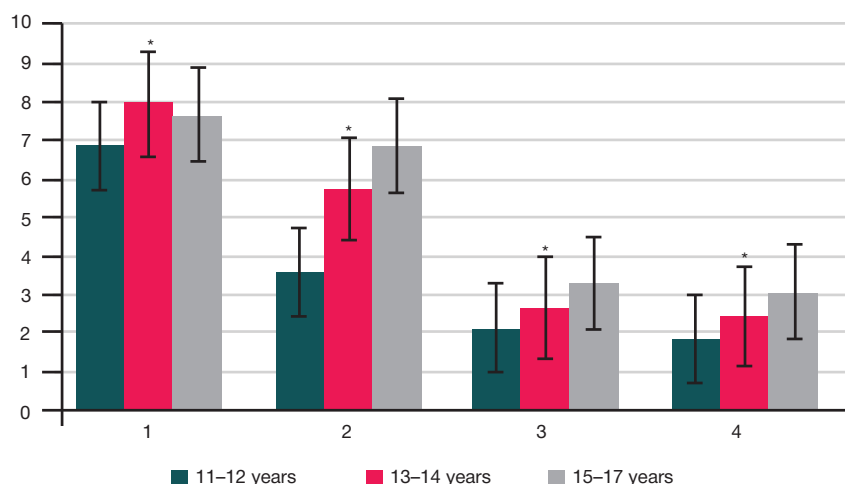
Fig. 4. Bar graph showing the average values of the auditory-speech and visual-figurative memory span obtained in the control groups after exposure to interference

The following specific features of the information consolidated observed in the control groups of adolescents should be noted. Adolescents of the control group aged 11–12 retell mostly in short simple sentences (consisting of 4–5 words on average). The number of semantic units is lower than the number of sentences: the same semantic content is represented using several sentences. When retelling, adolescents recall mostly the contents of the last 20–25 sentences they have read. In 90% of cases, retelling of the prior content is reduced to the description of the pictures watched. When retelling the recently read fragment of the book, adolescents aged 13–14 in the control group use enlarged simple sentences. They reproduce the semantic content that reflects interaction between the characters as dialogs. The semantic content is recalled in fragments and is correlated with the pictures found in the recently read pages. In the retelling, the detailed description of pictures predominates over the semantic content of the recently read text. The more precise and detailed retelling of the recently read fragment is typical for the 15–17 age group (control group). Adolescents of this group provide the most precise description of the characters' actions compared to other groups. The sequence disruptions observed in the retelling are minimal, the pictures are described using 5–7 sentences that are represented by mentioning the objects depicted and specifying their characteristics, without regard to the recently read text.

Assessment of the recently read text interference effects on memory consolidation in adolescents of the control groups shows distortion of the substantial amount of information. Distortions are manifested as the disrupted sequence of actions committed by the characters observed during retelling of the text and the lack of semantic correspondences between the recently read textual information and the pictures. The maximum distortions are reported in the control group of adolescents aged 11–12.

Step three

Reconsolidation of the auditory-speech and visual-figurative memory was assessed during phase three. After watching two series of videos (visual-acoustic and visual-speech content), adolescents of the experimental groups were offered to recall 10 words; groups of three words; and five images of the figures that are hard to verbalize together with the symbol (letter of Greek alphabet) they had memorized before watching. Adolescents of the control group were offered to complete a similar task after reading a fragment of the picture book.

A significant decrease in the amount and quality of the information recalled was observed in all experimental groups of adolescents during reconsolidation after exposure to the social media interference. Assessment of the significance of differences in the auditory-speech memory span values observed in the experimental groups of adolescents before and after exposure to interference revealed the significantly decreased values in the groups of adolescents aged 11–12 ($p = 0.026$), 13–14 ($p = 0.022$), and 15–17 ($p = 0.024$). Similar results were obtained when assessing the visual-figurative memory span. The maximum significant decrease in the amount of information recalled is reported in the experimental group of adolescents aged 11–12 ($p = 0.024$). The visual-figurative memory span is also decreased in the experimental groups aged 13–14 ($p = 0.022$) and 15–17 ($p = 0.021$) (Fig. 3).

The quantitative indicator of the amount of information recalled and the information content are modified in the context of social media interference. The group of subjects aged 11–12 replace the stimulus words to be recalled by the names of objects or produced speech (words) from the videos constituting the visual-speech content. Elements of the videos constituting the visual-acoustic content are also reported in the visual imagery recalled (particular movements resembling the contours of the figures recalled, contours of the displayed objects, etc.). In the group of adolescents aged 13–14 and 15–17, the qualitative transformation of the information recalled occurs primarily in the form of reduction. The interfering social media contents "blocks" the information content consolidated before the interference exposure. This, in turn, results in the loss of information content.

A significant decrease in the amount and quality of information recalled after exposure to the text reading interference is also reported in the control groups of adolescents. Assessment of differences in the auditory-speech memory span values obtained in the control groups of adolescents before and after the exposure to interference has revealed the significantly decreased values in the group of adolescents aged 11–12 ($p = 0.044$), 13–14 ($p = 0.049$), and 15–17 ($p = 0.047$). Similar results have been obtained when assessing the visual-figurative memory span. The maximum significant decrease in the amount of information recalled is observed in the control group of adolescents aged 11–12 ($p = 0.042$). The visual-figurative memory span is also significantly decreased in the groups aged 13–14 ($p = 0.044$) and 15–17 ($p = 0.044$) (Fig. 4).

In the context of interference provided by reading the text with illustrations, the quantitative reduction of the amount of information recalled is observed along with the modified

qualitative context. Adolescents aged 11–12 in the control group replace the stimulus words recalled with the names of objects presented in the illustrations to the text they have read. They also record the elements of illustrations in the recalled visual images. In the groups of adolescents aged 13–14 and 15–17, the qualitative transformation of the information recalled occurs primarily in the form of reduction. The interfering content of the recently read text "blocks" the information content consolidated before the interference exposure, just like the recently viewed video content. This is the cause of the information content loss.

Assessment of the significance of differences showed that the decrease in both auditory-speech and visual-figurative memory span was more pronounced in the experimental groups of adolescents where watching video content was used as interference compared to the control group where interference was provided by reading the fragment of the fiction picture book. In adolescents aged 11–12, significance of differences (p) between the indicators of auditory-speech memory was 0.021, and that of visual-figurative memory was 0.024; in adolescents aged 13–14, significance of differences between the indicators of auditory-speech memory was 0.024, while that of visual-figurative memory was 0.024; in adolescents aged 15–17 significance of differences in auditory-speech memory between the experimental and control groups was 0.019, and that of visual-figurative memory was 0.018.

The findings indicate more severe interfering effects of video content compared to reading textual information.

DISCUSSION

According to the review of domestic and foreign studies [15], the findings do not allow us to speak about the unified and consolidated effects extending to the whole population of children and adolescents. The authors of the review believe that the lack of definitive evidence of the effects of digital technology, including social media, is due to non-linear and differential effects. The power of these effects depends on the number of factors: individual characteristics, intensity of using the technologies, and socio-economic characteristics of the child's environment. Our findings also confirm the adverse impact of the factor of continuous long-term video stream viewing. The more the duration of the maximum continuous video stream and the total time spent on Internet (including social media) by adolescents, the larger is the information loss.

The results of the study conducted cofirm the earlier results [16]. The author points out to the fact that the efficiency of memory processes decreases within a year and a half since the start of mastering the Internet; the more prolonged online activity (over three years) leads to the increase in memorizing due to increased interaction of functional and operational mechanisms. Furthermore, the author believes that the methods used for processing of the material memorized become less differentiated and more automated with the increase in the duration of online activity. According to our empirical findings, the maximum decrease in the short-term (both auditory-speech and visual-figurative) memory span and substantial distortion of information due to interference are observed in the groups of adolescents aged 11–12. The 13–14- and 15–17-year-old subjects show less prominent reduction and distortion of information.

CONCLUSIONS

Adolescents aged 11–12, 13–14, and 15–17 show the decrease in the short-term (both auditory-speech and visual-figurative) memory span. The reduced short-term memory span results in impaired consolidation. The distorted information content is consolidated at the stage of storing. Either partial loss of information content (13–14 and 15–17 age ranges), or information content transformation in terms of form (for example, simplification) and the contents (for example, when recalling two series of three words, the stimulus words are recalled chaotically: words of one series are transferred to another series; the stimulus words are replaced by consonant words, the visual-figurative information is simplified and clarified) occurs.

Thus, the findings should be included in the programs of mental hygiene and development of the younger generation in the context of digital reality. The danger is not the digital reality itself, but its unconscious and uncontrollable effects on the fundamental mechanism that links the short-term and long-term memory systems.

References

1. Repovs G, Baddeley A. The multi-component model of working memory: explorations in experimental cognitive psychology. Neuroscience. 2006. 139: 5–21

2. Alberini CM. Memory Reconsolidation, 2013; 81–117. DOI: 10.1016/B978-0-12-386892-3.00005-6.

3. Grigoryan GA, Markevich VA. Konsolidaciya, reaktivaciya i rekonsolidaciya pamyati. Zhurnal Vysshej nervnoj deyatel'nosti. 2014; 64 (2): 123–36. Russian.

4. Velichkovskij BB. Rabochaya pamyat' cheloveka: Struktura i mexanizmy. M: Kogito-centr, 2015; 247 s. Russian.

5. Dozorceva EG., Kiryuxina D. V. Kiberbulling i sklonnost' k deviantnomu povedeniyu u podrostkov. Prikladnaya yuridicheskaya psixologiya. 2020; 1 (50): 80–87. Russian.

6. Andreeva AO. Manipulirovanie v seti Internet. Informacionnaya bezopasnost' i voprosy profilaktiki kiberehkstremizma sredi molodezhi. 2015: 21–28. Russian.

7. Kudryavcev IA. Deviantologiya izmenenij lichnosti podrostkov v social'nyx setyax (fenomeny i zakonomernosti deficitarnoj transformacii). Deviantologiya. 2021; 5 (2–9): 3–13. DOI: 10.32878/devi.21-5-02(9)-3-13. Russian.

8. Yudeeva TV. Motivaciya destruktivnogo kommunikativnogo povedeniya podrostkov v social'nyx setyax. Mezhdunarodnyj nauchno-issledovatel'skij zhurnal. 2022; 2–2 (116): 178–82. DOI: https://doi.org/10.23670/IRJ.2022.116.2.066. Russian.

9. Pis'mo Ministerstva obrazovaniya i nauki Rossijskoj Federacii ot 28.04.2014 N DL-115/03 «O napravlenii metodicheskix materialov dlya obespecheniya informacionnoj bezopasnosti detej pri ispol'zovanii resursov seti Internet». Dostupno po ssylke: https://www.consultant.ru/document/cons_doc_LAW_123707/8968082babe2e09c403b4254022a2abd2ff908e1/. Russian.

10. Lewis DJ. Psychobiology of active and inactive memory. Psychol. Bull. 1979. 86: 1054–83

11. Lewis DJ, Bregman NJ, Mahan JJ Jr. Cue dependent amnesia in rats. J Comp Physiol Psychol. 1972; 81 (2): 243–47

12. Roozendaal B, McGaugh JL. Memory modulation. Behav Neurosci. 2011; 125 (6): 797–824. DOI: 10.1037/a0026187. PMID: 22122145; PMCID: PMC3236701.

13. Velichkovskij BB. Testirovanie rabochej pamyati: ot prostogo k slozhnomu i snova k prostomu. Teoreticheskaya i ehksperimental'naya psixologiya. 2014; 7 (2): 133–42. Russian.

14. Anoxin KV. Mozg i pamyat': biologiya sledov proshedshego vremeni. Vestnik Rossijskoj akademii nauk. 2010; 80 (5-6): 455. Russian.

15. Isaacs E, Vargha-Khadem F. Differential course of development of spatial and verbal memory span: A normative study. British Journal of Developmental Psychology. 1989; 7: 377–80. DOI: 10.1111/j.2044-835X.1989.tb00814.x.

16. Bochaver AA, Dokuka SV, Sivak EV, Smirnov IB. Ispol'zovanie social'nyx setej v internete i depressivnaya simptomatika u podrostkov. Klinicheskaya i special'naya psixologiya. 2019; 8 (3): 1–18. DOI: 10.17759/psyclin.2019080301. Russian.

Литература

1. Repovs G, Baddeley A. The multi-component model of working memory: explorations in experimental cognitive psychology. Neuroscience. 2006. 139: 5–21

2. Alberini CM. Memory Reconsolidation, 2013; 81–117. DOI: 10.1016/B978-0-12-386892-3.00005-6.

3. Григорьян Г. А., Маркевич В. А. Консолидация, реактивация и реконсолидация памяти. Журнал Высшей нервной деятельности. 2014; 64 (2): 123–36

4. Величковский Б. Б. Рабочая память человека: Структура и механизмы. М: Когито-центр, 2015; 247 с.

5. Дозорцева Е. Г., Кирюхина Д. В. Кибербуллинг и склонность к девиантному поведению у подростков. Прикладная юридическая психология. 2020; 1 (50): 80–87.

6. Андреева А. О. Манипулирование в сети Интернет. Информационная безопасность и вопросы профилактики киберэкстремизма среди молодежи. 2015: 21–28.

7. Кудрявцев И. А. Девиантология изменений личности подростков в социальных сетях (феномены и закономерности дефицитарной трансформации). Девиантология. 2021; 5 (2–9): 3–13. DOI: 10.32878/devi.21-5-02(9)-3-13.

8. Юдеева Т. В. Мотивация деструктивного коммуникативного поведения подростков в социальных сетях. Международный научно-исследовательский журнал. 2022; 2–2 (116): 178–82. DOI: https://doi.org/10.23670/IRJ.2022.116.2.066.

9. Письмо Министерства образования и науки Российской Федерации от 28.04.2014 N ДЛ-115/03 «О направлении методических материалов для обеспечения информационной безопасности детей при использовании ресурсов сети Интернет». Доступно по ссылке: https://www.consultant.ru/document/cons_doc_LAW_123707/8968082babe2e09c403b4254022a2abd2ff908e1/.

10. Lewis DJ. Psychobiology of active and inactive memory. Psychol. Bull. 1979. 86: 1054–83

11. Lewis DJ, Bregman NJ, Mahan JJ Jr. Cue dependent amnesia in rats. J Comp Physiol Psychol. 1972; 81 (2): 243–47

12. Roozendaal B, McGaugh JL. Memory modulation. Behav Neurosci. 2011; 125 (6): 797–824. DOI: 10.1037/a0026187. PMID: 22122145; PMCID: PMC3236701.

13. Величковский Б. Б. Тестирование рабочей памяти: от простого к сложному и снова к простому. Теоретическая и экспериментальная психология. 2014; 7 (2): 133–42.

14. Анохин К. В. Мозг и память: биология следов прошедшего времени. Вестник Российской академии наук. 2010; 80 (5-6): 455.

15. Isaacs E, Vargha-Khadem F. Differential course of development of spatial and verbal memory span: A normative study. British Journal of Developmental Psychology. 1989; 7: 377–80. DOI: 10.1111/j.2044-835X.1989.tb00814.x.

16. Бочавер А. А., Докука С. В., Сивак Е. В., Смирнов И. Б. Использование социальных сетей в интернете и депрессивная симптоматика у подростков. Клиническая и специальная психология. 2019; 8 (3): 1–18. DOI: 10.17759/psyclin.2019080301.